IN SITU ABSORPTION AND FLUORESCENCE STUDIES OF ELECTROGENERATED SPECIES

A Thesis Submitted for the Degree of Doctor of Philosophy of the University of London and for the Diploma and Membership of Imperial College of Science and Technology

Cameron William Miller McLeod B.Sc.

September 1977

Department of Chemistry
Imperial College of Science & Technology
London S.W.7

ABSTRACT

The thesis describes analytical studies which are concerned with the measurement, at electrode surfaces, of highly absorbing/fluorescent species electrogenerated (invariably under controlled potential conditions) from inorganic and organic precursors. Introductory chapters outline research proposals, include a review of solution spectroelectrochemical studies and provide details of instrumentation and cell design. Chapter 3 is concerned with metal ion investigations, particularly cadmium. In situ monitoring during electrolysis indicated that highly absorbing cadmium hydroxide particles were produced when the solution layer at the working electrode became alkaline. The reduction reactions of dissolved oxygen and platinum surface oxide and the hydrogen evolution reaction accounted for hydroxide formation. In chapters 4 and 5 model compounds, o-tolidine and ferrocyanide, were used to illustrate the analytical value of the spectroelectrochemical approach (in stationary and flowing solutions) and to check cell performance. The electro-initiation of fluorogenic reactions utilising a gold micromesh cell is described in chapter 6. Morphine, heroin (after hydrolysis), laudanosine, reserpine, thioguanine and homovanillic acid were successfully examined and analysis of pharmaceutical products containing morphine and reserpine was performed. The penultimate chapter discusses absorption and fluorescence studies of some polycyclic aromatic hydrocarbons in acetonitrile. Finally, a general conclusion and suggestions for future work are presented.

ACKNOWLEDGEMENTS

I am grateful to Professor T.S. West for giving me the opportunity and encouragement to perform this research; his suggestions and comments during the programme were invaluable. My thanks also go to fellow research workers, J.F. Tyson, H.B. Sadeghi, A.J.C.L. Hogarth and S. Cooke for helpful discussion.

The latter part of research was conducted at the Department of Chemistry, University of Aberdeen and it gives me pleasure to acknowledge the co-operation and assistance of R.A. Chalmers and I.L. Marr.

Thanks are also due to staff at Imperial College and Aberdeen University and in particular to R. Cobley and A. Barclay for the construction of cells and to S. Black for drawing and photographic services.

Financial support from the Chemical Society/ Analytical Division is acknowledged.

C O N T E N T S

		Page
Abstract		2
Acknowledgements		3
CHAPTER 1	General Introduction	7
1.1.	Introduction	7
1.2.	Literature Review of Spectroelectrochemistry	10
CHAPTER 2	Equipment	23
2.1.	Spectroelectrochemical Instrumentation	23
2.2.	Spectroelectrochemical Cells	30
2.3.	Miscellaneous Equipment	39
CHAPTER 3	Studies with Metal Ions	40
3.1.	Introduction	40
3.2.	Preliminary Studies	43
3.3.	Absorption Monitoring during Controlled Potential Electrolysis	60
3.4.	Absorption Studies of Chemically Prepared Metal Hydroxide Solutions	82
3.5.	Conclusions	98
CHAPTER 4	Studies with Potassium Ferrocyanide and O-Tolidine	99
4.1.	Introductory Remarks	99
4.2.	Experimental Details	100

		Page
4.3.	Potassium Ferrocyanide	101
4.4.	o-Tolidine	116
4.5.	Conclusions	122
CHAPTER 5	Studies in Flowing Solution	123
5.1.	Introduction	123
5.2.	Experimental Procedure	125
5.3.	Oxidation of Ferrocyanide	126
5.4.	Oxidation of o-Tolidine	128
5.5.	Reduction of Dissolved Oxygen	134
5.6.	Reduction of Methyl Viologen	138
5.7.	Conclusions	144
CHAPTER 6	Aqueous Fluorescence Studies	145
6.1.	Introductory Remarks	145
6.2.	Morphine	147
6.3.	Laudanosine	184
6.4.	Reserpine	189
6.5.	Thioguanine	195
6.6.	Homovanillic Acid	200
6.7.	Instrumental Sensitivity	205
6.8.	Conclusions	207
CHAPTER 7	Studies with Polycyclic Aromatic Hydrocarbons	209
7.1.	Introduction	209

		Page
7.2.	Experimental Details	212
7.3.	Reduction Experiments	215
7.4.	Oxidation Experiments	222
7.5.	Conclusions	225
CHAPTER 8	General Conclusion and Recommendations	226
REFERENCES		228

ERRATUM

o-Tolidine and o-methyl flavinantine should be o-tolidine and o-methyl flavinantine respectively.

CHAPTER 1 General Introduction

1.1. Introduction

The techniques of ultraviolet-visible absorption and fluorescence spectroscopy play an important role in the field of instrumental analysis providing a means for the rapid determination of organic and inorganic constituents in samples from diverse origins. In an attempt to extend their range of application, the possibility of coupling spectroscopic and electrochemical methods and utilising *in situ* absorption and fluorescence monitoring of electrogenerated species for analytical purposes was investigated. The spectroelectrochemical technique has already been established over the last decade as a powerful tool for elucidation and characterisation studies of electrode reaction mechanisms[1,2], but it has only recently been shown to have analytical potential[3-7]. Combined methods of analysis are already well-established, none more so than gas chromatography-mass spectroscopy, and it is hoped that spectroelectrochemistry can eventually occupy a position of similar standing.

The basis of the approach is simply that a redox reaction alters the atomic/molecular structure of the reactant producing a new species. Providing the species is stable, the resulting change in spectroscopic properties may provide analytically important information: changes in absorption and fluorescence spectra assist in the characterisation of the parent compound while increased molar extinction coefficients and fluorescence yields

improve detection limits for trace determinations. The spectroelectrochemical technique, in effect, provides a convenient and reproducible method for performing selective chromogenic/fluorogenic reactions with simultaneous *in situ* absorption/fluorescence measurement. Although the above comments apply equally to inorganic and organic systems, studies with the latter group are potentially more rewarding due primarily to the large number of electroactive organic structures which exhibit characteristic absorption and possible fluorescence. In addition, organic electrode reactions seldom involve only electron transfer in contrast to inorganic ions. The initially formed radical ion species are generally highly reactive and subsequent follow-up chemical reactions occur; the lifetimes of the reactive intermediates can, however, usually be prolonged by suitable choice of non-aqueous solvent. The possibility therefore exists, with organic systems, of spectrally monitoring not only changes in the oxidation state of the parent compound, but also monitoring the formation of new chemical compounds.

To investigate the proposals, instrumentation was built to accomodate spectroelectrochemical cells utilising working electrode materials based on carbon, platinum and gold. Studies were performed in quiescent and flowing solutions where mass transport was controlled by diffusion and convective diffusion respectively. Initial investigations were concerned with heavy metal ions, particularly cadmium, and the reduction reactions of dissolved oxygen and platinum surface oxide were of particular importance. Model compounds,

potassium ferrocyanide and σ-tolidine, were used to check the monitoring performance of the cells and to illustrate the analytical value of the combined approach. Fluorescence research was directed at analytically important compounds including alkaloids, pharmaceutical products and polycyclic aromatic hydrocarbons. The results for morphine using a gold micromesh cell were particularly promising.

Before the experiments are discussed a short review of spectroelectrochemistry is presented.

1.2. Literature Review of Spectroelectrochemistry

1.2.1. Introductory remarks

The combination of electrochemical and spectroscopic methods is a subject in which considerable research has been done in the last decade. Coupling the appropriate spectroscopic technique to the electrochemical experiment has enabled significant progress to be made in a number of areas notably in electrode surface characterisation studies and in the field of electrochemical reaction mechanisms. Extensive and authoratative reviews by Kuwana and Winograd[1,2] which deal primarily with the latter subject are available while a series of papers edited by Muller[8] and which appear in one volume are concerned with the former subject. Electron spin resonance(ESR) coupled studies are reviewed by Adams[9] and also more recently by McKinney[10].

The main features of spectroelectrochemical methods are presented by referring individually to the principal optical techniques and to considerations such as equations, cells, electrodes, instrumentation and applications. Since this thesis is concerned with ultraviolet-visible monitoring in the solution phase, techniques used primarily for surface studies such as ellipsometry, holography and microscopy are not considered and the reader should refer to the volume edited by Muller[8]; an exception is the specular reflection technique. ESR work is also not considered, but studies in the infrared are included.

1.2.2. Transmission spectroscopy

In situ spectral monitoring by transmission spectroscopy provides the simplest route for relating solution spectroscopic changes to electrochemical parameters. The basis of the approach is to record the absorbance - time profile of the product species during electrochemical excitation and compare the results with theory. For electrode processes under semi-infinite linear diffusion(SILD) control, Kuwana[1,11] has derived definining equations basically modifications of the Beer-Lambert law. For an uncomplicated electrode reaction

$$a \rightarrow b + ne$$

the absorbance(A) - time equation for chronoamperometry is

$$A_b(t;\lambda) = \frac{2}{\pi^{\frac{1}{2}}}(D_a t)^{\frac{1}{2}}\epsilon_b(\lambda)C_a$$

where D is the diffusion coefficient ($cm^2.s$), ϵ is the molar extinction coefficient ($LM^{-1}cm^{-1}$) and C is the concentration (ML^{-1}). The expression predicts that the absorbance of electrogenerated product is directly proportional to the square root of time. Also the optical pathlength, $2(D_a t/\pi)^{\frac{1}{2}}$, continually increases with time and is essentially equivalent to the diffusion layer thickness. A similar equation exists for chronopotentiometry and linearity of absorbance with time is predicted.

The transmission cell of Kuwana shown in fig 1.1 is

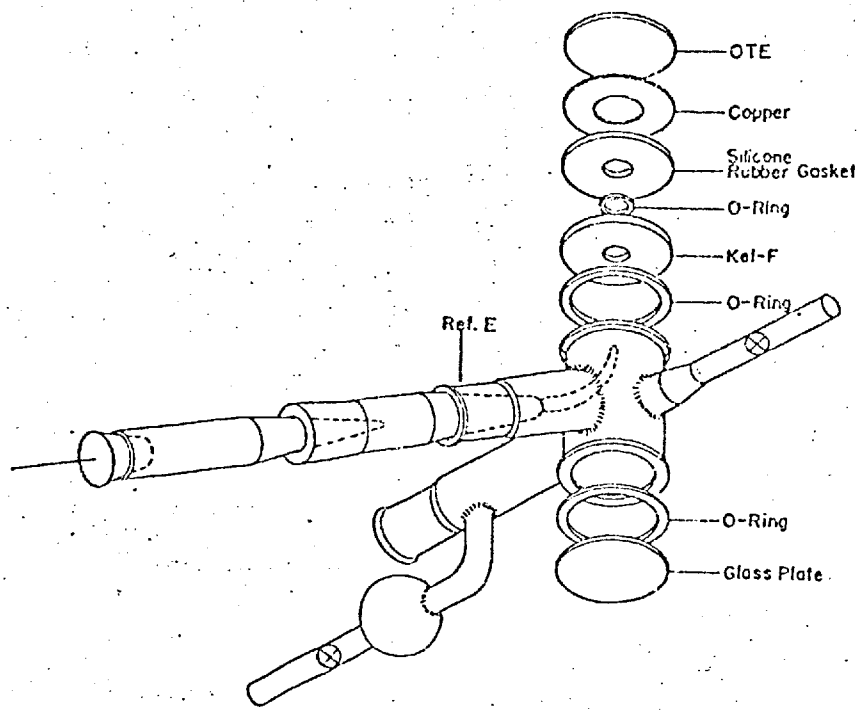

FIG. 1.1. Sandwich cell for transmission experiments. (Reproduced from Ref. 1)

fairly representative in that it utilises a planar optically transparent working electrode(OTE) as part of a three-electrode cell. Monochromatic light traverses the entire cell pathlength and OTE before being processed by the detection system. Single-beam optical equipment has been adequate for most purposes but for studies in the infrared double-beam instrumentation has been recommended[1] to eliminate solvent absorption peaks. Experiments have generally been performed under controlled potential or current conditions and electrochemical systems are based on a potentiostat with an X-Y recorder and an oscilloscope. Typical spectroelectrochemical apparatus employed by Kuwana is given in fig 1.2. Additional refinements have included the use of signal averaging to improve instrumental sensitivity; this is particularly important for the internal reflection spectro-

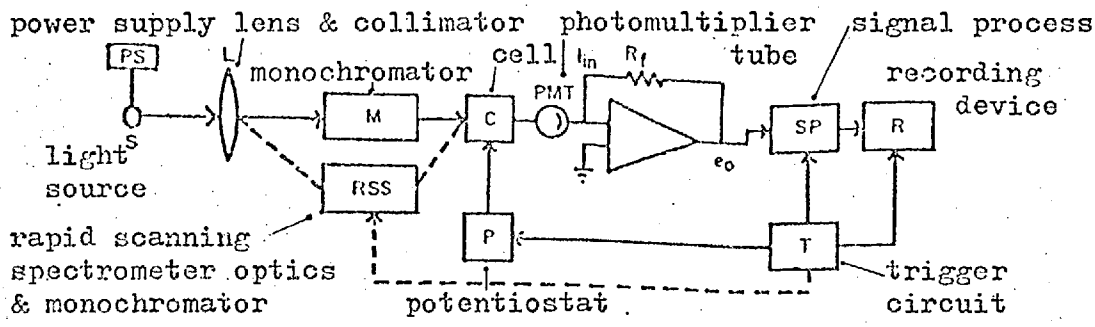

FIG. 1.2. Block diagram of spectroelectrochemical apparatus. (Reproduced from Ref. 1)

scopic (IRS) technique where extremely short pathlengths are experienced. Also a rapid scanning spectrometer (RSS)[12] has been employed for recording the spectra of reactive intermediates. Both these techniques can be interfaced with the mini-computer to improve data collection and processing and are discussed by Kuwana in his review paper[1].

OTE are prepared by depositing a thin film of metal or metal oxide on a transparent material such as a quartz slide. They should have good mechanical stability, favorable electrochemical properties and be optically transparent. The transmission characteristics are very dependent on the coating material and this determines to some extent the suitability of the OTE for any particular experiment. Doped tin oxide and indium oxide films are the preferred choice and are almost totally transparent in the visible but have a sharp cut-off at approximately 300nm. The electrodes tend to have potential ranges in aqueous solution similar to platinum but the tin oxide surface is unsuited to alkaline conditions[1]. Platinum film is reported to be the most suitable for experiments in the ultraviolet and visible for although it absorbs radiation,

the level remains fairly constant from 200nm - 800nm. The situation for the gold OTE is similar.

The first optically coupled experiment performed by Kuwana and co-workers[13] utilised a tin oxide OTE and involved the chronopotentiometric oxidation of o-tolidine and ferrocyanide; transition times and diffusion coefficients were subsequently spectrally determined by solving the appropriate equations for chronopotentiometry and chronoamperometry respectively[11].

In addition to obtaining fundamental parameters, monitoring the products of the electron transfer and follow-up chemical reactions has assisted the interpretation of electrode reaction mechanisms. For instance optical monitoring during cyclic scan showed that, in the case of o-tolidine, the oxidation products depended on the pH of the solution[14]. At pH 2 a single two-electron transfer occurred giving a species with an absorption maximum (λmax) of 437nm. At pH 4, however, two consecutive one-electron transfers resulted and a dimeric species (λmax 365nm, 630nm) was formed in addition to the one generated at pH 2. This latter electrode behaviour, two consecutive one-electron transfers, is termed an EE reaction mechanism. Strojek[15] verified this mechanism by comparing the absorbance - time behaviour during the potential step with the computer-simulated concentration profiles of the various species derived from the appropriate kinetic equations. Kinetic analyses of this type have also been employed for other important organic electrode mechanisms

*

including the EC, ECE and EEC schemes.

Spectroelectrochemical investigations have not been limited to aqueous solution and a number of non-aqueous solvents have been accessed for suitability with OTE[16]. The spectra of the radical anions of the polycyclic aromatic hydrocarbons (PAH), 9, 10-diphenylanthracene, pyrene, perylene and benzopyrene, were recorded by RSS at a tin oxide OTE in acetonitrile[1,17]. The compounds exhibited EEC behaviour, the post chemical reaction being proton abstraction by the dianion. Considerable variation in the stability of the dianion species was reported[1].

A versatile electrode which is suitable for studies in the ultraviolet, visible and infrared regions is the electroformed gold micromesh. A typical mesh, which consists of a regular array of microscopic holes and contains 1000 wires per inch, has a transparency of approximately 45%. Its electrochemical properties are similar to bulk gold[18]. Although the gold micromesh has been used for spectroelectrochemical experiments under SILD control[19], it is particularly suited to thin-layer studies. Reviews on thin-layer electrochemistry by Reilley[20] and Hubbard and Anson[21,22] refer to spectroscopic applications. The essential feature of the thin-layer cell is that the reactant is confined to a thin solution layer ($\sim 10^{-3}$ cm) next to the electrode so that exhaustive electrolysis can be carried out in a short period of time. The absorption response is then due solely to electrogenerated product and relatively simple spectroelectrochemical equations apply.

* E represents electron transfer. C represents chemical reaction.

The value of the gold micromesh thin-layer cell for spectral monitoring was first demonstrated by Murray[23]: the absorbance and charge were simultaneously recorded during cyclic sweep and potential step oxidation of σ-tolidine. More recently, the gold micromesh thin-layer cell has been used for kinetic studies, the reaction investigated being the hydrolysis of quinone-imine to p-quinone[24]. One important application of the spectroelectrochemical thin-layer technique has been in the study of biochemical reactions: cells utilising gold micromesh[25] and tin oxide[26] working electrodes were used to investigate the electron transfer reactions of redox enzymes.

Although most experiments have been concerned with monitoring the products of the electron transfer and follow-up reactions of organic molecules, a number of inorganic applications have been reported. The molar absorptivities of metals (cadmium, lead, zinc) dissolved in mercury as a result of electrodeposition were determined by monitoring the light attenuation through a mercury-plated platinum OTE[27,28]; the measurement was made at 609nm and no variation in absorbance with wavelength was found. The molar extinction coefficient of titanium (III) at 354nm was evaluated for the current-step reduction of titanium (IV) using the gold micromesh electrode[19]. The results were in good agreement with the true value (ε_{354} = 410) at low current densities where 100% current efficiency was obtained. In an extension of the work, titanium(IV) was regenerated through the oxidation of titanium(III) by hydroxylamine and analysis of the absorbance - time response

enabled the kinetics of the catalytic electrode reaction to be determined[29].

Absorption studies have been performed in flow cells with separated electrochemical and spectroscopic sections. The lifetimes and spectra of the radical anion and cation of 9,10-diphenylanthracene in acetonitrile were recorded by Sioda[30,31] in a flow cell containing a porous platinum wire grid as working electrode. The cell was also employed for recording the visible spectra of the free radical anions of nitrobenzene, p-nitrotoluene and anthraquinone in dimethylformamide[32]. A small-volume flow cell (solution volume 10ml) has also been designed by Mark and Janata[33] for simultaneous polarographic, coulometric and absorption measurement; the electrode reactions of corannulene and 4,5-methylenephenanthrene were investigated.

The combination of spectrophotometry and coulometry has been used directly for analytical purposes. A sensitive coulometer, based on the oxidation of iodide to iodine, was described by Ellis and Baker[34]. Absorption measurements were performed on the bulk solution after a specified period of electrolysis and the number of coulombs passed was calculated from the equation derived by combining Beer's and Faraday's laws. The reported detectability of the coulometer was 1.35×10^{-4}C. Similar bulk solution absorption measurements have been used to indicate the equivalence point in acid-base coulometric titrations[35-37].

Recently, Tyson demonstrated the analytical potential of the spectroelectrochemical experiment controlled by SILD. A long pathlength cell was achieved by arranging for a narrow analysing beam to sample the solution layer in contact with a platinum electrode in a direction parallel to the electrode surface; application to metal ions[3,4] and dyestuffs[4] was reported. Two other workers have used cells of similar design for analytical absorption studies. Sadeghi[6] investigated interference effects with respect to cadmium and also studied a number of anions including iodide, cyanide and iodate while Hogarth[7] performed investigations on cadmium, azo-dyes and hydroquinone.

1.2.3. Internal reflection spectroscopy

Internal reflection spectroscopy (IRS) enables one to monitor processes occurring within the electrode-solution interface and on the electrode surface itself. The IRS cell is designed so that the light beam penetrates the OTE from its outer surface and is critically reflected at the solution boundary. A penetration distance of up to 300nm can be achieved and electrogenerated species in this region cause light attenuation. The IRS technique, therefore, has the capability of monitoring essentially the surface concentration of electrogenerated species in contrast to transmission experiments where the concentration of species in the thickness of the diffusion layer is measured. To improve sensitivity it is possible to arrange for multiple reflections of the light beam. Detailed reviews on the theory, experimental details and

applications have been described elsewhere[1,8,38] so that the subject will only be considered briefly.

The absorbance - time behaviour derived by Kuwana[1] for a species monitored by IRS under SILD control is

$$A_b(t,\lambda) = \varepsilon_b(\lambda)\delta N_{eff} C_a \left(\frac{D_a}{D_b}\right)^{\frac{1}{2}} [1-\exp(x^2 t)\operatorname{erfc}(xt^{\frac{1}{2}})]$$

where δ is the penetration depth, N_{eff} is a sensitivity factor characteristic of the particular OTE, $x = D_b^{\frac{1}{2}}/\delta$ and the remaining terms are defined as previous. At times greater than one millisecond the absorbance reaches a steady state since the diffusion layer expands to regions not sampled by the light beam and the above expression reduces to

$$A_b(\lambda) = \varepsilon_b(\lambda)\,\delta N_{eff} C_a \left(\frac{D_a}{D_b}\right)^{\frac{1}{2}} .$$

Initial IRS studies by Kuwana and co-workers[38] were concerned with demonstrating the technique's ability to monitor the surface concentration of electrogenerated species. The oxidation of σ-tolidine under cyclic sweep, potential step and current step excitations provided absorbance results which agreed with theory. Subsequent work established that the IRS technique was a sensitive monitor of very fast reactions and enabled the rate constants for many homogeneous electron transfer processes to be determined. The reduction of methylviologen, (MeV^{2+}), at a tin oxide OTE in acetonitrile, performed by Kuwana and Winograd[1,39], illustrates this. The compound undergoes two reversible one-electron reductions at Ep_1 = -0.36V vs SCE and Ep_2 = -0.76V vs SCE corresponding

to formation of the species, $MV^{+\bullet}$ and MV^{o}. The free radical cation, $MV^{+\bullet}$, is intensely absorbing with bands at 390nm and 602nm. When the potential was stepped to values more negative than -0.76V an equilibrium was quickly established

$$MV^{2+} + MV^{o} \underset{K_b}{\overset{K_f}{\rightleftharpoons}} 2MV^{+\bullet}$$

through the reproportionation reaction which favoured the $MV^{+\bullet}$ species. Analysis of the absorbance - time curves recorded during excitation enabled the rate constant, K_f, for the homogeneous electron transfer reaction to be calculated.

Studies in the infrared have been concerned with monitoring the formation or removal of typical functional groups such as carbonyl and hydroxyl. The reduction of ninhydrin at gold micromesh in acetonitrile was followed by observing the decrease in the carbonyl stretching vibrations at $1725cm^{-1}$ and $1750cm^{-1}$ [40]. Similar studies with p-benzoquinone, benzil, benzophenone and acetophenone at a germanium OTE in dimethylsulfoxide were also performed[41].

In addition to solution - interface studies, IRS has been used for examining species adsorbed on the electrode surface and also for detecting changes in optical properties of the OTE with potential[2,8].

1.2.4. Fluorescence spectroscopy

There has been little application of fluorescence in spectroelectrochemical studies. A thin-layer cell utilising a thin-film platinum electrode was designed by Kissinger and co-workers[42] for fluorescence monitoring of polycyclic aromatic hydrocarbons. In a typical experiment, the fluorescence decay of rubrene in acetonitrile-40% benzene was monitored during oxidation at 1.0V vs SCE.

1.2.5 Specular reflection spectroscopy

Specular reflection spectroscopy, although primarily employed for studying the formation and optical behaviour of monolayer films on electrode surfaces, has been employed for detecting reactive intermediates and products from electrode reactions. An interesting thin-layer application reported by Kissinger and Reilley[43] concerned studies with 9,10-diphenylanthracene (DPA) and 5,5-diethylbarbituric acid(DBA). Oxidation of DPA in acetonitrile afforded a well-resolved spectrum of the free radical cation, DPA^+ while for DBA the infrared specta recorded before and after reduction indicated the loss of the carbonyl band.

1.2.6. Electrogenerated Chemiluminescence

Luminescence has been observed during the electrolysis of solutions of polycyclic aromatic hydrocarbons and reviews on the subject are available by Hercules[44], Guibault[45] and Bard and Faulkner[46]. The principal mechanisms proposed for emission involve either annihilation or recombination reactions

between electrogenerated anions and/or cations which lead to excited states of the parent hydrocarbon. Analytical studies were first performed by Cruser and Bard[47,48] and later by Pickford and co-workers[49].

1.2.7. Photoelectrochemistry

Photoelectrochemistry is concerned with studying the effect of light irradiation on electrochemical output parameters such as current and potential. It can be considered to be complimentary to the spectroelectrochemical experiment where current and potential are the input signals. A comprehensive review on the subject has been written by Kuwana[50] and various photoeffects undergone by organic systems are discussed. Photopolarographic studios of inorganic species have been reported by Crow[51] and the possibility of using the technique for analysis and structural determinations was mentioned. In more recent work by Perone[52,53], electroanalytical techniques were used to study organic intermediates formed by flash photolysis.

CHAPTER 2 Equipment

2.1. Spectroelectrochemical Instrumentation

2.1.1. Purpose-built instrument

A single-beam ultraviolet-visible spectrometer constructed on the building-block principle was designed to record absorption and fluorescence spectra of electrogenerated species. The instrument, illustrated in plate 1, consisted of the following modular electrochemical and spectroscopic units:

(1) Radiation sources

Deuterium (Cathodeon C70-2V-S) and tungsten lamps were employed in the ultraviolet and visible range respectively for absorption studies. A low pressure mercury source was also used for the range 250nm - 800nm. For fluorescence studies a xenon arc lamp (Hanovia 901C-1,150W) and a low pressure mercury source were utilised. Each light source had its respective power supply.

(2) Cell assembly

The cell assembly consisted of a platform and holder(s) which accomodated the spectroelectrochemical cells (described later).

(3) Electrochemical units

A PAR 174A polarographic analyser (Princeton Applied Research) and a Chemtrix 804 potentiostatic waveform source provided potential step and potential sweep excitations and were generally operated in the three-electrode mode. Cell currents after passage through a standard resistor were

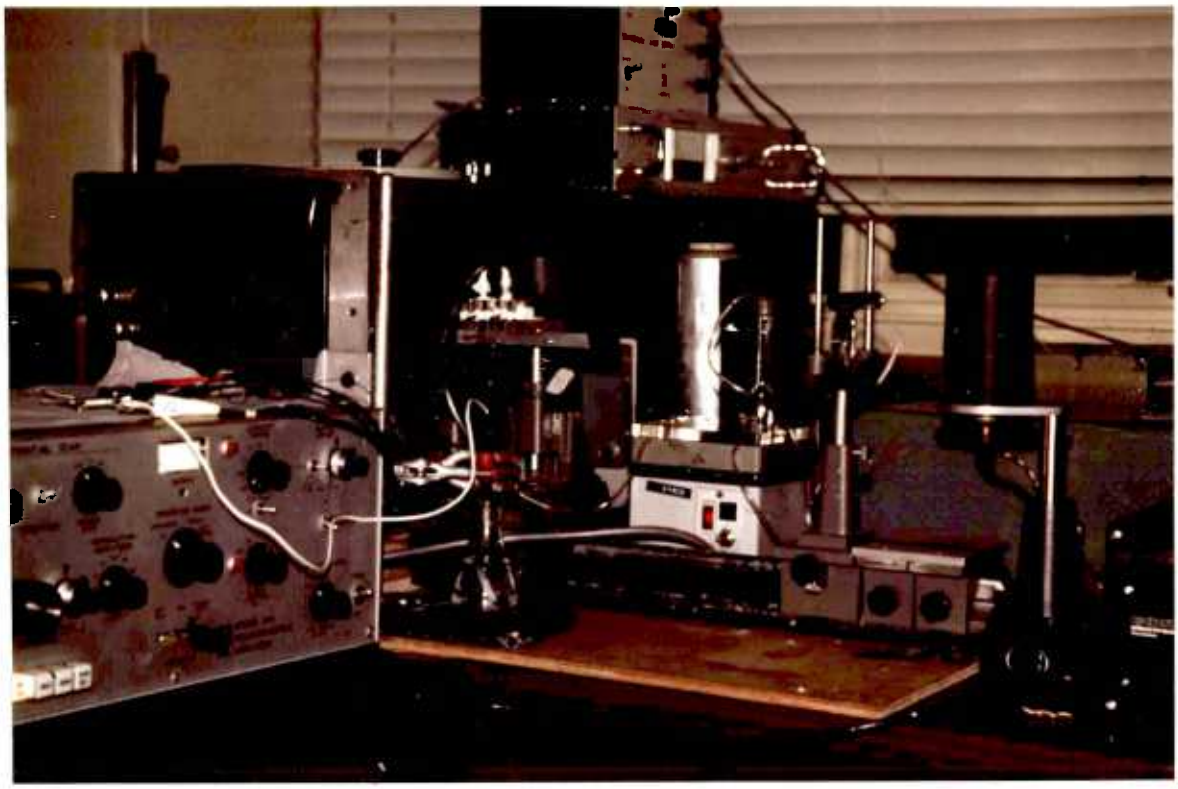

PLATE **1**

PURPOSE-BUILT INSTRUMENT

recorded on a potentiometric recorder (Servoscribe IS) or measured directly with a digital voltmeter (Fenlow type 701). The Chemtrix instrument was also employed as a constant-current source after modification; the appropriate circuit diagram is given in fig 2.1. The constant-current level was selected by adjusting the voltage output control of the source or by varying resistor, Rv. The two-way switch (S) initiated the electrolysis by transferring the current from the fixed dummy resistor (Rd) to the cell. The potential of the working electrode (V vs SCE) versus time was monitored on a Servoscribe recorder.

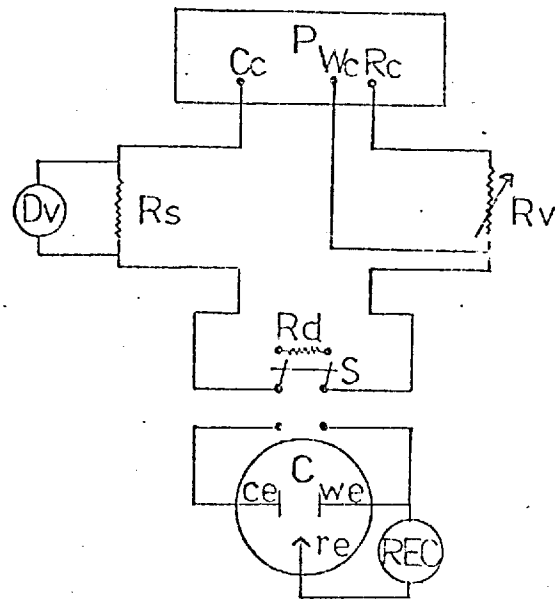

FIG. 2.1. Circuit diagram for constant current experiment.

P, potentiostat (Chemtrix); Cc, counter electrode connection; Wc, working electrode connection; Rc, reference electrode connection; Dv, digital voltmeter; REC, recorder; S, switch; C, spectroelectrochemical cell; ce, counter electrode; we, working electrode; re, reference electrode; Rs = 250Ω Rd = 500Ω Rv = 300Ω

(4) Dispersive systems

The monochromator (Optica CF4) was of the Littrow type and utilised a plane grating ruled at 600 lines per mm. It had a reciprocal linear dispersion of 1.9nm mm^{-1} over the wavelength range 190nm - 1000nm which was graduated in 0.5nm steps. The width of the entrance and exit slits which were coupled could be varied between 0 and 0.6mm in steps of 0.02mm. Interference filters (Baird-Atomic) were used to select a narrow wavelength band for excitation during fluorescence experiments.

(5) Detection system

An end-window photomultiplier tube (EM19592) which had an S-11 response was operated with an EHT supply (Brandenburg 475R). The photo-current was converted to a voltage by passage through a standard resistor (IMΩ) and the signal (% absorption) was displayed directly without amplification on a Servoscribe recorder. A two-channel recorder (Servoscribe 2S) was employed for simultaneous registration of the current and optical signal.

A schematic diagram of the component parts is given in fig 2.2. A peristaltic pump used for sample delivery to flow cells is also included in the diagram.

The cell assembly and light sources were mounted on carriers (Ealing Beck) to an optical bar (Ealing Beck) which was secured to the monochromator. The carriers provided fine horizontal and vertical adjustment so that optimum optical alignment of the spectroelectrochemical cell

with respect to the monochromator entrance slit could be achieved. Vertical/horizontal slits (0.5mm, 1.0mm) situated at either end of the cell holder enabled a narrow analysing beam of radiation to be selected.

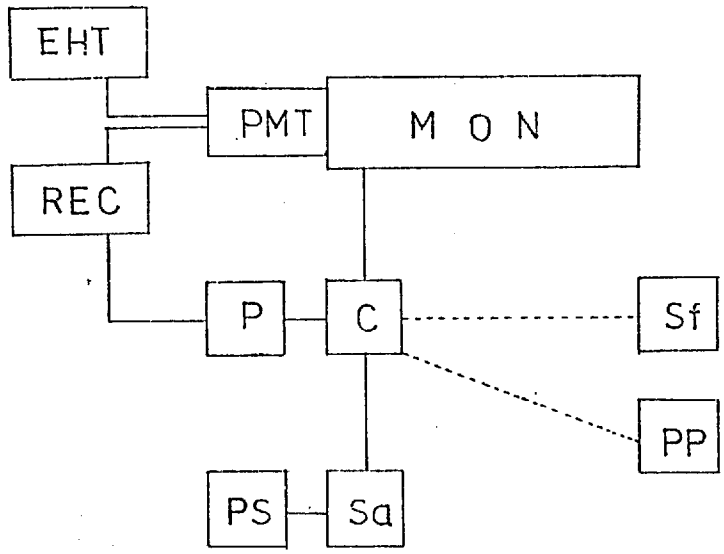

FIG. 2.2. Block diagram of spectroelectrochemical instrumentation.

PS, power supply; Sa, light source (absorption);
Sf, light source (fluorescence); C, cell assembly;
P, potentiostat; MON, monochromator;
PMT, photomultiplier tube; EHT, high voltage supply;
REC, recorder; PP, peristaltic pump.

2.1.2. Modified Farrand instrument

The Farrand spectrofluorimeter in conjunction with the PAR174A was employed for fluorescence studies in preference to the previous instrumentation except in the case of metal ion solutions. This arrangement was more convenient since automatic recording of fluorescence spectra (uncorrected) could be obtained unlike the previous instrumentation where manual measurements had to be performed. The fluorimeter utilised a xenon arc lamp (Hanovia 901C-1, 150W), two modified Czerny-Turner type monochromators (reciprocal linear dispersion 10nm mm^{-1}), an IP28 photomultiplier and a Honeywell potentiometric recorder (Electronik 15). Slits providing a bandpass of 20nm on both monochromators were used unless stated otherwise. To reduce scattered exciting light in frontall illumination measurements, Corning filters, 7-54 (maximum transmission 330nm) and 3-73 (maximum transmission 550nm), were fitted to the excitation and emission monochromators respectively. The spectrofluorimeter containing the gold mesh cell is illustrated in plate 2. Please note that a cell enclosure made from polystyrene and black cotton cloth is omitted from the photograph.

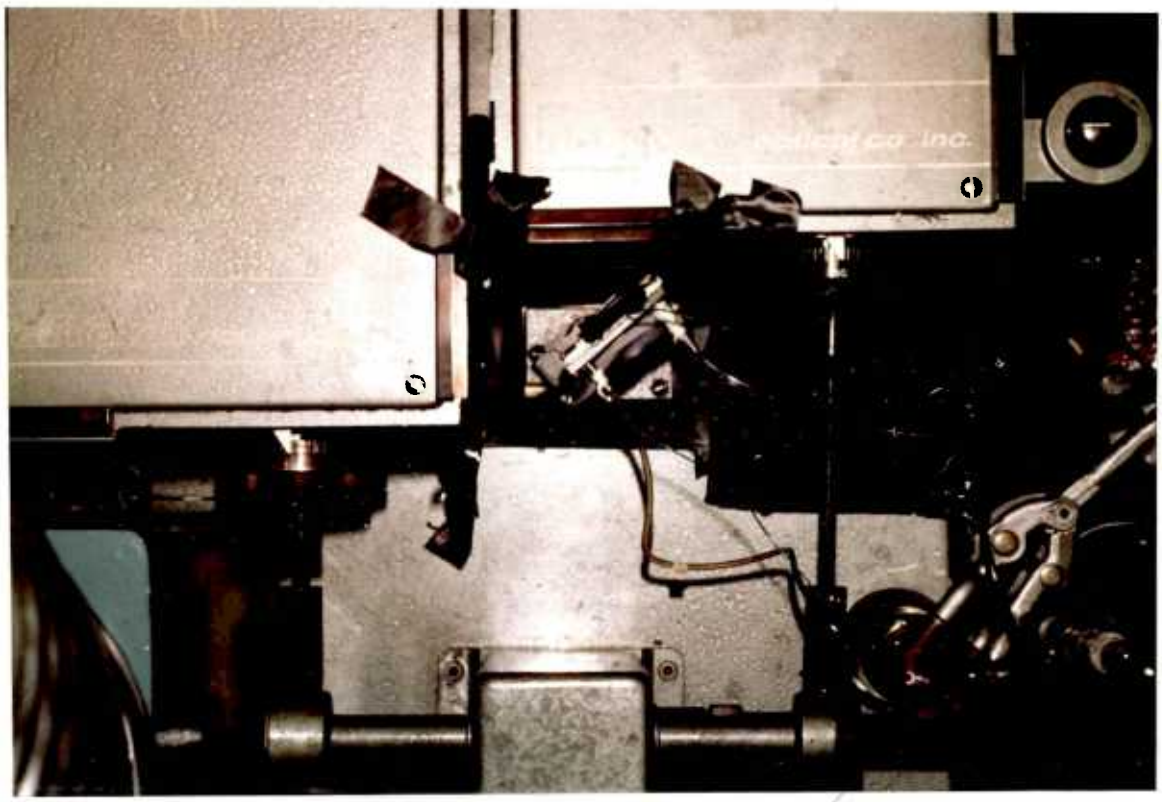

PLATE **2**

GOLD MICROMESH CELL

AND FARRAND INSTRUMENT

2.2. Spectroelectrochemical Cells

2.2.1. General remarks

The spectroelectrochemical cells were based on a standard three-electrode arrangement and which with normal potentiostatic-mode operation the working electrode potential was monitored with respect to the reference electrode while current flowed between the working and counter electrodes. The relative placement of the electrodes was dictated primarily by spectroscopic considerations and in the case of micro-cells a non-uniform potential distribution over the electrode surface and consequently an unequal current distribution would result. This feature was only significant for non-aqueous studies.

The absorption cells were designed so that a narrow light beam traversed the entire length of and parallel to the working electrode surface and optical pathlengths of magnitude similar to that encountered in solution spectrophotometry were realised. The thickness of the light beam varied, but was generally less than 1mm. The electrode areas were necessarily large and in the case of the micro absorption and fluorescence cells the ratio of electrode area to cell volume was high so that exhaustive electrolysis could be achieved in a short period of time. This enabled measurements to be recorded without possible spectral interference from the reactant and was particularly important for fluorescence work. The fluorescence cells were also of relatively short

pathlength and this was desirable for preventing inner filter effects.

The counter electrode placement in the various cells did not obstruct the light beam and was either located in a region far-removed from the working electrode or was separated from the test solution to prevent unwanted products from interfering. The reference electrode similarly did not obstruct the light beam and was positioned as close to the working electrode as possible subject to cell design.

2.2.2. Absorption cells

(1) Silica cuvette containing platinum electrode unit

Absorption studies in quiescent solution were performed with a standard silica cuvette (pathlength 20mm) which contained a platinum electrode unit. The unit which was machined from tufnol consisted of a pair of platinum plate electrodes (dimensions 5mm x 15mm) cemented to tufnol brackets which were attached to a cell cap. Platinum wire spot-welded to the electrodes led to the cap terminal for electrical connection. The wire was coated with epoxy resin (araldite) to ensure electrolysis occurred only at the monitoring region. Small holes were machined in the cap to enable sample introduction (by syringe) and withdrawal (narrow-bore tube connected to water pump) and also degassing; solution volumes were approximately 5ml. A fritted glass tube (diameter 2mm), positioned close to the working electrode, was connected to a reference electrode (SCE) via a salt bridge. A schematic

diagram of the electrode unit is given in fig. 2. 3.

A minor modification of the unit enabled fluorescence measurements to be performed. Instead of two parallel electrodes, the counter electrode was replaced by a small platinum wire so that it was possible to collect radiation at right angles to the direction of the exciting light beam. This arrangement is also shown in fig. 2.3.

FIG. 2.3. Platinum electrode unit.

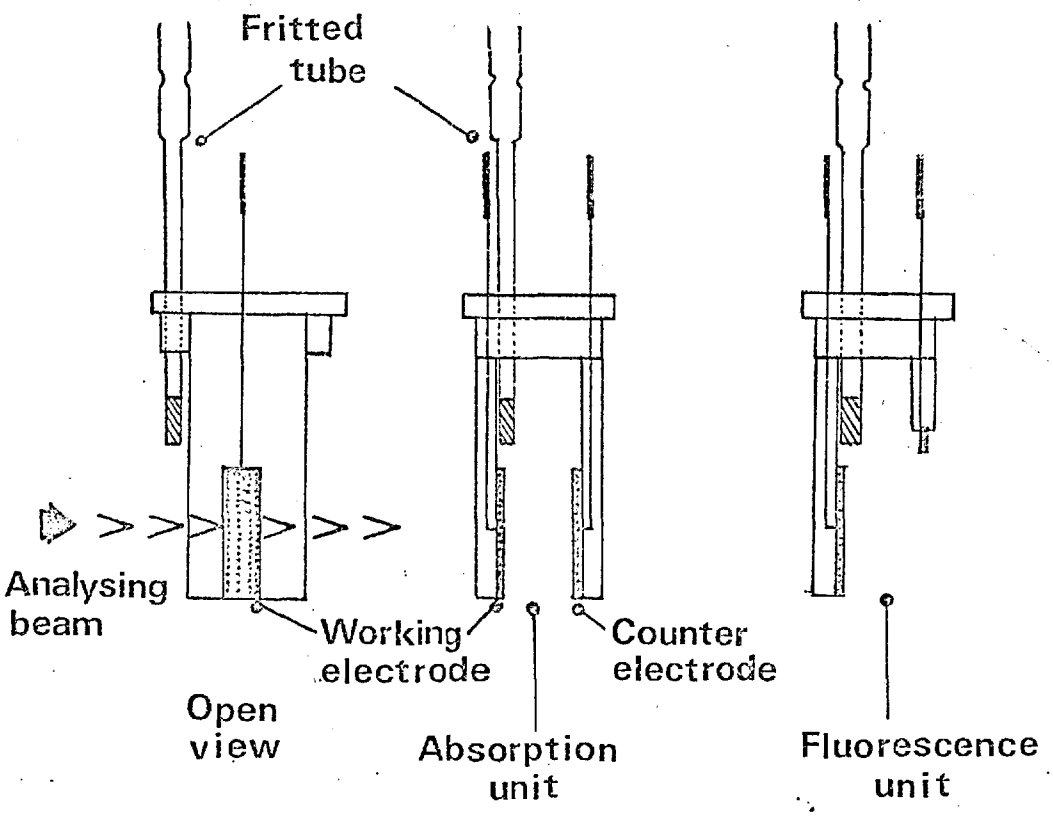

(2) Carbon fibre flow cell

Two micro-flow cells incorporating carbon fibres as the working electrode were designed for monitoring in flowing solutions. The design was based on the carbon fibre flow cell of Das Gupta[54]. The cells, the main features of which are illustrated in fig. 2.4, were machined from perspex block and could be readily dismantled. The internal cell volumes were approximately 300μl and 70μl with respective pathlengths of 50mm and 20mm. For assembly, a packed bed of carbon fibres (Courtaulds Ltd) was attached to double-sided sticky tape and placed in the recessed channel of the lower block. Electrical connection to the electrode was obtained by placing further fibres secured to brass strip along the connecting channels at right angles. Additional tape then covered the connecting channels and the cell was assembled. Screw-in quartz windows were situated at either end of the cell enabling a narrow analysing beam to traverse the entire length of the carbon fibre surface.

Sample solution was delivered by a single-channel peristaltic pump (Varioperpex, LKB Produckter) and tubing (Technicon 116-05 22-11). Platinum tube (internal diameter 1mm) situated at the outflow was employed as the counter electrode while the reference electrode (SCE) was placed downstream in the waste reservoir. The system is identical to that described for the gold micromesh cell illustrated in fig. 2.5.

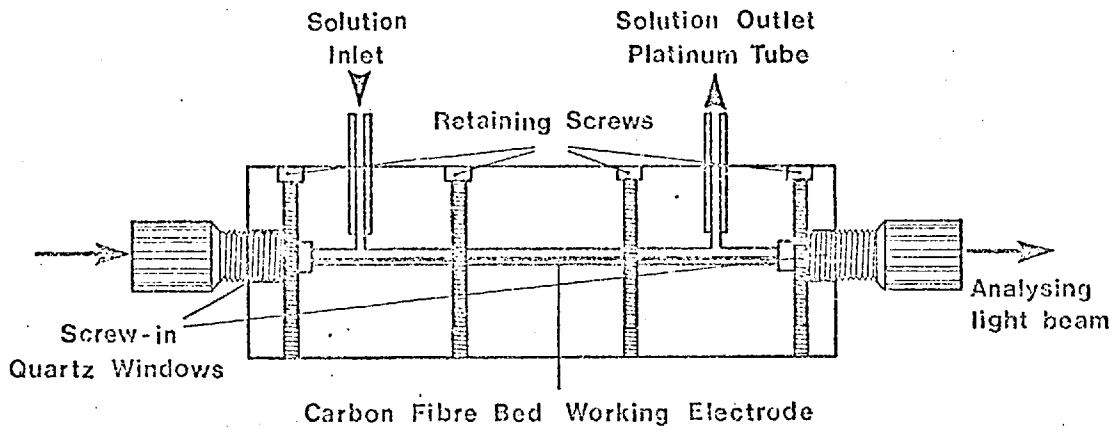

SIDE VIEW

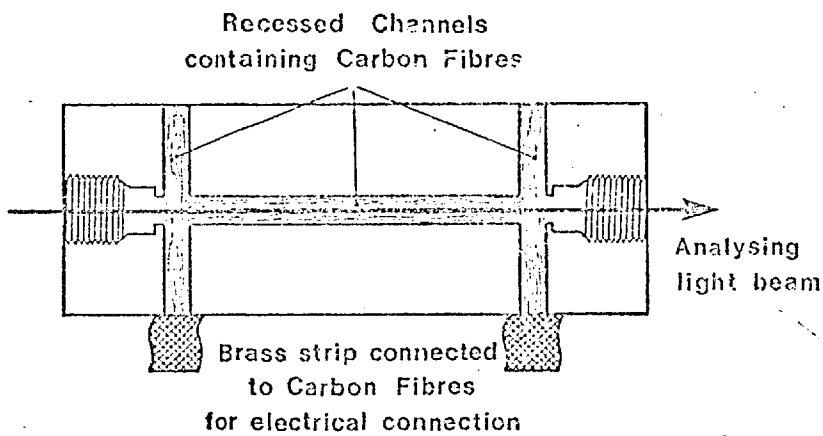

TOP VIEW

FIG. 2.4. Carbon fibre flow cell

2.2.3. Fluorescence cells

(1) Gold micromesh cell

A piece of transparent (45% transmission) gold micromesh (1000 lines per inch; Buckbee Mears Ltd) was inserted between the two halves of a standard micro-flow cell (Hellma Ltd; cell no. 136 in suprasil; pathlength 0.5mm) and the unit made leakproof by sealing with silicone rubber adhesive (Devcon). The cell volume was approximately 120μl. Electrical connection to the gold mesh was made with thin brass strip which was permanently attached to the cell. It is stressed that the mesh was extremely fragile and care must be exercised when handling. Platinum tube (internal diameter 1mm) sealed to the cell outlet served as the counter electrode. Sample was fed to the cell with peristaltic pump and tubing as previous. A saturated calomel electrode (SCE) placed in the downstream reservoir completed the three-electrode cell. The cell was mounted on a holder (Ealing Beck) and positioned in the Farrand spectrofluorimeter for frontal illumination studies (quiescent solution), being placed at an angle of approximately 30 degrees to the exciting beam. The penetration depth of the existing light was just less than 0.5mm. A schematic diagram of the cell and associated equipment is shown in fig. 2.5.

(2) Quartz cell containing platinum wire unit

The cell for fluorescence studies in non-aqueous media consisted of a three-electrode unit which fitted a circular quartz cell with a vacuum-tight seal. This is shown

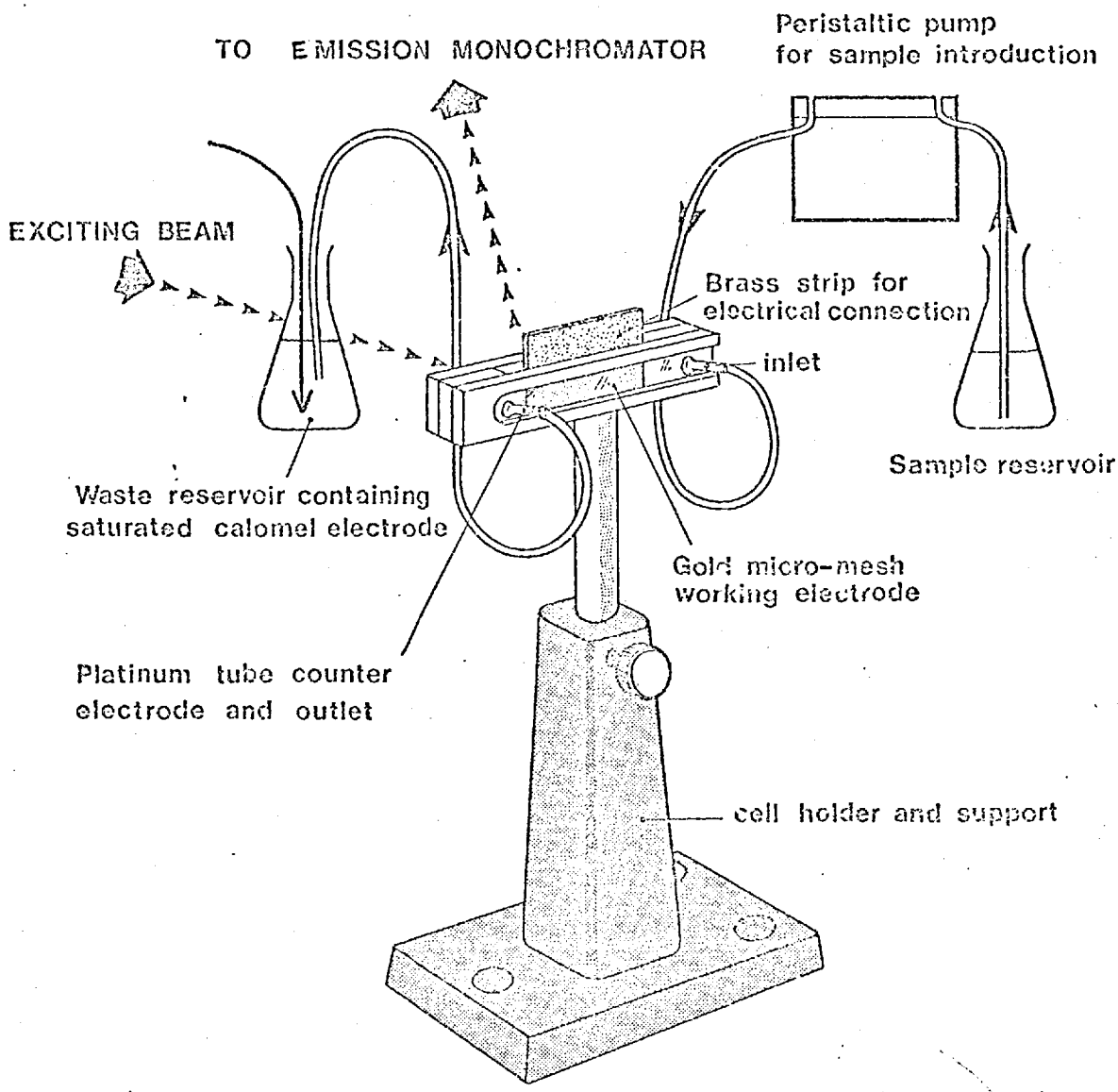

FIG. 2.5. Gold micromesh cell and associated equipment

in fig. 2.6. Various cells were made by fusing together two sizes of quartz tubing and sealing at the narrow end. The tubing diameters at the narrow end (viewing area) were 1mm, 2mm and 3mm while that of the main body was 10mm. The cell cap contained a silicone rubber septum (Hamilton 75807 diameter 12mm) through which the electrodes were introduced. Platinum wire (length 27mm; diameter 0.8mm) sealed in soft glass served as the working electrode while the counter electrode (platinum wire) and the reference electrode (silver/silver ion) were contained in fritted tubes with the appropriate electrolyte solution. The assembly was accommodated in the standard Farrand cell holder for right-angled fluorescence measurements. Sample introduction and removal was achieved using a Hamilton gas-tight syringe (1005LLCH) with extended needle. High-purity argon (99.999%) was employed for degassing and for maintaining an inert atmosphere; the gas was presaturated (acetonitrile with molecular sieve 3A) and dried (column of molecular sieve 5A) before introduction to the cell.

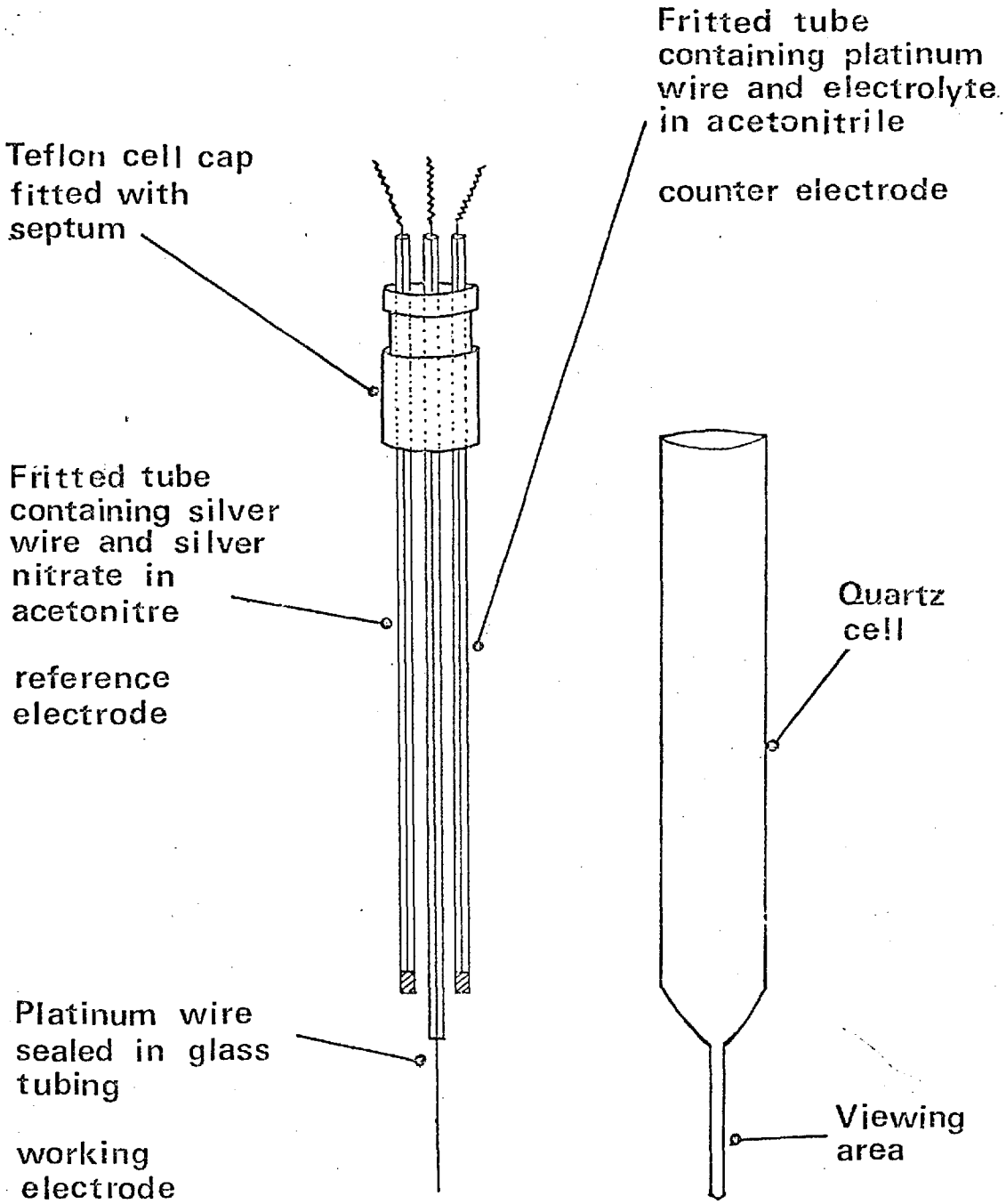

FIG. 2.6. Quartz cell and platinum electrode unit

2.3. Miscellaneous Equipment

The ultraviolet-visible spectra of standard solutions were recorded with the Unicam SP 800 spectrometer.

The PAR 174A or the Chemtrix 804 instrument was used in conjunction with a Metrohm cell (EA875-20) and the two-channel Servoscribe recorder for obtaining current - potential curves.

CHAPTER 3 Studies with Metal Ions

3.1. Introduction

The immediate aim of research was to develop a selective analytical technique for trace metals in solution based on measuring the absorption and fluorescence of "hydrated metal atoms" generated at an inert electrode surface. Previous experiments by Tyson[3,4] had indicated that the monitoring of absorption changes at the cathode surface during diffusion-controlled electrolysis of dilute metal ions had analytical potential; many metal ions including cadmium(II), cobalt(II), chromium(III), copper(II), iron(II), iron(III), nickel(II), lead(II), zinc(II) were shown to exhibit sensitive absorption in the ultraviolet. The absorption depended on a number of experimental parameters and typical absorbance - voltage, spectral distribution and calibration curves are presented in fig 3.1. for zinc. The identity of the absorbing species had not been established, but because of the resemblance between the absorbance - voltage curve and a polarographic wave it was thought that reduction of the cation was required. It was suggested that hydrated metal atoms were responsible for absorption and also that hydrated electrons were involved in the reduction mechanism. The similarity in the wavelength maxima of the electrogenerated species and the corresponding gas phase resonance line of the atomic species supported the proposal.

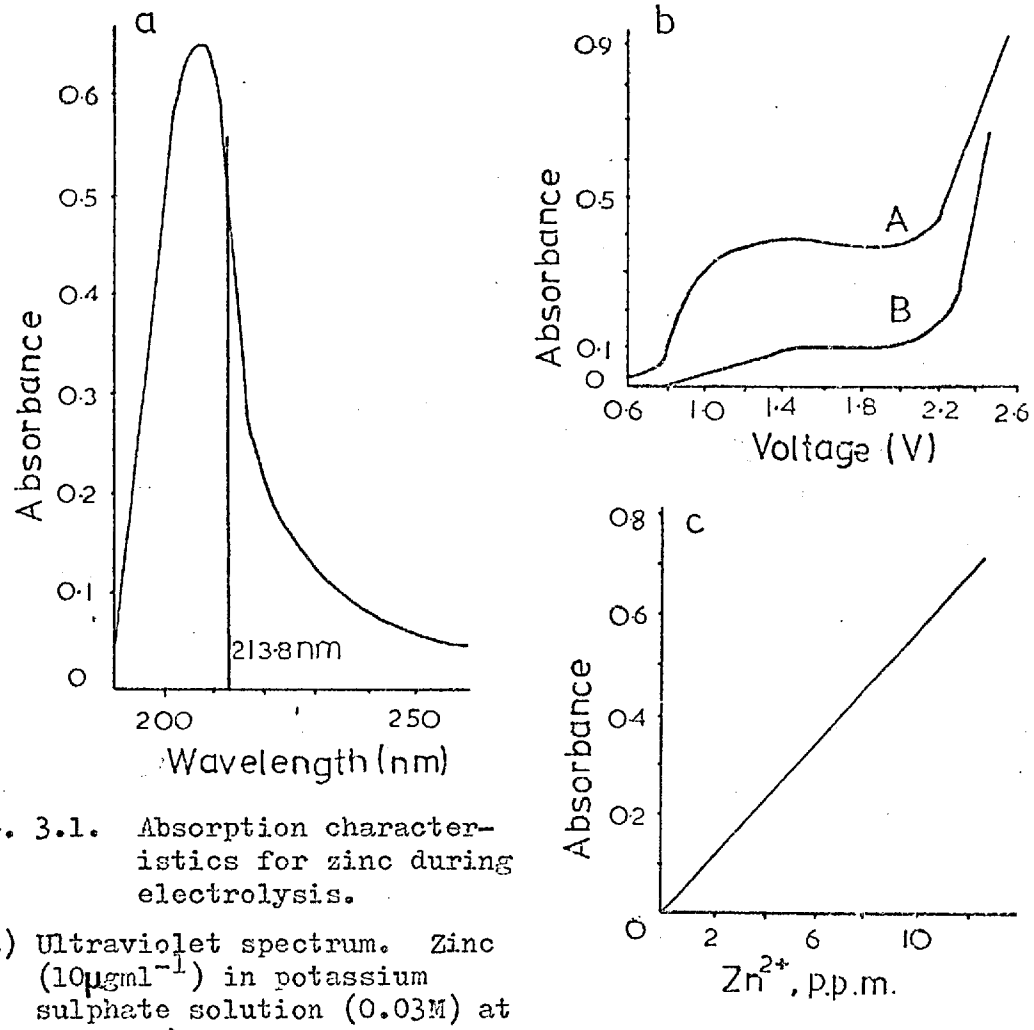

FIG. 3.1. Absorption characteristics for zinc during electrolysis.

(a) Ultraviolet spectrum. Zinc ($10\mu g ml^{-1}$) in potassium sulphate solution (0.03M) at -1.4V; λmax 207nm; the position of the zinc gas-phase resonance line at 213.8nm is indicated.

(b) Voltage dependence of absorption signal at 207nm.

(A) Zinc ($10\mu g ml^{-1}$) in potassium sulphate solution (0.03M);

(B) Potassium sulphate solution (0.03M) only.

(c) Calibration graph for zinc in potassium sulphate solution (0.03M) at 207nm; applied voltage -1.4V. (Reproduced from Ref. 5.)

Initial studies were directed at investigating the possibility of obtaining a fluorescence signal by sufficiently exciting these species generated at the cathode, but it soon became apparent that the experimental results did not fit the hydrated atom theory. Instead the formation of precipitated metal hydroxides particles at the cathode were thought to be

responsible for the absorption and apparent fluorescence behaviour. Further detailed experiments subsequently confirmed this and provided an insight into the electrode reaction mechanism.

The identity of the absorbing species, particularly in experiments with cadmium, was also considered by Tyson[4], Sadeghi[6] and Hogarth[7].

3.2. Preliminary Studies

Cadmium(II) was thought suitable for investigation since previous studies by Tyson[4] showed that it exhibited sensitive and well-defined absorption behaviour during electrolysis; the spectrum with an absorption maximum centred around approximately 220nm is given in fig 3.2. An intense absorption band with maximum absorption at 200nm was also reported during electrolysis of the blank solution. (potassium sulphate (0.03M)). The standard silica cuvette and the platinum electrode unit illustrated in fig 2.3. were employed in this work; the unit was initially operated in the two-electrode mode.

3.2.1. Experimental procedure

(1) Instrumental alignment

The instrument was set up so that the maximum amount of light entered the monochromator entrance slit; this was achieved by fine horizontal and vertical adjustment of the deuterium light source. At this stage the light beam was passing through the cuvette unobstructed. The cell platform was then horizontally adjusted until the tufnol bracket just interrupted the light beam to achieve grazing incidence at the electrode. Sample solution was injected into the cell and the detector gain adjusted so that 100% transmission (0% absorption) was registered on the chart recorder. 0% transmission (100% absorption) achieved by obstructing the light beam represented the situation when no source radiation entered the monochromator entrance slit.

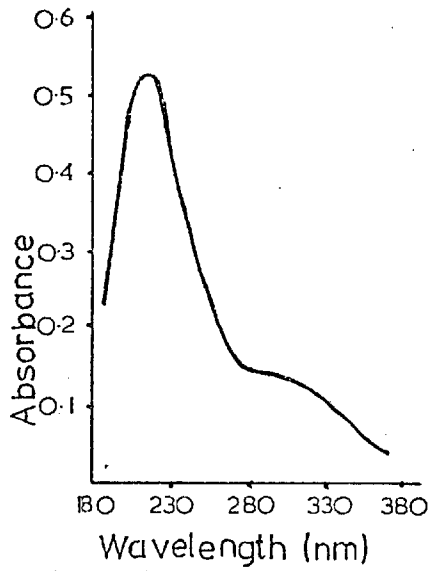

FIG. 3.2. Ultraviolet spectrum for cadmium during electrolysis. Cadmium ($10\mu gml^{-1}$) in potassium sulphate solution (0.03M); applied voltage -2.0V.

(Reproduced from Ref. 4.)

(2) Solution preparation

The appropriate amount of cadmium sulphate (Analar grade) was dissolved in distilled water (100ml) to give stock solutions (typically $1\%wv^{-1}$ or 0.01M with respect to cadmium). Standard solutions containing potassium sulphate (0.03M) as background electrolyte were prepared by dilution of the stock solution.

(3) Method for generating signal

The procedure developed by Tyson[3,4] to generate absorption signals consisted of applying, to a degassed solution, a step voltage (typically -2V) to the monitoring electrode which had previously been anodically pretreated at +5V. The high anodic pretreatment was found to be unnecessary and inconvenient. Instead a repetitive cycling procedure, -2V to +2V to -2V···, on a non-degassed sample gave reproducible signals indefinitely. The absorption - time profile for cadmium solution ($30\mu gml^{-1}$) during polarity reversal is given

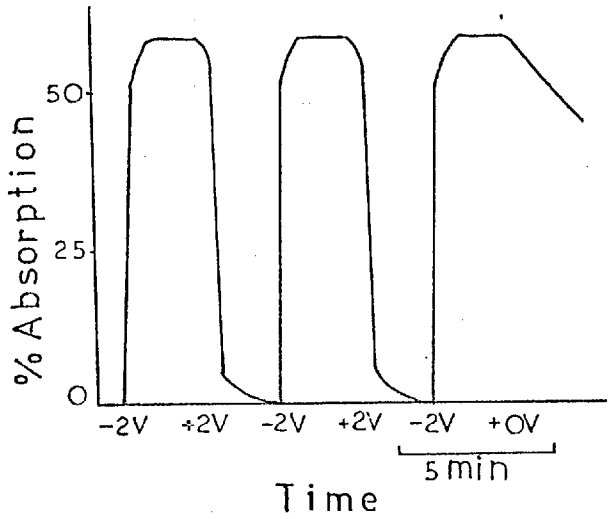

FIG. 3.3.
Absorption - time response for the cadmium species during changes in electrode polarity. Cadmium ($30\mu gml^{-1}$) in potassium sulphate solution (0.03M); monitoring wavelength 220nm.

in fig 3.3; the period for a complete cycle was 5 minutes. It can be seen that generation and removal of the absorbing species was achieved in a regular manner simply by reversing the electrode polarity. It was also noted that stepping the voltage from -2V to OV caused a slower absorption decay in contrast to the -2V to +2V step.

3.2.2. Effect of dissolved oxygen

The absorption - time behaviour for electrolysis (-2V to +2V) of cadmium solution ($30\mu gml^{-1}$) was recorded for (1) a non-degassed solution and (2) a degassed solution; the response curves are shown in fig 3.4. The rate of absorption development was quicker for the degassed solution, but more apparent was the behaviour when the electrode polarity was reversed to +2V. In contrast to the degassed solution whose absorption decay was slow, rapid decay for the non-degassed solution was observed. This experiment demonstrated that the chemistry/electrochemistry of oxygen played an important role in the formation and stability of the absorbing species.

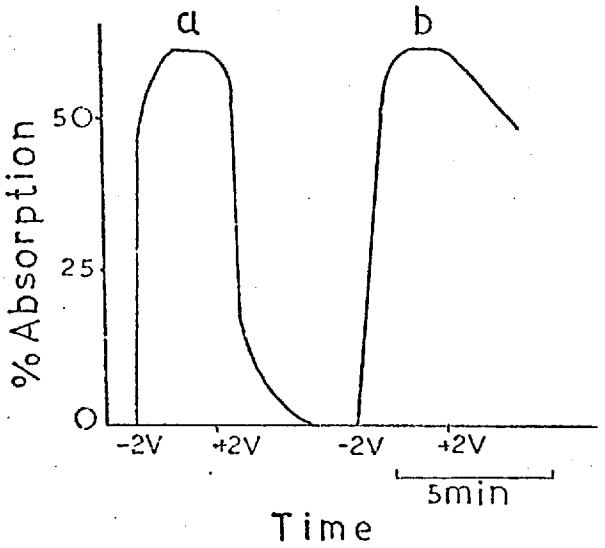

FIG. 3.4.
Effect of dissolved oxygen on the cadmium absorption response during electrolysis:
(a) non-degassed solution
(b) degassed solution (5min).
Cadmium ($30\mu gml^{-1}$) in potassium sulphate solution (0.03M); monitoring wavelength 220nm.

3.2.3. Light beam width and position with respect to the electrode

Experiments were performed in which the light beam did not graze the electrode, but instead sampled solution at distances up to approximately 0.5mm from the cathode. The result of the study is shown in fig 3.5. Progressively slower signal development occurred as the separation distance between the analysing light beam and the electrode surface increased; a constant absorption level was also not reached in the measurement time. For the corresponding degassed solutions, the signal response although still delayed was considerably quicker; this rate increase is consistent with the previous results obtained at grazing incidence.

Experiments also revealed that the narrower the light beam at the cathode surface, the quicker was the signal response and the shorter was the time to reach the absorption maximum.

The absorption responses for both experiments were consistent with stable species being generated, diffusing away from the electrode surface, and filling up a light beam of

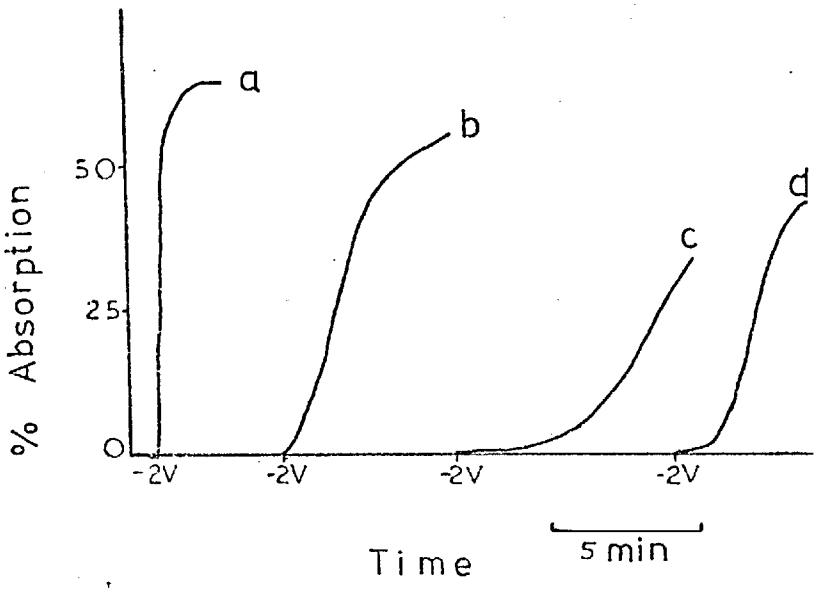

FIG. 3.5. Absorption - time response for the cadmium species when light beam samples solution at distances from the electrode surface: (a) grazing incidence (b) 0.2mm (c) 0.5mm (d) 0.5mm; solution first degassed. Cadmium ($30\mu gml^{-1}$) in potassium sulphate solution (0.03M); monitoring wavelength 220nm.

finite width. This behaviour was not consistent with the formation of highly reactive hydrated cadmium atoms.

3.2.4. Fluorescence experiments

The absorption maximum for the cadmium species is at approximately 220nm and excitation energy in the far-ultraviolet was, therefore, required to induce fluorescence. Unfortunately, the output energy of the xenon lamp in this region is relatively low so that interference filters were initially omitted from the excitation beam to ensure the maximum energy irradiated the electrode - solution layer.

Using the modified electrode unit depicted in fig 2.3, an apparent fluorescence signal (λmax 270nm) was recorded during the electrolysis (-2V) of cadmium solution ($30\mu gml^{-1}$). No signal was recorded for the blank solution. The results of

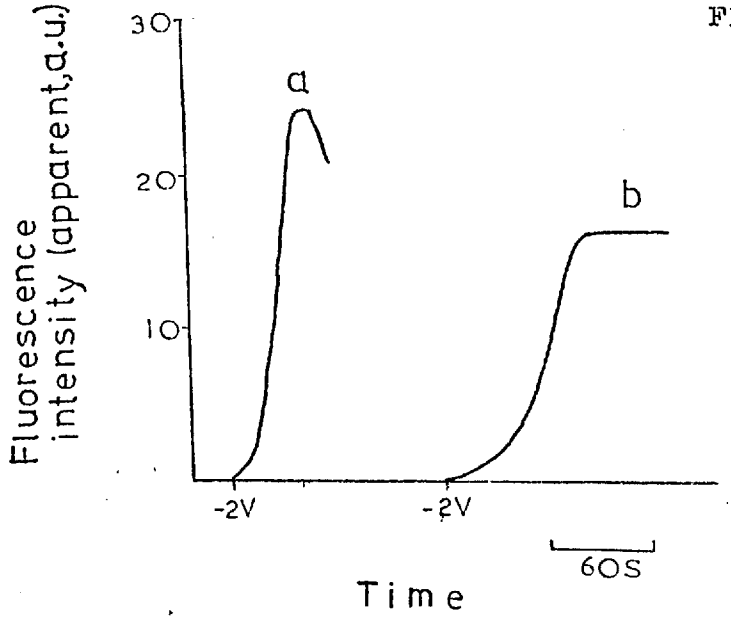

FIG. 3.6. Effect of dissolved oxygen on the apparent fluorescence signal for the cadmium species during electrolysis (-2V):
(a) degassed solution (5min).
(b) non-degassed solution.
Cadmium ($30\mu gml^{-1}$) in potassium sulphate solution (0.03M); monitoring wavelength 270nm; a.u., arbitrary units.

these preliminary studies were reported in the literature[5].

(1) Effect of dissolved oxygen

A marked difference in signal form occurred if the solution was not degassed. The signal response for the degassed cadmium solution ($30\mu gml^{-1}$) was fast and reached a maximum after approximately 40s and then decayed. The non-degassed solution gave a weaker, but permanent signal. The response curves are given in fig 3.6 and it can be seen that the influence of dissolved oxygen on the rate of signal development was similar to previous absorption results.

(2) Calibration

The apparent fluorescence signal was recorded for various concentrations of cadmium solutions ($1 - 500\mu gml^{-1}$) and the calibration curve which is presented in fig 3.7 illustrated the dependence of the signal on the cadmium ion concentration. The graph was linear in the range $1 - 50\mu gml^{-1}$, approximately constant between 50 and $100\mu gml^{-1}$, but then

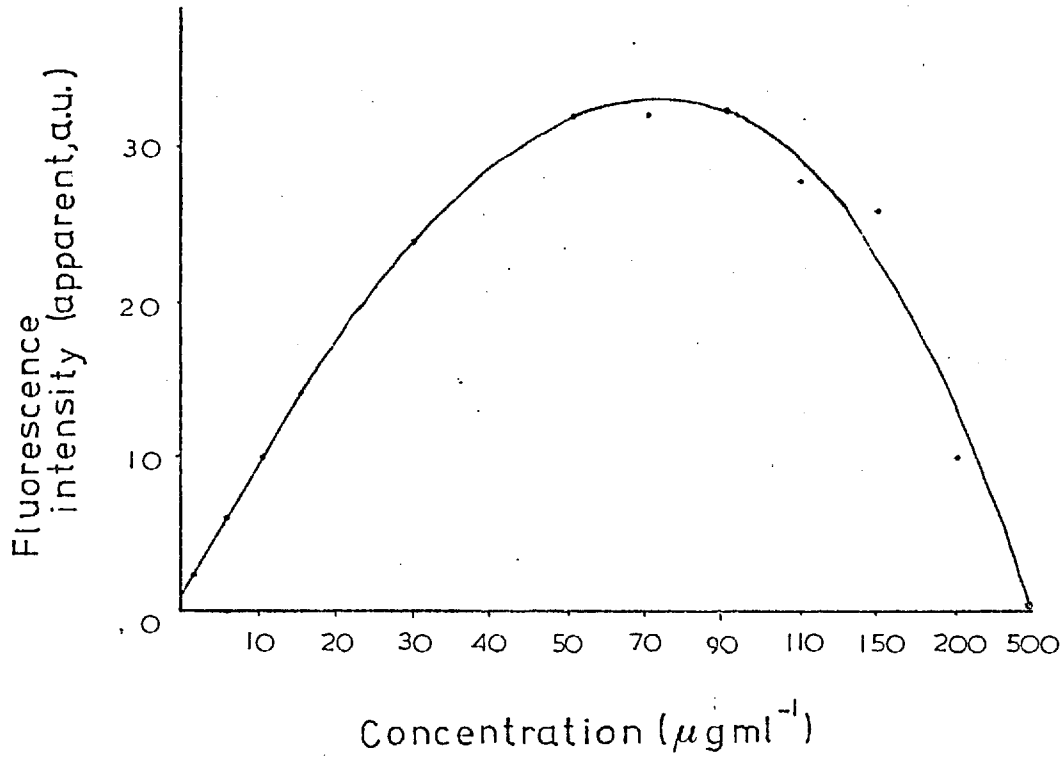

FIG. 3.7. Fluorescence (apparent) calibration curve for the cadmium species during electrolysis (-2V). Monitoring wavelength 270nm; solution degassed (5 minutes).

decreased quite sharply at higher concentrations. This behaviour was typical of fluorescence calibration curves where the phenomena of self-absorption becomes significant at higher concentrations.

(3) Spectral distribution of signal

Inspection of the cadmium absorption spectrum given in fig 3.2 would indicate that only exciting wavelengths less than approximately 380nm would be successful in inducing fluorescence since at longer wavelengths little or no absorption occurs. To investigate this, the wavelength dependence of the signal on the excitation energy was studied; this was achieved by inserting interference filters between the light source and sample cell. The results are presented for irradiation by (1) a xenon arc lamp and (2) a low pressure mercury lamp.

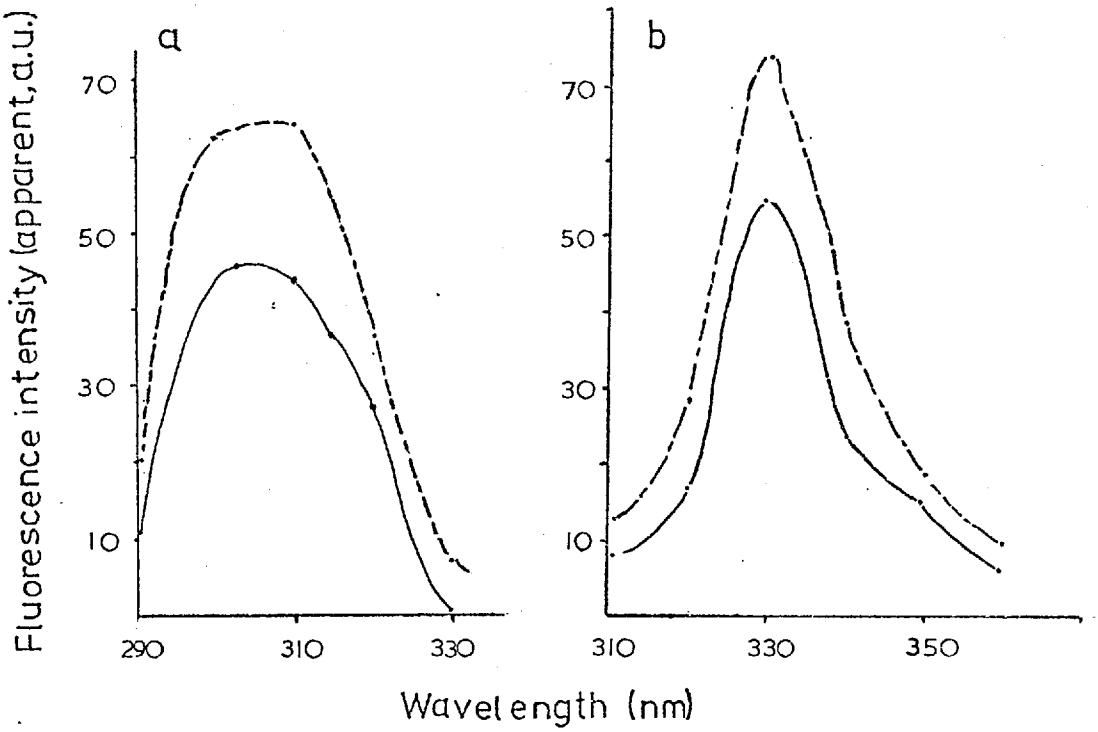

FIG. 3.8. Fluorescence signal (apparent) versus wavelength (nm) during electrolysis of cadmium ($40\mu gml^{-1}$):
(a) 300nm interference filter
(b) 325nm interference filter
(c) 375nm interference filter.

Solid line, +2V on monitoring electrode; broken line, -2V on monitoring electrode; xenon arc lamp as light source.

(1) Xenon arc lamp.

The signal intensity as a function of wavelength was recorded for cadmium solution ($40\mu gml^{-1}$) during electrolysis (+2V to -2V) with excitation at (1) 300nm, (2) 325nm and (3) 375nm.

Although strong signals were obtained for each exciting waveband, the spectra which are illustrated in fig 3.8 consisted essentially of a recording of the bandpass of the interference filter. Since no signal was recorded at wavelengths outside the bandpass of the filters, particularly at longer wavelengths, the results strongly suggested scatter of the incident radiation.

(2) Low-pressure mercury lamp. This type of source, unlike the xenon arc lamp (strong continuum emission), emits strong lines in the ultraviolet and visible which are superimposed on a weak continuum. Scatter signals should only be recorded at the wavelengths of the emitting mercury lines and this method should decide unequivocally that the signal was due to scattered radiation. The appropriate interference filter was used to select the principal mercury lines at 253nm, 312nm, 366nm and 546nm and the measuring procedure of the previous experiment was repeated. The spectral distribution of the signals was essentially a recording of the source output and consisted of strong signals at the main mercury lines with much reduced signals at other wavelengths; these findings are shown in fig 3.9 and confirm the scattering proposal of the previous study.

Concluding this section, the results indicate that scattering species were formed near the cathode during the electrolysis (+2V to -2V) of dilute cadmium solutions giving rise to an apparent fluorescence signal. The previously

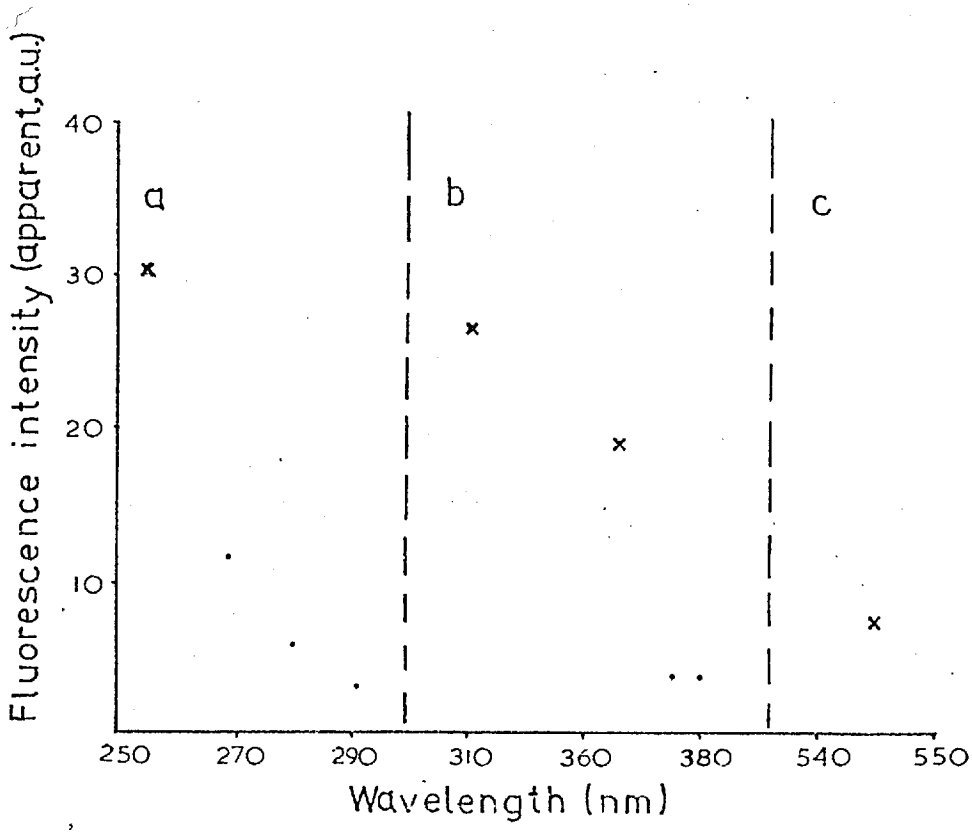

FIG. 3.9. Fluorescence signal (apparent) versus wavelength (nm) during electrolysis (-2V) of cadmium ($40\mu gml^{-1}$): (a) 250nm interference filter (b) 375nm interference filter (c) 525nm interference filter. Starred points correspond to main mercury lines (253nm, 312nm, 366nm, 546nm); low-pressure mercury lamp as light source; dots correspond to measurements at arbitrary wavelengths.

reported cadmium signals[5] were, therefore, incorrectly assigned as fluorescence.

3.2.5. Absorption spectrum of the electrogenerated cadmium species

Since scatter signals were unexpectedly obtained in the visible region, the possibility of absorption in this region was also investigated. Due to the high intensity of the mercury lamp a rather narrow light beam was selected to sample the electrode - solution layer. The absorption signal

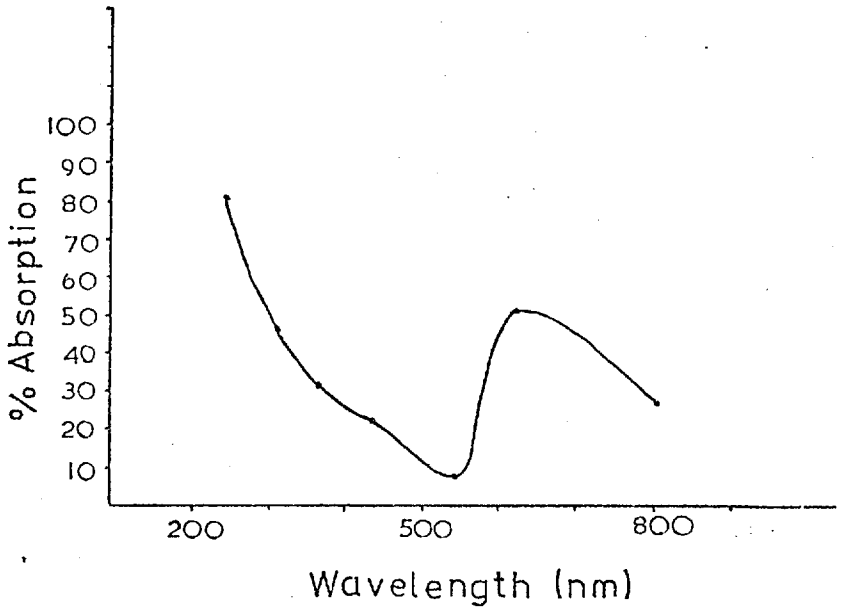

FIG. 3.10. Absorption spectra for the cadmium species during electrolysis (-2V). Cadmium (50μgml^{-1}) in potassium sulphate solution (0.03M).

was obtained for cadmium solution (50μgml^{-1}) using a +2V to -2V cycle at wavelengths corresponding to the principal mercury lines. The spectral distribution shown in fig 3.10 revealed absorption in the ultraviolet, but also an unexpected absorption band in the visible region centred around 626nm.

3.2.6. Visual examination of the cathode-solution layer

After a short period of electrolysis, a layer of particles was noted to form near the cathode for cadmium solution (50μgml^{-1}); the layer was only visible under illumination from the xenon arc lamp. Further, reversal of electrode polarity (-2V to +2V) caused the dissolution of the particles. At this stage, it was thought that the particles were precipitated cadmium hydroxide and that their production and removal was due to pH changes occurring at the monitoring electrode - alkalinity at the cathode (-2V) acidity at the anode (+2V). This proposal explained qualitatively

the signal - time behaviour for both the absorption and fluorescence experiments during the -2V to +2V cycle and suggested that the same precipitated particles were responsible for both signals.

3.2.7. Absorption response in acidic solutions

If the cadmium hydroxide theory is correct then a reduced absorption signal would be expected in acidic solutions due to the neutralisation of hydroxide and the increased solubility of the cadmium hydroxide particles. Cadmium solutions ($50\mu gml^{-1}$) were prepar containing potassium sulphate (0.03M) and various concentrations of sulphuric acid (0.01M - 0.1M H_2SO_4). The absorption results at 220nm for a +2V to -2V electrolysis cycle are presented in table 3.1.

Table 3.1. The effect of sulphuric acid concentration on the absorption signal (220nm) of the cadmium species during electrolysis (-2V).

Sulphuric acid concentration (M)	0	0.01	0.05	0.1
% Absorption	82	25	15	12

Solution, cadmium ($50\mu gml^{-1}$) in potassium sulphate (0.03M).

The downward trend of absorption with increasing acid concentration suggested that there was a progressive removal of hydroxide and consequently less cadmium hydroxide was precipitated. Although significant absorption was still recorded for sulphuric acid solutions (0.05M, 0.1M), the signals were temporary and lasted approximately 5s from the start of

electrolysis; this indicated rapid dissolution of the precipitate. A similar experiment was performed for electrolysis of potassium sulphate solution (0.03M) and the absorption results for wavelength monitoring at 210nm are given in table 3.2.

Table 3.2. The effect of sulphuric acid concentration on the absorption signal (210nm) for the blank solution during electrolysis (-2V).

Sulphuric acid concentration (M)	0	0.01	0.05	0.1
% Absorption	62	52	27	17

A gradual reduction in absorption occurred on going to higher acid concentrations indicating a progressive removal of hydroxide. Only temporary signals were recorded in sulphuric acid solutions (0.05M and 0.1M) as before, but nevertheless highly alkaline layers next to the cathode were momentarily produced.

3.2.8. Absorption spectra of (1) the species generated for the blank solution and (2) sodium hydroxide solution

The spectral distribution of the absorption signal was obtained during the electrolysis (-2V) of potassium sulphate solution (0.03M). The spectrum of sodium hydroxide (0.005M) was also recorded on the same instrument and it can be seen from fig 3.11 that the two spectra are identical. A rough value of the pH near the cathode was obtained, assuming hydroxide absorption obeys Beer's law. Direct comparison of the respective absorbance values at 200nm and also taking

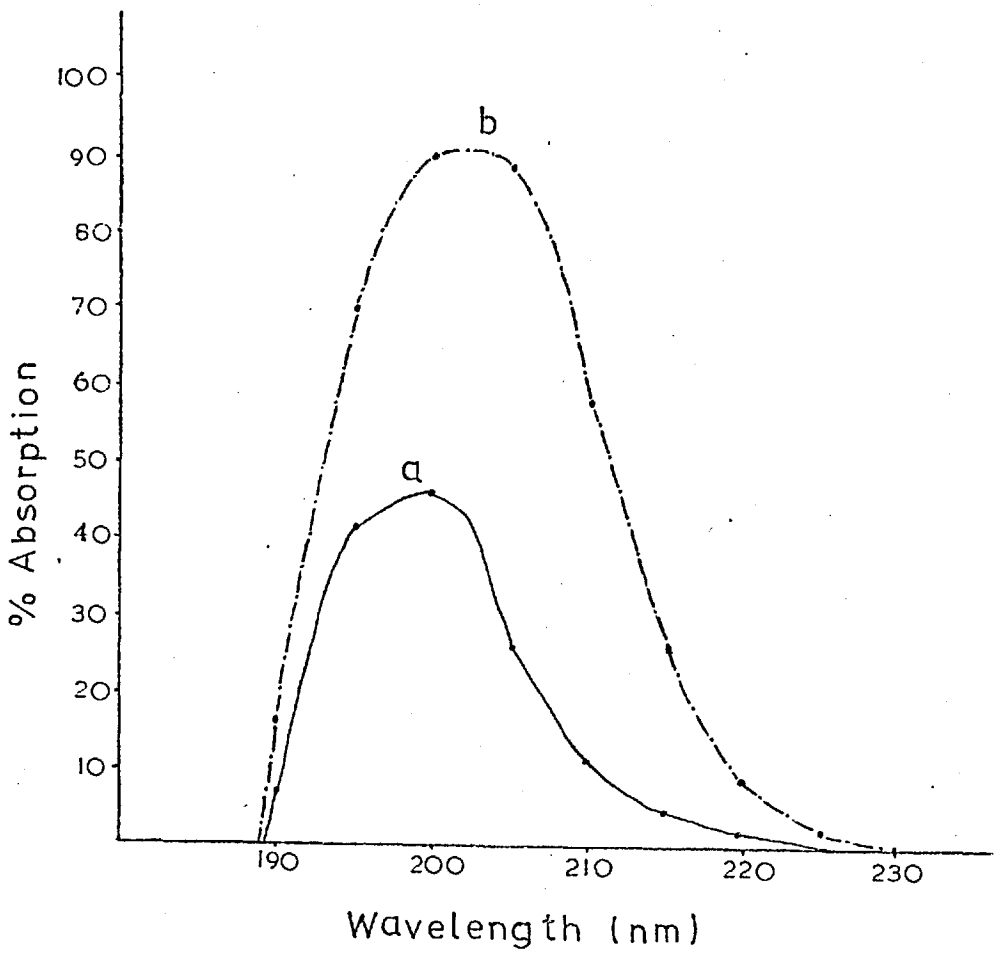

FIG. 3.11. Ultraviolet spectra of (a) the species produced during electrolysis (-2V) for potassium sulphate solution (0.03M) and (b) sodium hydroxide solution (0.005M).

into account the reduced optical pathlength* of the spectro-electrochemical cell relative to that of the standard solution (1:4), provided a pH value of 12. This procedure for estimating the pH of the electrode - solution layer will be considered in more detail later on.

3.2.9. Absorption spectrum of cadmium hydroxide solution

A simplified model which accounts for the process occurring during electrolysis is the production of a thin layer of hydroxide ions which diffuse away from the cathode

* It was assumed that the optical pathlength was equal to the electrode length (5mm).

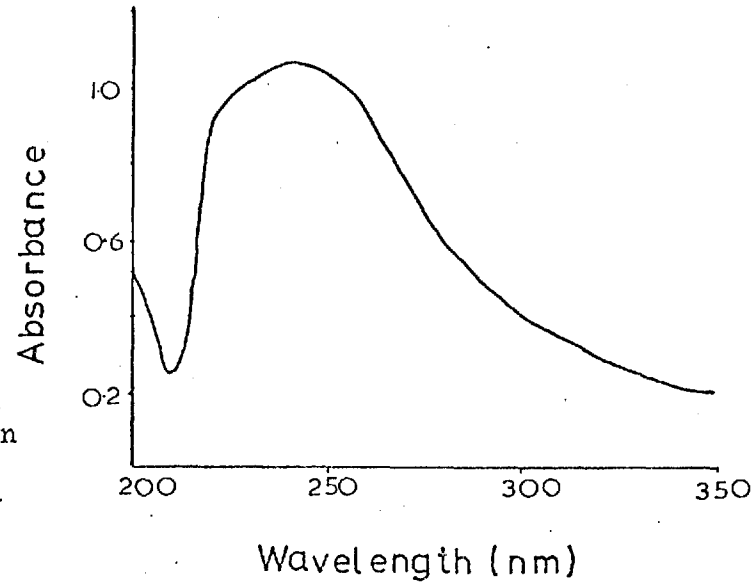

FIG. 3.12. Ultraviolet spectrum (Unicam SP 800) of cadmium hydroxide solution. Cadmium ($20\mu gml^{-1}$) in sodium hydroxide solution (0.005M); sodium hydroxide solution (0.005M) as reference; path-length 40mm.

and react with cadmium ions to give absorbing species. It would be expected from solubility product considerations ($K_{sp}\ Cd(OH)_2 = 2.5 \times 10^{-14}$) that the high pH generated would precipitate cadmium ions.

In an attempt to reproduce the situation, a solution of precipitated cadmium hydroxide was prepared by adding cadmium solution (10ml, $200\mu gml^{-1}$) to sodium hydroxide solution (50ml, 0.01M) contained in a volmetric flask (100ml). The solution was made up to the mark and after thorough mixing, a fine suspension of particles was clearly visible. The ultraviolet spectrum recorded against sodium hydroxide solution (0.005M) as reference is presented in fig 3.12 and the strong resemblance to the electrogenerated counterpart (fig 3.2) is evident. This comparison provides fairly convincing evidence that cadmium hydroxide particles selectively absorb light, but it is not conclusive since other soluble cadmium hydroxy species will be formed which may be light-absorbing. This is given consideration later.

3.2.10. Evidence for pH changes and metal hydroxide formation at electrodes

The previous experiments demonstrated that a high concentration of hydroxide ion sufficient to precipitate metal hydroxides was generated at the cathode during electrolysis. Experimental evidence, although not well documented in the literature, supports this.

Kemula[55], using the polarographic technique with microscopic observation of the area around the dropping mercury electrode (DME), observed the alkaline form of phenolphthalein and cadmium hydroxide precipitate during the reduction of dissolved oxygen. Ultramicroscopy has been used to monitor aqueous solutions of silver nitrate, mercurous nitrate and copper sulphate during electrolysis and the formation of colloidal particles were noted as soon as the cathode solution layer became alkaline (purple form of phenolphthalein); the particles were considered to be oxides or hydroxides[56]. The colloidal precipitate of uranium hydroxide, generated at the DME, has also been detected by optical means[57]. Further references to the formation of colloidal particles near the cathode and their examination using ultramicroscopic procedures are contained in a review by Ibl[58]. Direct electrochemical evidence supporting metal hydroxide formation is the decreased limiting currents recorded in amperometric titrations[59].

Using acid-base indicators (thymol blue; neutral red; alizarin yellow R; σ-cresol red; phenolphthalein), the pH changes accompanying the hydrogen and oxygen evolution reactions

(alkality at the cathode; acidity at the anode) have been accurately measured colorimetrically, the reactions providing the basis for acid-base coulometric titrations with photometric detection of equivalence[35-37].

A theoretical investigation of the solution pH at the cathode during hydrogen evolution has been undertaken by Hansen[60] in connection with the electrodeposition of insoluble hydroxides. He concluded that a relatively high pH (pH 11 - 13) existed at the cathode even in rather acidic solutions (pH 1) and subsequent experiments confirmed this[61].

Procedures for determining the pH of the electrode - solution layer have been reviewed by Taran and co-workers[62] and also by Stender and co-workers[63]; the principle methods employed have been colorimetry, use of microelectrodes and sample removal.

Clearly, there is ample evidence in the literature supporting the proposal that hydroxide ion and cadmium hydroxide were formed at the monitoring electrode during electrolysis and it remains to demonstrate conclusively that they selectively absorb ultraviolet radiation. Before that ,however, the electrode reactions responsible for the high pH at the cathode are investigated.

3.3. Absorption Monitoring during Controlled Potential Electrolysis

In order to examine the electrode reactions responsible for generating hydroxide ion, namely reduction of platinum surface oxide and dissolved oxygen, controlled potential electrolysis (CPE) with simultaneous monitoring of current and absorption was performed. Before describing the experiments, a brief literature review of the reduction reactions is presented, emphasis being placed on the final reduction products.

3.3.1. The cathodic reactions of dissolved oxygen and platinum surface oxide

(1) Reduction of dissolved oxygen

Considerable research has been carried out on the reduction of dissolved oxygen and unfortunately there is disagreement regarding the mechanism and products of the reaction. The subject has been treated extensively by Hoare[64] and Damjanovic[65]. It is known that the mechanism and ultimate products, hydrogen peroxide, water and hydroxide ion, are critically dependent on a number of factors including the pH of the solution, the electrode material (and its surface condition), electrode potential/current density and the presence of impurities.

Polarographic reduction of dissolved oxygen gives curves containing two separate waves, the reduction potential of which are unaffected by pH[66]. It is generally accepted[67] that the waves correspond to the reactions

1st Wave
(0.05V vs SCE)

$$O_2 + 2H^+ + 2e^- \longrightarrow H_2O_2 \quad \text{(Acid)}$$

$$O_2 + H_2O + 2e^- \longrightarrow HO_2^- + OH^- \quad \text{(Alkali)}$$

2nd Wave
(-0.6 to -1.4V vs SCE)

$$H_2O_2 + 2H^+ + 2e^- \longrightarrow 2H_2O \quad \text{(Acid)}$$

$$HO_2^- + H_2O + 2e^- \longrightarrow 3OH^- \quad \text{(Alkali)}$$

indicating that hydrogen peroxide and water are prevalent in acidic solution while hydroxide is produced in alkali. Similar reactions have been proposed for platinum electrodes but the oxidation state and the catalytic activity of the electrode surface tend to complicate the situation. In addition owing to the low overpotential for hydrogen evolution, the second wave is not normally recorded in acidic solution. The main controversy is whether hydrogen peroxide is formed initially as a stable intermediate or whether the reduction, corresponding to a 4-electron transfer proceeds directly to water or hydroxide ion. The reactions and possible mechanisms are considered by Damjanovic[65] and he reports the experimental evidence for and against. Conflicting results are provided by Myuller and Nekrasov[68] who detected hydrogen peroxide in both acidic and alkaline solutions whereas Damjanovic and co-workers[69] found the peroxide only in base. Blurton and McMullin[70] showed that the formation of hydrogen peroxide and hydroxide were dependent on electrode potential: in alkaline solution between the open-circuit voltage and 0.4V vs HE, hydrogen peroxide was produced whereas between 0.4 and 0.0V vs HE, hydroxide was formed with hydrogen peroxide as an intermediate.

The catalytic behaviour of the electrode material was demonstrated in tracer experiments by Davies and co-workers[71] with the O^{18} isotope. Using active carbon electrodes in potassium hydroxide solution (1M), the reduction produced hydrogen peroxide and the O-O bond was not broken whereas with a platinum cathode the peroxide was not detected at low current densities and only at high current densities. This difference was interpreted as being due to the poor catalytic qualities of carbon for decomposing the peroxide relative to platinum. Other studies have shown that the adsorbed oxygen layer promotes the catalytic decomposition of hydrogen peroxide[68], but also inhibits the reduction of molecular oxygen[72].

The reaction of Ti(IV) with hydrogen peroxide to form the orange peroxo complex has been employed by a number of workers[73,74] for detection of hydrogen peroxide in electrode reactions.

(2) Reduction of platinum surface oxide

It is well known that the platinum electrode surface is not electrochemically inert, but is covered with a layer of adsorbed hydrogen atoms or oxygen species depending on the electrode potential. The potential regions for film formation are clearly seen by considering a typical current-potential curve shown in fig 3.13 and recorded by Bold and Breiter[75] for platinum in sulphuric acid solution (2.3M). The adsorption - desorption of hydrogen, occurring in the region 0.10V to 0.35V vs HE is rapid and reversible. Between 0.4V and 0.8V vs HE

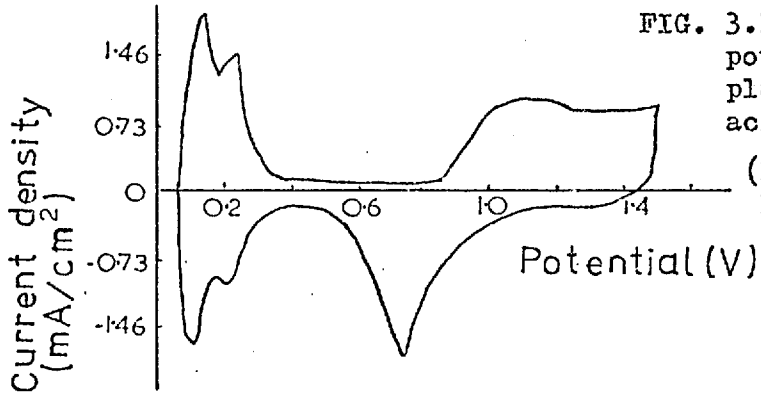

FIG. 3.13. Current - potential curve for platinum in sulphuric acid solution (2.3M) (Reproduced from Ref. 75).

there is a low current region where the platinum surface is essentially free of adsorbed species. Beyond 0.8V vs HE the formation of the oxygen film occurs with evolution commencing at about 1.4V vs HE. Film formation is slow and irreversible since the oxygen reduction wave observed on the reverse scan is displaced to less positive potentials.

Although the hydrogen layer has been well characterised[76], there is controversy regarding the exact nature of the oxygen film. Depending on experimental conditions such as electrode potential and time, the oxygen surface has been described as (i) a chemisorbed oxygen layer and (2) a metal oxide; inter-conversion between the two forms is possible. Various methods, electrochemical and optical, have been employed for studying the oxide layer and the review by Woods[76] summarises the more recent work.

There is strong evidence that the platinum electrode at potentials less than approximately 1.0V vs HE is free of surface oxide, the film consisting of chemisorbed oxygen species such as OH_{ad}. The chemisorption reaction

$$H_2O \rightleftharpoons PtOH + H^+ + e^-$$

has been proposed by a number of workers[77-80] to explain this. At potentials greater than 1.0V vs HE, a further oxidation step

$$PtOH \longrightarrow PtO + H^+ + e^-$$

results in the growth of surface oxide[81-85]. Higher oxides such as PtOx are reported to form under severe anodic conditions[86].

Various mechanisms have been suggested for surface oxide reduction in acidic solution and the scheme proposed by Feldberg[87]

$$PtOx + xH^+ + xe^- \longrightarrow Pt(OH)_x$$

$$Pt(OH)_x + xH^+ + xe^- \longrightarrow Pt + xH_2O$$

is a good representation of the picture. Unfortunately there has been little research aimed at identifying the product(s) of reduction although recently, spectroelectrochemical experiments by Tyson[4] indicated that hydroxide ion was produced in neutral solution. A plausible mechanism to account for the high alkalinity in neutral solutions is simply cathodic stripping of the adsorbed hydroxy radicals without involvement of protons:

$Pt(OH)x + xe^- \longrightarrow Pt + xOH^-$. Another possibility is that just in the same way as the hydrogen evolution reaction in neutral solution

$$H_2O + e^- \longrightarrow H_{ad} + OH^-$$

generates a high pH at the cathode [88], the requirement for hydrogen ions in surface oxide reduction in neutral solution

will cause a similar breakdown of water and result in excess hydroxide.

Clearly it is not possible, due to the conflicting results in the literature, to predict the final products from surface oxide and dissolved oxygen reduction reactions in our system. It is hoped that simultaneous absorption and current monitoring can resolve the situation and provide unambiguous identification of the product(s) from the respective reactions.

3.3.2. Absorption - potential curve for reduction of dissolved oxygen

The absorption of the product of dissolved oxygen reduction (non-degassed solution of potassium sulphate (0.03M) and a non-oxidised electrode) was recorded at 200nm while potential steps (initial potential 0.2V vs SCE) of increasing magnitude were applied to the working electrode. The absorption - potential curve is shown in fig 3.14a and indicates that the absorption increases fairly rapidly up to about -0.2V vs SCE and then remains constant. The steep rise in absorption at potentials beyond -0.8V vs SCE marks the onset of hydrogen evolution and results in a further rise in the pH of the electrode - solution layer. A small correction to the signals at -0.9V vs SCE and -1.1V vs SCE was made for light attenuation by hydrogen gas bubbles.

3.3.3. Absorption - potential curve for reduction of platinum surface oxide.

The working electrode was pretreated at +5V for 30s and then held at +0.8V vs SCE while the potassium sulphate

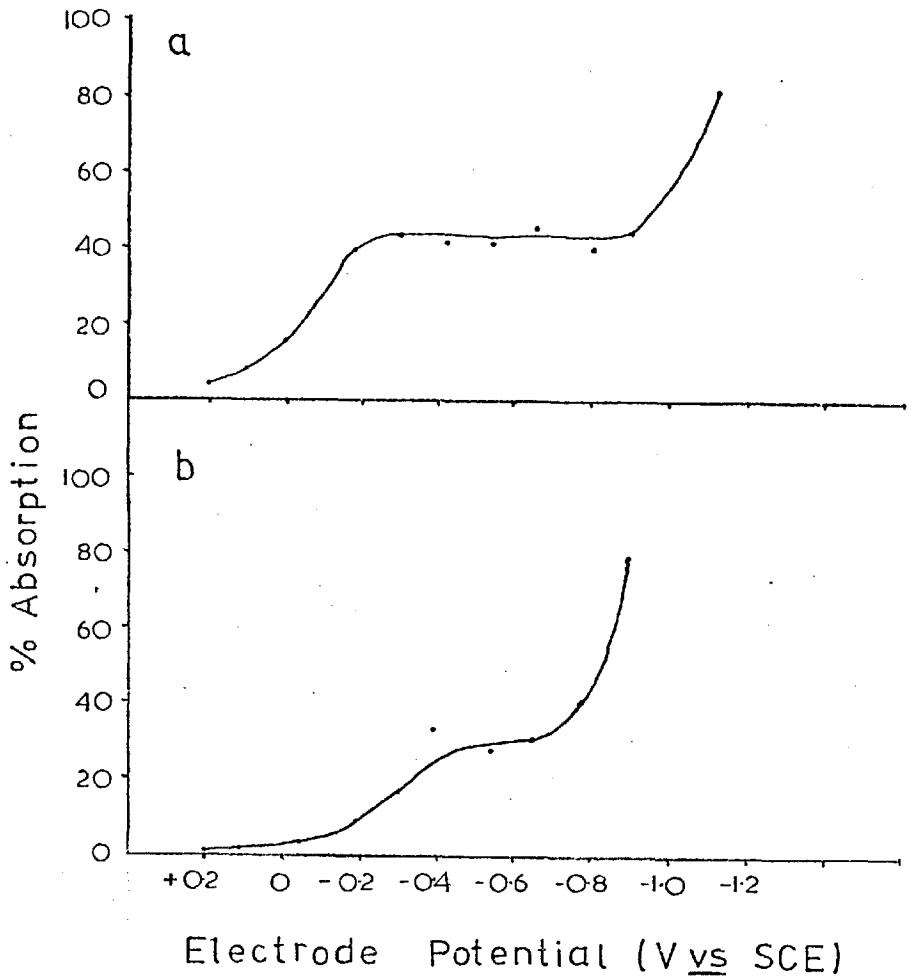

FIG. 3.14. Absorption – electrode potential curves for (a) reduction of dissolved oxygen and (b) reduction of surface oxide. Solution, potassium sulphate (0.03M); monitoring wavelength 200nm.

solution (0.03M) was degassed for 5 minutes. The electrode potential was returned to +0.2V vs SCE and then stepped as before to negative potentials. A nitrogen blanket was kept over the solutions during the experiment. The absorption response shown in fig 3.14b is similar to previous except that it is displaced by approximately 0.2V vs SCE to more negative potentials. This agrees with the findings of Tyson[4] and suggests that surface oxide reduction is occurring at more negative potentials than dissolved oxygen reduction.

For potentials up to about -0.20V, a small increase in absorption occurred and this was attributed to reduction of residual dissolved oxygen. The response at -0.30V was quicker than previous, but because maximum absorption was not attained, it was considered that reduction was only partially complete. At potentials beyond -0.40V, the absorption level was fairly constant until the onset of hydrogen evolution. The hydrogen evolution reaction commenced at less negative potentials than for the non-oxidised electrode.

3.3.4. Absorption spectra of the species generated for the blank solution

The spectral distribution of the species generated at the working electrode for potassium sulphate solution (0.03M) was recorded for the following reactions:

(1) Reduction of dissolved oxygen (non-degassed solution; non-oxidised electrode; potential step, +0.2V to -0.6V vs SCE).

(2) Reduction of surface oxide (degassed solution; oxidised electrode; potential step, +0.2V to -0.6V vs SCE).

(3) Reduction of dissolved oxygen and surface oxide (non-degassed solution; oxidised electrode; potential step, +0.2V to -0.6V vs SCE).

(4) Hydrogen evolution (potential step, +0.2V to -1.1V vs SCE).

The spectra corresponding to each reaction are presented in fig 3.15 and comparison with the spectrum for sodium hydroxide solution (0.001M) given in fig 3.16(a) is very good indicating that hydroxide ion was produced in all four cases. The dissimilarity

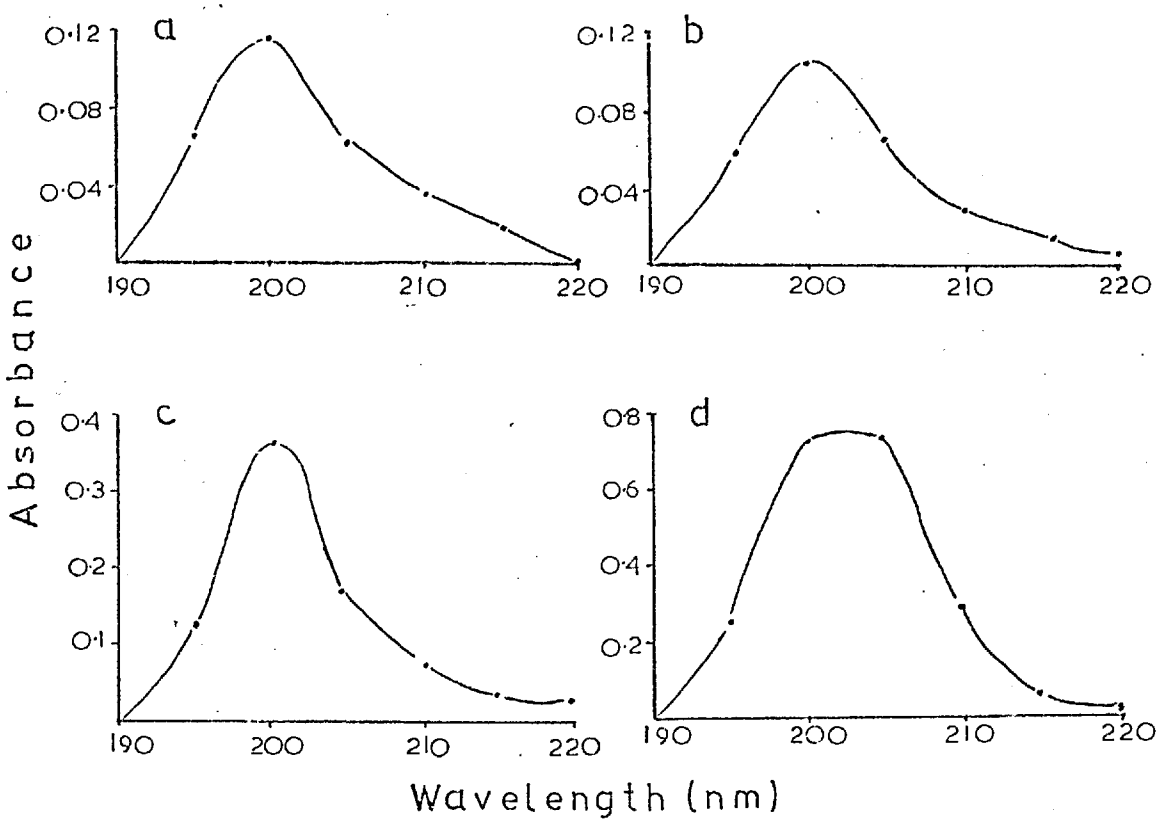

FIG. 3.15. Ultraviolet spectra of the products from (a) dissolved oxygen reduction, (b) platinum surface-oxide reduction (c) dissolved oxygen and platinum surface-oxide reduction and (d) the hydrogen evolution reaction. Solution, potassium sulphate (0.03M).

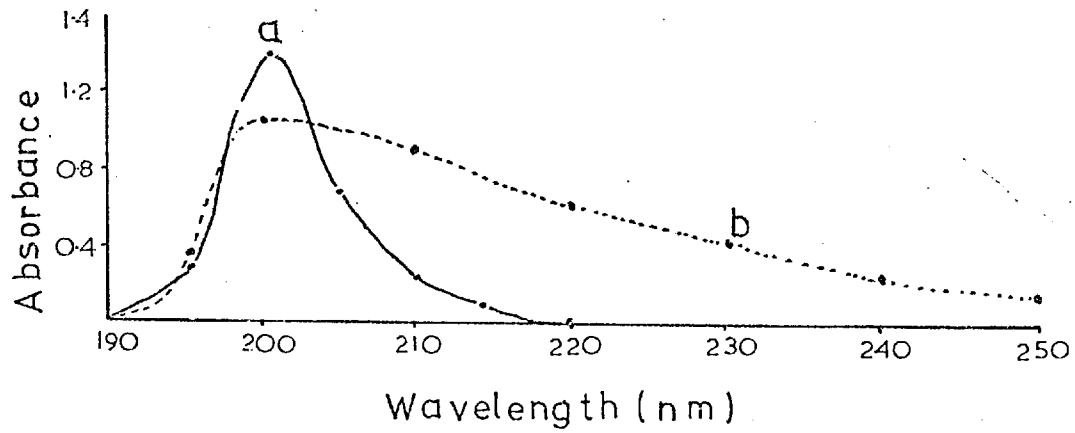

FIG. 3.16. Ultraviolet spectra (Unicam SP 800) for (a) sodium hydroxide solution (0.001M) and (b) hydrogen peroxide solution (0.005M). Pathlength 10mm.

of the spectra with that of hydrogen peroxide (0.005M) enables the formation of peroxide in any significant quantity to be ruled out. This result agrees with earlier findings of Tyson[4]. Incidentally the spectrum of hydrogen peroxide is displaced to longer wavelengths in alkaline solution due to the formation of the peroxo anion[89]; this feature would have assisted the detection of hydrogen peroxide had it been produced.

3.3.5. Estimation of the pH of the electrode-solution layer

An estimation of the pH at the electrode - solution layer corresponding to each electrode reaction was obtained from a comparison of the "electrogenerated" absorbance values with those of standard sodium hydroxide solutions. The ultra-violet spectra of sodium hydroxide solutions (0.001M - 0.0001M) provided linear calibration at 200nm in accordance with Beer's law; this is illustrated in fig 3.17. Linear calibration and similar spectral behaviour for sodium hydroxide solutions (0.0001M - 0.0014M) were recently reported by Zuman and Szafranski[90]. The absorbance results for electrogenerated hydroxide together with the estimated pH near the electrode surface for the respective reductions are given in table 3.3. The absorbance values were computed from the spectra of fig 3.15. Since the optical pathlength of the spectroelectrochemical cell (5mm; assumed equal to the length of the working electrode) was one half that used for recording the spectra of the standard solutions (pathlength 10mm) the concentrations read from the calibration graph were doubled to provide an estimate of the

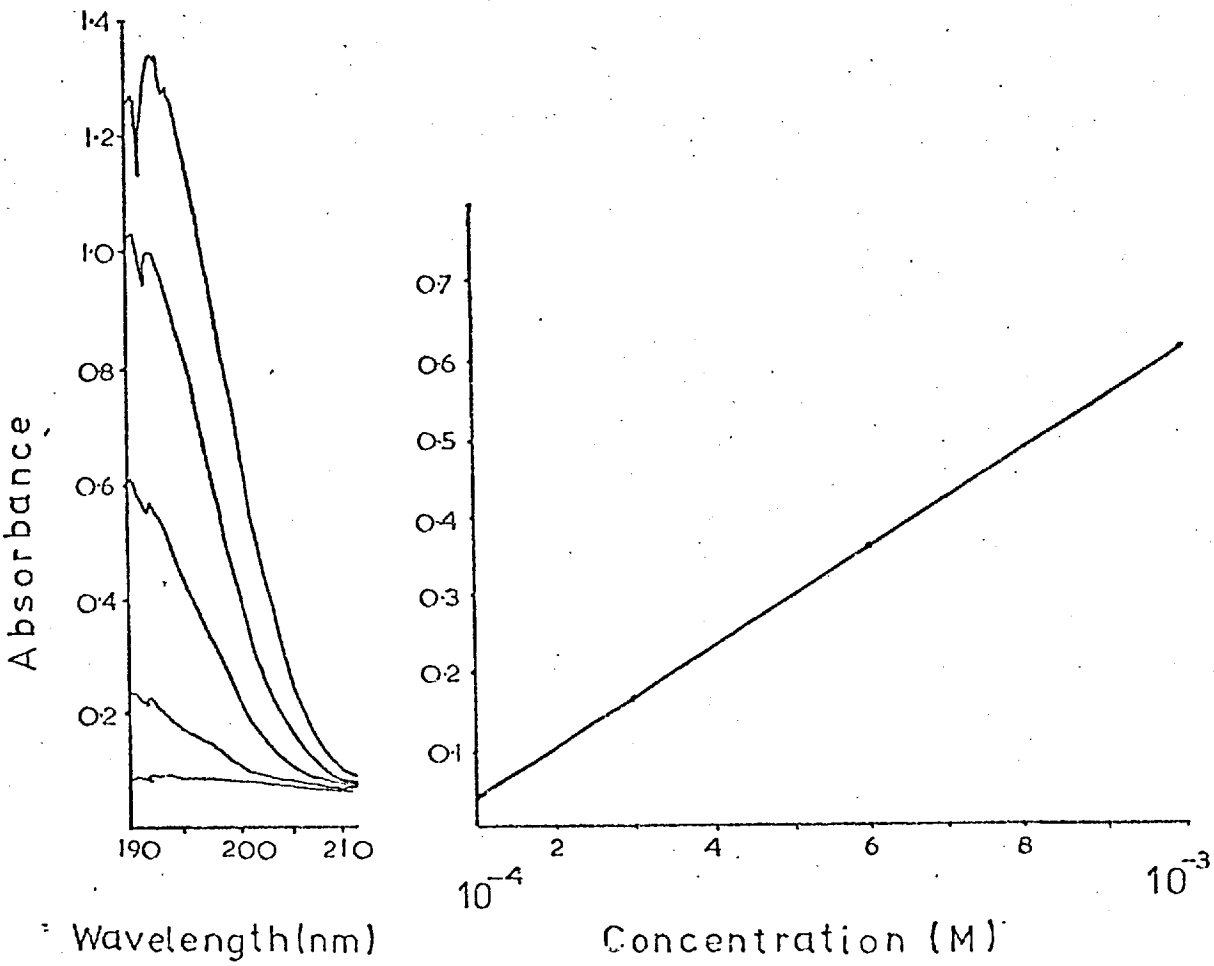

FIG. 3.17. Ultraviolet spectra (Unicam SP 800) of sodium hydroxide solutions (10^{-4}M - 10^{-3}M) and calibration graph at 200nm. Pathlength 10mm.

actual pH near the working electrode.

The values confirm that a high pH is generated at the electrode - solution layer increasing in the reaction order (1) dissolved oxygen reduction ~ (2) surface oxide reduction < (3) dissolved oxygen and surface oxide reduction < (4) hydrogen evolution. The comparison does assume a uniform hydroxide concentration distribution within the width of the light beam and if this is not the case then solution layers very close to the electrode surface would be at an even higher pH.

Table 3.3. Absorbance values for electrogenerated hydroxide and estimated pH of the electrode - solution layer.

Route for Hydroxide Production	Absorbance (200nm)	Estimated Concentration (M)	Calculated pH
Dissolved oxygen reduction	0.12	4.4×10^{-4}	10.4
Surface oxide reduction	0.10	4.2×10^{-4}	10.3
Dissolved oxygen and surface oxide reduction	0.36	1.2×10^{-3}	10.9
Hydrogen evolution	0.72	5×10^{-3}	11.2

Solution, potassium sulphate (0.03M).

3.3.6. Absorption monitoring of the blank solution during cyclic sweep excitation

The absorption and current were simultaneously monitored during a cyclic sweep (+0.1V to -0.8V to +0.1V vs SCE at $30 mVs^{-1}$) of the working electrode for potassium sulphate solution (0.03M). The following situations were investigated:

(1) No electroreducible species (non-oxidised working electrode, degassed solution).

(2) Dissolved oxygen reduction (non-oxidised working electrode, non-degassed solution).

(3) Surface oxide reduction (oxidised working electrode, degassed solution).

(4) Reduction of surface oxide and dissolved oxygen (oxidised working electrode, non-degassed solution).

The current - potential and absorption - potential curves shown

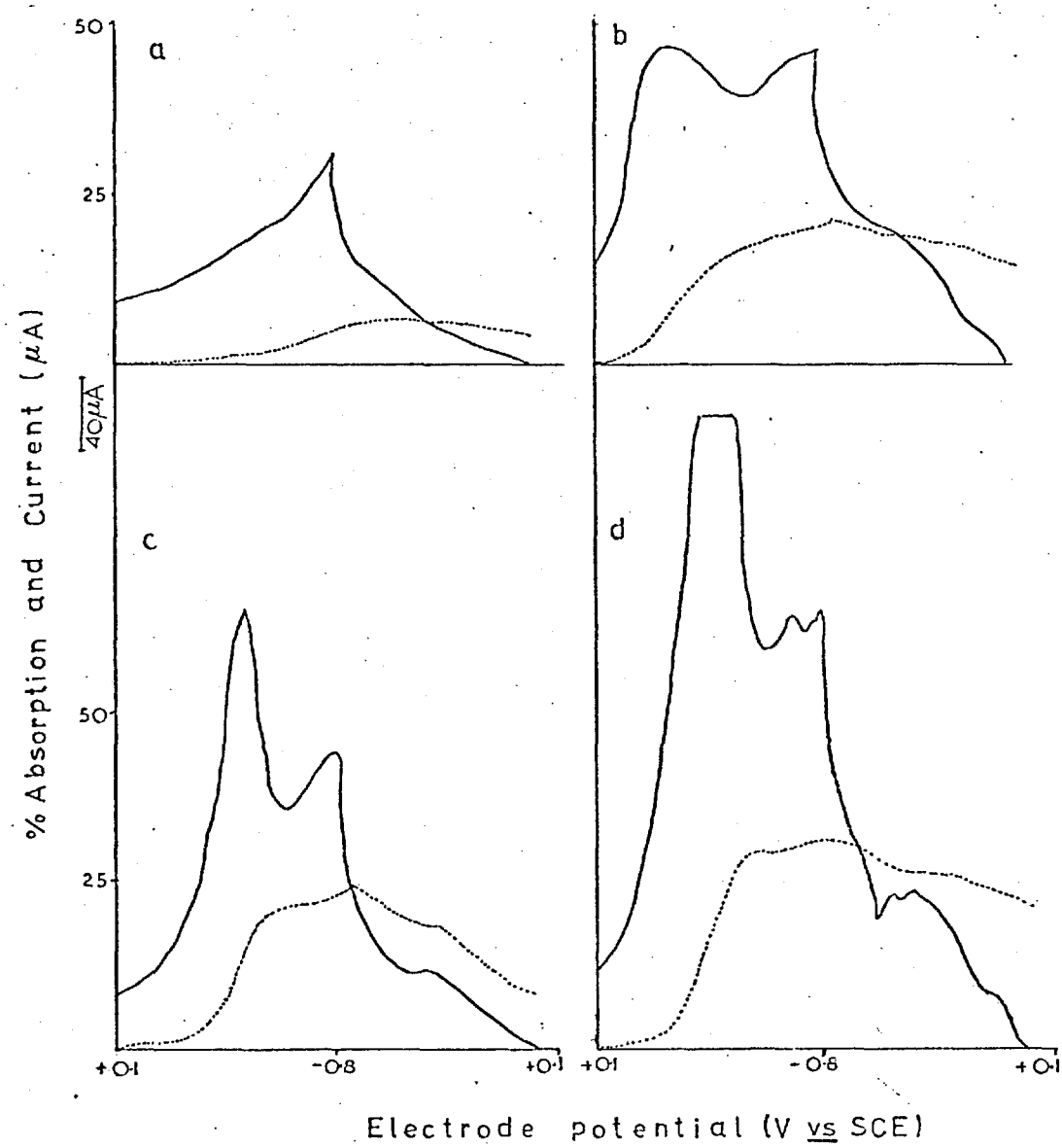

FIG. 3.18. Current/absorption - potential curves during cyclic sweep of the working electrode:
(a) no electroreducible species
(b) reduction of dissolved oxygen
(c) reduction of surface oxide
(d) reduction of dissolved oxygen and surface oxide.
Solution, potassium sulphate (0.03M); scan rate 30mVs^{-1}; monitoring wavelength 200nm; solid lines, current; broken lines, % absorption.

in fig 3.18 indicate that reduction of dissolved oxygen and/or surface oxide is a prerequisite for hydroxide production since the increase in sweep currents (solid lines) at potentials more negative than 0.0V vs SCE is accompanied by a simultaneous rise in absorption (broken lines). The concentration of hydroxide generated from the various routes agrees with previous experiments and increases in the reaction order: (1)<(2)~(3)<(4). Close inspection of the response curves reveals that the reduction wave for surface oxide and the initial rise in absorption (curve c) are displaced to more negative potentials that the corresponding responses for dissolved oxygen reduction (curve b). This behaviour is in agreement with the findings for the potential step experiment in section 3.3.3.

3.3.7. Absorption monitoring of the blank solution during potential step excitation

An identical set of experiments to the previous were performed for potential step excitation (+ 0.1V to -0.8V vs SCE) and the response curves are shown in fig 3.19. The potential step excitation characterised by the initially high double-layer charging current (solid line) caused an increase in the rate of reduction relative to the potential sweep and is evidenced by the rapid response of the absorption signal (dotted line). The absorption from the solution containing no reducing species was unusually high and indicated that degassing was not complete.

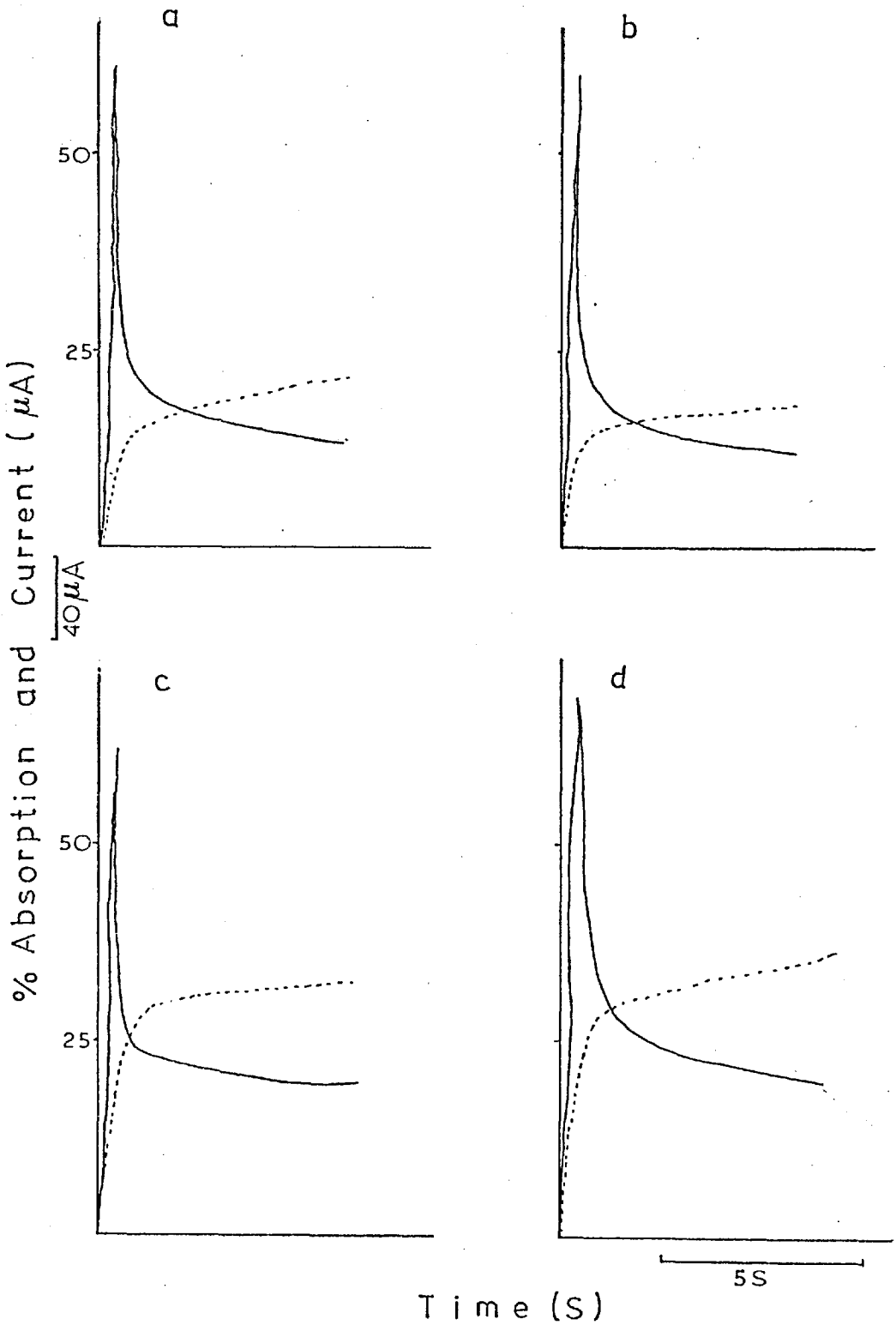

FIG. 3.19. Current/absorption - time curves during potential step excitation: (a) no electroreducible species (b) reduction of dissolved oxygen (c) reduction of surface oxide (d) reduction of dissolved oxygen and surface oxide. Solution, potassium sulphate (0.03M); monitoring wavelength 200nm; solid lines, current; broken lines, % absorption; potential step, +0.1V to -0.8V vs SCE.

3.3.8. Absorption monitoring of cadmium solutions during cyclic sweep excitation

By choosing the experimental conditions such that the production of hydroxide was minimised (non-oxidised working electrode, degassed solution) it was hoped to show that cadmium ion was reduced and no concurrent absorption occurred. The absorption - potential and current - potential curves were recorded for cadmium solutions ($50\mu gml^{-1}$, $100\mu gml^{-1}$) during a cyclic sweep (+0.1V to -0.8V to +0.1V *vs* SCE at $40mVs^{-1}$) of the working electrode and are given in fig 3.20. The current - potential curves revealed small increases in sweep current relative to the blank potassium sulphate solution (0.03M) suggesting reduction of cadmium(II); the corresponding absorption responses at 220nm showed no increases. Generally, cathodic scans with platinum working electrodes show high background currents and in this study with dilute cadmium solutions it was not possible to state categorically that reduction was occurring. For confirmation, the linear sweep voltammogram for cadmium solution ($900\mu gml^{-1}$), using micro-platinum wire as working electrode, was recorded and this did reveal a reduction wave commencing at approximately -0.6V *vs* SCE; the corresponding scan for the blank solution is also included. This is shown in fig 3.21a. The study clearly demonstrated that cadmium(II) was reduced without concurrent absorption and enabled the hydrated metal atom theory, which was originally postulated to explain the absorption signals, to be ruled out.

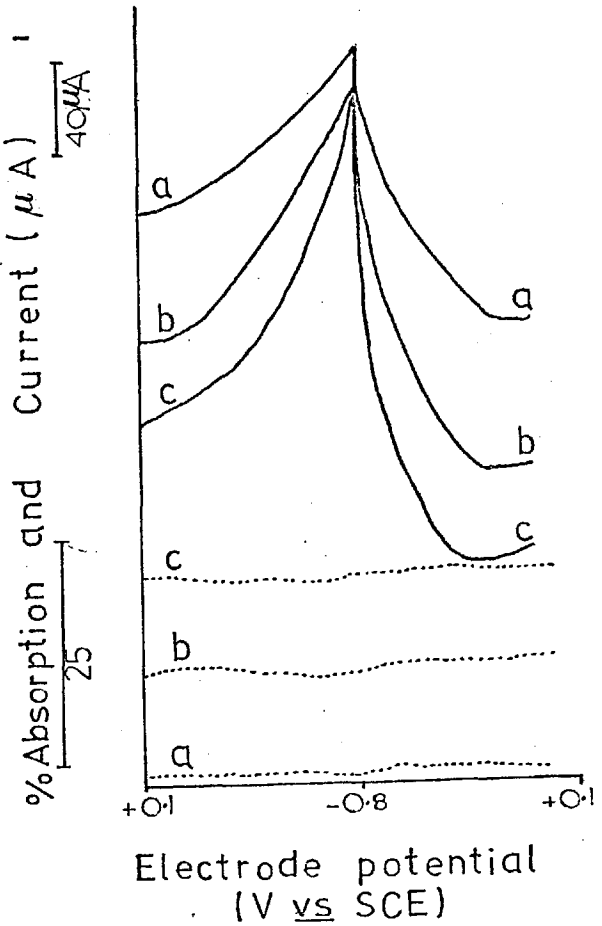

FIG. 3.20. Current/absorption - potential curves during cyclic sweep of the working electrode: (a) potassium sulphate solution (0.03M) (b) cadmium (50μgml^{-1}) in potassium sulphate solution (0.03M) (c) cadmium (100μgml^{-1}) in potassium sulphate solution (0.03M). Scan rate 40mVs^{-1}; monitoring wavelength 220nm; solid lines, current; broken lines, % absorption.

In contrast, using experimental conditions which generated hydroxide ion (oxidised working electrode and non-degassed solution) enabled strong absorption signals at 220nm to be recorded for cadmium (50μgml^{-1}) during the scan. The absorption and current responses during reduction of (1) dissolved oxygen and (2) surface oxide are presented in fig 3.22. It can be seen that the reduction wave for surface oxide reduction and the initial rise in absorption are displaced to more negative potentials than the responses for dissolved oxygen reduction; this agrees with the response behaviour observed for the corresponding scans of the blank solution (fig 3.18b, c).

3.3.9. Absorption spectra of the electrogenerated cadmium species

The ultraviolet spectra of the electrogenerated cadmium

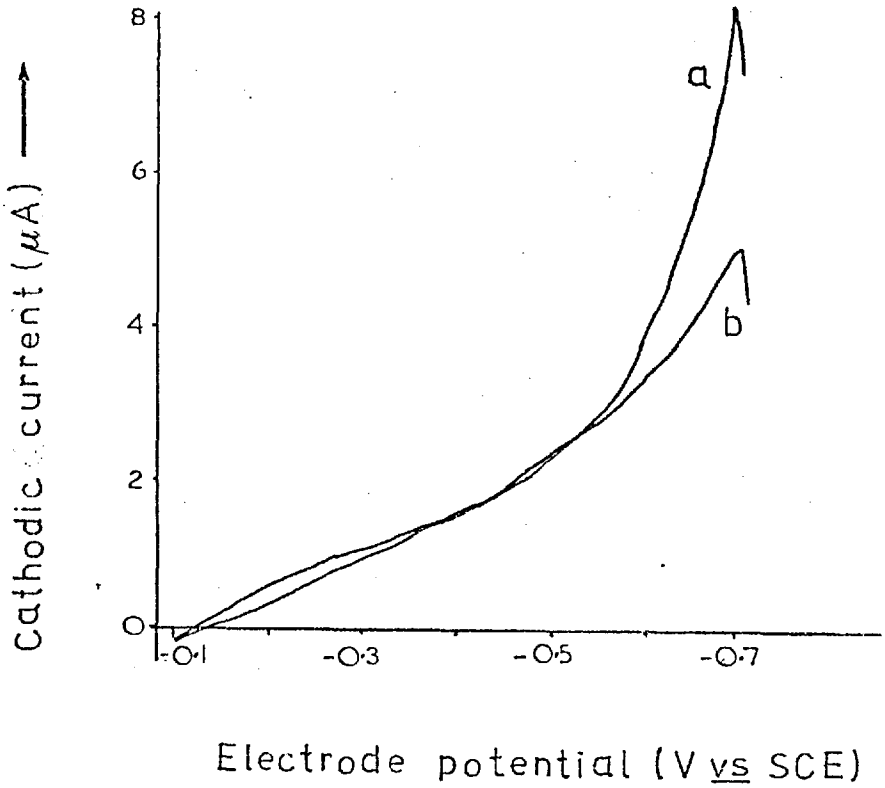

FIG. 3.21. Linear sweep voltammogram for (a) cadmium ($900\mu gml^{-1}$) in potassium sulphate solution (0.03M) and (b) potassium sulphate solution (0.03M). Scan rate $80mVs^{-1}$.

species was recorded using hydroxide derived from (1) reduction of dissolved oxygen, (2) reduction of dissolved oxygen and surface oxide and (3) the hydrogen evolution reaction.

The spectra which are presented in fig 3.23 for cadmium solutions ($2x10^{-5}M$) are very similar with maximum absorption occurring at approximately 200nm. (N.B. The recorded spectra include a contribution from hydroxide ion). No absorption was recorded for cadmium solutions ($2x10^{-4}M$) with hydroxide derived from reaction (1) or reaction (2). Further, failure to record the characteristic hydroxide signal at 200nm indicated the complexation of hydroxide with cadmium ions to give non-absorbing species. The absorption results at 200nm (λmax hydroxide) and

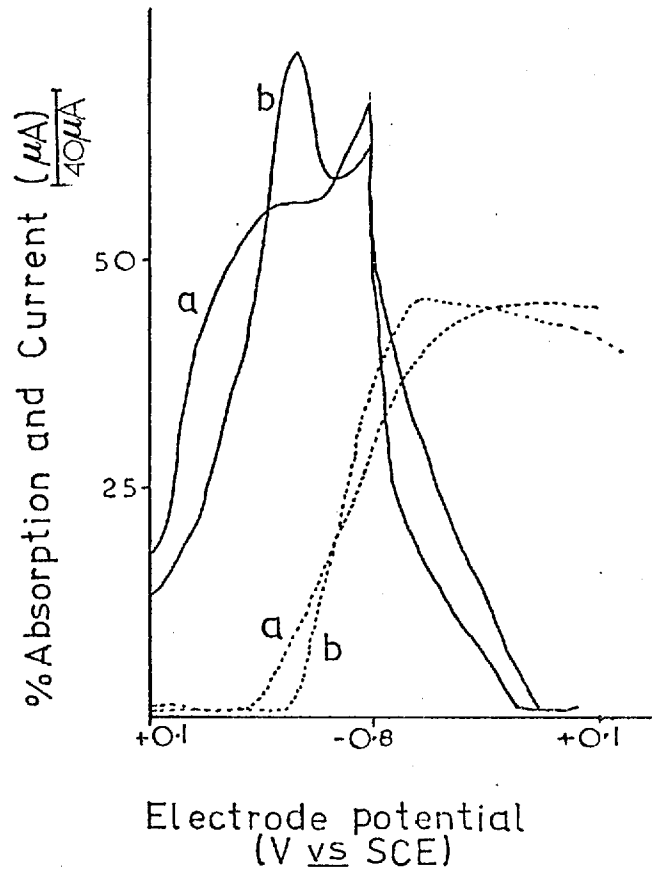

FIG. 3.22.
Current/Absorption - potential curves during cyclic sweep of the working electrode:
(a) reduction of dissolved oxygen
(b) reduction of platinum surface oxide. Cadmium ($50\mu g ml^{-1}$) in potassium sulphate solution (0.03M); monitoring wavelength 220nm; scan rate $40mVs^{-1}$; solid lines, current; broken lines, % absorption.

220nm (λmax cadmium) for the cadmium solutions and the blank potassium sulphate solution (0.03M) are given in table 3.4.

Table 3.4. The electrogenerated absorption values at 200nm and 220nm for cadmium and the blank solutions.

	% Absorption					
	Potassium sulphate (0.03M)		Cadmium ($2x10^{-5}$M)		Cadmium ($2x10^{-4}$M)	
	200nm	220nm	200nm	220nm	200nm	220nm
Reduction of dissolved oxygen	27	2	26	18	3	2
Reduction of dissolved oxygen and surface oxide	44	3	46	31	1	2

Sufficient hydroxide was, however, generated during the hydrogen evolution reaction and the spectrum for cadmium solution ($2x10^{-4}$M) is shown in fig 3.24. An interesting

spectral feature is the bathochromic shift in the absorption maximum of the cadmium species which provides partial resolution of the hydroxide ion and cadmium absorption bands.

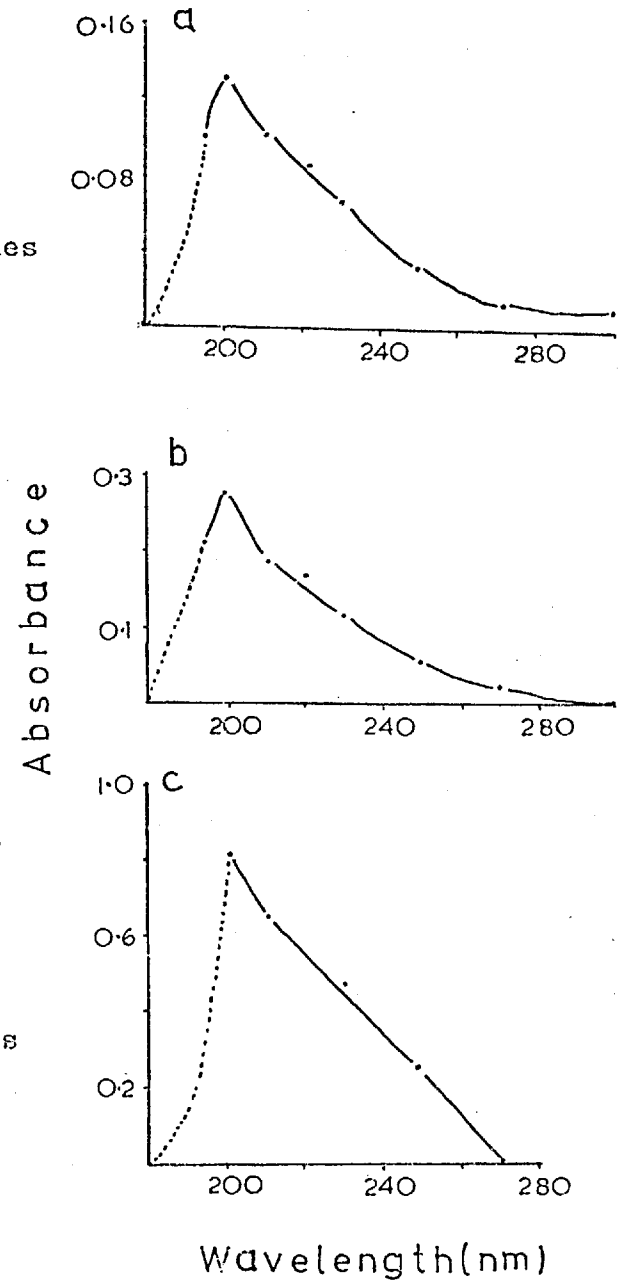

FIG. 3.23. Ultraviolet spectra of the cadmium species during (a) reduction of dissolved oxygen (b) reduction of dissolved oxygen and surface oxide (c) the hydrogen evolution reaction. Cadmium (2×10^{-5}M) in potassium sulphate solution (0.03M).

3.3.10 Calibration for the electro-generated cadmium species

The absorbance values for the electro-generated cadmium species were obtained from the reaction of cadmium solutions ($5\mu g ml^{-1}$ - $200\mu g ml^{-1}$) with hydroxide ion derived from the three main sources. The calibration curves are presented in fig 3.25 for (1) reduction of dissolved oxygen (2) reduction of dissolved oxygen and platinum surface oxide and (3) the hydrogen evolution reaction and the unusual absorbance - concentration dependence is readily explained in terms of cadmium hydroxide

formation. The linearity observed up to approximately 20μgml^{-1} indicates that the amount of precipitate increased in a regular manner with increasing cadmium concentration. The decreasing absorbance values (curves a and b) beyond this concentration level, however, signified that there was insufficient hydroxide to ensure the continued precipitation of cadmium hydroxide. The absorbance values at the 30μgml^{-1} level clearly provide an indication of the quantities of hydroxide available from the three routes. The high pH resulting from the hydrogen evolution reaction did not extend the range of linearity but rather high absorbance values were still noted even for cadmium concentrations of 800μgml^{-1} (curve c).

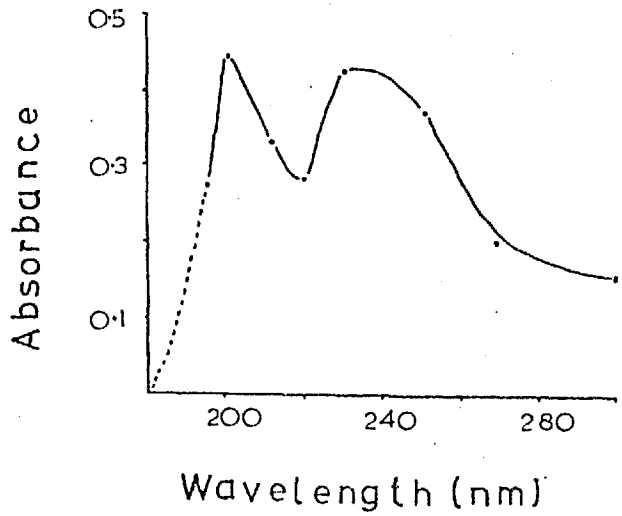

FIG. 3.24. Ultraviolet spectrum of the cadmium species during the hydrogen evolution reaction. Cadmium ($2x10^{-4}M$) in potassium sulphate solution (0.03M).

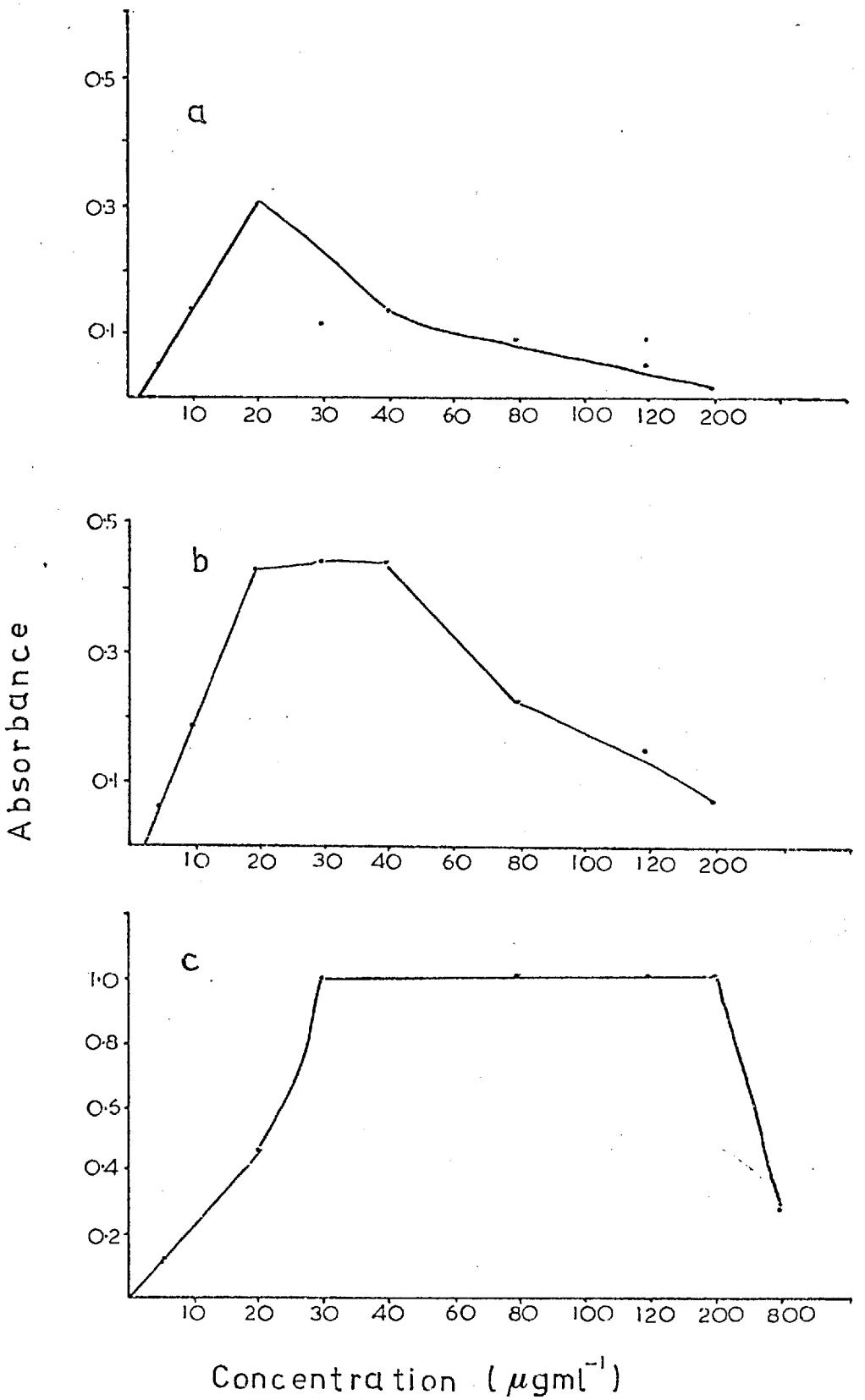

FIG. 3.25. Calibration graphs for the electrogenerated cadmium species: (a) reduction of dissolved oxygen (b) reduction of dissolved oxygen and platinum surface oxide and (c) the hydrogen evolution reaction. Monitoring wavelength 220nm.

3.4. Absorption Studies of Chemically Prepared Metal Hydroxide Solutions

3.4.1. Ultraviolet spectra of cadmium hydroxide solutions

As shown previously (fig 3.12), a chemically prepared solution of cadmium hydroxide exhibits sensitive absorption in the ultraviolet. This is not conclusive, however, that the absorbing species are precipitated cadmium hydroxide particles since other soluble cadmium hydroxy complexes are formed and these may absorb the radiation. The principle cadmium-containing species in alkaline solution depend on the concentration of hydroxide ion[91]. The following reactions give a representation of the dynamic equilibria existing between the various species that are formed:

$$Cd^{2+} + OH^- \rightleftharpoons Cd(OH)^+$$

$$Cd(OH)^+ + OH^- \rightleftharpoons Cd(OH)_{2\,soln} \rightleftharpoons Cd(OH)_2\downarrow$$

$$Cd(OH)_{2\,soln} + OH^- \rightleftharpoons Cd(OH)_3^-$$

$$Cd(OH)_3^- + OH^- \rightleftharpoons Cd(OH)_4^{2-} .$$

The $Cd(OH)^+$ and $Cd(OH)_4^{2-}$ complexes predominate at high (pH14) and low pH (pH8) respectively[91].

To determine whether any of the soluble cadmium species absorb ultraviolet radiation, it was decided to prepare cadmium hydroxide solutions containing various concentrations of sodium hydroxide and compare the absorption spectra of the unsettled and settled solutions. The settled solutions would not contain precipitated particles (provided the particles are not colloidal) and any absorption (neglecting hydroxide ion absorption) would

be due to soluble cadmium hydroxy complexes.

The preparation consisted of the addition of various microlitre aliquots of stock cadmium solution (0.01M) to volumetric flasks (25ml) containing various concentrations of sodium hydroxide solution (0.1M - 0.001M); final cadmium concentrations were $2x10^{-4}$M and $2x10^{-5}$M. After thorough mixing, the ultraviolet spectrum of each solution was recorded. The solutions were then left overnight to allow precipitate to settle and portions of the clear solution were withdrawn for a second ultraviolet scan. Care was taken not to disturb the fine settled precipitate. The solutions were then thoroughly mixed again for a final scan.

The results of a visual inspection of the cadmium hydroxide solutions are summarised in table 3.5 while the corresponding spectra of the unsettled (solid line) and settled (broken line) solutions are presented in figs 3.26 and 3.27. The final ultraviclet scan is not included. For fig 3.26 (cadmium $2x10^{-5}$M), the spectra of the unsettled solutions bear a strong resemblance to their electrogenerated counterparts (fig 3.23) and it can be seen that the hydroxide concentration does not significantly influence the spectral properties of the species. For cadmium concentrations of $2x10^{-4}$M, no absorption was recorded for solutions 0.001M and 0.003M with respect to sodium hydroxide. Also the lack of hydroxide absorption at 200nm indicated that soluble non-absorbing cadmium hydroxy complexes were formed. This agrees with the previous electrogenerated results reported in table 3.4. Strong

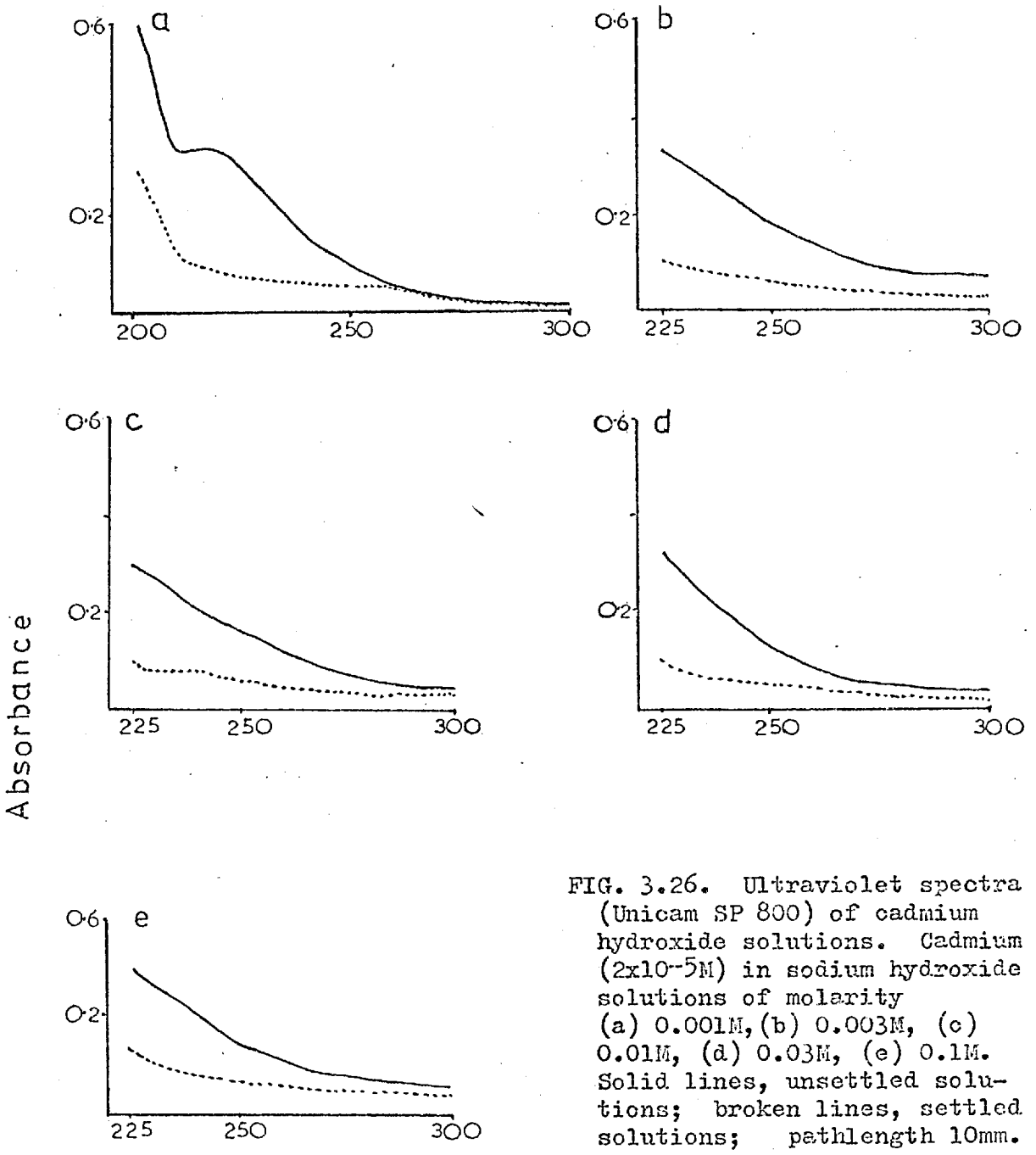

FIG. 3.26. Ultraviolet spectra (Unicam SP 800) of cadmium hydroxide solutions. Cadmium (2×10^{-5}M) in sodium hydroxide solutions of molarity (a) 0.001M, (b) 0.003M, (c) 0.01M, (d) 0.03M, (e) 0.1M. Solid lines, unsettled solutions; broken lines, settled solutions; pathlength 10mm.

absorption was noted for the remaining unsettled solutions, but differences in the spectra were evident. The spectral features are illustrated in fig 3.27.

The most important findings of these experiments, however, were that (1) there was no significant absorption for

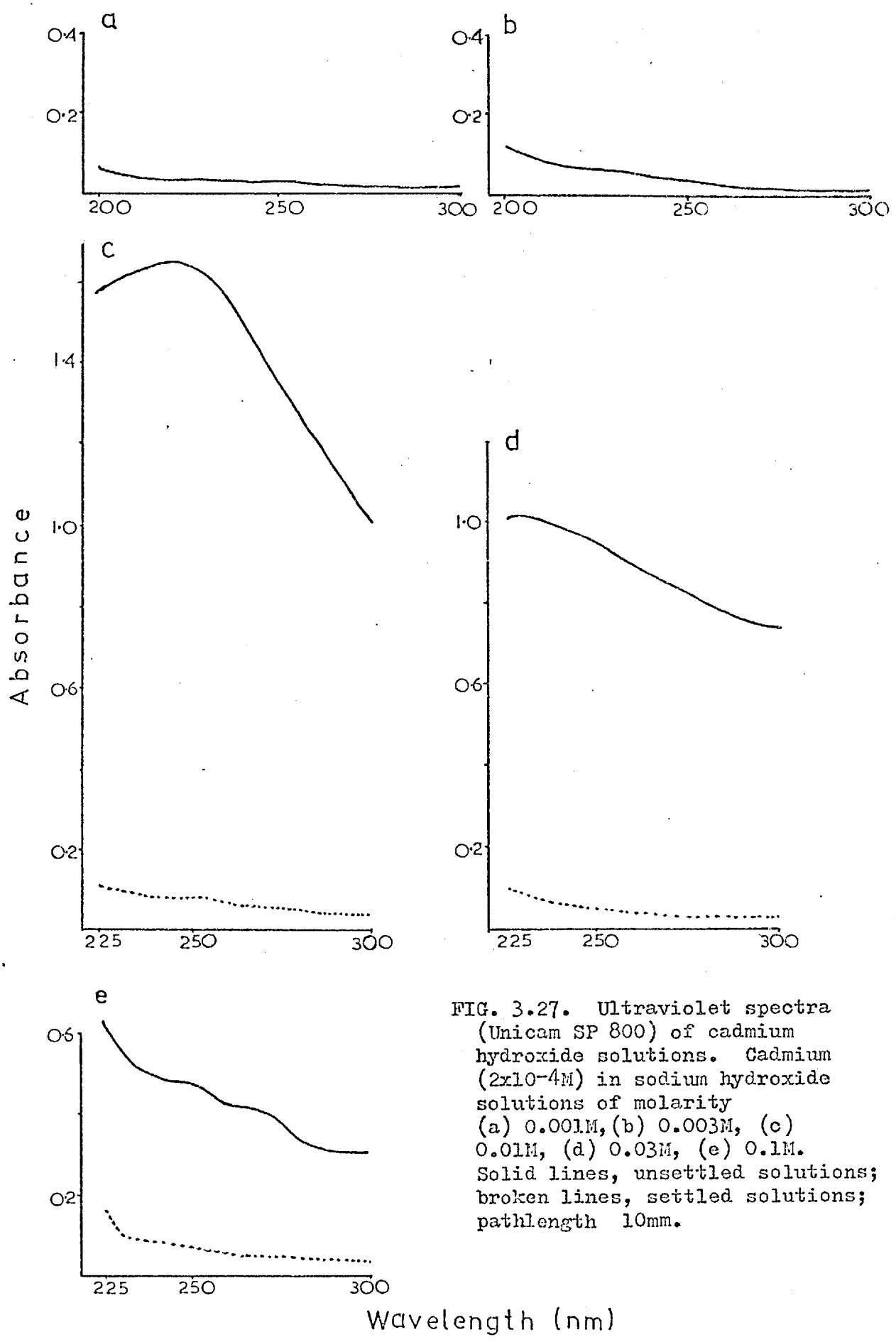

FIG. 3.27. Ultraviolet spectra (Unicam SP 800) of cadmium hydroxide solutions. Cadmium (2×10^{-4}M) in sodium hydroxide solutions of molarity (a) 0.001M, (b) 0.003M, (c) 0.01M, (d) 0.03M, (e) 0.1M. Solid lines, unsettled solutions; broken lines, settled solutions; pathlength 10mm.

any of the clear settled solutions (aged overnight) and (2) the original spectra were restored when the scan was made on the unsettled solution containing precipitate. This indicated that soluble complexes such as $Cd(OH)^{+}$, $Cd(OH)_2$, $Cd(OH)_3^{-}$ and $Cd(OH)_4^{2-}$ did not exhibit significant ultraviolet absorption. Comparison of the result in table 3.5 with the corresponding spectra reveals that absorption was only recorded for those solutions in which cadmium hydroxide particles were produced.

This study demonstrates that the absorption signals measured in the spectroelectrochemical experiments previously described were caused by fine precipitated particles of cadmium hydroxide. This conclusion is also applicable to those cadmium studies performed by Sadeghi[6], Tyson[3,4] and Hogarth[7] where in the case of the former two workers soluble hydroxy complexes, particularly $CdOH^{+}$, were thought to be responsible.

3.4.2. Calibration for chemically prepared cadmium hydroxide

The analytical growth curve recorded for electrogenerated cadmium hydroxide (fig 3.25) should be duplicated for the chemically prepared precipitate and thus provide confirmation of the previous conclusion. Standard cadmium solutions ($5\mu gml^{-1}$ - $200\mu gml^{-1}$) were prepared containing various concentrations of sodium hydroxide solution (0.01M, 0.001M, 0.00075M). After thorough mixing of the solutions, the ultraviolet scan

Table 3.5. Visual description of chemically prepared cadmium hydroxide solutions.

Hydroxide Concentration(M)	Cadmium Concentration $2x10^{-5}M$	$2x10^{-4}M$
0.001	Clear solution Small precipitate	Clear solution No precipitate
0.003	Clear solution Small precipitate	Clear solution No precipitate
0.01	Clear solution Small precipitate	Cloudy solution Precipitate
0.03	Clear solution Small precipitate	Cloudy solution Precipitate
0.1	Clear solution Small precipitate	Cloudy solution Precipitate

was recorded and the absorbance at 220nm was noted, due correction being made for the blank solution absorbance. The calibration curves presented in fig 3.28 indicate that the range of linearity is approximately the same for curves b and c, that is 0 - 40μgml^{-1}, while linearity is only observed up to 20μgml^{-1} for curve a. For curves a and b, the absorbance then tends to level off and approach the x-axis. This behaviour is very similar to that obtained electrochemically: initially there is sufficient hydroxide to enable the concentration of precipitate to increase in a regular manner providing a linear analytical growth curve. Eventually, however, this condition is not met and the solution equilibria governing the reactions of cadmium and hydroxide ions favour the dissolution of precipitate and the formation of the soluble non-absorbing mono-hydroxy cadmium complex ($CdOH^+$). The calibration plot (curve c) for sodium hydroxide

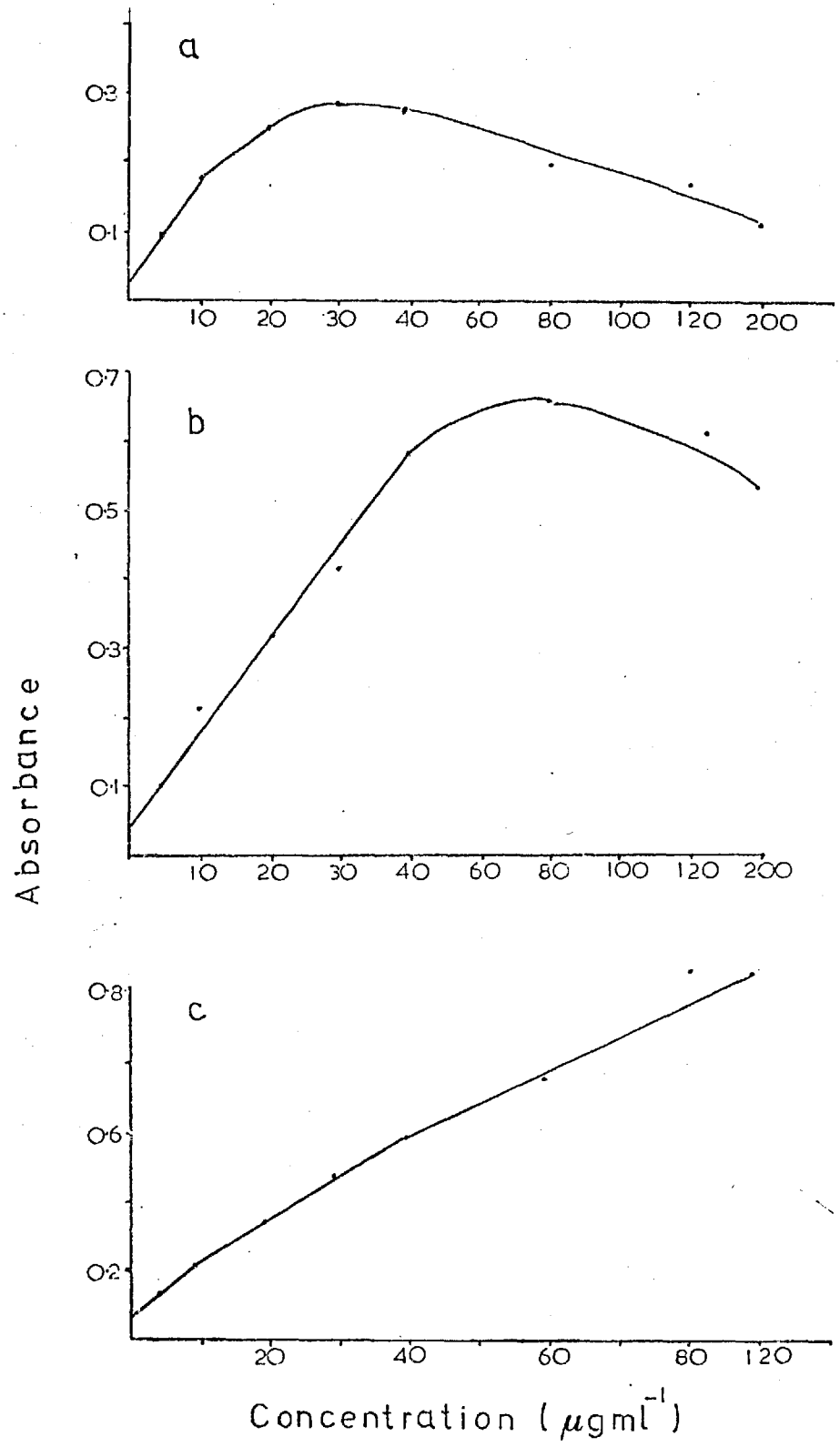

FIG. 3.28. Calibration curves for chemically prepared cadmium hydroxide solutions. Molarity of sodium hydroxide solution: (a) 7.5×10^{-4}M (b) 0.001M (c) 0.01M; absorbance measured at 220nm (Unicam SP 800); pathlength 10mm.

solution (0.01M) is linear in the range 0 to 40μgml^{-1} and then increases erratically up to 200μgml^{-1}; this behaviour indicates that there is sufficient hydroxide to maintain the continued production of precipitate with increasing cadmium ion although Beer's law is not obeyed. Insignificant absorption was recorded for the ultraviolet spectra of the clear settled solutions.

3.4.3. Absorption spectra of metal hydroxide solutions

The results for cadmium(II) suggest that the spectra reported by Tyson[4] for a number of metal ions including chromium(III), cobalt(II), copper(II), iron(II), lead(II), nickel(II) and zinc(II) were also due to precipitated metal hydroxide particles. Consideration of the solubility product values of the metal hydroxides given in table 3.6 indicates that the pH of the electrode - solution layer(pH10-11) is high enough to precipitate the ions at concentrations of 10^{-5}M.

Table 3.6.
Solubility products of metal hydroxides at 18°C or 25°C .

$Cd(OH)_2$	=	2.5×10^{-14}
$Cr(OH)_3$	=	6.3×10^{-31}
$Co(OH)_2$	=	1.6×10^{-15}
$Cu(OH)_2$	=	2.2×10^{-20}
$Fe(OH)_2$	=	8.0×10^{-16}
$Pb(OH)_2$	=	1.2×10^{-15}
$Ni(OH)_2$	=	2.0×10^{-15}
$Zn(OH)_2$	=	1.2×10^{-17}

Taken from Ref. 92.

Solutions of the above metal ions (2×10^{-5}M or 8×10^{-5}M) containing sodium hydroxide (0.001M) were prepared in a similar manner to cadmium(II). The results of a visual examination of the solutions are summarised in table 3.7 while the spectra of the metal hydroxide solutions before and after settling are

presented in fig 3.29. The results in all cases are similar to the cadmium situation: sensitive absorption was only exhibited by the unsettled solutions, while insigificant absorption was recorded for the settled solutions. The original spectra were restored when the scan was repeated on the aged and thoroughly mixed solution containing precipitate. Although no precipitate was visibly noticeable for cobalt, the differences in spectra suggest that very fine precipitated particles were formed, possibly of colloidal dimensions.

Table 3.7. Description of chemically prepared metal hydroxide solutions.

Cr ($2x10^{-5}$M)	precipitate
Co ($2x10^{-5}$M)	no precipitate
Cu ($8x10^{-5}$M)	brown precipitate
Fe ($2x10^{-5}$M)	orange suspension
Pb ($8x10^{-5}$M)	precipitate
Ni ($8x10^{-5}$M)	precipitate
Zn ($8x10^{-5}$M)	precipitate

Hydroxide concentration (0.001M).

This study demonstrates once again that the precipitated metal hydroxide particles were most probably responsible for light absorption and soluble metal hydroxy complexes of the type $M(OH)_x$ can largely be discounted as possible absorbers.

3.4.4. Light scattering considerations and graphical analysis of absorption spectra

The experiments have demonstrated that precipitation of metal hydroxides occurs at the working electrode and these particles scatter and absorb the incident radiation. It is possible that the decrease in light transmission during

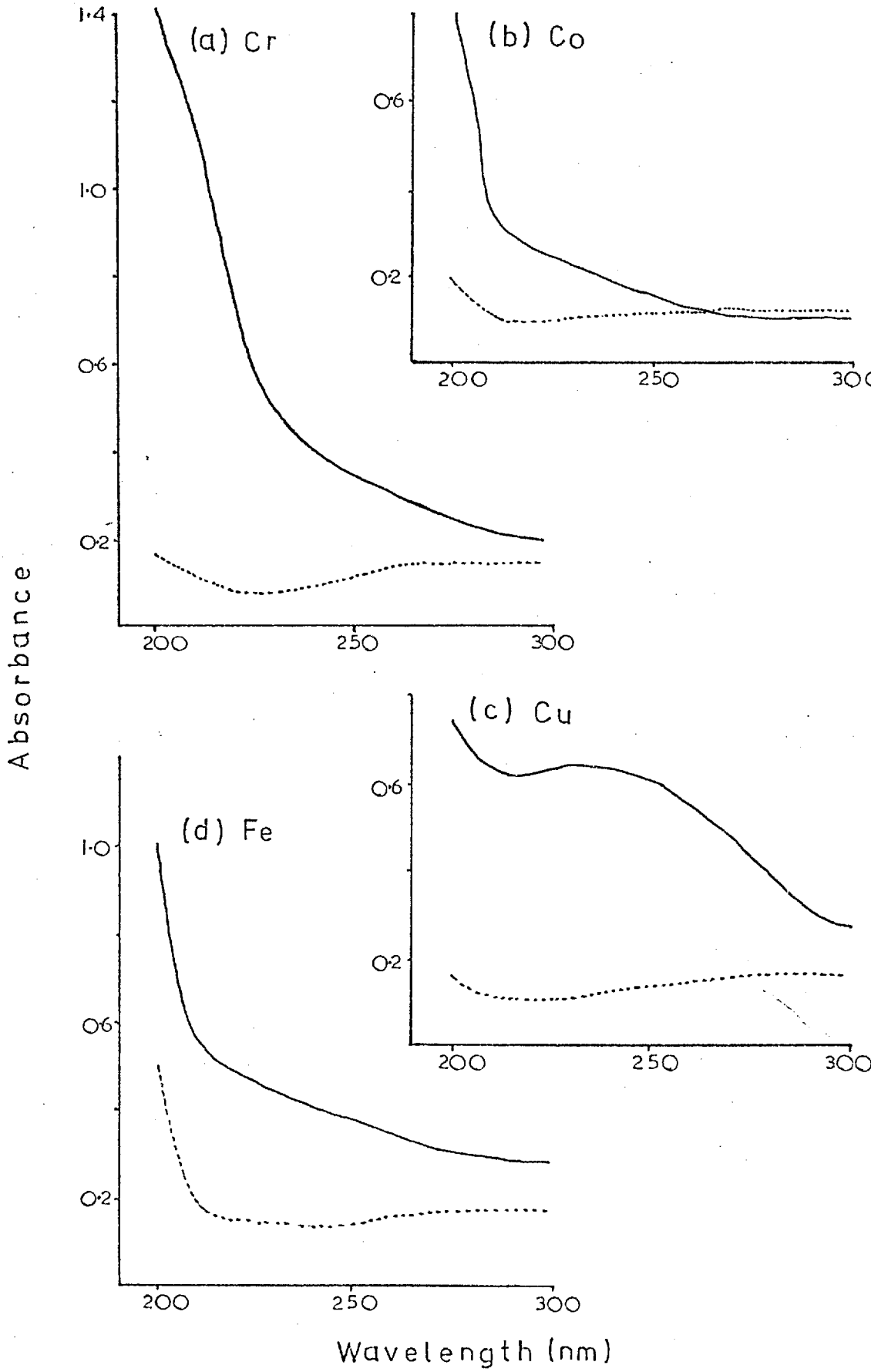

FIG. 3.29. Ultraviolet spectra (Unicam SP 800) of metal hydroxide solutions. Metal ion (2×10^{-5}M or 8×10^{-5}M) in sodium hydroxide solution (0.001M); (cont.)

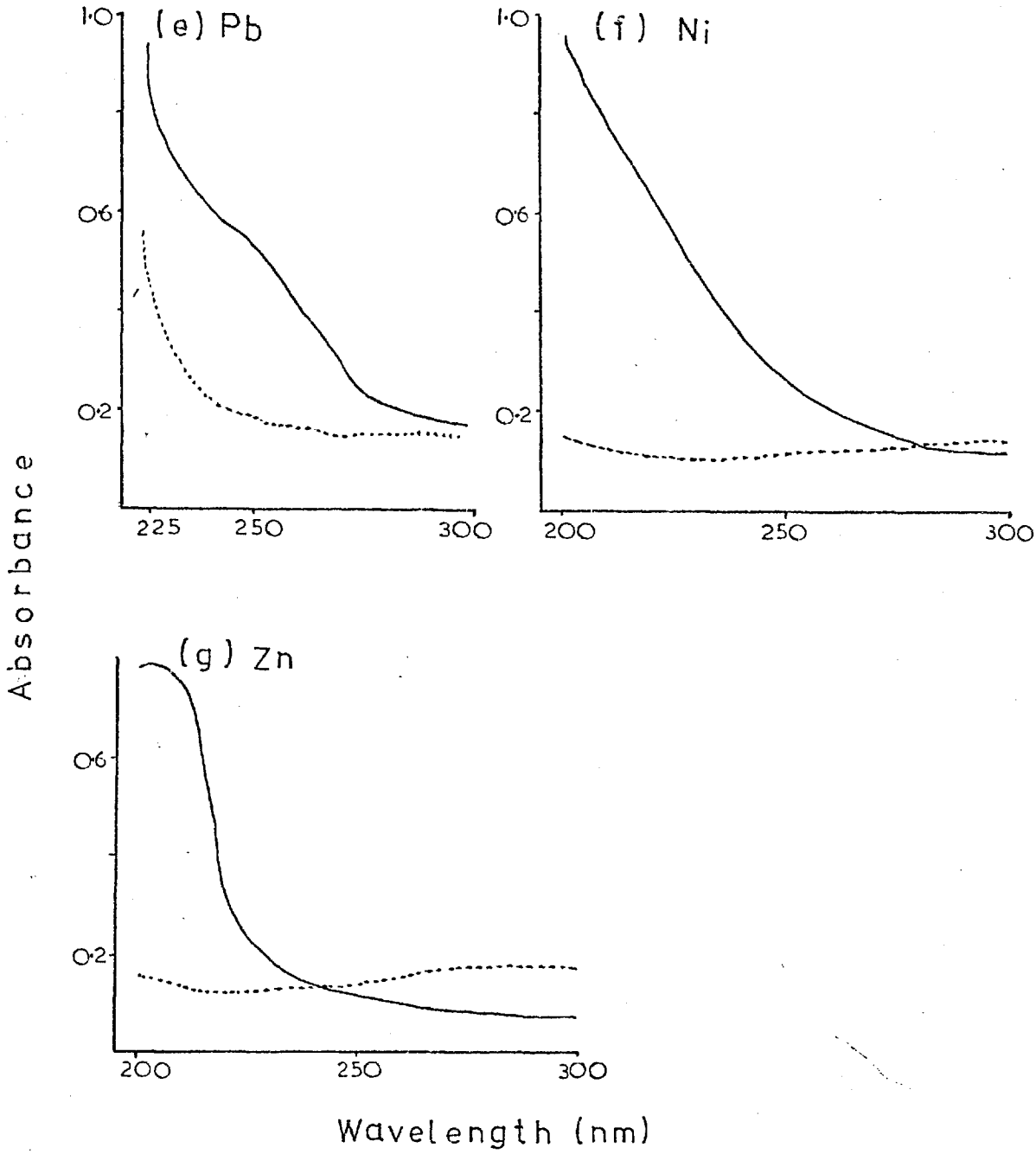

FIG. 3.29. (contd.)

(a) Cr(III) (2×10^{-5}M); (b) Co(II) (2×10^{-5}M)
(c) Cu(II) (8×10^{-5}M); (d) Fe(II) (2×10^{-5}M)
(e) Pb(II) (8×10^{-5}M); (f) Ni(II) (8×10^{-5}M)
(g) Zn(II) (8×10^{-5}M);

solid line, unsettled solution; broken line; settled solution; pathlength 10mm.

electrolysis is also caused by light scattering. The measurement of such scattered signals is in fact the basis of the nephelometric and turbidimetric techniques which enable the solids content of dilute suspensions to be determined.

Before describing a procedure purported to distinguish between true absorption and apparent absorption (scatter), it is necessary to consider briefly the effect of particle size on the properties of scattered light. The intensity and spatial distribution of scattered light generally depends on the size and shape of the particles. Rayleigh scattering is observed for dissolved ions or molecules where the particle sizes are much less than the wavelength of light (particle diameter $< \lambda/20$); the intensity of the scattered radiation is inversely proportional to the 4th power of the wavelength. As the size of the particle exceeds about $\lambda/20$, interference effects become increasingly significant and the simple Rayleigh theory no longer applies. Various equations have been derived by Rayleigh, Gans and Mie to describe the scattering properties of such systems but a discussion of this complex subject is outside the scope of the thesis. Instead the reader should refer to the review paper on light scattering by Billmeyer[93] which provides an introduction to the topic. Particles of colloidal dimensions (1nm - 100nm) exhibit Tyndall scattering, but there is no simple intensity - wavelength relationship; the Mie theory predicts scattering to vary irregularly with wavelength.

Clearly, the metal hydroxide particles would not exhibit Rayleigh scattering since the particle dimensions are colloidal

(1nm - 100nm) and/or in the fine particle size range (10^{-5}cm - 10^{-3}cm). The latter size range is of course supported experimentally by the visual observation of precipitate, prepared electrochemically and chemically (except cobalt), and also by the fact that the chemically prepared particles settled on standing. Particles of colloidal dimensions would, however, exist during the growth of precipitate.

It seemed appropriate, therefore, to examine the recorded absorption spectra with a view to determining whether the metal hydroxide particles were exhibiting true absorption or scatter or both. Actually it is not easy to distinguish between the two. The turbidimetric equation

$$I = I_o \exp(-\tau l) \text{ and } \log\frac{I_o}{I} = \frac{\tau l}{2.3}$$

which describes the decrease in light intensity in passage through a sample of length l and turbidity, τ, is of comparable form to the Beer-Lambert law

$$I = I_o \exp(-2.3\ \epsilon l c) \text{ and } \log\frac{I_o}{I} = A = \epsilon l c.$$

For unit pathlength, the apparent or true absorbance depends only on the concentration of the scattering or absorbing species respectively and is independent of the incident light intensity. A further complication is that certain colloidal suspensions, for example silver sulphide and lead chromate, selectively absorb light in addition to scattering it[94].

A graphical procedure has been used by Heller and Vassy[95] to indicate the presence of true absorption in systems exhibiting Tyndall spectra. The equation

$$-\log K = C + n\log\lambda$$

where K is an absorption coefficient, C is a constant and n is the wavelength exponent, was proposed to characterise the spectrum if nothing but the wavelength was varied. Values of n (very much) greater than 4 were reported to indicate the presence of true absorption whereas values between 0 and 4 were attributed to scatter; also as n approached zero, the particle size increased. If true absorption was absent then n = 4 was indicative of Rayleigh scattering. The procedure has been applied to indicate the presence of strong absorption in iron oxide solutions at wavelengths less than 550nm and also for the determination of particle sizes in gelatin and polystyrene solutions [95,96].

The spectra of cadmium hydroxide particles (prepared electrochemically and chemically), metal hydroxide particles and electrogenerated hydroxide were analysed according to the graphical method. The calculated "n" values for a number of spectra are listed in table 3.8 while representative $\log A^{*}$ - $\log \lambda$ plots for hydroxide absorption and electrogenerated cadmium hydroxide are presented in fig 3.30 to illustrate the graphical technique. The graph for the hydroxide spectrum (fig 3.15c) yielded two large "n" values of opposite sign, -40 and +140, as expected for a system undergoing true absorption. The "n" values (-8.3 and -13.3) for electrogenerated cadmium hydroxide (fig 3.23b) were also significantly greater than 4 and indicated the presence of absorption. Referring to table 3.8,

* Absorbance is assumed proportional to K in the Heller - Vassy equation.

Table 3.8. n values for logA - logλ plots for spectra of metal hydroxides and hydroxide ion.

Spectrum	Metal ion concentration	Hydroxide ion concentration	n value(s)	Location of spectrum
Electro-generated OH^-	-	-	-40, +140	fig 3.15a
Electro-generated $Cd(OH)_2$	$2x10^{-5}M$	-	-8.3,-13.3	fig 3.23b
Electro-generated $Cd(OH)_2$	$50\mu gml^{-1}$	-	-4.0,+16.7, -3.2	fig 3.10
$Cd(OH)_2$	$2x10^{-5}M$	0.01M	-8.7,-6.0	fig 3.26c
$Cd(OH)_2$	$2x10^{-4}M$	0.01M	-2.8	fig 3.27c
$Cr(OH)_3$	$8x10^{-5}M$	0.001M	-6.7	fig 3.29a
$Co(OH)_2$	$2x10^{-5}M$	0.001M	-6.7	fig 3.29b
$Cu(OH)_2$	$8x10^{-5}M$	0.001M	-0.9,-8.0	fig 3.29c
$Fe(OH)_2$	$2x10^{-5}M$	0.001M	-3.0,-10.0	fig 3.29d
$Pb(OH)_2$	$8x10^{-5}M$	0.001M	-13.3	fig 3.29e
$Ni(OH)_2$	$8x10^{-5}M$	0.001M	-9.2	fig 3.29f
$Zn(OH)_2$	$8x10^{-5}M$	0.001M	-25.0	fig 3.29g

an absorption band for the electrogenerated particles in the visible region (about 626nm) is indicated since analysis of the spectrum (fig 3.10) yielded "n" values of opposite sign. Values of n less than 4 and signifying scatter were also obtained for cadmium hydroxide spectra; this was particularly true for cadmium solutions of concentration $10^{-4}M$ and greater. Also the analysis of the spectra of aged solutions where particle size growth would have occurred resulted in a lowering of n relative to the freshly prepared solution. The results for the metal hydroxide solutions signified the presence of absorption, but in some cases ($Cu(OH)_2$, $Fe(OH)_2$) scatter was also indicated.

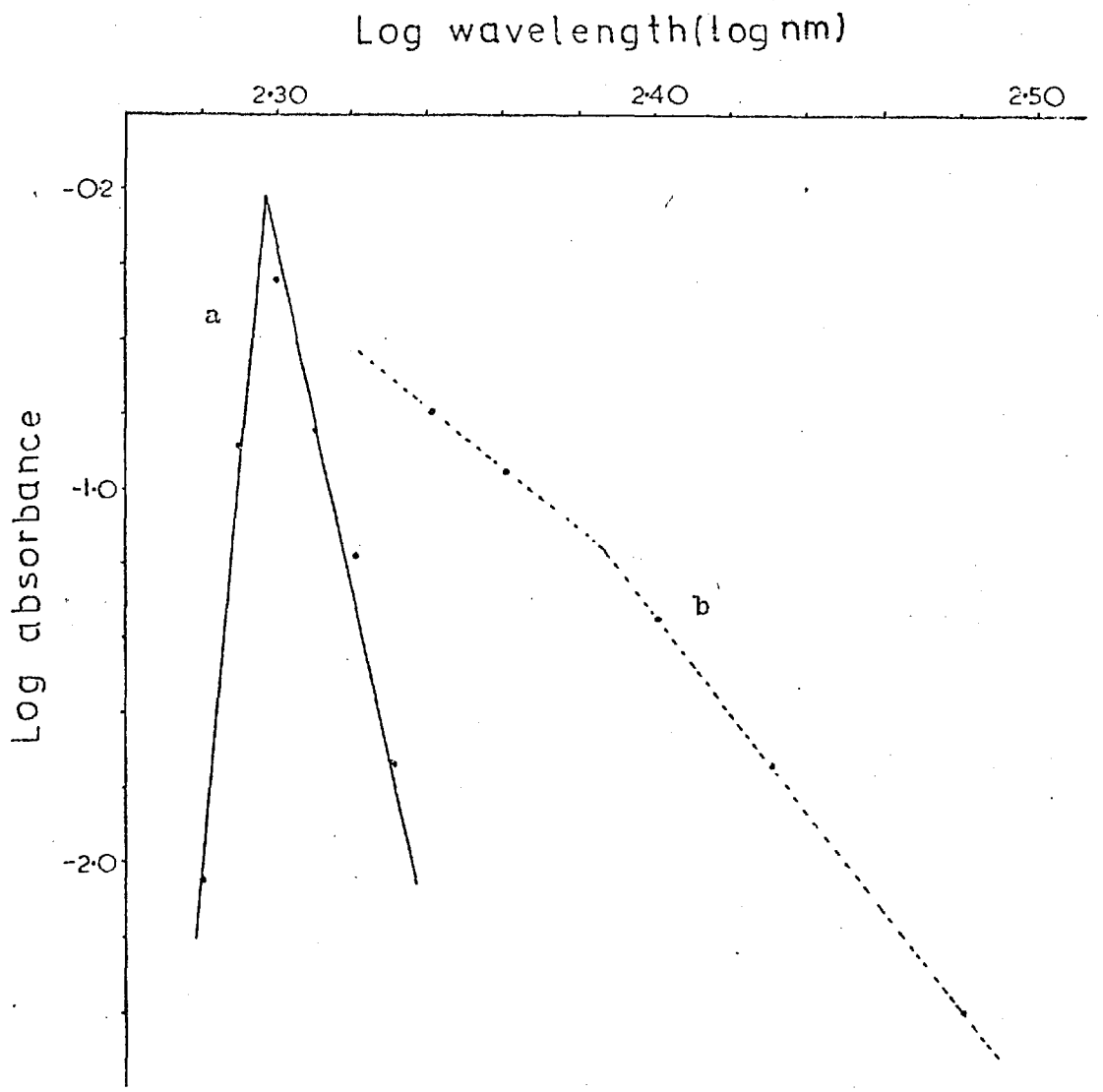

FIG. 3.30. Log absorbance versus log wavelength for (a) electrogenerated hydroxide ion (fig. 3.15(c)) and (b) electrogenerated cadmium hydroxide (fig. 3.23(b)).

Judging the results as a whole it would seem that the method is valid for indicating the presence of absorption and/or scatter in systems composed of colloidal or fine particles. It must be remembered, however, that since scatter signals were recorded for precipitated cadmium hydroxide particles in the fluorescence measurements, the presence of scatter cannot be ruled out from the above metal hydroxide systems with "h" values greater than 4.

3.5. Conclusions

The studies have demonstrated that during the electrolysis of dilute cadmium solutions precipitated cadmium hydroxide particles were generated when the cathode - solution layer became alkaline. Alkalinity at the cathode, depending on experimental conditions, arose from (1) reduction of dissolved oxygen, (2) reduction of platinum surface oxide and (3) the hydrogen evolution reaction. The particles caused light scattering, but they also exhibited sensitive absorption and the measurement of such signals may be used for analytical determinations. Although reproducible generation was achieved, there would not appear to be any analytical advantage in employing electrogeneration, save for convenience, since the absorption characteristics (spectra and calibration curves) of the particles were duplicated for chemical preparation. Further, lack of selectivity in the reaction between hydroxide ion with metal ions would make the technique unattractive for general application.

The spectroelectrochemical technique was shown to be suitable for monitoring the course of electrochemical reactions, providing new and important spectroscopic information on the reduction products of platinum surface oxide and dissolved oxygen. *In situ* monitoring during the respective reduction reactions indicated that hydroxide ion was produced in preference to hydrogen peroxide. This kind of study assists in the understanding of electrode reaction mechanisms.

CHAPTER 4 Studies with Potassium Ferrocyanide and o-Tolidine

4.1. Introductory Remarks

Potassium ferrocyanide and o-tolidine were used to indicate the analytical potential of spectrally monitoring electrogenerated species formed as a direct result of an electrode reaction. They serve as model compounds since (1) their electrochemical behaviour is well-characterised and (2) the absorption spectra of the respective oxidation products are significantly different from the parent compound to enable interference - free monitoring at an appropriate wavelength. Studies with potassium ferrocyanide were primarily concerned with comparing the experimental absorbance - time results for chronoamperometric and chronopotentiometric oxidations with the respective Beer's law-type relationships. In the case of o-tolidine, the experiments were designed to illustrate the potential of the technique for the determination of organic compounds at the trace level and the experimental procedures to be adopted when performing spectroelectrochemical investigations of new compounds.

4.2. Experimental Details

The silica cuvette containing the platinum unit described in section 2.2.2 was employed exclusively in this work. Electrolysis was carried out at constant voltage or controlled potential using the Chemtrix function generator. Current - potential curves using micro-platinum wire as working electrode were also obtained with the Chemtrix source.

A pretreatment process for the electrode was adopted. This conisted of soaking the wire in nitric acid ($50\%VV^{-1}$), rinsing with distilled water and finally "holding" at -0.1V vs SCE with pulses(3) of short duration (~1s). This procedure provided an non-oxidised platinum surface with little adsorbed hydrogen.

Solution preparation

Potassium ferrocyanide. Standard solutions of potassium ferrocyanide were prepared containing potassium sulphate (0.03M) as background electrolyte.

o-tolidine. Stock o-tolidine solution ($1000\mu gml^{-1}$ and 0.01M) was prepared by dissolving the appropriate weight of the compound in acetic acid solution (0.5M) containing a few drops of glacial acetic acid and adjusting the volume to 100ml. Standard solutions in either perchloric acid (0.5M) or hydrochloric acid (0.5M) as background electrolyte were prepared by diluting the stock solution with acetic acid (0.5M).

4.3. Potassium Ferrocyanide

The quantitative basis of the spectroelectrochemical experiment [1] is provided by the equation derived by combining Beer's and Faraday's law

$$A = \varepsilon l Q/nFV \qquad (1)$$

and relates the absorbance of electrogenerated product to the quantity of charge passed in the electrode reaction. Before analysing the respective absorbance responses for chronoamperometric and chronopotentiometric oxidations of potassium ferrocyanide, the spectroelectrochemical behaviour of the ferro-ferricyanide system

$$Fe(CN)_6^{4-} - \bar{e} \rightleftharpoons Fe(CN)_6^{3-}$$

is presented.

4.3.1. Voltammetric behaviour

The current - potential curve for potassium ferrocyanide (0.001M) in potassium sulphate solution (0.03M) recorded during a cyclic sweep (0V to 0.6V to 0V vs SCE at $29mVs^{-1}$) is given in fig 4.1. Well-developed anodic (Ep= 0.25V) and cathodic (Ep= 0.16V) waves were obtained and the peak separation* of 90 mV indicated near-reversibility for the one-electron redox reaction. To ensure the maximum absorption response for *in situ* monitoring of electrogenerated ferricyanide, potentials greater than 0.25V vs SCE should be selected.

4.3.2. Absorption spectrum of ferricyanide

The ultraviolet-visible spectrum of potassium ferri-

* For an electrochemically reversible (fast) electrode reaction the difference in peak potentials for the anodic and cathodic processes is given by the relationship[97]

$$Ep(a) - Ep(c) = 0.059/n .$$

cyanide solution (10^{-4}M) given in fig 4.2 (solid line) and recorded on the Unicam SP 800 instrument shows two prominent absorption peaks at 305nm and 420nm. Potassium ferrocyanide solution (10^{-4}M) did not absorb in the wavelength region investigated.

The spectrum of electrogenerated ferricyanide (broken line) is also included in fig 4.2.

Signals at the appropriate wavelength were obtained by monitoring, at the anode, the decrease in light transmission during the application of a step voltage (-0.9V to 1.5V) to potassium ferrocyanide solution (0.001M) containing background electrolyte; fresh sample solution was used for measurement at each wavelength.

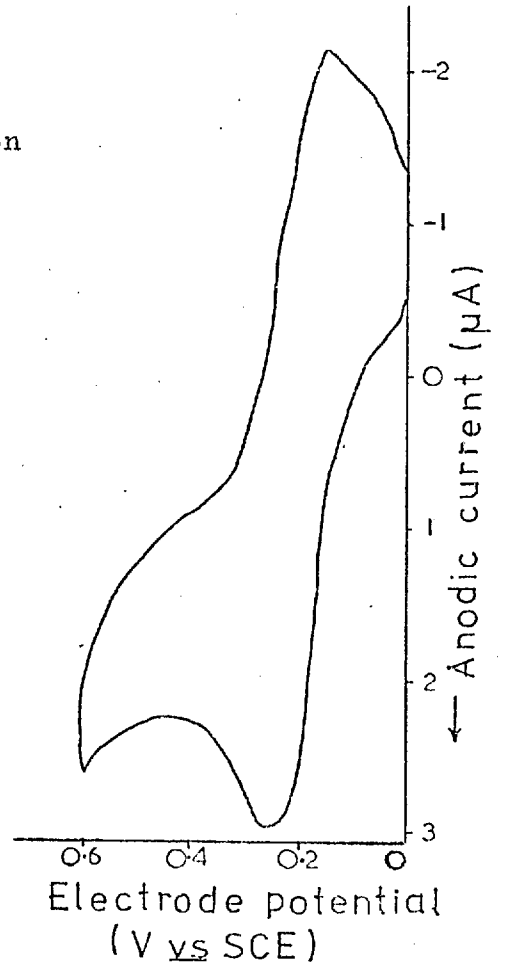

FIG. 4.1. Current - potential curve for ferrocyanide during cyclic sweep. Potassium ferrocyanide (0.001M) in potassium sulphate solution (0.03M); scan rate 29mVs^{-1}; working electrode, platinum wire.

Insertion of the absorbance value at 420nm (broken line) into the Beer's law equation provided an estimate of the optical pathlength of the cell ($A = 0.4, \varepsilon = 1020, C = 0.001M$). The value, 4mm, was in approximate agreement with the length of the platinum electrode (5mm) and validates the calculations of the provious chapter concerning hydroxide generation at the

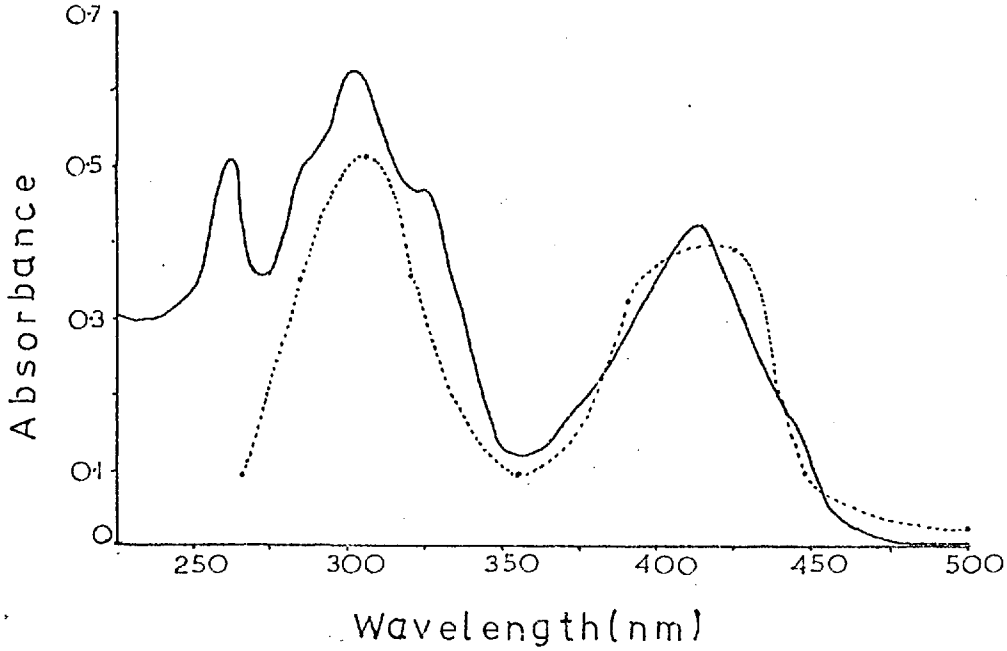

FIG. 4.2. Absorption spectrum of ferricyanide. Solid line (Unicam SP 800), potassium ferricyanide solution (10^{-4}M); path length, 40mm. Broken line, potassium ferroxyanide (10^{-3}M) in potassium sulphate solution (0.03M) during electrolysis (+1.5V).

cathode - solution layer.

4.3.3. Absorption monitoring during cyclic sweep

In experiments similar to that described in section 3.3.6, the absorption/current - potential curves were recorded simultaneously for potassium ferrocyanide (0.001M) in potassium sulphate solution (0.03M) during a cyclic sweep (0V to 0.6V to 0V *vs* SCE at 16mVs^{-1}) of the platinum working electrode. The response is shown in fig 4.3. It can be seen that the increase in absorption (broken line) at 305nm follows closely behind the increase in sweep current (solid line) until the reaction becomes diffusion-controlled whereupon the absorption begins to level-off. When the potential reaches a point where the reduction of ferricyanide occurs, as evidenced by the increase in cathodic current, the absorption decreases to a low value. This kind of study utilising

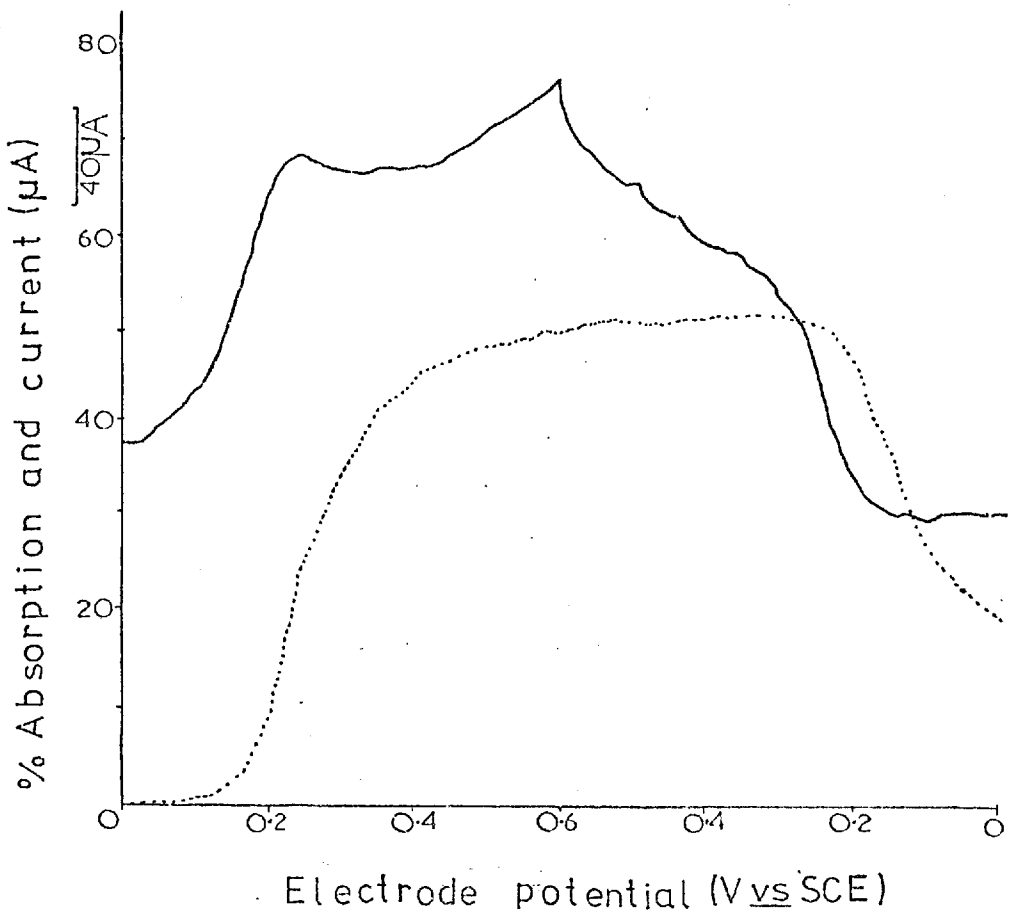

FIG. 4.3. Absorption and current response for ferrocyanide during cyclic sweep. Potassium ferrocyanide (0.001M) in potassium sulphate solution (0.03M); solid line, current; broken line, absorption; monitoring wavelength 305nm; scan rate 16mVs^{-1}.

simultaneous current and absorption monitoring provides convincing though qualitative evidence that the spectrally observed product is the direct result of the electrode reaction.

4.3.4. Absorption monitoring during chronoamperometry

Chronoamperometry involves the application of a potential step to the working electrode and monitoring the resultant current as a function of time. The potential is of sufficient magnitude to oxidise/reduce completely the electroactive material in the immediate area of the electrode. For a reversible electrode reaction, the instantaneous current flowing is controlled by the

rate of diffusion of electroactive material to the electrode surface and is given by the Cottrell equation[97]

$$i = nFac(D/\pi t)^{\frac{1}{2}} \qquad (2)$$

where i is the current(A), F is Faraday's constant (96493C), n is the number of electrons involved in the electrode reaction, a is the electrode area (cm^2), C is the bulk concentration (Mml^{-1}), D is the diffusion coefficient (cm^2s^{-1}) and t is the time (s). Integration of the Cottrell equation with respect to time provides the chronoamperometric charge - time expression

$$Q = 2nFac(Dt/\pi)^{\frac{1}{2}} \qquad (3)$$

and when substituted in equation (1) yields tho corresponding absorbance - time expression,

$$A = \frac{\varepsilon l 2ac(Dt)^{\frac{1}{2}}}{\pi^{\frac{1}{2}}V} \qquad (4)$$

For the arrangement where the light beam is directed normal to the electrode surface, (as in transmission experiments of Kuwana) the equation reduces to

$$A = \frac{2}{\pi^{\frac{1}{2}}}\varepsilon c(Dt)^{\frac{1}{2}} \qquad (5)$$

where c is the concentration (ML^{-1}). The change in concentration units arises from elimination of the terms l(cm), a(cm^2) and V(L). The equation predicts that for a reversible reaction under semi-infinite linear diffusion (SILD) control, the absorbance of the electrogenerated product is directly proportional to the square root of time. A graph of A versus $t^{\frac{1}{2}}$ should, therefore, be a straight line and evaluation of the gradient enables parameters such as ε or D to be determined. This type of analysis has been

performed by Kuwana[11]. Linearity of A versus $t^{\frac{1}{2}}$ and also incidentally i versus $t^{-\frac{1}{2}}$ serves to check whether linear diffusion conditions are being maintained during electrolysis. For the situation where the light beam is parallel to the electrode surface the absorbance will not increase indefinitely, but will approach a steady-state level since diffusing material will eventually reach solution not sampled by the light beam. The absorbance - time expression

$$A = \frac{\varepsilon l 2c(Dt)^{\frac{1}{2}}}{\pi^{\frac{1}{2}}w} \qquad (6)$$

where l, the electrode length, is assumed equal to the optical pathlength and w is the light beam width, may be valid for the short period in which the diffusing product fills up the width of the light beam.

Results

The absorption/current - time curves at 420nm were recorded for the potential-step oxidation (-0.05V to 0.40V vs SCE) of potassium ferrocyanide solution (0.001M) containing potassium sulphate (0.03M). The current - time curve was also recorded for the background electrolyte solution alone and this enabled a correction for the background current to be made. The absorbance response curve given in fig 4.4 gradually approaches a constant level and is consistent with a steady-state concentration profile of ferricyanide being established within the width of the light beam. Inspection of the curve for $t^{\frac{1}{2}} < 2s$ reveals a linear relationship between absorbance and the square root of time suggesting adherence to equation (6). A rough check on the

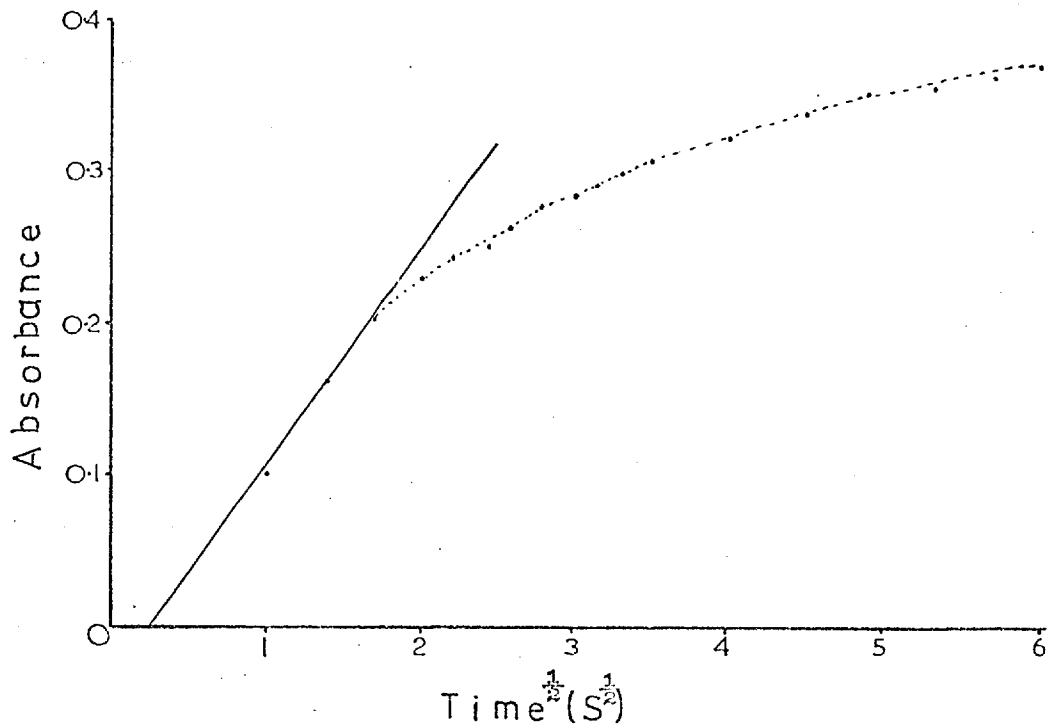

FIG. 4.4. Absorbance - time response for ferrocyanide during chronoamperometric oxidation. Potassium ferrocyanide(0.001M) in potassium sulphate solution (0.03M); monitoring wavelength 420nm; potential step, -0.05V to 0.40V vs SCE.

validity of the equation was possible by determining the gradient of the absorbance - time graph and through the relationship

$$\text{gradient} = \varepsilon l 2cD^{\frac{1}{2}}/w\pi^{\frac{1}{2}}$$

(ε = 1020, l = 0.5(cm), c = 0.001M, $D^{\frac{1}{2}} = 2.55\times10^{-3}$, $\pi^{\frac{1}{2}} = 1.77$)

calculating the width of the light beam, w. A result of 1.2mm was obtained and this is a sensible value.

The current - time measurements were used to determine whether linear diffusion conditions were maintained during electrolysis. The necessary results are presented in table 4.1 which also includes the absorbance values. According to the Cottrell equation, the product "$it^{\frac{1}{2}}$" should be constant for linear diffusion conditions; also linearity of the i versus

Table 4.1. Current - time and absorbance - time results for chronoamperometric oxidation of ferrocyanide.

i_t (μA)	i_{bl} (μA)	i (μA)	t (s)	$t^{\frac{1}{2}}$ ($s^{\frac{1}{2}}$)	$t^{-\frac{1}{2}}$ ($s^{-\frac{1}{2}}$)	$it^{\frac{1}{2}}$ ($\mu As^{\frac{1}{2}}$)	Absorbance
260	124	136	1	1	1	136	0.10
204	104	100	2	1.4	0.71	140	0.16
184	98	86	3	1.73	0.58	149	0.20
172	92	80	4	2.0	0.50	160	0.22
162	90	72	5	2.23	0.45	161	0.24
154	88	66	6	2.45	0.41	162	0.25
149	87	62	7	2.64	0.38	164	0.26
144	86	58	8	2.83	0.35	164	0.27
142	85	57	9	3.00	0.33	171	0.28
139	84	55	10	3.16	0.32	174	0.29
136	83	53	11	3.32	0.30	176	0.30
132	82	49	12	3.46	0.29	171	0.30
124	80	44	16	4.00	0.25	176	0.32
118	78	40	20	4.47	0.22	179	0.34
114	76	38	24	4.9	0.20	186	0.35
111	74	37	28	5.29	0.19	196	0.35
108	73	35	32	5.66	0.18	198	0.36
106	71	35	36	6.00	0.17	210	0.37
103	70	33	40	6.32	0.16	208	0.37
101	70	31	44	6.33	0.16	196	0.38
100	68	32	48	6.93	0.14	222	0.39
98	68	30	52	7.21	0.14	216	0.40
97	68	29	56	7.48	0.13	217	0.39

Potassium ferrocyanide (0.001M) in potassium sulphate solution (0.03M); potential step, -0.05V to 0.40V vs SCE; i_t, total current; i_{bl}, current for potassium sulphate solution (0.03M) alone; $i = i_t - i_{bl}$; Absorbance at 420nm.

$t^{-\frac{1}{2}}$ plot should be observed. Inspection of column 7 in table 4.1 shows that there is a gradual increase in the "$it^{\frac{1}{2}}$" product indicating non-adherence to exact linear diffusion conditions. This is not surprising since, generally, shielded horizontal electrodes are required before constant values can be obtained. The text by Adams[97] may be consulted for a discussion of this subject. An approximate straight-line relationship was, however,

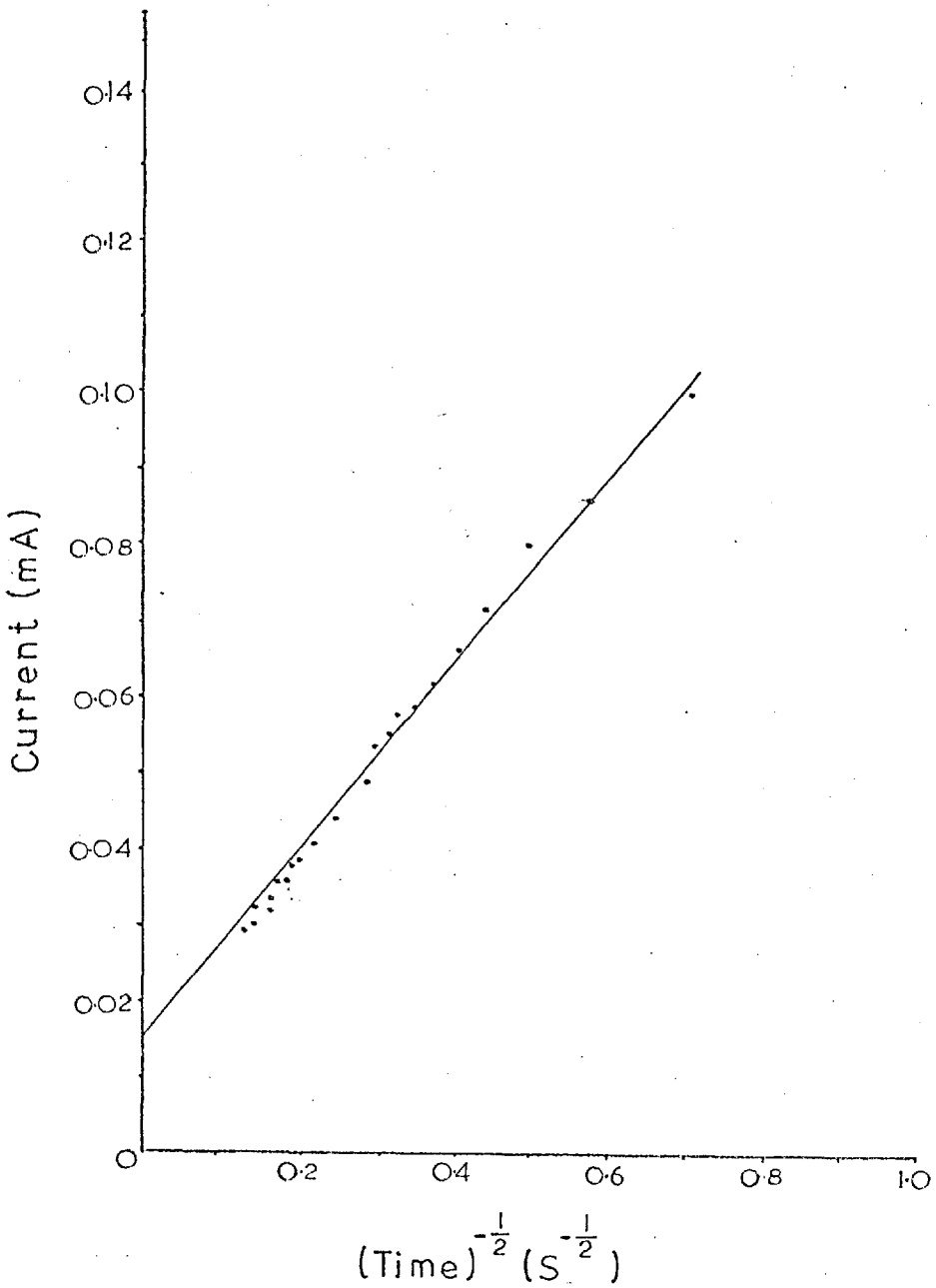

FIG. 4.5. Current versus the reciprocal square root of time for ferrocyanide during chronoamperometric oxidation. Potassium ferrocyanide (0.001M) in potassium sulphate solution(0.03M); potential step, -0.5V to 0.40V vs SCE.

observed for the i versus $t^{-\frac{1}{2}}$ graph which is given in fig 4.5 and indicates that approximate linear diffusion conditions were established at the vertical platinum electrode.

The gradient value of the i versus $t^{-\frac{1}{2}}$ plot, 0.13×10^{-3}, enabled the electrochemical area of the electrode to be calculated from the expression, gradient = $nFacD^{\frac{1}{2}}/\pi^{\frac{1}{2}}$ ($n = 1$, $F = 96493C$, $c = 10^{-6}(Mml^{-1})$, $D^{\frac{1}{2}} = 2.55 \times 10^{-3}$, $\pi^{\frac{1}{2}} = 1.77$). The area, a, was found to be $0.93cm^2$ and this compares favourably with the geometric area of $0.8cm^2$. Generally, agreement between the electrochemical and geometric areas would be unusual.

4.3.5. Absorption monitoring during chronopotentiometry

The chronopotentiometric technique involves the measurement of the working electrode potential versus time during constant current electrolysis under linear diffusion control. Application of a constant current to the electrolysis cell causes the surface concentration of the most readily oxidised/reduced species to decrease and eventually become zero. At this point the potential of the working electrode is forced to a value where another reaction can accommodate the current (in the case of ferrocyanide oxidation this would be oxidation of water). The time taken to reach this sharp change in working electrode potential is termed the transition time (τ) and is given by the Sand equation[97]

$$\tau^{\frac{1}{2}} = \frac{\pi^{\frac{1}{2}} nFaD^{\frac{1}{2}} c_b}{2i} \qquad (7)$$

where i is the current density (μAcm^{-2}), c is the bulk concentration of reactant (mML^{-1}), n is the number of electrons involved in the electrode reaction, F is Faraday's constant (96,493C),

D is the diffusion coefficient ($cm^2 s^{-1}$) and a is the electrode area (cm^2). For the equation to be valid the function, $i\tau^{\frac{1}{2}}/c$, termed the transition - time constant, should be independent of the current density, i; also linearity of $\tau^{\frac{1}{2}}$ with concentration is predicted.

The absorbance - time expression for chronopotentiometry is

$$A = \frac{\varepsilon l i t}{nFV} \qquad (8)$$

since for constant - current electrolysis the charge-time expression is simply the product of the current and time. This equation is for a light beam directed normal to the electrode surface and a linear variation of absorbance with time can be expected. The expression is only valid, however, up to the transition time (τ) since after this, 100% current efficiency with respect to ferrocyanide oxidation is not achieved. Beyond the transition time, the concentration of ferrocyanide at the electrode surface is zero and the rate of oxidation is governed by the rate of diffusion of the reactant to the electrode surface. The situation becomes identical to chronoamperometry with the current and absorbance having a square root dependence on time. The departure from linearity on the absorbance - time graph provides a value for the transition time and this method has been demonstrated by Kuwana[11].

For an analysing beam projected parallel to the electrode surface the absorbance would not increase indefinitely, due to considerations outlined previously, and the absorption response

would be primarily characteristic of diffusing product filling up a light beam of finite width. Depending on the level of constant current selected, it should be possible to record an initial linear variation of absorbance with either time or the square root of time. It is unlikely that both sets of behaviour could be recorded in the manner reported by Kuwana[11] and estimation of transition times would not be possible.

Results

The absorption/potential - time curves at 305nm were recorded for controlled current oxidation of potassium ferrocyanide solution (0.001M) containing potassium sulphate (0.03M), constant current levels of 0.50mA, 0.47mA, 0.44mA and 0.39mA being selected to ensure a sensitive absorption response. The absorption - time curves are shown in fig 4.6. The absorption behaviour for current levels 0.47mA (curve b), 0.44mA (curve c) and 0.39mA (curve d) showed linearity for a certain period and then gradually approached the same steady-state level; the range of linearity and the time taken to approach the constant absorption level increased with decreasing current. This behaviour was in agreement with ferricyanide being generated under constant current conditions with absorbance initially exhibiting linear dependence on the current and time as predicted by equation (8). The absorbance - time curve for the current level of 0.50mA (curve a) was not linear and was of similar appearance to the chronoamperometric behaviour. The corresponding potential - time curves were poor in that no sharp changes in

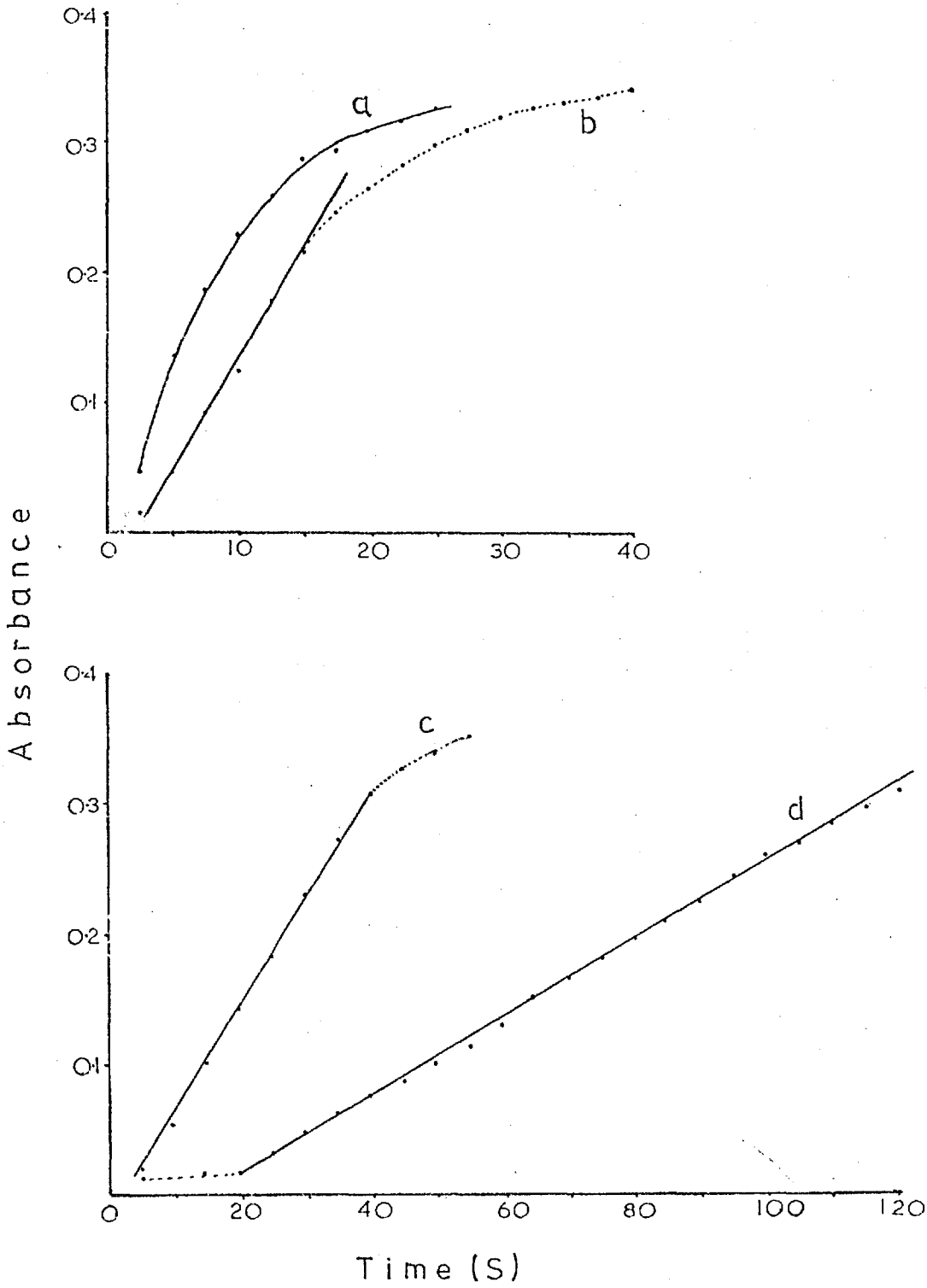

FIG.4.6. Absorbance - time response for ferrocyanide during chronopotentiometric oxidation. Potassium ferrocyanide (0.001M) in potassium sulphate solution (0.03M); monitoring wavelength 305nm; constant current levels, (a) 0.50mA, (b) 0.47mA, (c) 0.44mA, (d) 0.39mA.

potential which could be attributed to a new oxidation process occurring were noticed; estimation of the transition times was, therefore, impossible. This was not surprising since current levels were selected corresponding to transition times of less than 1s. A more rapid shift to higher potentials with increasing current was, however, noted. To determine whether the absorbance results conformed to equation (8), the experimental gradients were compared to the theoretical ones; the results are given in table 4.2.

Table 4.2. Experimental and theoretical gradient values of Absorbance - time plots for chronopotentiometric oxidation of ferrocyanide.

Current level (mA)	Gradient	
	Experimental	Theoretical
0.39	0.003	0.036
0.44	0.008	0.040
0.47	0.017	0.043

Potassium ferrocyanide (0.001M) in potassium sulphate solution (0.03M); Absorbance - time plots, fig 4.6.

The theoretical gradients were calculated from the expression $\varepsilon l i/nFV$ ($\varepsilon_{305} = 1420$; $l = 0.5$(cm); $n = 1$; $F = 96493$C; $V = a \times w = 0.08 \times 10^{-3}$L) where the volume term, V, was calculated based on a light beam width of 0.1cm. It can be seen that although the experimental values are significantly less than the calculated ones, the comparison improves as the current level rises.

A possible explanation for this effect is that side reactions, particularly surface oxide formation, which consume a portion of the electrolysis current may become less important at the higher current levels so that electrolysis efficiency with respect to

ferricyanide generation is improved.

Finally a comparison was made between the theoretical transition times, calculated from equation (7), and the values determined from the linear portion of the absorbance - time curves. The results are presented in table 4.3. The gross discrepancy between the respective $\tau^{\frac{1}{2}}$ and $i\tau^{\frac{1}{2}}/c$ values indicates that the method is not valid for estimating transition times.

Table 4.3. Theoretical and spectrally determined transition times for chronopotentiometric oxidation of ferrocyanide.

$i(\mu Acm^{-2})$	$\tau^{\frac{1}{2}}$ theor	τ theor	$i\tau^{\frac{1}{2}}/c$ theor	τ abs	$\tau^{\frac{1}{2}}$ abs	$i\tau^{\frac{1}{2}}/c$ abs
487	0.447	0.20	218	120	10.9	5308
550	0.396	0.16	218	40	6.3	3465
587	0.371	0.14	218	16	4.0	2348
625	0.348	0.12	218	11	3.3	2062

Potassium ferrocyanide (0.001M) in potassium sulphate solution (0.03M); abs, absorbance.

4.4. Experiments with o-Tolidine

The oxidation of o-tolidine (4,4'-diamino-3,3'-dimethyl-biphenyl) was studied to illustrate the potential of the spectro-electrochemical technique for trace determinations of organic compounds. o-tolidine undergoes a diffusion - controlled two-electron oxidation at pH 2 corresponding to the reaction

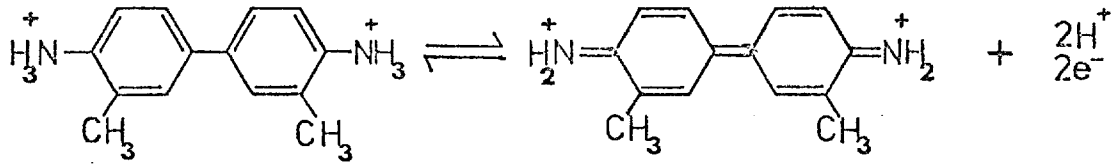

The oxidation product (quinonediimine) absorbs at 437nm with a molar extinction coefficient (ε_{437}) of 61000. At pH 4, two successive one-electron steps occur: the product of the 1st wave has been identified as a dimer and gives absorption bands at 365nm and 635nm while the product of the 2nd wave is identical to that obtained at pH 2. These reactions have provided the basis for the spectroelectrochemical studies performed by Kuwana[1,14].

Experiments were similar to initial ferrocyanide investigations, but also included a calibration study. Low pH solutions were employed to eliminate the possibility of dimer formation.

4.4.1. Voltammetric behaviour

The current - potential curve for o-tolidine solution

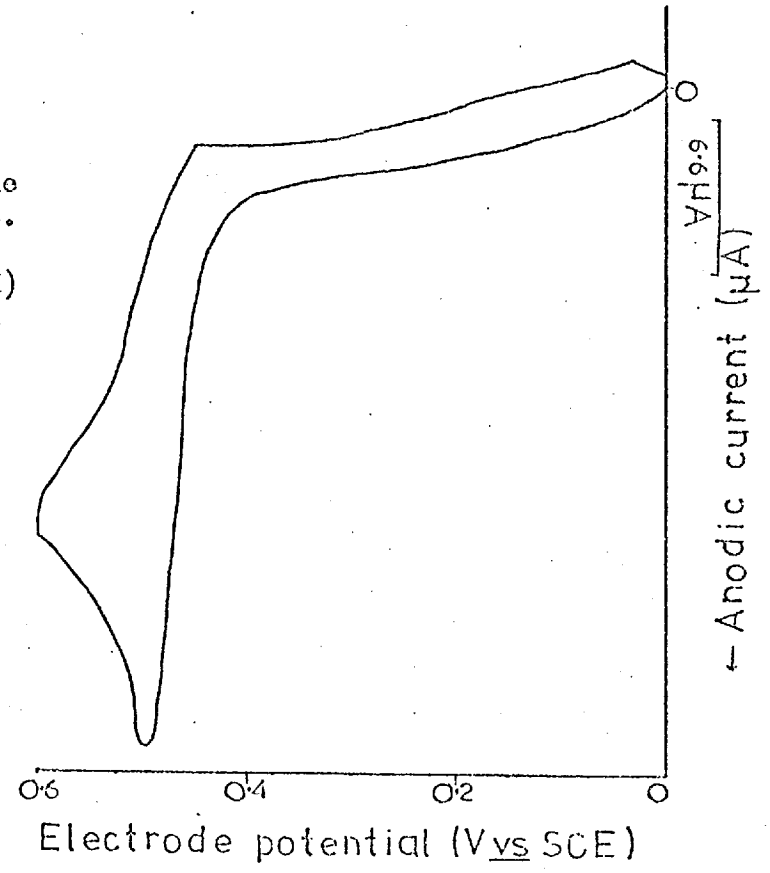

FIG. 4.7.
Current - potential curve for σ-tolidine during cyclic sweep. σ-tolidine (0.005M) in acetic acid (0.5M) and perchloric acid (0.5M); scan rate $15mVs^{-1}$; working electrode, platinum wire.

(0.005M) containing acetic acid (0.5M) and perchloric acid (0.5M) recorded for the cyclic sweep (0V to 0.6V to 0V vs SCE at $15mVs^{-1}$) is given in fig 4.7. A peak potential (E_p) of 0.50V vs SCE was recorded for the oxidative wave, but lack of a cathodic wave on the reverse scan suggested irreversible behaviour for the σ-tolidine system.

4.4.2. Absorption spectra of σ-tolidine and the oxidation product

The ultraviolet spectrum of σ-tolidine solution ($5x10^{-5}M$) containing acetic acid (0.5M) and perchloric acid (0.5M) was recorded on the Unicam SP 800 instrument with the background electrolyte solution as reference. The spectrum with a single absorption band centred around 249nm is presented in fig 4.8(a); the molar extinction coefficient (ε_{249}) was calculated to be

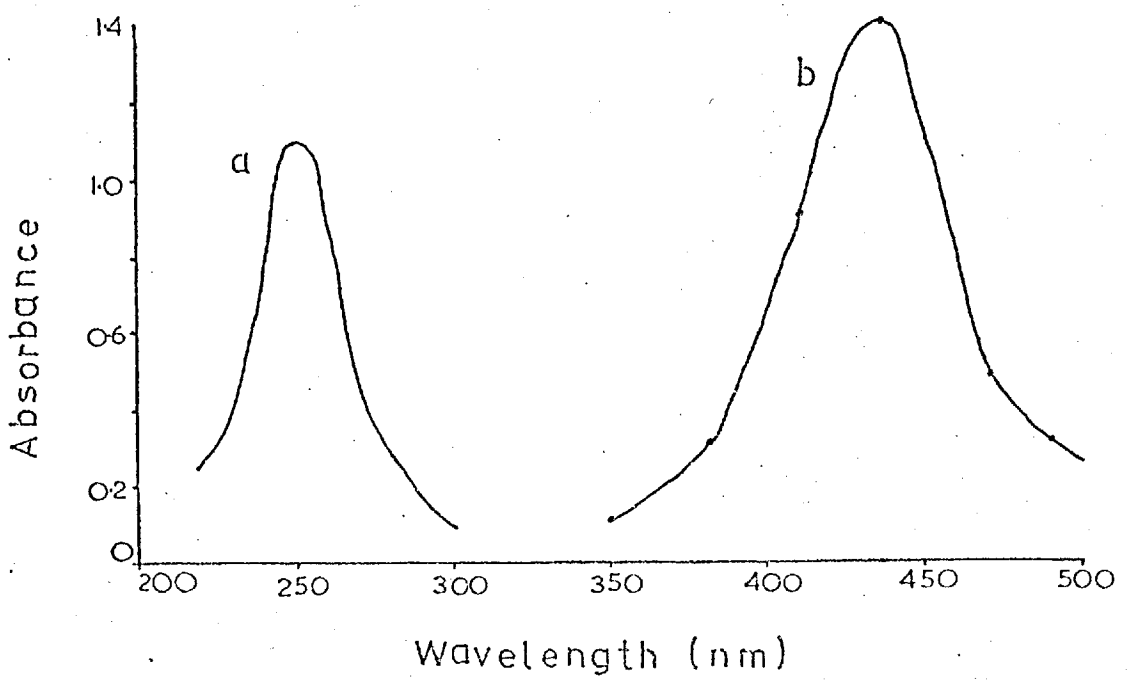

FIG. 4.8. Absorption spectra of o-tolidine and the oxidation product. (a) o-tolidine ($5x10^{-5}$M) in background electrolyte; reference, background electrolyte; pathlength, 10mm (b) o-tolidine ($5x10^{-5}$M) in background electrolyte during controlled potential electrolysis (0.75V vs SCE); background electrolyte; acetic acid (0.5M) and perchloric acid (0.5M).

20,000($LM^{-1}cm^{-1}$). The visible spectrum of the oxidation product was recorded manually for potential step oxidation (0V to 0.75V vs SCE) of o-tolidine solution ($5x10^{-5}$M) containing background electrolyte. The spectrum also given in fig 4.8(b) consists of a single band with an absorption maximum around 440nm. The molar extinction coefficient (ε_{437}) was estimated from Beer's law (assuming the optical pathlength of 5mm was applicable) and a value of 56,000 was obtained. This is in approximate agreement with the value reported by Kuwana (ε_{437}=61,000).

This simple study neatly illustrates the analytical value of the technique. A two-electron transfer reaction has resulted in the formation of a product with a large molar

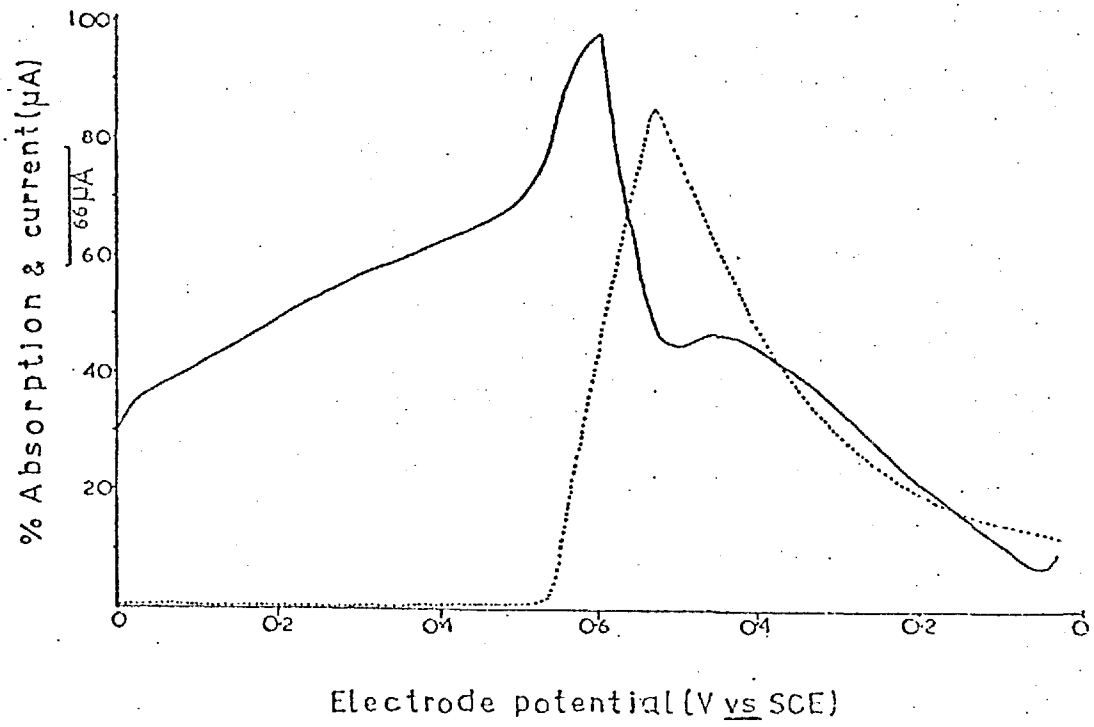

FIG. 4.9. Absorption and current response for σ-tolidine during cyclic sweep. σ-tolidine(0.005M) in acetic acid(0.5M) and perchloric acid(0.5M). Solid line, current; broken line, absorption; monitoring wavelength 437nm; scan rate 15mVs^{-1}.

extinction coefficient (ε); the high value, readily explained by the degree of conjugation existing in the structure, enables sensitive *in situ* absorptions measurements to be performed. Further, the oxidation reaction generated a new spectrum in the more accessible visible region providing additional characterisation for the σ-tolidine system.

4.4.3. Absorption monitoring during cyclic sweep

The absorption/current - potential curves were recorded simultaneously for the cyclic sweep oxidation (0V to 0.6V to 0V *vs* SCE at 15mVs^{-1}) of σ-tolidine solution (0.005M) containing background electrolyte. The response behaviour shown in fig 4.9

was similar to the ferro-ferricyanide system with the increase in absorption (broken line) coinciding with the increase in anodic sweep current (solid line) for the forward direction. On scan reversal, the absorption decreased to a low value indicating reduction of the oxidation product. The high background current associated with platinum surface oxide formation and removal is evident from the current trace. If scan rates greater than about $25mVs^{-1}$ were selected the absorption signal could not follow the current response in the anodic and cathodic reactions.

4.4.4. Calibration

The absorbance of the oxidation product at 437nm was recorded for standard o-tolidine solutions ($5x10^{-7}M$ - $2x10^{-5}M$) in acetic acid (0.5M) and hydrochloric acid (0.5M) during potential step excitation (0V to 0.6V vs SCE). Duplicate measurements were taken for each standard solution and the results are presented in table 4.4. The absorbance of electrogenerated product versus the molar concentration of o-tolidine, is given in fig 4.10. It can be seen that, for the concentration range investigated, the graph is linear in two distinct regions namely between (1) $1.25x10^{-6}M$ and $10^{-5}M$ and (2) $10^{-5}M$ and $2x10^{-5}M$. The gradients (28731, 29000) of the straight-line portions of the curve were used to determine the respective molar extinction coefficients(ε) through application of Beer's law. The values (57462 and 58000) were in reasonable agreement with the theoretical value (61000) confirming that electrogeneration, in the case of o-tolidine,

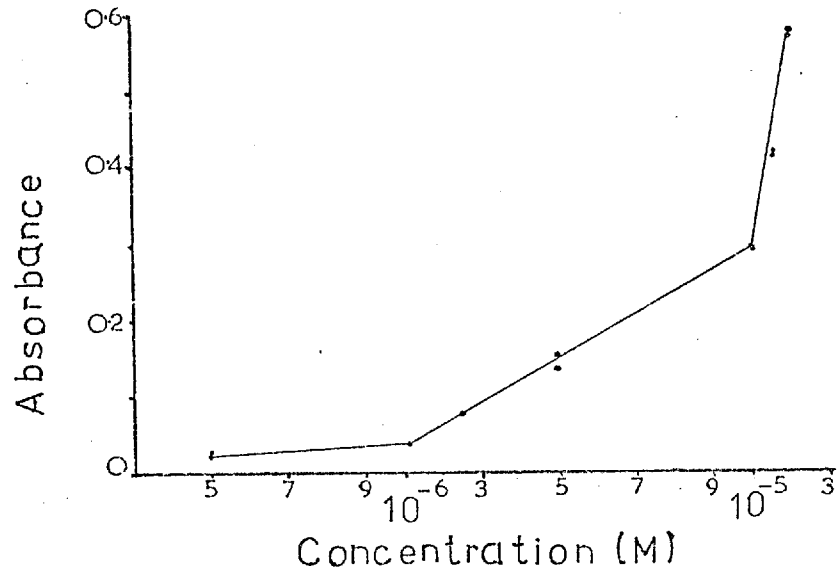

FIG.4.10. Absorbance versus σ-tolidine concentration during controlled potential electrolysis. σ-tolidine in acetic acid (0.5M) and hydrochloric acid(0.5M); electrode potential 0.6V vs SCE; monitoring wavelength 437nm.

Table 4.4. Absorbance versus σ-tolidine concentration during potential step excitation.

σ-tolidine Concentration(M)	Absorbance	
$5x10^{-7}$	0.021	0.025
$1.25x10^{-6}$	0.039	0.039
$2.5x10^{-6}$	0.075	0.072
$5x10^{-6}$	0.152	0.137
10^{-5}	0.294	0.289
$1.5x10^{-5}$	0.418	0.427
$2x10^{-5}$	0.569	0.577

σ-tolidine in acetic acid (0.5M) and hydrochloric acid (0.5M); potential step, 0V to 0.6V vs SCE; monitoring wavelength 437nm.

was a reliable procedure providing results in approximate agreement with Beer's law.

4.5. Conclusions

Potassium ferrocyanide and σ-tolidine were shown to be valuable compounds for illustrating the principles of the spectroelectrochemical experiment and checking the operating performance of the cell. Controlled potential oxidation with concurrent *in situ* monitoring provided a novel route for generating and recording the spectra of highly absorbing species and enabled sensitive and reproducible absorption measurements to be made. Such procedures should be applicable to a large number of organic compounds enabling the aquisition of new and valuable analytical information.

The absorbance behaviour for ferrocyanide oxidation, although showing initially linear dependence on time or the square root of time (depending on the excitation technique) as predicted, did not fit the spectroelectrochemical equations and evaluation of parameters by this route was unsatisfactory. The steady-state absorbance values, however, tended to agree with Beer's law and enabled the optical pathlength of the cell to be equated to the electrode length without incurring too great an error.

CHAPTER 5 Studies in Flowing Solution

5.1. Introduction

Since *in situ* absorptiometric monitoring of electrogenerated species in stationary solutions was demonstrated to have analytical potential it was decided to construct flow cells incorporating carbon fibres as the working electrode and perform similar experiments on flowing solutions. The flow cells are described in section 2.2.2. Continuous flow cells are widely used in automatic analysis systems and a possible application envisaged for the cell was as a redox unit for performing chromogenic reactions with simultaneous absorption measurement in Technicon auto-analyser systems. Another possibility was as a combined electrochemical-absorption detector in continuous flow chromatographic systems. Clearly, one important requirement for spectroscopic observation is that the desired species is produced within the short time the solution resides in the cell.

The choice of carbon fibres as the working electrode was due primarily to their suitability for incorporating into micro-cells with long optical pathlengths. Advantages of using the fibres are their large surface area which enables 100% conversion of electroactive material and ensures the maximum electrochemical and absorption response. In addition, the fibres exhibit favourable electrochemical characteristics. The electrode material is relatively new and unfortunately little published data on electroanalytical applications are available.

Das Gupta[54] found that the electrochemical behaviour of the material was comparable to other forms of carbon, such as pyrolytic graphite and glassy carbon and that the fibres suffered less from adsorption effects. A carbon fibre flow cell based on controlled potential amperometric monitoring was shown to be an extremely sensitive electrochemical detector for flowing solutions and application to environmental pollutants was demonstrated. More recently, Jennings and Pearson[98] successfully utilised a single strand of fibre as a pH indicator electrode for the determination of the end points of acid-base titrations.

For an initial appraisal of the carbon fibre flow cells, the redox reactions of ferrocyanide, o-tolidine and dissolved oxygen were investigated. Experiments in stationary solutions were also performed with Paraquat, an important herbicide.

5.2. Experimental Procedure

Sample solution was delivered to the cell at a flow rate of approximately 0.4mlmin^{-1} and the absorption response was recorded during electrolysis. Generally the micro-cell (volume ~ 70µl; path length ~ 20mm) was operated in the three-electrode mode with potentiostatic control of the working electrode while the macro-cell (volume ~ 300µl; pathlength ~ 50mm) was employed for two-electrode studies. Operating problems included light beam attenuation by air bubbles and also a drifting baseline; the latter was particularly significant for the micro-cell. The collection of experimental data was, therefore, slow and tedious and generally only single measurements were obtained for each sample. Solution preparation for potassium ferrocyanide, O-tolidine and dissolved oxygen studies was as previously described.

Current - potential curves were obtained in the Metrohm cell using a small bunch of carbon fibres as the working electrode. The electrode was prepared by inserting the fibres into narrow-bore glass tubing and sealing one end either by heat treatment or with silicone rubber sealant. Electrical connection was made by securing fine brass strip to the fibres at the opposite end of the tubing. Electrode pretreatment was not necessary.

5.3. Oxidation of Ferrocyanide

The performance of the cells was checked by monitoring electrogenerated ferricyanide. Using the macro-cell in the two-electrode mode, potassium ferrocyanide solution (0.001M) containing background electrolyte was oxidised during an electrolysis cycle of -1.6V to 1.6V and the absorption response was recorded at 305nm. The signal response was similar to previous static experiments with the platinum electrode unit, but the time to reach maximum absorbance, approximately six minutes, was longer. Although the maximum absorbance, 0.3 , was well below that expected theoretically (7.1A for l = 50mm), the experiment did confirm the suitability of the cell for monitoring in flowing solutions. Possible reasons to account for the discrepancy, assuming 100% current efficiency, were (1) an unfavourable current distribution along the carbon fibre surface which reduced the effective optical pathlength and/or (2) electrogenerated ferricyanide resided in a very narrow solution layer close to the electrode surface and only partial filling-up of the light beam thickness was achieved.

The micro-cell was employed for controlled potential studies and the absorbance at 420nm was recorded for various concentrations of potassium ferrocyanide solution (10^{-4}M - 8×10^{-4}M) during oxidation at 0.5V vs SCE. In addition, the absorbance of potassium ferricyanide solution (10^{-4}M) was recorded in the flow cell (zero applied potential) and in a standard cuvette (pathlength 20mm) on the Unicam instrument. The results are presented in table 5.1.

Table 5.1. Absorbance values for potassium ferricyanide solution and electrogenerated ferricyanide.

(a) Potassium ferrocyanide		(b) Absorbance, potassium ferricyanide (10^{-4}M)	
Concentration (M)	Absorbance	Carbon fibre cell	Standard cell
10^{-4}	0.113	0.194	0.22
$2x10^{-4}$	0.229		
$4x10^{-4}$	0.456		
$8x10^{-4}$	0.620		

Wavelength 420nm; micro-cell, pathlength approximately 20mm; flow rate 0.4mlmin^{-1}.
(a) Potassium ferrocyanide in potassium sulphate solution (0.03M); electrode potential 0.5V vs SCE.
(b) Standard cell, pathlength 20mm (Unicam SP 800).

At the 10^{-4}M level, the absorbance value for electrogenerated ferricyanide, 0.11A, was still lower than that for the standard solution, 0.19A, but there was a considerable improvement in the comparison relative to the previous result for the macro-cell. Also the larger absorbance value recorded for the standard cell (st), 0.22A, indicated that the carbon fibre cell (cf) pathlength was less than 20mm. A calculation involving Beer's law

$$l_{cf} = \frac{A_{cf} l_{st}}{A_{st}} = \frac{0.194x2}{0.22} \doteq 1.76cm$$

indicates that the actual pathlength of the carbon fibre cell was approximately 18mm. The calibration graph given in fig 5.1 shows that linearity was observed for ferrocyanide concentrations between 10^{-4}M and $4x10^{-4}$M.

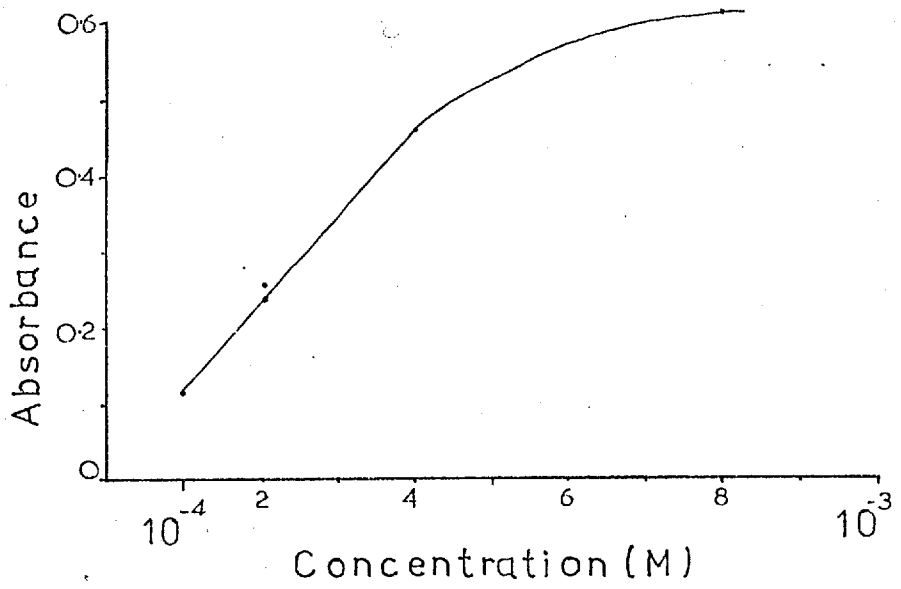

FIG. 5.1. Absorbance versus ferrocyanide concentration during controlled potential electrolysis. Monitoring wavelength, 420nm; electrode potential, 0.5V vs SCE; flow rate, 0.4ml min^{-1}; background electrolyte, potassium sulphate(0.03M).

5.4. Oxidation of σ-Tolidine

5.4.1. Voltammetric behaviour

The current - potential curve for σ-tolidine (10^{-4}M) in acetic acid (0.5M) and hydrochloric acid (0.5M) solution during a cyclic sweep (0V to 1.0V to 0V vs SCE at 125mVs^{-1}) of the carbon fibre working electrode is given in fig 5.2. Well-developed anodic (E_p = 0.48V vs SCE) and cathodic waves (E_p = 0.40V vs SCE) are apparent and the peak separation of approximately 80mV indicates a reversible two-electron oxidation process.

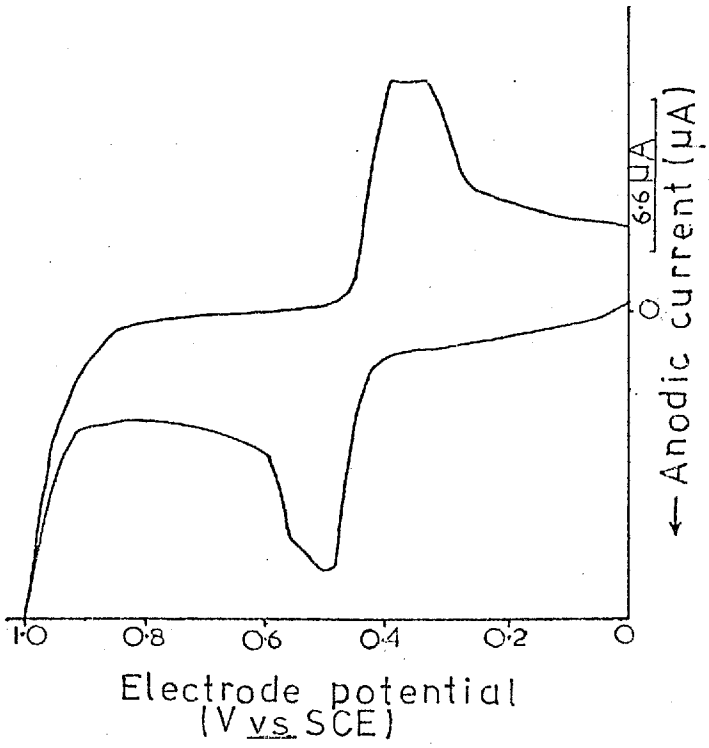

FIG. 5.2. Current - potential curve for σ-tolidine during cyclic sweep. σ-tolidine (10^{-4}M) in acetic acid (0.5M) and hydrochloric acid (0.5M); scan rate 125mVs^{-1}; working electrode, carbon fibres.

5.4.2. Absorption and current monitoring during controlled potential oxidation

The absorption and current responses were simultaneously recorded in the micro-cell during controlled potential electrolysis (0.9V vs SCE) of flowing σ-tolidine solutions ($5x10^{-7}$M - $2x10^{-5}$M). The cell was rinsed with blank solution for a period of ten minutes between each run. A typical response curve is presented in fig 5.3 for σ-tolidine ($2x10^{-5}$M); the solid line represents current and the broken line absorption. The sample solution was presented to the peristaltic pump for delivery to the cell at t = 0 and the rise in current from the steady state level (0.42μA) of the blank solution (acetic acid (0.5M) and perchloric acid (0.5M)) after approximately three minutes indicates the delay time before sample reached the cell. The steady-state current level was reached after about five minutes although for less concentrated solutions this time was reduced. One noticeable

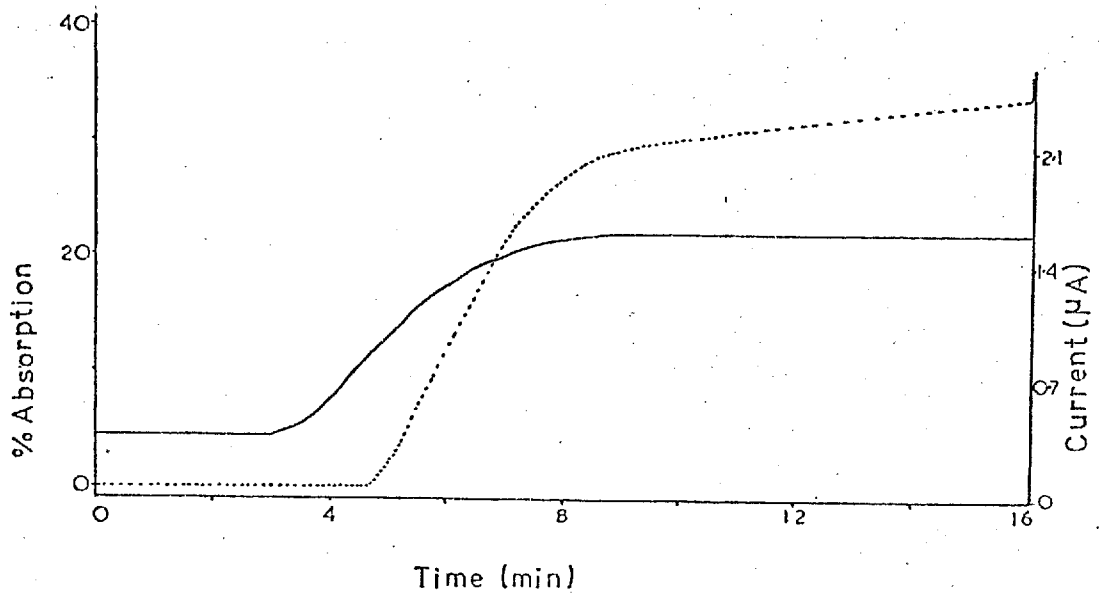

FIG. 5.3. Absorption and current response for o-tolidine during controlled potential oxidation. o-tolidine (2×10^{-5}M) in acetic acid (0.5M) and hydrochloric acid (0.5M); monitoring wavelength, 437nm; electrode potential, 0.9V vs SCE; flow rate 0.4ml min^{-1}.

and contrasting feature to previous static experiments was the time lag after the increase in oxidation current before the commencement of the absorption signal. This was probably due to the irregular and macroscopically rough surface of the carbon fibre bed (cf. smooth platinum electrode surface) which prevented the analysing light beam from sampling the electro-generated product as soon as it had formed. A steady-state absorption signal was not attained in a satisfactory time and absorbance values were calculated after nine minutes. The results of the study are given in table 5.2. while the calibration plots, current (solid line) and absorbance (broken line) respectively versus concentration, are shown in fig 5.4. The interesting

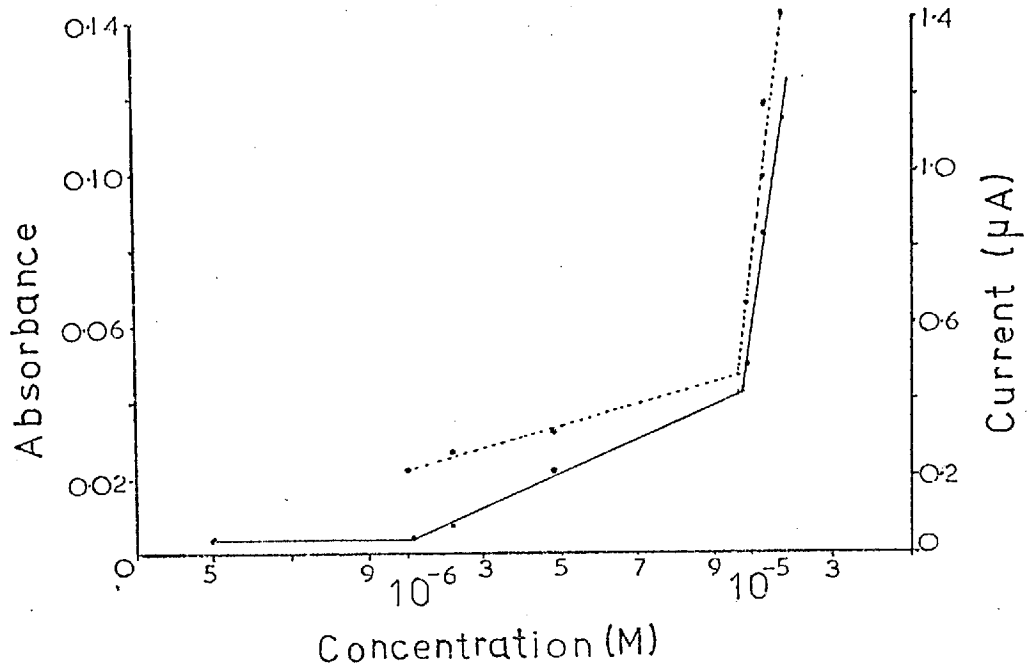

FIG. 5.4. Absorbance and current versus σ-tolidine concentration during controlled potential oxidation. σ-tolidine in acetic acid (0.5M) and hydrochloric acid (0.5M); monitoring wavelength, 437nm; electrode potential, 0.9V vs SCE; flow rate 0.4ml min^{-1}.

Table 5.2. Absorbance and current results for σ-tolidine solutions during controlled potential electrolysis.

σ-tolidine concentration(M)	Current(μA)	Absorbance
$5.0x10^{-7}$	0.03	0
$1.2x10^{-6}$	0.03	0.022
$2.4x10^{-6}$	0.07	0.027
$5.0x10^{-6}$	0.21	0.031
$1.0x10^{-5}$	0.49	0.060
$1.5x10^{-5}$	0.84	0.100
$2.0x10^{-5}$	1.14	0.140

Micro-cell, path length approximately 20mm; σ-tolidine in acetic acid (0.5M) and perchloric acid (0.5M); monitoring wavelength 437nm; electrode potential 0.9V vs SCE; flow rate 0.4mlmin^{-1}; current (0.42μA) due to background electrolyte was subtracted.

feature of the calibration curves is the similar dependence of the analytical signals on concentration with linearity being observed in two distinct concentration regions.

The spectroelectrochemical equation governing the flow system was obtained by combining the Beer-Lambert law with the current expression for the controlled potential amperometric technique[54]

$$i = nFuc \qquad (1)$$

where i is the current (A), u is the flow rate (mls^{-1}), c is the concentration (Mml^{-1}) and the remaining terms are defined as previous. Elimination of the concentration terms in both equations yields the absorbance expression

$$A = \frac{\varepsilon l i 10^3}{nFu} \qquad (2)$$

for the flow cell which predicts that the absorbance is directly proportional to current (i) and inversely proportional to the flow rate (u). To check the validity of the equation, the absorbance - current graph was plotted for values corresponding to the linear portion of the absorbance and current calibration curves and the experimental value of the gradient was compared to theory. The graph is shown in fig 5.5 and the gradient was found to be 0.109×10^{-6}. The value for the theoretical gradient calculated from the expression

$$\text{Gradient}_{theor} = \frac{\varepsilon l 10^3}{nFu} \qquad (3)$$

where $\varepsilon = 61000$ (cm), $l = 1.76$, $n = 2$, $F = 96493C$ and $u = 0.0066$ (mls^{-1}) came to 0.084×10^{-6}. This comparison is surprisingly good and indicates that essentially all the electro-generated product was sampled by the light beam. Discrepancy between the experimental absorbance (0.14) and the theoretical

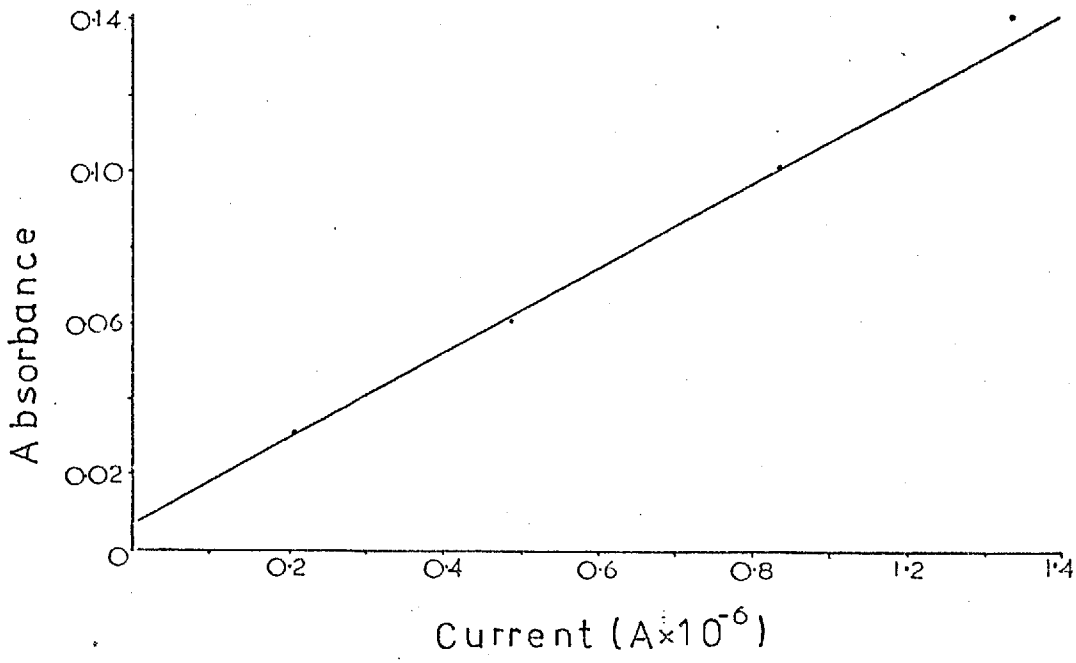

FIG. 5.5. Absorbance versus current for o-tolidine during controlled potential oxidation. o-tolidine (5×10^{-6}M, 10^{-5}M, 1.5×10^{-5}M, 2×10^{-5}M) in acetic acid (0.5M) and hydrochloric acid (0.5M); monitoring wavelength, 437nm; electrode potential 0.9V vs SCE; flow rate 0.4mlmin^{-1}.

value (2.15) at a concentration of 2.0×10^{-5}M was, however, still significant.

5.5. Reduction of Dissolved Oxygen

The reduction of dissolved oxygen on carbon fibre was investigated to see whether this electrode material produced results similar to platinum. Evidence for hydrogen peroxide formation at carbon electrodes which was mentioned earlier in section 1.2 was reported by Davis and co-workers[71].

Potassium sulphate solution (0.03M) was delivered to the macro-cell at a flow rate of $0.4 ml min^{-1}$ and the absorption signal for the product of dissolved oxygen reduction was recorded at various wavelengths during application of a step voltage (-2V). The ultraviolet spectrum is given in fig 5.6 and it bears a strong resemblance to that of hydrogen peroxide (fig 3.16b). To confirm and also to obtain a quantitative determination of the hydrogen peroxide concentration, titanium(IV) solution was delivered to the carbon fibre cell. A similar test for hydroxide ion was performed with phenolphthalein solution.

5.5.1. Quantitative test for hydroxide ion

Direct comparison of the absorbance values at 200nm for dissolved oxygen reduction with standard sodium hydroxide solutions (section 3.3.5) was not possible in this study since absorption of hydrogen peroxide would interfere. It was, therefore, necessary to employ a colorimetric acid-base indicator for the measurement of the hydroxide concentration[62,63]. Previous experiments by Tyson[4] indicated that phenolphthalein absorption at 552nm was sensitive to the pH of the solution and the absorbance values provided an accurate measure of the pH.

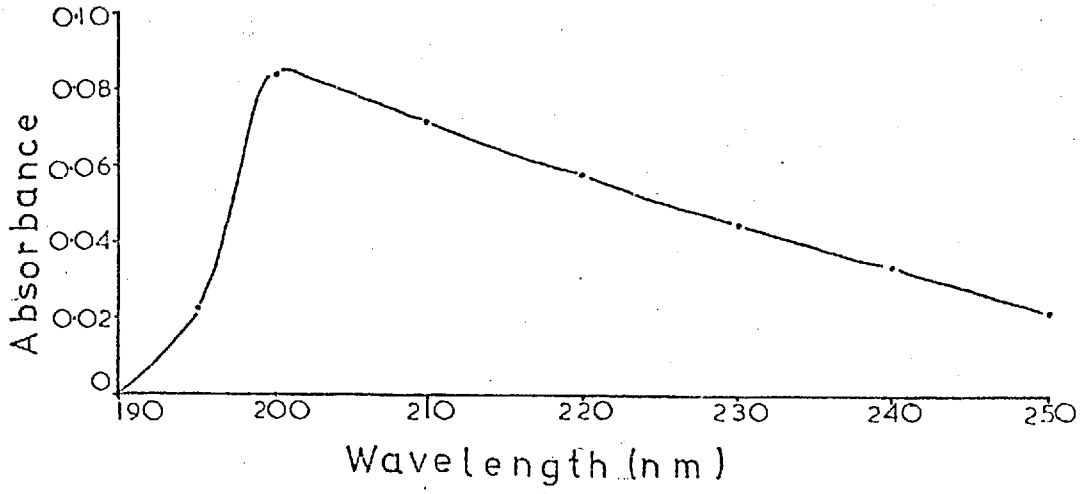

FIG. 5.6. Ultraviolet spectrum of the product for dissolved oxygen reduction. Solution, potassium sulphate (0.03M); flow rate 0.4mlmin^{-1}; applied voltage, -2V.

Procedure

The macro-cell was first calibrated by flowing through, consecutively, phenolphthalein solutions (10μgml^{-1} in potassium sulphate (0.03M)) containing various concentrations of sodium hydroxide at zero applied volts and noting the absorption at 552nm. The absorption recorded during electrolysis (-2V) of

Table 5.3. Effect of hydroxide ion concentration on the absorption of phenolphthalein solution.

Sodium hydroxide Concentration(M)		% Absorption (522nm)
(a)	5×10^{-5}	18
	10^{-4}	73
	5×10^{-4}	100
(b)	Electrogenerated Hydroxide	76

Macro-cell, pathlength approximately 50mm; monitoring wavelength 522nm; flow rate 0.4mlmin^{-1};
(a) phenolphthalein (10μgml^{-1}) containing sodium hydroxide in potassium sulphate solution (0.03M).
(b) phenolphthalein (10μgml^{-1}) in potassium sulphate solution (0.03M) at -2V.

an identical phenolphthalein solution, but without added sodium hydroxide was next recorded. The results are given in table 5.3 and since the electrogenerated value is in approximate agreement with the absorption at the 10^{-4}M level, it was decided that a hydroxide concentration of 10^{-4}M would be the most appropriate. This value is probably an underestimate of the actual hydroxide concentration in the electrode - solution layer since previous comparisons have established that the absorbance of electrogenerated product is always less than that for the standard solution. Further caution should be exercised since phenolphthalein is electroreducible[55] and a reduction reaction would destroy the acid-base properties of the indicator.

5.5.2. Quantitative test for hydrogen peroxide

The reaction of titanium(IV) with hydrogen peroxide in aqueous solution produces an orange-red complex with an absorption maximum centred around 405nm[99]. A determination of the concentration of electrogenerated hydrogen peroxide was made by comparing the absorbance of the electrogenerated complex with the values of standard solutions. Titanium(IV) solutions ($700\mu gml^{-1}$) in potassium chloride (0.1M) and containing hydrogen peroxide (0.001M and 0.005M) were delivered to the macro-cell at zero volts and the absorption values recorded. Next the absorption of the titanium - peroxo complex resulting from electrogeneration of hydrogen peroxide was recorded during electrolysis (-2V) of a flowing solution of titanium(IV) containing potassium chloride (0.1M). The appropriate results are given in table 5.4.

Table 5.4. The effect of hydrogen peroxide concentration on the absorbance of titanium(IV) - peroxo complex.

Hydrogen peroxide Concentration (M)		Absorbance
(a)	0.001	0.16
	0.005	0.66
(b)	Electrogenerated	0.10

Macro-cell, pathlength approximately 50mm; monitoring wavelength 405nm; flow rate $0.4 ml min^{-1}$.
(a) Titanium ($700 \mu g ml^{-1}$) containing hydrogen peroxide in potassium chloride solution (0.1M).
(b) Titanium ($700 \mu g ml^{-1}$) in potassium chloride (0.1M) at -2V.

A determination of the concentration of hydrogen peroxide at the electrode-solution layer was obtained by extrapolation of the calibration curve constructed from the two absorbance values for the standard solutions; the approximate hydrogen peroxide concentration was found to be $9 \times 10^{-5} M$.

In addition to the consideration mentioned for the hydroxide comparison, the validity of the peroxide result depends on a number of other factors which were not investigated. It was assumed that (1) colour development was complete within the cell residency time, (2) hydroxide ion did not effect the formation and stability of the peroxo complex and (3) the concentration of titanium(IV) was not significantly altered by reduction.

5.6. Reduction of Methyl Viologen

The final study with the carbon fibre cell concerned the compound methyl viologen (1,1'-dimethyl-4,4'-bipyridylium cation), better known as Paraquat, a very effective herbicide used extensively for weed control. Of the number of methods proposed for its determination the solution spectrophotometric method of Calderbank[100] is particularly sensitive. The basis of the method is the chemical reduction of methyl viologen in alkaline medium by sodium dithionite to give a deep-blue coloured solution of the free radical species with subsequent absorption measurement at 396nm (ε=38000) or at 600nm (ε=9000).

Spectroelectrochemical investigations of the compound have been performed by Kuwana[1]. In aqueous medium, methyl viologen undergoes a pH-independent reversible one-electron reduction at the dropping mercury electrode (DME) giving the free radical cation; the half-wave potential ($E_{\frac{1}{2}}$) is -0.68V vs SCE. A second wave at -1.1V vs SCE shows irreversibility due to the insolubility of the fully reduced neutral species. The reduction waves correspond to the reactions

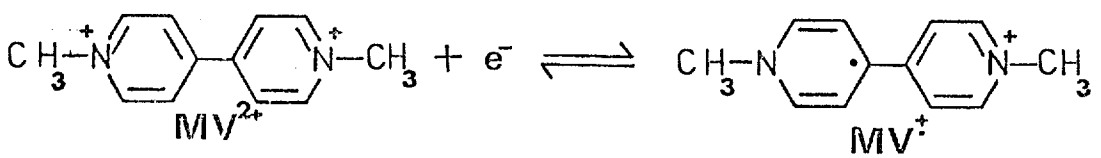

MV^{2+} $MV^{+\cdot}$

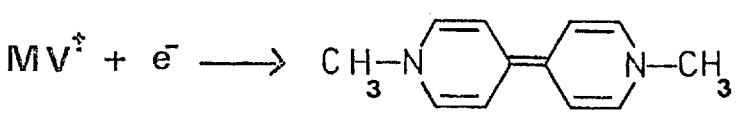

MV

It was hoped to develop a spectroelectrochemical method for Paraquat based on electrogenerating the free radical species in the carbon fibre cell and measuring in situ the concurrent absorption signal. Experiments were performed using static solution conditions since only small absorption signals were recorded for flowing solutions.

Solution Preparation

Stock Paraquat solutions ($1000\mu g ml^{-1}$ and 0.03M) were prepared by dissolving the appropriate amount of methyl viologen dihydrate (previously dried at 100° C for two hours) in distilled water (100ml). Aliquots were diluted to give the required standard solutions in either sodium hydroxide (0.1M) or sulphuric acid (0.2M) solution.

5.6.1. Voltammetric behaviour

The current - potential curve was recorded for methyl viologen (0.003M) in (1) sodium hydroxide solution (0.1M) and (2) sulphuric acid solution (0.2M) during a cyclic sweep of the working electrode. The result for the carbon fibre electrode was virtually identical to the DME[1] in that a pH-independent reversible one-electron reduction occurred, the difference in peak potentials of the cathodic (E_{pc} = -0.73V vs SCE) and the anodic (E_{pa} = -0.69V vs SCE) waves being approximately 30mV. The cyclic voltammogram in alkaline solution is given in fig 5.7.

5.6.2. Absorption spectrum of the radical ion of methyl viologen

The spectral distribution of the absorption signal was recorded in 40nm steps from 350nm - 720nm for Paraquat ($120\mu g ml^{-1}$)

FIG. 5.7.
Current - potential curve for methyl viologen during cyclic sweep. Methyl viologen (0.003M) in sodium hydroxide solution (0.1M); scan rate 20mVs^{-1}; working electrode, carbon fibre

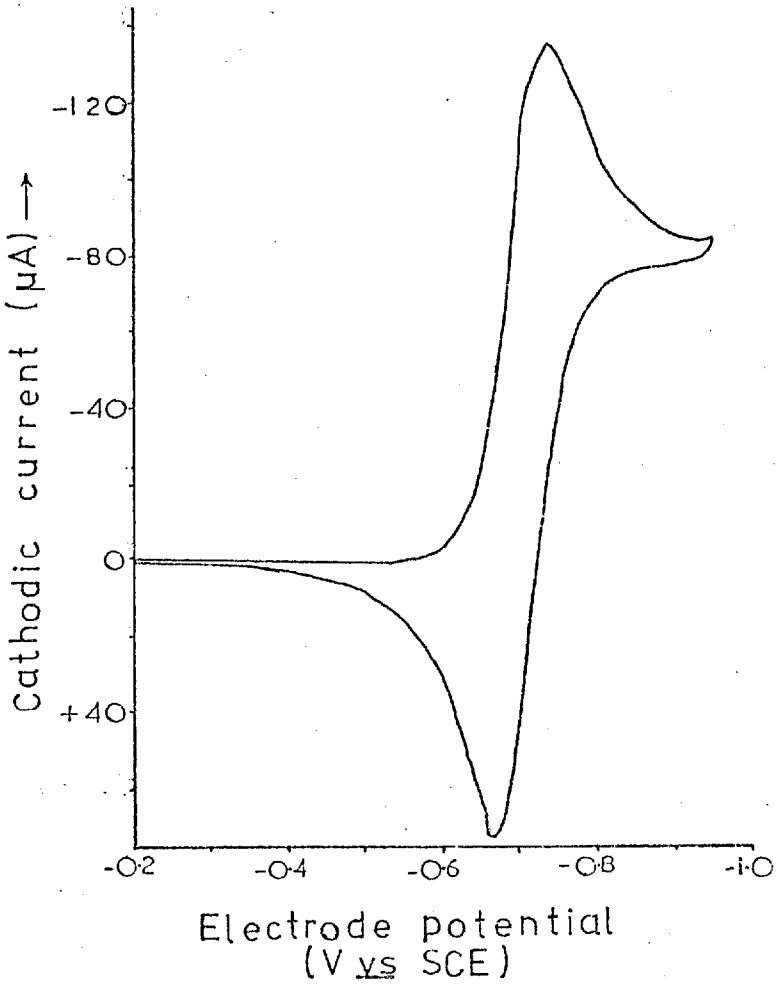

in sulphuric acid solution. The signal which was generated by applying a step potential of -0.85V vs SCE to the static solution reached a maximum in approximately three minutes. A solution of the free radical species (60μgml^{-1}) was also prepared chemically by adding sodium dithionite solution (2ml, 2% wv^{-1}) to Paraquat (60μgml^{-1}) contained in sodium hydroxide solution (0.1M) and the spectrum was recorded on the Unicam SP 800 instrument (pathlength 10mm). The spectra are presented in fig 5.8 and it can be seen that the absorbance of the electrogenerated product (broken line) is significantly less than expected considering the lower concentration and shorter path-length for the chemically prepared solution (solid line).

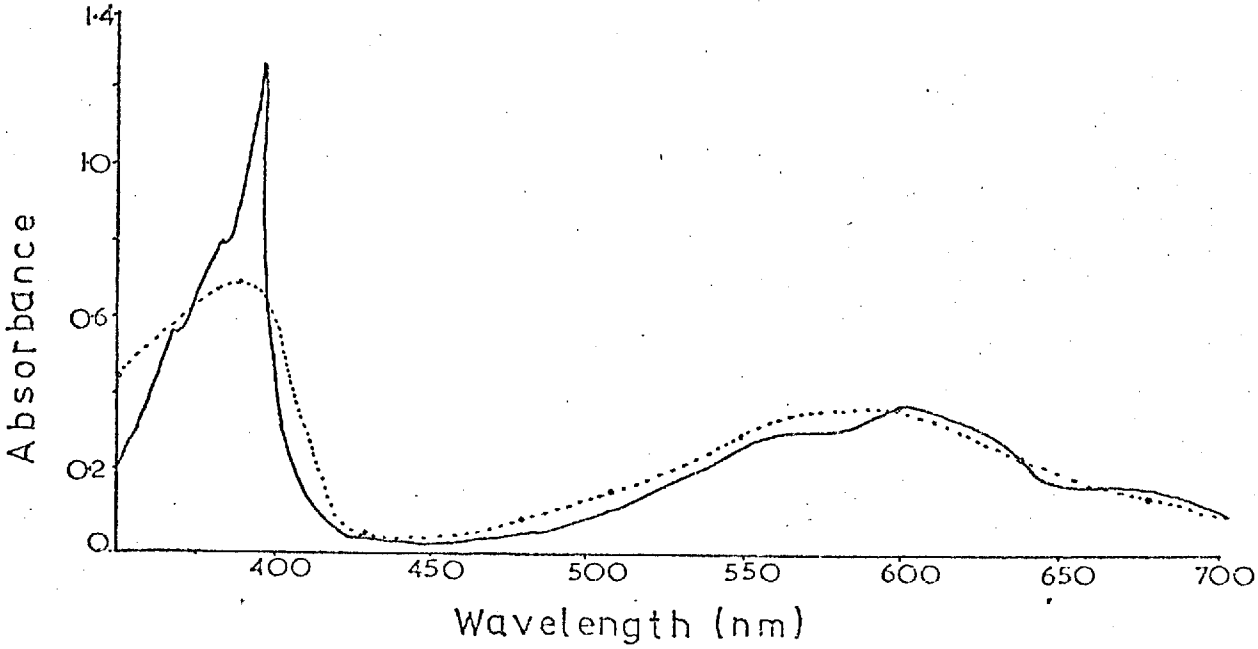

FIG. 5.8. Absorption spectrum of methyl viologen radical ion. Solid line (Unicam SP 800), Methyl viologen (60μgml^{-1}) in sodium hydroxide solution (0.1M) after chemical reduction; path length, 10mm; Broken line, Methyl viologen (120μgml^{-1}) in sulphuric acid solution (0.2M) during controlled potential electrolysis (-0.85V vs SCE), static solution.

5.6.3. Calibration

(1) Acidic solution

The absorbance values for Paraquat (10-120μgml^{-1}) in sulphuric acid solution (0.2M) were obtained for excitation at -0.85V vs SCE. Measurements for each standard solution were repeated at least once and the calibration graph is presented in fig 5.9. Although approximate linearity was obtained, the absorbance measurements at each concentration showed considerable scatter. This lack of reproducibility may have been caused by partial poisoning of the electrode surface since the cell had been operated continuously without replacing the carbon fibre bed. Returning the electrode to zero applied potential resulted in the immediate decay of the

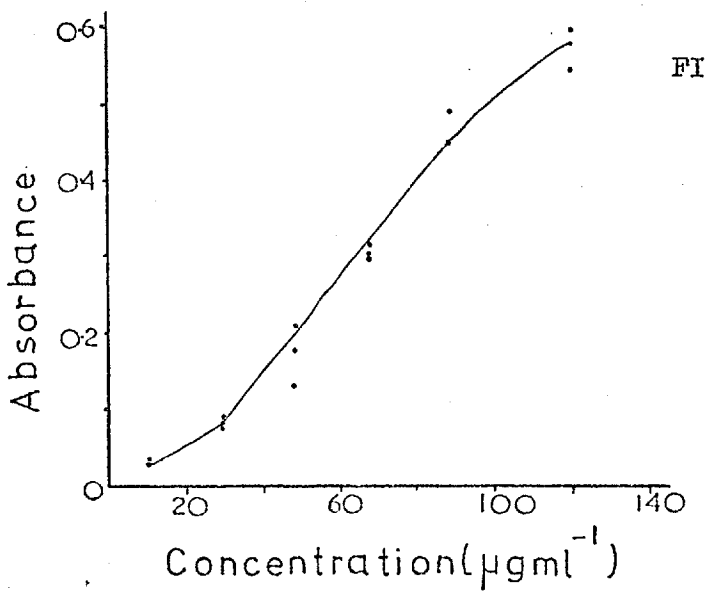

FIG. 5.9. Absorbance versus methyl viologen concentration during controlled potential electrolysis. Methyl viologen in sulphuric acid (0.2M); monitoring wavelength 390nm; electrode potential, -0.85V vs SCE; static solution.

absorption signal to the base line indicating instability of the free radical species in acidic solution. Instability of the free radical would not have been expected on the basis of the voltammetric behaviour of the compound where a reversible wave (indicating a stable free radical species) was recorded in both acidic and alkaline solution. This result serves to demonstrate that the degree of reversibility of the electrode reactions as evidenced by the current - potential behaviour during cyclic sweep may not necessarily apply to the controlled-potential experiment on the longer time scale.

(2) Basic solution

The absorption response in alkaline solution with excitation at -1.0V vs SCE was more sensitive so that lower concentrations of Paraquat solutions were investigated. In addition, a steady-state signal was maintained on returning the electrode to zero applied potential indicating the stability of the free radical cation in alkali; this

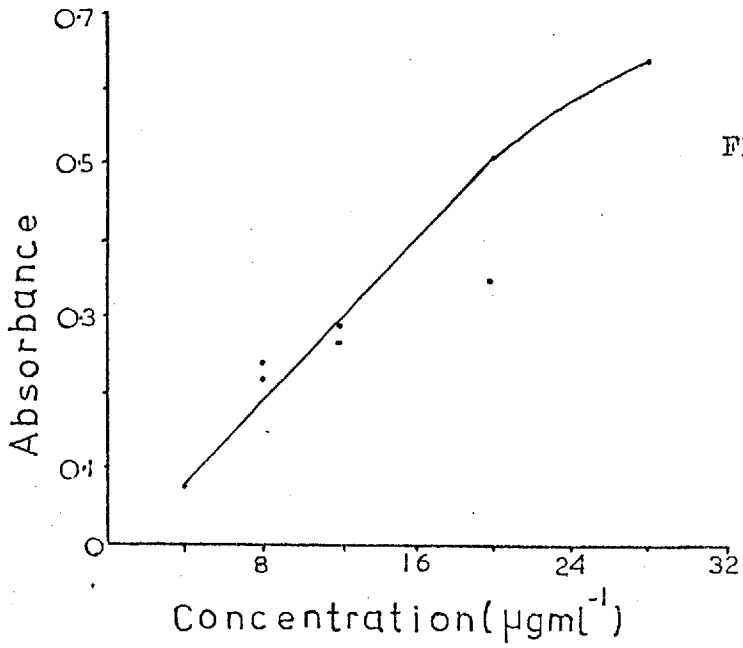

FIG. 5.10. Absorbance versus methyl viologen concentration during controlled potential electrolysis. Methyl viologen in sodium hydroxide solution (0.1M); monitoring wavelength 390nm; electrode potential, -1.0V vs SCE; static solution.

accounts for the increased sensitivity relative to acidic solution. The calibration graph for Paraquat (1 - 28μgml^{-1}) in sodium hydroxide solution (0.1M) is presented in fig 5.10. Reproducibility was poor once again and only approximate linearity was observed. Comparison of the absorption signal for chemical reduction at the 4μgml^{-1} level indicated that chemical preparation was more sensitive by a factor of approximately ten: an absorbance value of 0.77 for chemical preparation was obtained relative to 0.07 for electrogeneration.

5.7. Conclusions

In situ absorption monitoring of electrogenerated species in flowing solutions met with partial success. Linear calibration curves were established over narrow concentration ranges for ferrocyanide and o-tolidine solutions, but absorbance values were significantly less than expected. For o-tolidine the current and absorption behaviour was in approximate agreement with theory and confirmed the validity of the derived spectro-electrochemical equation. The absorption and current responses were fairly rapid although in the former case only an approximate steady-state signal was obtained. These findings generally applied to static experiments with Paraquat solutions, but unfortunately reproducible generation of product was not obtained; the absorbance was also low relative to the chemical preparation. The flow cells were plagued with operating problems which included light beam attenuation by air bubbles, drifting baseline and possible poisoning of the carbon fibre surface and as such make the present cell design unsuitable for direct analytical application.

Investigation of the dissolved oxygen reduction reaction illustrated once more the value of the spectroelectrochemical technique for monitoring the course of electrode reactions. In contrast to the results using platinum, dissolved oxygen reduction on carbon fibre yielded hydrogen peroxide and hydroxide ion as stable products.

CHAPTER 6 Aqueous Fluorescence Studies

6.1. Introductory Remarks

Fluorescence spectroscopy is an extremely powerful analytical technique that is used extensively in many areas for sensitive qualitative and quantitative analysis. Its importance lies in its additional selectivity and increased sensitivity (potentially by at least two orders of magnitude) relative to absorption methods. These advantages would be inherited by the fluorescence coupled electrochemical experiment. A particularly important fluorescence assay route is the fluorogenic reaction whereby a weakly or non-fluorescent compound is converted by appropriate chemical reaction into a highly fluorescent species. Although it is difficult to predict accurately the structural requirements for fluorescence, a fluorogenic reaction is generally aimed at increasing (1) the complexity and/or (2) the molecular rigidity and/or (3) the degree of resonance and/or (4) the degree of unsaturation of the reactant molecule. The principal reaction types, condensation, hydrolysis and redox, are employed for trace determinations of a wide range of biochemically important compounds, particularly those of pharmaceutical and clinical interest. The texts by Guibault[45], White and Argauer[101] and Udenfrieund[102] are a valuable source of reference for fluorogenic reactions.

It was decided to investigate the possibility of electrochemically initiating typical fluorogenic reactions and measuring *in situ* the subsequent fluorescence. A micro-fluorescence cell incorporating gold micromesh as the working electrode and

described in section 2.2.3 was designed for the purpose. The gold micromesh, ideally suited to sandwiching between the two halves of the flow cell, was chosen since it had been successfully used in spectroelectrochemical thin-layer studies[19,23-25,29]. Initial research directed at morphine was particularly successful and detailed studies indicated that the technique was suitable for sensitive morphine determination in the presence of the main opium alkaloids. The technique was shown to have wide application and other compounds briefly investigated which underwent electro-oxidation to highly fluorescent species included heroin (after hydrolysis), laudanosine, reserpine, thioguanine and homovanillic acid.

6.2. Morphine

6.2.1. Introduction

Morphine, an alkaloid obtained from opium which is the dried juice of the poppy plant Papaver somniferum, is an extremely potent but, unfortunately, addictive analgesic. Its importance in medicine, its addictive properties and its ever-increasing use in the illegal narcotics market necessitates rapid and sensitive methods for its qualitative and quantitative determination. Analytical methods, both chemical and physical, have been reviewed by Ehrlich-Rogozinsky and Cheronis[103] while the text by Evans[104] is another useful source listing official assay procedures. Although a number of direct fluorimetric methods have been reported[103,105], they lack sensitivity since morphine is only weakly fluorescent; they are not generally applicable to biological samples where high sensitivity is required. Fortunately morphine can be oxidised to the highly fluorescent dimer, pseudomorphine, when treated with weakly alkaline potassium ferricyanide solution[106]. Analytical advantage of the reaction was first realised by Kupferberg and co-workers[107] enabling sub-μg determinations of morphine in biological tissue. The sensitivity of the method was later substantially improved (at least ten-fold) by Takemori[108] who performed the oxidation in low volume to improve dimerisation efficiency. More recently, forensic analysts using high-pressure liquid chromatography with fluorescence detection have utilised the reaction for morphine quantitation in urine[109]. A fluorogenic procedure whereby morphine

is converted to a fluorophore by treatment with acid and alkali is also available[110,111]. The reaction has been employed for the semi-automatic assay of sub-μg quantities in biological material[112].

In the present study, oxidative dimerisation of morphine

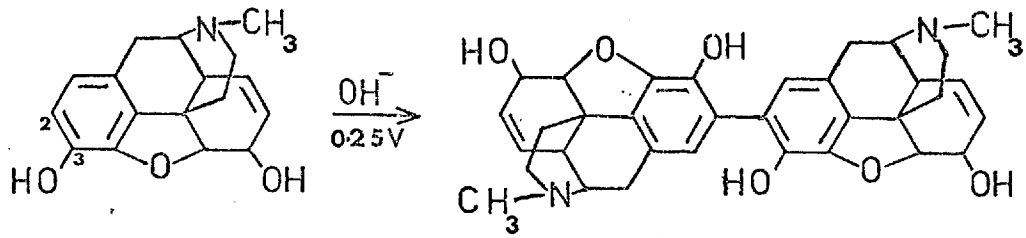

initiated by excitation at 0.25V vs SCE was successfully performed in the gold micromesh cell and provided sensitive fluorescence. The electrode reaction involves the one-electron oxidation of the ionised phenolic hydroxy group and subsequent coupling of the phenolate radicals. Since pseudomorphine also contains phenolic hydroxy groups further oxidation is likely. The dimerisation reaction is very sensitive to the solution pH. The chemical oxidation studies by Kupferberg[107] showed that the rate of formation and stability of pseudomorphine depended on the pH of the solution and also the initial concentration of morphine. Maximum fluorescence was recorded at pH 9.0, but the stability of the product was short lived (~2 min). For solutions of pH 8.0 the product was stable, but the fluorescence development was slow and maximum fluorescence was not attained. At pH 8.5 the product was stable for at least twenty minutes and the fluorescence intensity was only slightly less than that for pH 9.0. A pH of 8.5 was, therefore, considered by Kuperberg to be optimum. These results have been

confirmed by Jackson[113].

In initial fluorescence - electrochemical experiments the fluorescence characteristics of pseudomorphine were obtained in pH 8.5 solution. The optimum conditions for the formation and stability of electrogenerated pseudomorphine were then determined and the dimerisation efficiency was compared to the chemical method. The analytical growth curves were found to be reliable and enabled an accurate single-tablet assay of morphine sulphate to be performed. Finally, once interference studies were evaluated the technique was shown to be suitable for the direct determination of morphine in the presence of the principal opium alkaloids.

6.2.2. Experimental details

(1) Apparatus

The Farrand spectrofluorimeter described in section 2.1.2 was used in conjunction with the PAR 174A for fluorescence monitoring during controlled potential excitation. Corning filters (7 - 54, 3 - 73) were fitted to the excitation and emission monochromators, unless stated otherwise, to reduce the intensity of scattered exciting light. The transmission characteristics of the 3-73 filter (max transmission 530nm) were such that only radiation of wavelengths greater than about 400nm was detected. The slit-widths of both monochromators were chosen to provide a bandpass of 20nm except for spectral recording when 5nm or 10nm bandpass was used. It should be noted that the spectra presented later do not represent the "true" spectra but include contributions from

the wavelength - dependent components of the instrument such as light source, filters and photomultiplier tube.

(2) Operating procedure for cell

Sample solution was delivered to the cell by peristaltic pump and tubing. With a stationary solution, a potential (typically 0.25V vs SCE), sufficient to effect oxidation, was applied to the mesh and the resulting fluorescence with time was monitored at the appropriate wavelength combination (λ_{ex} 320nm, λ_{em} 442nm). The fluorescence response, depending on the pH of the solution and the electrode potential, increased steadily and went through a maximum before decaying to the background level. The procedure could be repeated by returning the electrode potential to zero volts and delivering fresh solution to the cell. Blank solution was generally passed through the cell for a period of ten minutes between different sample runs. This cleaning cycle was required for consistent results and was particularly important when examining solutions of differing pH.

(3) Solution preparation

Morphine. Stock morphine solution (calculated as the free base or as the hydrochloride) was prepared by dissolving the required quantity of morphine in dilute sulphuric acid (0.1M). Microlitre aliquots of the appropriate stock were then diluted to 25ml with background electrolyte solution to give the required standard solutions. This procedure was also adopted for preparing solutions of the other alkaloids investigated except in the case of pseudomorphine.

Pseudomorphine. Stock pseudomorphine (0.002M) was prepared by dissolving the required quantity of alkaloid in dilute sodium hydroxide solution (0.1M). Standard solutions were then prepared by dilution. The solubility of the alkaloid was low in acidic and weakly alkaline solution.

Background Electrolyte. The required quantity of sodium pyrophosphate (Analar grade) was dissolved in distilled water (500ml) and adjusted to pH 8.5 (or the appropriate pH) with a small quantity of sulphuric acid (1M). The solution was prepared fresh each day.

(4) Voltammetric studies

The electroactivity of the compound under investigation was determined by recording the current - potential curve at a micro-gold wire working electrode in the Metrohm cell. Satisfactory voltammograms were obtained when an electrode cleaning procedure was adopted. This consisted of soaking the wire in concentrated nitric acid (50% vv^{-1}), rinsing with distilled water and wiping with tissue paper. The electrode was then pretreated at -0.2V vs SCE for a short period before commencement of the scan.

6.2.3. Fluorescence spectra of pseudomorphine

The excitation and emission spectra of the fluorescence signal were recorded in situ during the controlled potential oxidation of morphine hydrochloride ($2x10^{-4}$M) in pH 8.5 sodium pyrophosphate solution (0.1M) at 0.20V vs SCE. The spectra which

were obtained with a bandpass of 5nm on both monochromators and without filters (Corning 7-54, 3-73) were recorded at a point corresponding to the plateau region of the fluorescence - time curve. The spectra presented in fig 6.1 reveal the characteristic excitation (3 peaks at 250nm, 280nm, 320nm) and emission pattern (one peak at 442nm) for pseudomorphine previously reported by Kupferberg[107]. The spectra recorded with the complimentary filters fitted to the respective monochromators were slightly distorted, but the excitation and emission maxima remained the same. Subsequent fluorescence monitoring was performed at the wavelength combination, λ_{ex} 320nm and λ_{em} 442nm.

6.2.4. Effect of electrode potential

Morphine hydrochloride (8×10^{-5}M) in pH 8.5 sodium pyrophosphate solution (0.1M) was oxidised in the gold micromesh cell at various electrode potentials. The fluorescence results are summarised in table 6.1 and the response curves for excitations at 0.25V, 0.30V, 0.40V and 0.60V vs SCE are given in fig 6.2. For potentials less than that required for oxidation, for example 0.15V vs SCE, no pseudomorphine was formed and consequently no fluorescence was recorded. At potentials up to 0.2V vs SCE, the fluorescence developed slowly and did not reach a maximum value in an acceptable time. For increasingly positive potentials (>0.2V vs SCE), the rate of fluorescence development and decay increased and the fluorescence maxima progressively decreased. The fluorescence behaviour indicated the increasing oxidation rate of the phenolic hydroxy groups of morphine and pseudomorphine

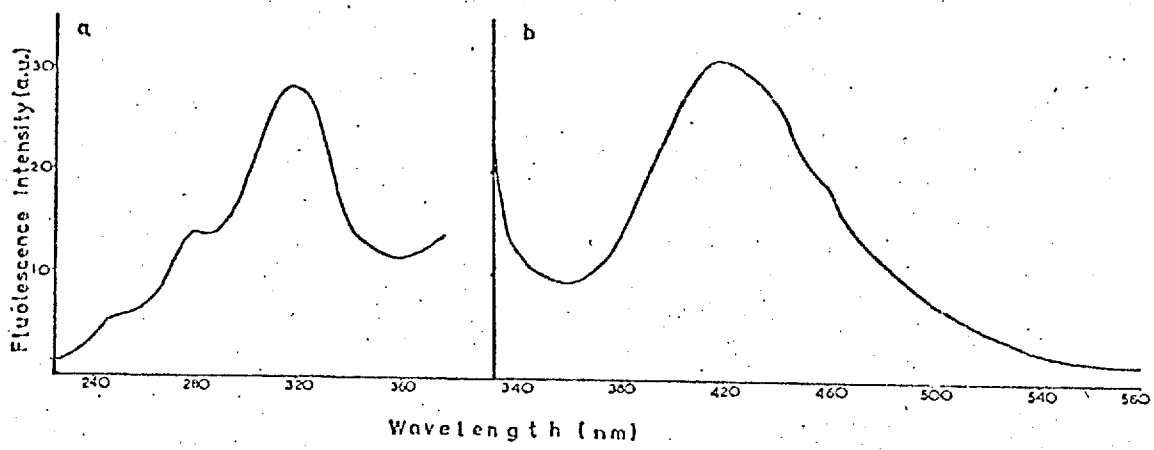

FIG. 6.1. Fluorescence excitation (a) and emission (b) spectra of electrogenerated pseudomorphine. Morphine hydrochloride ($2x10^{-4}M$) in pH 8.5 sodium pyrophosphate solution (0.1M); electrode potential 0.20V vs SCE; excitation wavelength 320nm, emission wavelength 442nm; bandpass, 5nm for both monochromators.

with increasing electrode potential, the oxidation product of the latter compound being non-fluorescent. Maximum fluorescence was obtained for an applied potential of 0.25V vs SCE.

6.2.5. Effect of pH

Morphine hydrochloride solutions ($8x10^{-5}M$) containing sodium pyrophosphate (0.1M) and covering the pH range 6.0 to 10.2 were individually oxidised at 0.3V vs SCE and the fluorescence response was recorded. The rate of fluorescence development and decay increased as the solution became more alkaline and the response curves were of similar appearance to fig 6.2. The results of the study are summarised in table 6.2. Maximum fluorescence was obtained for the pH 7.7 solution. Fluorescence was not recorded for solutions of pH 6.0 and 6.4 and in the case of pH 7.2 the time to reach maximum fluorescence was considerable. These results indicated that the oxidation of morphine and pseudomorphine was pH-dependent and a study of the voltammetric behaviour of the two compounds with respect to pH should confirm this. Incidentally

Table 6.1. Effect of electrode potential on the fluorescence of electrogenerated pseudomorphine.

Electrode Potential (V vs SCE)	Maximum Fluorescence Intensity (a.u.)	$Time_{MF}$ (minutes)
0.15	-	-
0.20	-	-
0.25	40	9.8
0.30	35	6.2
0.40	22	3.2
0.50	18	2.4
0.60	16	2.2

Morphine ($8x10^{-5}$M) in pH 8.5 sodium pyrophosphate solution; excitation wavelength 320nm; emission wavelength 442nm; MF, maximum fluorescence.

Table 6.2. Effect of pH on the fluorescence of electrogenerated pseudomorphine.

pH	Maximum Fluorescence Intensity (a.u.)	$Time_{MF}$ (minutes)
6.0	-	-
6.4	-	-
7.2	40	17.7
7.7	53	7.5
8.0	41	3.7
8.6	28	2.6
9.1	20	2.3
9.6	16	1.9
10.2	12	1.4

Morphine ($8x10^{-5}$M) in sodium pyrophosphate solution (0.1M); electrode potential 0.3V vs SCE; excitation wavelength 320nm; emission wavelength 442nm.

with excitation at 0.25V vs SCE differences in the fluorescence maxima for solutions in the pH range 7.5 to 8.5 were less pronounced. Maximum fluorescence was still recorded for the

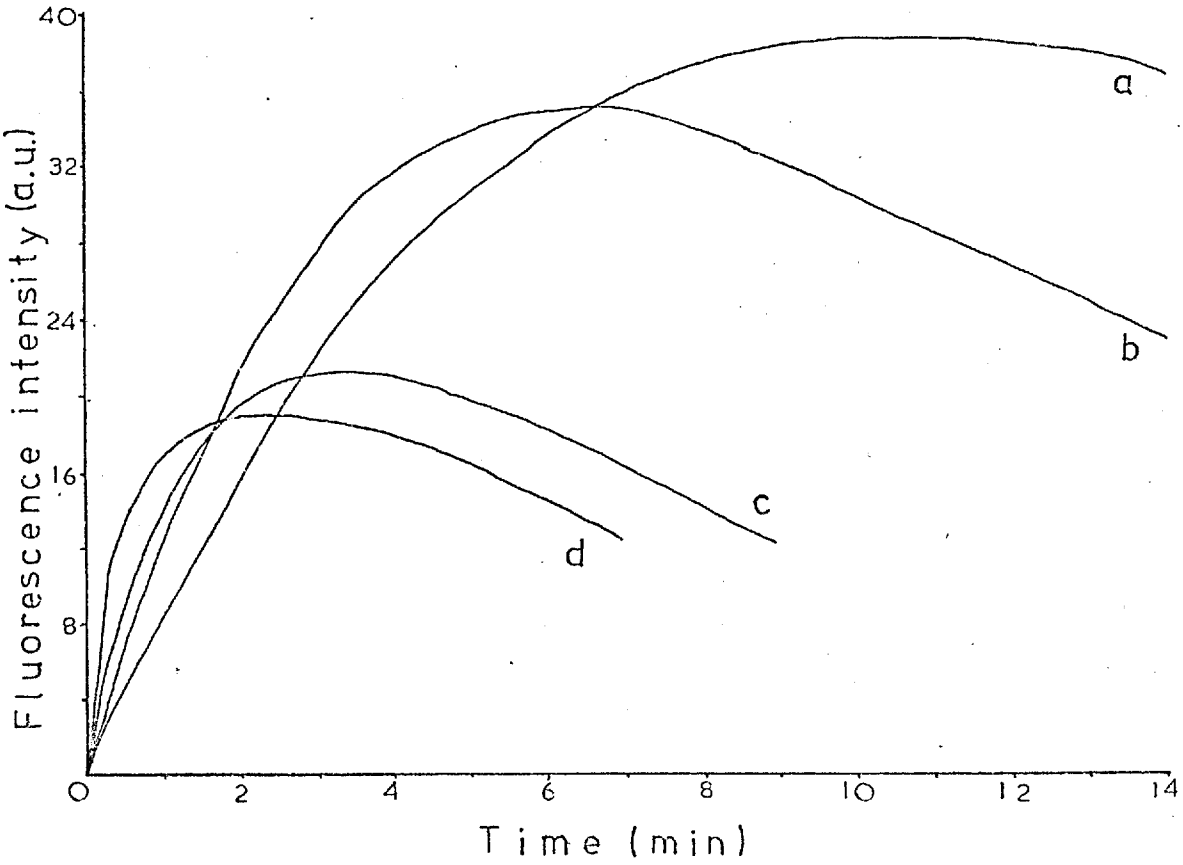

FIG. 6.2. Fluorescence response curves of electrogenerated pseudomorphine for various applied potentials. Morphine ($8x10^{-5}$M) in pH 8.5 sodium pyrophosphate solution (0.1M); electrode potentials (V vs SCE), (a) 0.25V (b) 0.30V (c) 0.40V (d) 0.60V; excitation wavelength 320nm; emission wavelength 442nm.

pH 7.7 solution, but the time to reach the maximum was excessive. Summarising, to obtain maximum fluorescence an excitation potential of 0.25V vs SCE with a solution pH of about 7.7 should be chosen. If the development time is unacceptable then a faster fluorescence response can be obtained at the expense of sensitivity by increasing either (or both) parameter(s).

6.2.6. Efficiency of electrochemical conversion and comparison with potassium ferricyanide oxidation

The efficiency of electrochemical dimerisation was determined by comparing the maximum fluorescence of electrogenerated pseudomorphine with the fluorescence of standard pseudomorphine

solutions. The molar concentrations of the morphine and pseudomorphine solutions were in the ratio of 2 to 1 since two molecules of morphine are required for dimerisation. The efficiency was also compared to the chemical oxidation method of Kupferberg[107].

Procedure

The maximum fluorescence of pseudomorphine was recorded in the gold micromesh cell for three situations. First, morphine ($2x10^{-5}$M) in pH 8.5 sodium pyrophosphate solution (0.1M) was oxidised at (1) 0.25V *vs* SCE and (2) 0.30V and the respective fluorescence signals recorded. Next, morphine ($2x10^{-5}$M) in pH 8.5 sodium pyrophosphate solution (0.1M) was oxidised by potassium ferricyanide ($6x10^{-5}$M)/potassium ferrocyanide ($3.7x10^{-6}$M) solution in (1) high-volume (25ml) conditions and (2) low-volume (1.5ml) conditions { For the low-volume reaction, the oxidant (250µl of potassium ferricyanide ($6x10^{-3}$M)/potassium ferrocyanide ($3.7x10^{-4}$M) solution) was added to morphine (250µl, $2x10^{-3}$M) in pH 8.5 sodium pyrophosphate (1ml, 0.1M) and left for two minutes before the final dilution to 25ml. } and the fluorescence of the respective solutions were recorded by flowing them through the cell separately at zero applied potential. Finally, the fluorescence of standard pseudomorphine solution (10^{-5}M) in pH 8.5 sodium pyrophosphate solution (0.1M) was recorded for zero applied potential. The comparison was repeated again for alkaloid solutions of pH 7.5 and pH 8.0, but omitting chemical oxidation (Previous experiments had established that

chemical oxidation was very inefficient at pH 7.5 and pH 8.0 agreeing with Kupferberg's finding). The fluorescence results are presented in table 6.3 together with the appropriate percent conversion values.

Table 6.3. Fluorescence results and efficiency of electrochemical and chemical oxidation.

	Maximum fluorescence intensity(a.u.) of pseudomorphine				
	pseudomorphine (10^{-5}M)	Morphine (2×10^{-5}M) oxidation Chemical		Electrochemical	
		low volume	high volume	0.25V	0.30V
pH 7.5	30.5	-	-	-	14.2
% Conversion	-	-	-	-	46.5
pH 8.0	29.3	-	-	-	16.2
% Conversion	-	-	-	-	55.3
pH 8.5	27.5	18.2	15.5	15.2	11.4
% Conversion	-	66.2	56.4	55.3	41.4

Alkaloids in sodium pyrophosphate solution; excitation wavelength 320nm, emission wavelength 442nm.

Inspection of the results for electrogeneration indicates that the maximum fluorescence (and efficiency) was achieved for either the pH 8.0 and 0.30V combination or with pH 8.5 and 0.25V. For solutions of pH 7.5 and 8.0 at 0.25V, fluorescence developed very slowly and a maximum value was not reached in an acceptable time; this agreed with previous findings. Comparing the electrochemical and chemical results it can be seen that electrogeneration was almost as efficient as chemical oxidation performed at high volume. Dimerisation efficiency was, however, improved for the low volume oxidation agreeing qualitatively

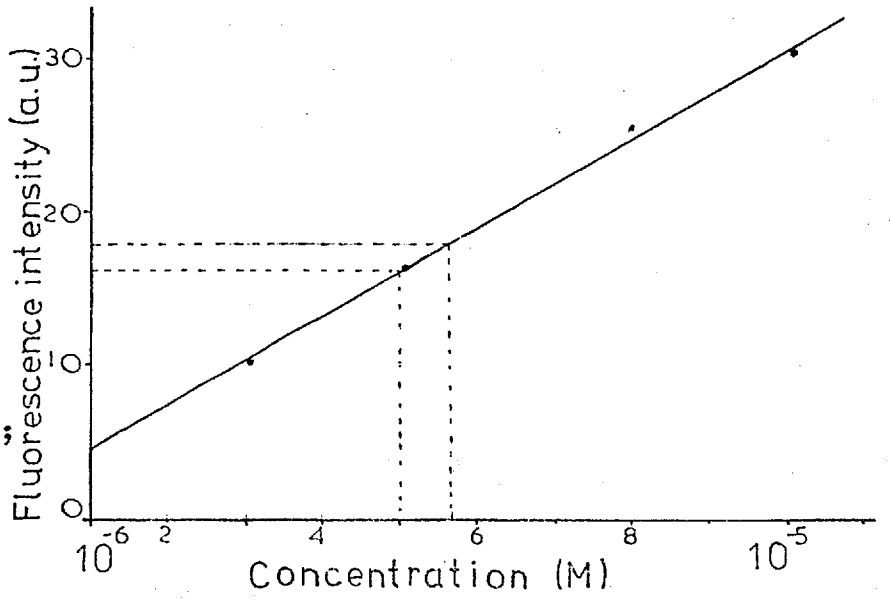

FIG. 6.3. Fluorescence versus concentration of pseudomorphine. Pseudomorphine in pH 8.5 sodium pyrophosphate solution (0.1M); excitation wavelength 320nm; emission wavelength 442nm.

with Takemori's proposals[108].

In a further experiment designed to check the previous results, the fluorescence calibration graph was constructed for standard pseudomorphine solutions ($3x10^{-6}$M - 10^{-5}M) in pH 8.5 sodium pyrophosphate (0.1M). The fluorescence intensity measurements for morphine ($2x10^{-5}$M) oxidation, electrochemical (0.25V vs SCE) and chemical (high volume), in pH 8.5 sodium pyrophosphate (0.1M) were obtained as before and the corresponding pseudomorphine concentrations were read from the pseudomorphine calibration graph which is given in fig 6.3. The fluorescence and efficiency results are given in table 6.4. It can be seen that the results were in approximate agreement with the previous study, chemical oxidation being only slightly more efficient.

In summary, the study has provided a rough guide to the efficiency of electrochemical dimerisation (also chemical dimerisation). It should be noted, however, that pseudomorphine undergoes further oxidation and this factor was not taken into

Table 6.4. Fluorescence results and efficiency of electrochemical and chemical oxidation.

Pseudomorphine Concentration (M)	Fluorescence intensity (a.u.)	Morphine (2×10^{-5}M) Fluorescence intensity (a.u.)	
		Chemical high vol.	Electrochemical 0.25V
3×10^{-6}	10.0		
5×10^{-6}	16.5		
8×10^{-6}	25.5		
10^{-5}	30.5	18.0	16.4
% Conversion (calculated)		59%	54%
% Conversion (read from calibration graph fig 6.3.)		57%	50%

Alkaloids in pH 8.5 sodium pyrophosphate solution; excitation wavelength 320nm, emission wavelength 442nm.

account when making the comparison. It is also possible that the cell area from which fluorescence was collected (in the case of electrogeneration) was less relative to the standard solution (and the chemically oxidised solution) due to an uneven current distribution over the gold micromesh. If either of these two factors were significant and were taken into account then a higher efficiency would result.

6.2.8. Voltammetric behaviour of morphine and pseudomorphine as a function of pH

The previous fluorescence studies with morphine and pseudomorphine demonstrated the importance of electrode potential and pH on the formation and stability of pseudomorphine. The increasing rate of development and decay of pseudomorphine

fluorescence with increasing solution pH and electrode potential indicated that the oxidation potentials of the phenolic hydroxy groups of morphine and pseudomorphine were pH-dependent.

A study of the voltammetric behaviour of the two compounds with respect to pH should confirm this. In addition, information about the stability of the morphine free radical species may be obtained. Although the overall electrode reaction corresponds to an ECE (oxidation of morphine, dimerisation, oxidation of pseudomorphine) process, the initially formed morphine free radical species may have sufficient stability on the time scale of the cyclic sweep to enable the reduction wave to be observed on the reverse scan.

The one-electron oxidation reaction of morphine in alkaline solution corresponds to the process

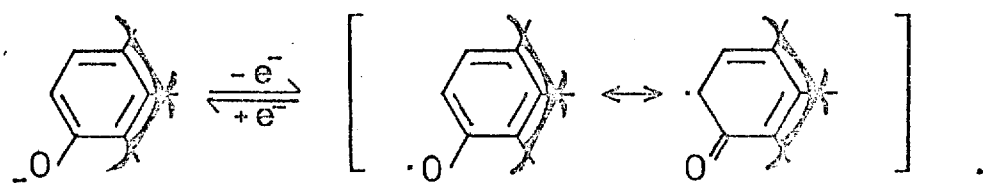

In acidic solution, however, the reaction would proceed by a different mechanism since according to Vermillon and Pearl[114] phenolic oxidation at low pH involves the irreversible removal of two electrons from the non-ionised phenol to give a phenoxonium ion

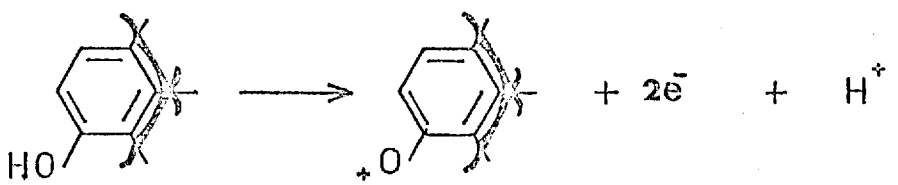

The formation of pseudomorphine could, therefore, not be realised in acidic solution.

The voltammetric behaviour of morphine and pseudomorphine in sulphuric acid solution (2M) has been studied by Deys[115]; he showed that pseudomorphine was oxidised at potentials ($E_{\frac{1}{2}}$ = 0.70V vs SCE) less positive the morphine ($E_{\frac{1}{2}}$ = 0.78 V vs SCE).

Procedure

Solutions of pseudomorphine in (1) sulphuric acid (0.1M), (2) pH 7.5 sodium pyrophosphate (0.1M), (3) pH 8.5 sodium pyrophosphate (0.1M), (4) pH 10.2 sodium pyrophosphate and (5) sodium hydroxide (0.1M) were prepared and the respective current - potential curves were obtained during a cyclic sweep (0V to 0.75V to 0V vs SCE at 20mVs^{-1}) of the micro-gold wire working electrode. The procedure was repeated for morphine solutions. Solubility of pseudomorphine was low in acidic and weakly alkaline solutions so that dilute solutions (~10^{-5}M) were employed. At the higher pH levels, however, solubility increased enabling greater concentrations to be used. This was fortunate since the background currents due to surface oxide reduction steadily increased as the solution became more alkaline and tended to obscure the waves for dilute solutions. The voltammetric curves for morphine (solid line) and pseudomorphine (broken line) as a function of pH are given in fig 6.4 and it is readily apparent that the potentials at which oxidation commences (E_c) and the half-wave potentials ($E_{\frac{1}{2}}$) for both compounds steadily increase at the pH decreases; determinations of E_c and $E_{\frac{1}{2}}$ values for morphine and pseudomorphine are given in table 6.5. It can be seen that pseudomorphine is oxidised at less positive potentials than morphine

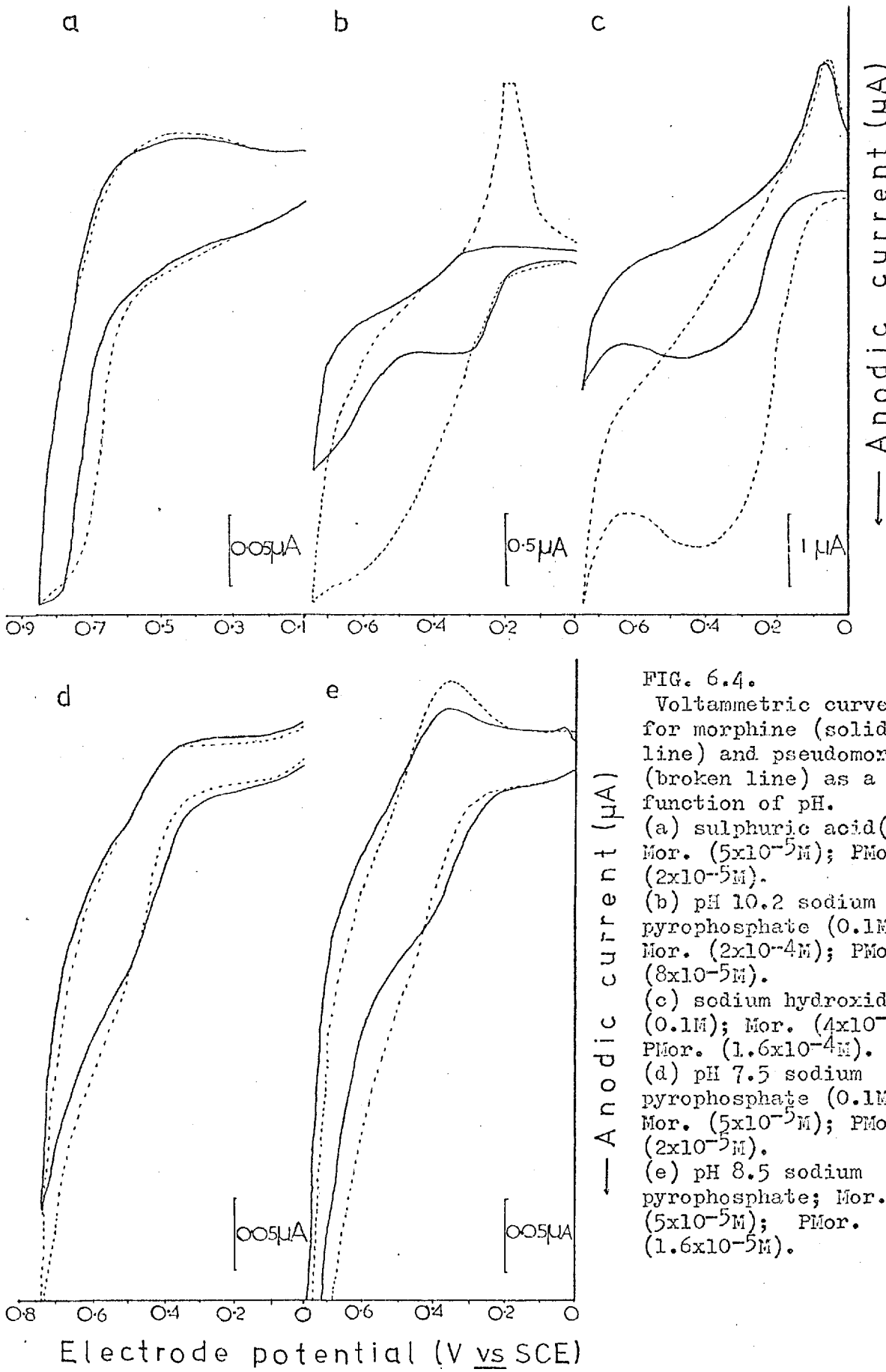

FIG. 6.4.
Voltammetric curves for morphine (solid line) and pseudomorphine (broken line) as a function of pH.
(a) sulphuric acid(0.1M); Mor. (5×10^{-5}M); PMor. (2×10^{-5}M).
(b) pH 10.2 sodium pyrophosphate (0.1M); Mor. (2×10^{-4}M); PMor. (8×10^{-5}M).
(c) sodium hydroxide (0.1M); Mor. (4×10^{-4}M); PMor. (1.6×10^{-4}M).
(d) pH 7.5 sodium pyrophosphate (0.1M); Mor. (5×10^{-5}M); PMor. (2×10^{-5}M).
(e) pH 8.5 sodium pyrophosphate; Mor. (5×10^{-5}M); PMor. (1.6×10^{-5}M).

Table 6.5. Half-wave potentials ($E_{\frac{1}{2}}$) and commencing potentials (E_c) for oxidation of morphine and pseudomorphine.

Background Electrolyte Solution	Morphine E_c	Morphine $E_{\frac{1}{2}}$	Pseudomorphine E_c	Pseudomorphine $E_{\frac{1}{2}}$
pH 1 Sulphuric acid (0.1M)	0.60	0.73	0.57	0.68
pH 7.5 Sodium pyrophosphate (0.1M)	0.32	0.42	0.32	0.42
pH 8.5 Sodium pyrophosphate (0.1M)	0.25	0.35	0.27	0.38
pH 10.2 Sodium pyrophosphate (0.1M)	0.19	0.28	0.19	*
pH 13 Sodium hydroxide (0.1M)	0.15	0.25	0.09	0.22

Data refer to fig 6.4. * difficult to determine.

in solutions of pH 1 (curve a) and pH 13 (curve c) while for pH 7.5 (curve d) and pH 8.5 (curve e) the reverse is true, but the difference is rather slight. At pH 10.2 (curve b) the behaviour is very similar for both compounds. On the basis of these results it would be predicted that maximum pseudomorphine fluorescence would be realised in weakly alkaline solution (pH 7.5 - 8.5) where the stability of pseudomorphine with respect to electrode potential is at a maximum.

As mentioned earlier, surface oxide reduction tended to obscure the current behaviour on the reverse scan so that information on morphine free radical stability was not obtained.

6.2.9. The effect of concentration

The effect of morphine concentration on the fluorescence of psuedomorphine was investigated for excitation in pH 8.5

solutions at (1) 0.25V and (2) 0.30V. The calibration graph in the former case was obtained over a wide concentration range and enabled the detection limit for the procedure to be established. A recovery experiment was also performed to give an idea of accuracy.

(1) Excitation at 0.25V

The maximum fluorescence for excitation at 0.25V vs SCE in pH 8.5 sodium pyrophosphate solution (0.1M) was determined for morphine hydrochloride solutions covering the range 10^{-3}M to 10^{-6}M. For solutions at low concentration the instrument was operated on the most sensitive range. This introduced considerable background noise and an associated uncertainty in measurement. Measurements were generally repeated at least once (except at higher concentrations where an unacceptable recording time was experienced) and the results are given in table 6.6. The logarithmic calibration graph shown in fig 6.5 indicates an extremely good fit of experimental data with linearity being nearly observed over the 1000 fold concentration range. Fluorescence measurements were not extended beyond 10^{-3}M because precipitation of morphine tended to occur in the pH 8.5 media. Fluorescence was, however, recorded for morphine concentrations up to 3×10^{-3}M in pH 11 solution. The calibration curve still exhibited a wide linear analytical range, but the onset of self-absorption, which became noticeable at concentrations beyond 10^{-3}M, brought a departure from linearity. Decreased sensitivity in the pH 11 media was observed as expected.

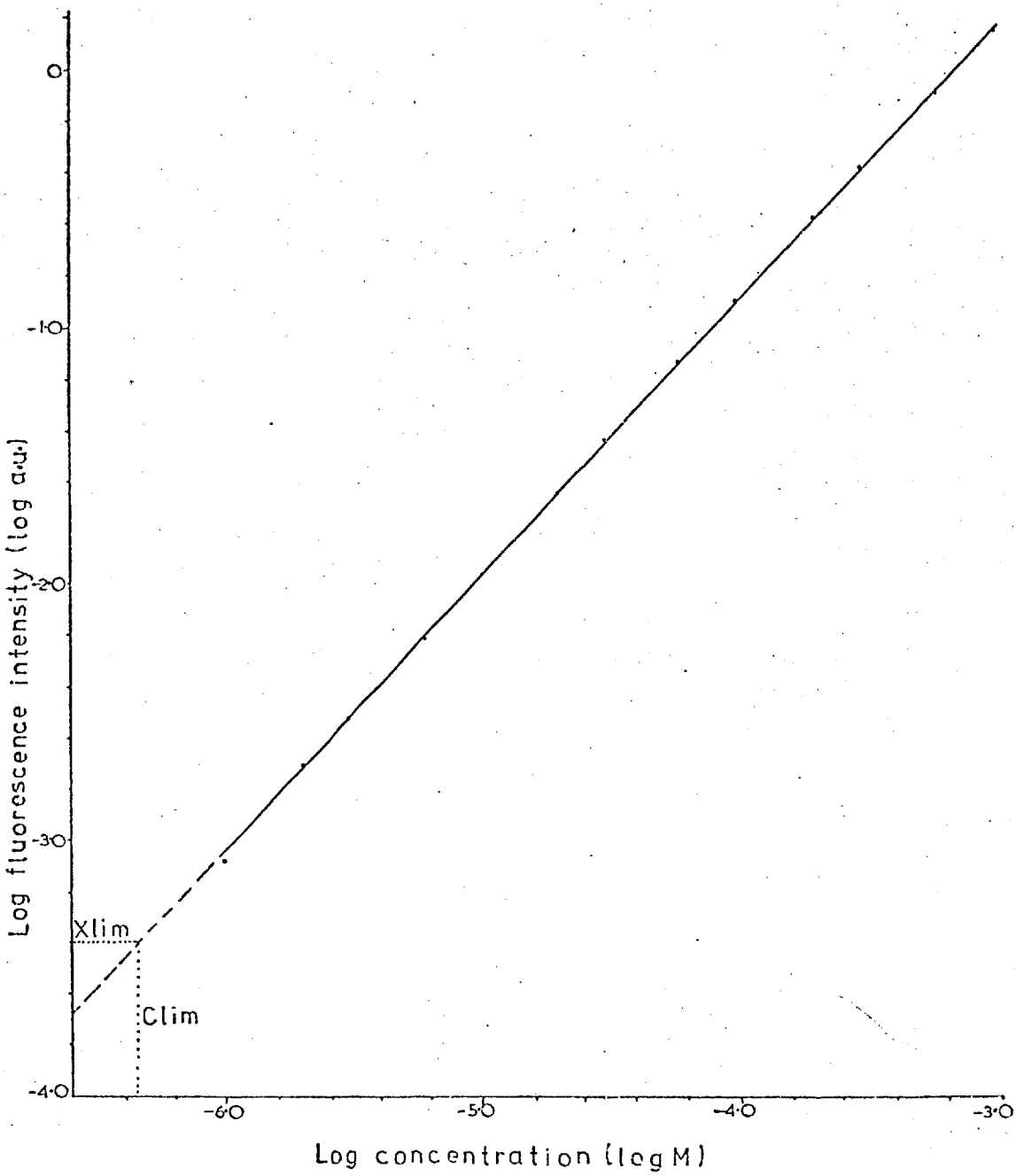

FIG 6.5. Logarithmic calibration graph for electrogenerated pseudomorphine. Morphine (10^{-3}M to 10^{-6}M) in pH sodium pyrophosphate solution (0.1M); electrode potential 0.25V vs SCE; excitation wavelength 320nm; emission wavelength 442nm.

Table 6.6. Fluorescence of electrogenerated pseudomorphine as a function of morphine concentration.

Morphine Concentration		Maximum Fluorescence Intensity(a.u.)				$Time_{MF}$
(M)	log(M)	1	2	Average	log Av.	(min)
10^{-6}	-6.00	0.0007	0.0009	0.0008	-3.10	5.5
$2x10^{-6}$	-5.70	0.0020	0.0019	0.0019	-2.72	5.5
$3x10^{-6}$	-5.52	0.0028	0.0030	0.0029	-2.54	5.2
$6x10^{-6}$	-5.22	0.0063	0.0064	0.0063	-2.20	4.8
10^{-5}	-5.0	0.0111	0.0108	0.0109	-1.96	5.1
$2x10^{-5}$	-4.70	0.0223	0.0230	0.0226	-1.65	4.8
$3x10^{-5}$	-4.52	0.0357	0.0361	0.0359	-1.44	5.0
$6x10^{-5}$	-4.22	0.0718	0.0720	0.0719	-1.14	5.2
10^{-4}	-4.00	0.1239	0.1260	0.1249	-0.90	5.6
$2x10^{-4}$	-3.70	0.2631	0.2570	0.260	-0.58	6.6
$3x10^{-4}$	-3.52		0.409	0.409	-0.39	7.5
$6x10^{-4}$	-3.22		0.807	0.807	-0.09	12.2
10^{-3}	-3.00		1.371	1.371	+0.14	13.8

Morphine in pH 8.5 sodium pyrophosphate solution (0.1M); electrode potential 0.25V vs SCE; excitation wavelength 320nm; emission wavelength 442nm.

The limit of detection based on the definition by Kaiser[116] was taken as that concentration of morphine hydrochloride which produced a flucrescence signal, $\bar{x}$, equal to twice the standard deviation of the background noise level, $2\sigma_{bl}$, ($2\sigma_{bl} = 3.54x10^{-4}$), once the blank value, $\bar{x}_{bl}$, had been subtracted. That is

$$\bar{x} - \bar{x}_{bl} = 2\sigma_{bl} = x_{lim} .$$

The value was found by extrapolating the logarithmic calibration graph to meet the limiting signal, x_{lim}, and reading from the graph the corresponding limiting concentration, c_{lim}. The procedure illustrated in fig 6.5 provided a limiting concentration of

5×10^{-7}M. The limiting detectable weight based on the cell volume of 120µl (0.5mmx0.9mmx27mm) was calculated to be 23ng of morphine hydrochloride or 19ng of morphine.

(2) Excitation at 0.30V

Excitation at 0.30V vs SCE although less sensitive than 0.25V provided a response curve which went through a maximum fairly rapidly and enabled the maximum fluorescence value to be readily computed. The results for morphine solutions (3-30µgml^{-1}) presented in table 6.7 provided a linear calibration graph; this is shown in fig 6.6. To obtain an indication of the accuracy of the procedure, known amounts of morphine were put through the method and the recoveries were determined from the calibration graph. The % relative error expressed as the amount taken - amount found/amount taken x 100 was then calculated. The results are summarised in table 6.8. The recoveries were a little on the low side, but the relative errors were acceptable. It was decided on the basis of these results to apply the procedure to the single-tablet assay of morphine sulphate.

Table 6.7. Fluorescence of electrogenerated pseudomorphine as a function of morphine concentration.

Morphine Concentration (µgml^{-1})	Maximum Fluorescence Intensity(a.u)			$Time_{MF}$
	1	2	Average	
3	3.8	3.8	3.8	2.7
6	7.4	7.4	7.4	3.7
12	16.3	15.9	16.1	3.8
18	24.0	23.7	23.9	3.6
24	32.3	32.3	32.3	4.0
30	40.6	40.7	40.6	3.8

Morphine in pH 8.5 sodium pyrophosphate solution (0.1M); electrode potential 0.30V vs SCE; excitation wavelength 320nm, emission wavelength 442nm.

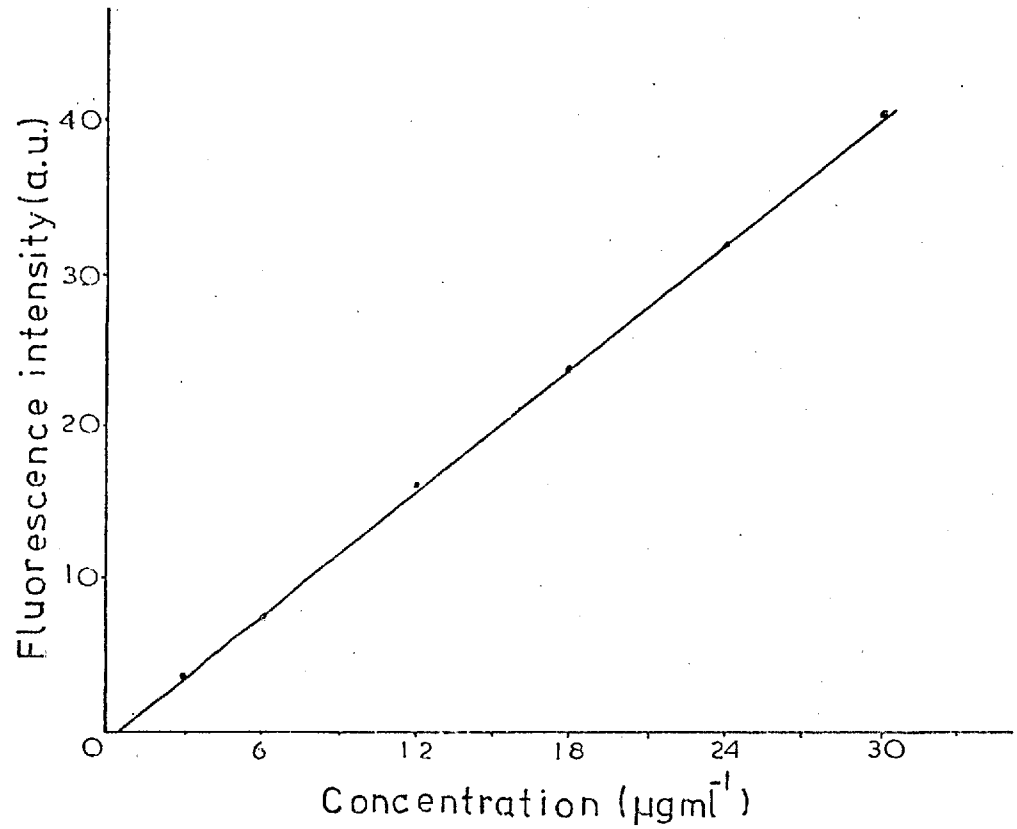

FIG. 6.6. Fluorescence of electrogenerated pseudomorphine versus concentration of morphine. Morphine in pH 8.5 sodium pyrophosphate solution (0.1M); electrode potential 0.30V vs SCE; excitation wavelength 320nm; emission wavelength 442nm.

Table 6.8. Recoveries of morphine.

Morphine Concentration ($\mu g ml^{-1}$)	Weight Taken (μg)	Maximum Fluorescence Intensity, au		Concentration Found ($\mu g ml^{-1}$)			Weight Found (μg)	% Relative error
				1	2	Av		
9	225	11.1	11.4	8.4	8.6	8.5	212.5	5.5%
15	375	19.6	19.8	14.6	14.8	14.7	367.5	2.0%
21	525	27.8	27.9	20.6	20.8	20.7	517.5	1.4%

Morphine in pH 8.5 sodium pyrophosphate solution (0.1M); electrode potential 0.30V vs SCE; excitation wavelength 320nm; emission wavelength 442nm; recoveries (as pseudomorphine) determined from fig 6.6.

6.2.10. Assay of morphine sulphate

Solution preparation

Morphine sulphate tablet (15mg, BPC) was powdered in

a volumetric flask (10ml) and dissolved in dilute sulphuric acid (~5ml). The solution, having been left overnight to allow extraction of morphine, was filtered and diluted to 10ml to provide the unknown stock solution. Sample solution was then prepared by diluting an aliquot (500µl) of the stock to 25ml with pH 8.5 sodium pyrophosphate solution (0.1M).

Stock morphine solution (1500μgml^{-1}; calculation based on free morphine) was prepared from morphine hydrochloride and standard solutions (6 - 60μgml^{-1}) were made up in pH 8.5 sodium pyrophosphate (0.1M) as previous.

Results

The fluorescence response curves of the standards and the unknown solution were recorded during excitation at 0.25V and the maximum values noted. Measurements on the same solution were generally repeated three times, but for solutions at the 6μgml^{-1} and 60μgml^{-1} level and for the unknown solution at least ten measurements were performed. Reproducibility was extremely good and the precision data are presented together with the fluorescence results in table 6.9. The mean fluorescence value was plotted against concentration and the calibration curve is given in fig 6.7. The fluorescence graph was not strictly linear over the entire concentration range, but linearity was observed in the range, 6μgml^{-1} to 30μgml^{-1}, corresponding to the fluorescence of the unknown solution. A reliable determination of the unknown concentration from the calibration graph was thus attained.

Table 6.9. Assay of morphine sulphate tablet - fluorescence results and precision data.

Morphine Concentration (μgml^{-1})	Maximum Fluorescence Intensity (a.u.)			
		Average	SD	RSD
6	1.21,1.25,1.26,1.25, 1.22,1.25,1.23,1.25, 1.28,1.29,1.32.	1.25	0.32	2.56
15	3.50,3.47,3.52.	3.50	0	
30	7.78,7.74,7.77.	7.76		
45	13.59,13.68,13.68.	13.65		
60	19.08,18.93,19.14, 19.08,19.08,19.14, 19.26,19.17,19.17, 19.44.	19.14	0.47	0.74
Unknown solution	5.78,5.77,5.74,5.71, 5.76,5.75,5.70,5.61, 5.51,5.70.	5.70	0.84	1.47

Morphine in pH 8.5 sodium pyrophosphate (0.1M); electrode potential 0.25V vs SCE; excitation wavelength 320nm, emission wavelength 442nm; SD, standard deviation; RSD, relative standard deviation.

Calculation

Concentration of unknown sample solution read from calibration graph = 22.5μgml

Concentration of stock solution (initial dilution 500μl to 25ml) = 1125.0μgml^{-1} = 11.25mg/10ml

∴ Quantity of morphine in tablet = 11.25mg

∴ Quantity of morphine sulphate in tablet = 14.95mg.

The final assay result given in table 6.10 was within 0.07% of the stated value and confirms the suitability of this approach for accurate single-tablet analysis.

Table 6.10. Assay of morphine sulphate tablet.

Specified content of Morphine sulphate	Amount found
15mg	14.95mg

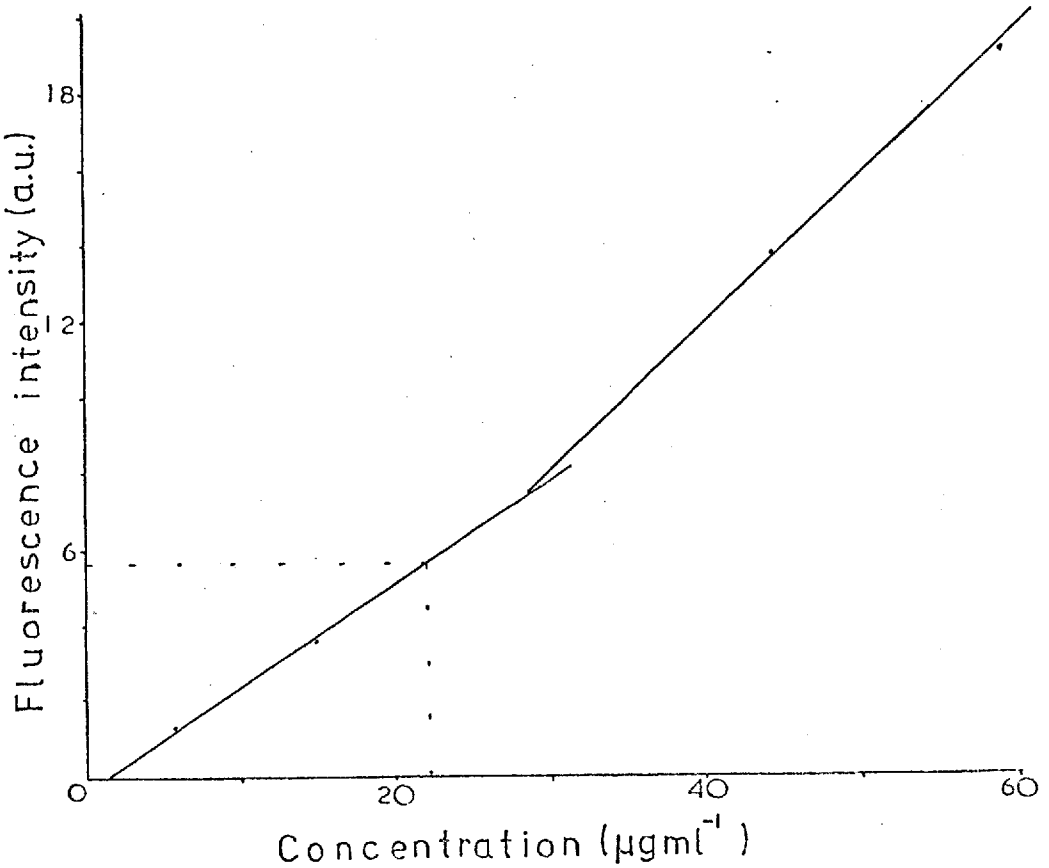

FIG. 6.7. Fluorescence of electrogenerated pseudomorphine versus concentration of morphine (Assay of morphine sulphate tablet). Morphine in pH 8.5 sodium pyrophosphate solution (0.1M); electrode potential 0.25V vs SCE; excitation wavelength 320nm; emission wavelength 442nm.

6.2.11. Interference studies

An important procedure in the development stages of a new analytical method is to examine and investigate possible interfering substances. Due to the large number of compounds structurally related to morphine which exhibit similar chemical and physical properties, a specific and interference-free method for morphine is difficult to obtain. Referring to the morphine dimerisation reaction on page 148 which involves oxidation of the ionised phenolic hydroxy group at the C-3 position and subsequent coupling of the phenolate radicals at C-2, it might be expected that this rather unusual reaction could offer the

necessary specificity and provide an interference-free route for morphine. Unfortunately, a large number of phenolic compounds undergo this reaction*. Kupferberg[107] reported that the phenolic alkaloids normorphine, n-allylmorphine, dihydromorphine and monoacetylmorphine yielded fluorescence characteristics identical to pseudomorphine and that they would interfere with the determination of morphine. Non-phenolic compounds including codeine and its derivatives and heroin (diacetylmorphine) did not yield fluorescence products similar to pseudomorphine and it was stated that such compounds would not cause interference although the conclusion was not substantiated by experiment. Essentially the same results were reported by Deys[115] for the anodic voltammetric determination of morphine in acidic solution: those alkaloids bearing a phenolic hydroxy group (pseudomorphine, dihydromorphine, dihydromorphinone, nalorphine, apomorphine) yielded oxidative waves similar to morphine causing interference whereas compounds containing alkylated hydroxy groups (codeine, narcotine, narceine, thebaine, papaverine)were not electroactive and did not interfere. With the results of Kupferberg and Deys providing the basis for interference studies,a selection of opium alkaloids that were readily available - codeine, narceine, narcotine, papaverine, cotarnine, laudanosine, sinomenine (phenolic alkaloid)-were examined for possible interference (papaverine, apomorphine, thebaine were considered, but were insoluble at pH 8.5.). Heroin (diacetylmorphine), a synthetic derivative of morphine, was

* Phenolic oxidation plays an important role in bio-organic synthesis particularly in the biogenisis of alkaloids; the interested reader may refer to reviews by Scott[117] and Fukumoto[118].

also investigated. The structures of the alkaloids are given in fig 6.8. Experiments were first concerned with establishing for each alkaloid their electroactivity and whether they exhibited oxidative fluorescence before conducting the interference studies proper. Possible interference mechanisms to be considered are spectral interference from either natural or oxidative fluorescence (not necessarily phenolic coupling) and chemical interference whereby the dimerisation reaction is inhibited.

(1) Voltammetric behaviour

It was hoped to demonstrate that the alkaloids having a free phenolic hydroxy group (morphine, sinomenine) would show an oxidative wave whereas the non-phenolic compounds would be electrochemically inactive. The current - potential curves for each alkaloid ($5x10^{-4}$M) in pH 8.5 sodium pyrophosphate solution (0.1M) were recorded during the cyclic sweep (0V to 0.75V to 0V vs SCE at $20mVs^{-1}$) of the gold wire. Oxidative waves were recorded for morphine, sinomenine and heroin solutions while solutions of codeine, narceine, cotarnine were electroinactive. The scan for laudanosine indicated possible electroactivity and a further sweep from 0.5V to 1.25V vs SCE confirmed this. A summary of the electrochemical behaviour of the alkaloids investigated is given in table 6.11. The voltammograms for sinomenine, morphine, codeine and heroin are presented in fig 6.9. The current - potential behaviour for sinomenine (curve a) being characteristic of phenolic oxidation was similar to morphine

Morphine

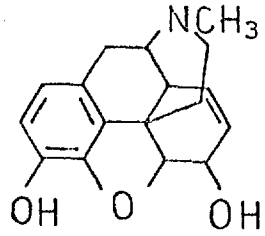

Codeine

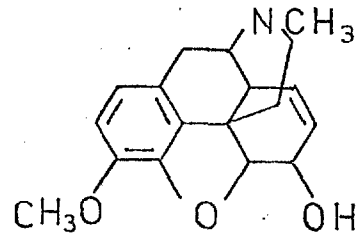

Heroin

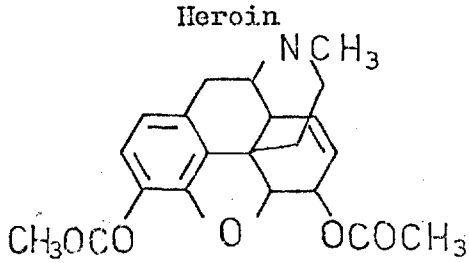

Apomorphine

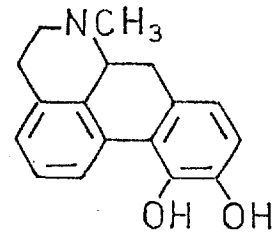

Sinomenine

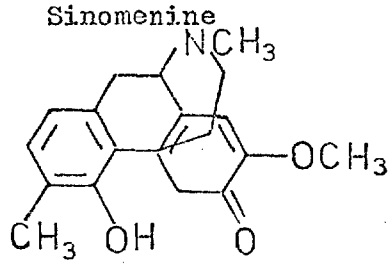

Cotarnine

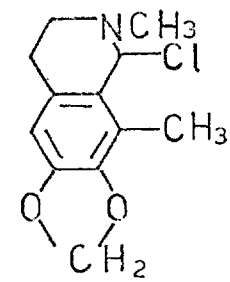

Papaverine

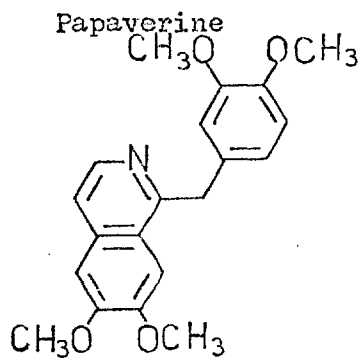

Laudanosine

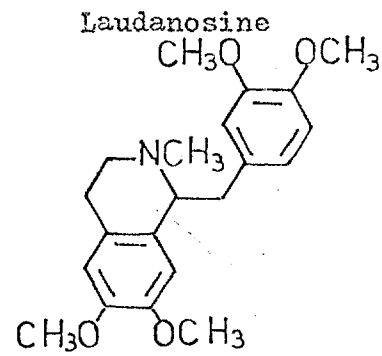

Narcotine

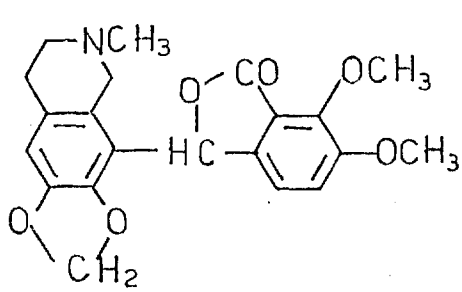

Narceine

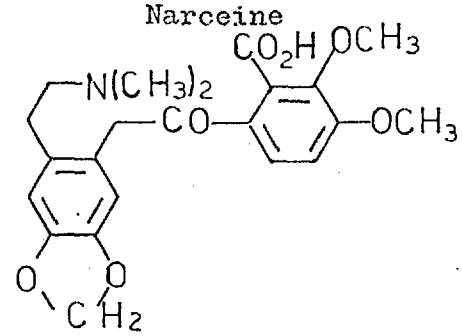

FIG. 6.8. Structures of some alkaloids.

(curve b) with oxidation commencing at approximately 0.15V vs SCE. Lack of cathodic current on the reverse scan for sinomenine indicated irreversibility in the sense that the unstable free radical species rapidly underwent a follow-up chemical reaction. A cathodic wave was similarly not observed for morphine and confirmed the irreversible nature of the oxidation process. The oxidative wave for heroin (curve d) was at first a little surprising and when recorded at high sensitivity (dotted line) was indicative of phenolic oxidation ($E_{\frac{1}{2}}$=0.27V). The compound, however, undergoes alkaline hydrolysis[119] to monoacetylmorphine and this enabled the characteristic oxidation wave to be recorded. The curve for laudanosine (solid line) in fig 6.10 reveals that oxidation commenced at approximately 0.8V vs SCE. Lack of cathodic current indicated an irreversible process. The scan for the background solution (broken line) is also given.

On the basis of this study it would be expected that sinomenine and heroin would cause interference either by (1) scavenging morphine free radicals and lowering the dimerisation efficiency and/or (2) undergoing self-coupling to give a fluorescent product. It cannot be predicted at this stage whether oxidation of laudanosine would interfere either chemically or spectrally. The remaining alkaloids should not interfere.

(2) Fluorescence studies

Solutions of each alkaloid (3×10^{-4}M) in pH 8.5 sodium pyrophosphate were examined individually in the gold micromesh

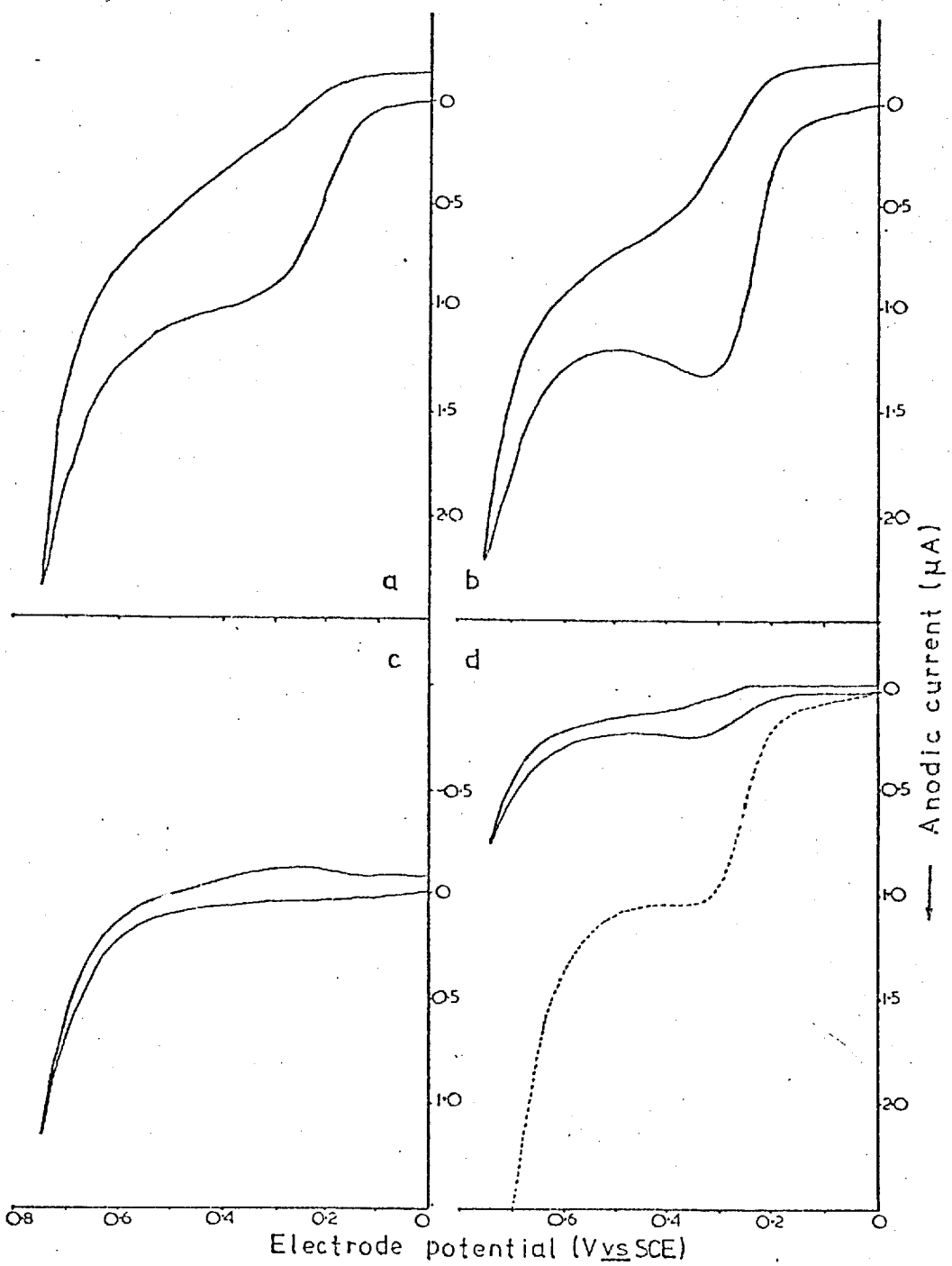

FIG. 6.9. Voltammetric curves for (a) sinomenine, (b) morphine, (c) codeine and (d) heroin. Alkaloid (5×10^{-4}M) in pH 8.5 sodium pyrophosphate solution (0.1M); working electrode, gold wire; scan rate $20 mVs^{-1}$; curve d, broken line: sensitivity, μA ÷ 5.

Table 6.11. Voltammetric characteristics of alkaloids.

Alkaloid	Oxidative Wave	$E_{\frac{1}{2}}$
Morphine	Yes	0.24
Sinomenine	Yes	0.21
Heroin*	Yes	0.27
Laudanosine	Yes	E_c 0.8
Codeine	No	-
Narceine	No	-
Cotarnine	No	-
Narcotine	No	-

Alkaloids (5×10^{-4}M) in pH 8.5 sodium pyrophosphate solution. Cyclic sweep, 0V to 0.75V to 0V *vs* SCE at $20 mVs^{-1}$ except laudanosine (0.5V to 1.25V to 0.5V *vs* SCE); * after hydrolysis.

cell during excitation at various positive applied potentials. Only the heroin and laudanosine solutions exhibited fluorescence (excitation, 320nm; emission, 442nm) during electrolysis. The emission spectrum for the heroin product was identical to pseudomorphine confirming Kupferberg's findings[107]. Also when the heroin solution was prepared immediately before examination only a small signal was recorded indicating that the hydrolysis to monoacetylmorphine at pH 8.5 was relatively slow. The laudanosine product exhibited sensitive fluorescence and the characteristics will be reported later. The remaining alkaloid solutions did not exhibit fluorescence. Sinomenine incidentally on oxidation is known to form the dimer, 1,1'-disinomenine[120] and on the basis of the previous study it is concluded that the dimer is non-fluorescent.

The possible interference of each alkaloid on the fluorescence of electrogenerated pseudomorphine was next investi-

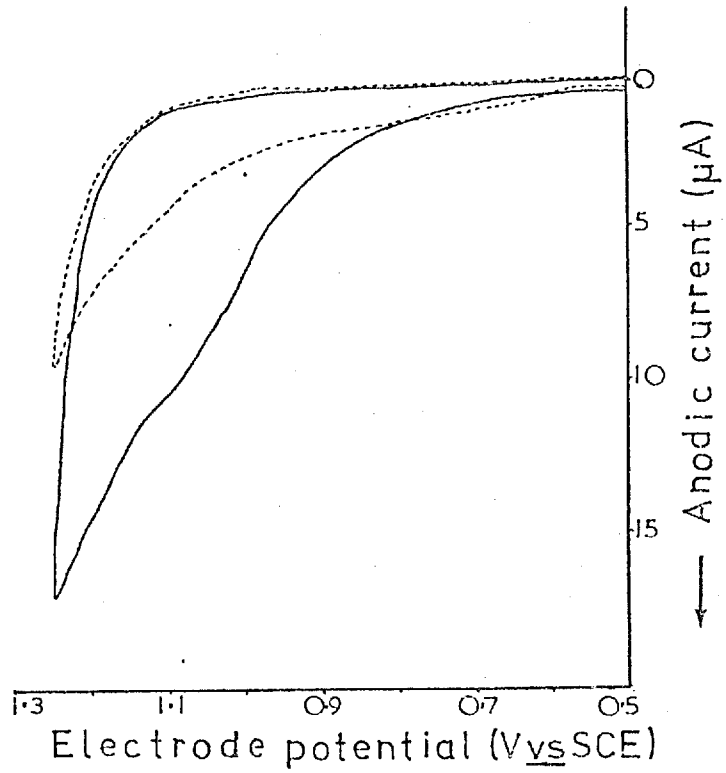

FIG. 6.10.
Voltammetric curve for laudanosine.
Laudanosine ($5x10^{-4}$M) in pH 8.5 sodium pyrophosphate solution (0.1M); working electrode, gold wire; scan rate $20mVs^{-1}$.

gated in a systematic manner. Morphine solutions ($3x10^{-5}$M) containing the particular alkaloid at (1) the same concentration ($3x10^{-5}$M), (2) 10 fold in excess ($3x10^{-4}$M), (3) 100 fold in excess ($3x10^{-3}$M), all in pH 8.5 sodium pyrophosphate solution (0.1M), were oxidised at 0.25V vs SCE and the maximum fluorescence recorded. This procedure was carried out for sinomenine, heroin, laudanosine, narceine, cotarnine and narcotine and in addition for codeine, concentrations 1000 fold in excess ($3x10^{-2}$M) were examined. The fluorescence results are summarised in table 6.12. The electroinactive alkaloids, codeine, narceine, cotarnine and narcotine caused no interference at all the concentration levels investigated except for cotarnine at the $3x10^{-3}$M level when natural fluorescence became significant. The remaining electroactive alkaloids, sinomenine, heroin and laudanosine caused interference. For sinomenine at the $3x10^{-5}$M level, the fluorescence signal was reduced to 33% of the original

Table 6.12. Interference of alkaloids on the fluorescence of electrogenerated pseudomorphine.

Alkaloid	Oxidative Fluorescence	Interference Results Alkaloid Concentration (M)			
		$3x10^{-5}$	$3x10^{-4}$	$3x10^{-3}$	$3x10^{-2}$
Morphine	Yes				
Sinomenine	No	X	X	X	
Heroin *	Yes	/	X	X	
Laudanosine	Yes	/	X	X	
Codeine	No	/	/	/	/
Narceine	No	/	/	/	
Cotarnine	No	/	/	/	
Narcotine	No	/	/	/	

Morphine ($3x10^{-5}$M) and alkaloid in pH 8.5 sodium pyrophosphate solution (0.1M); electrode potential 0.25V vs SCE; excitation wavelength 320nm, emission wavelength 442nm; X represents interference, / no interference; * After hydrolysis.

value while morphine solutions that were $3x10^{-4}$M with respect to sinomenine exhibited no fluorescence on electrolysis. Laudanosine and heroin solutions individually caused serious positive interference (increased fluorescence) at concentrations $3x10^{-4}$M and higher. Interference was not observed at the $3x10^{-5}$M level.

The results of this study are in good agreement with the predictions voiced on the basis of the voltammetric behaviour of the alkaloids. Alkaloids containing a phenolic hydroxy group undergo phenolic oxidation and prevent pseudomorphine formation by scavenging the morphine free radical species. This interference mechanism was exhibited by sinomenine. Although, in the case of sinomenine, fluorescence was not realised for the self-coupled product (1,1'-disinomenine) or the mixed dimer

species (sinomenine-morphine) such possibilities would have to be considered for other phenolic alkaloids. Spectral interference from non-phenolic alkaloids which become fluorescent on oxidation is also possible; this was demonstrated for laudanosine. The high specificity of the dimerisation reaction in the presence of electroinactive alkaloids (codeine, narcotine, cotarnine, narceine) was, however, evident and the result for codeine was particularly important.

6.2.12. Assay of papaveretum tablet and omnopon injection ampoule

The official assay methods for morphine in pharmaceutical preparations based on opium require a preliminary extraction procedure prior to titrimetric, gravimetric or colorimetric finish[104]. This applies to papaveretum, an important preparation based on the principal opium alkaloids. It consists of the hydrochloride salts of morphine (47.5 - 52.5% ww^{-1}), narcotine (16 - 22% ww^{-1}), codeine (2.5 - 5% ww^{-1}) and papaverine (2.5 - 7% ww^{-1}) and is obtained in the form of tablet (10mg papaveretum, BPC) or injection ampoule (Omnopon, 20mgml^{-1} papaveretum; Roche).

Procedure

One papaveretum tablet weighing 63.4mg was powdered in a mortar. An accurately weighed quantity (58.6mg) was transferred to a volmetric flask (10ml) containing dilute sulphuric acid (0.1M) and left overnight to allow extraction of the alkaloids. A few drops of sodium hydroxide solution (1M) were next added to precipitate papaverine and also some narcotine. The cloudy

solution was filtered (Whatman No 52) and diluted to 10ml giving stock solution P. Omnopon injection solution (1ml) was similarly treated giving stock solution O.

Stock morphine (1500μgml^{-1}) was prepared and suitable aliquots were diluted in pH 8.5 sodium pyrophosphate solution (0.1M) to 25ml giving standard solutions ranging from 3 to 30μgml^{-1}. Aliquots (500μl) of the stock P and O solutions were treated likewise. The fluorescence of the standard and unknown solutions was measured in the usual manner for excitations at 0.25V vs SCE and the results are presented in table 6.12. The unknown concentrations, solutions P and O, are also included in the table and were read from the linear calibration graph of fig 6.11.

Table 6.12. Assay of papaveretum tablet and omnopon injection ampoule - fluorescence results.

Morphine Concentration (μgml^{-1})	Max, Fluorescence Intensity (a.u.)		
			Av.
3.0	10.2	10.3.	10.2
6.0	26.8	26.6	26.7
12.0	51.0	50.6	50.8
18.0	75.9	74.3	75.1
24.0	95.4	93.6	94.5
30.0	117.0	115.8	116.4
Unknown solution P 9.6	42.6	41.9	42.2
Unknown solution O 19.8	81.0	80.4	8C.6

Solutions in pH 8.5 sodium pyrophosphate (0.1M); electrode potential 0.25V vs SCE; excitation wavelength 320nm; emission wavelength 442nm.

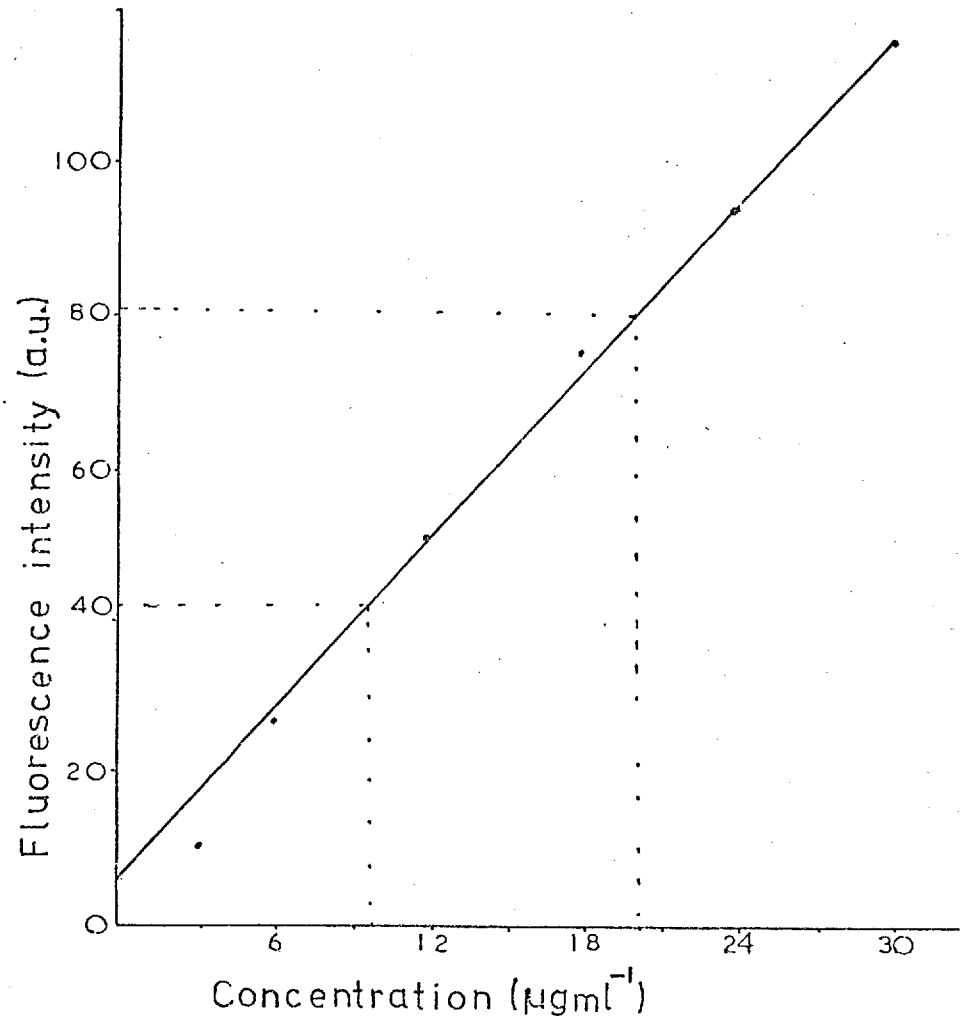

FIG. 6.11. Fluorescence of electrogenerated pseudomorphine versus concentration of morphine (Assay of papaveretum tablet and omnopon injection ampoule). Morphine in pH 8.5 sodium pyrophosphate solution (0.1M); electrode potential 0.25V vs SCE; excitation wavelength 320nm; emission wavelength 442nm.

Calculation

(1) Papaveretum tablet

Concentration of morphine in diluted P solution = $9.6\mu gml^{-1}$

∴ Concentration of morphine in stock P solution = $480\mu gml^{-1}$

∴ Weight of morphine in 10ml = 4.8mg

∴ Weight of morphine in tablet = 4.8 x 63.4/58.6 = 5.2mg

(2) Omnopon injection ampoule

Concentration of morphine in diluted O solution = $19.8\mu gml^{-1}$

∴ Concentration of morphine in stock O solution = $990\mu gml^{-1}$

∴ Concentration of morphine in ampoule = $990\mu gml^{-1} \times 10$

= $9.9mgml^{-1}$

The results of the assay are shown in table 6.13 and confirm that the procedure is interference-free and provides accurate results.

Table 6.13. Morphine assay in papaveretum tablet and omnopon injection ampoule.

	Morphine	
	Specified	Found
Papaveretum Tablet (10mg)	47.5-52.5% ww^{-1}	52.0% ww^{-1}
Omnopon Injection Ampoule ($20mgml^{-1}$)	$10mgml^{-1}$	$9.9mgml^{-1}$

6.3. Laudanosine

Laudanosine is one of the minor and lesser important of the alkaloids occurring naturally in opium. Previous interference studies with respect to morphine indicated that the compound exhibited fluorescence on oxidation at 0.25V vs SCE. This behaviour would not be expected on the basis of the laudanosine current - potential curve (fig 6.10) where the oxidation wave commenced at about 0.8V vs SCE. Further investigations showed that increments in electrode potential caused increased fluorescence development in a similar manner to the morphine experiments.

6.3.1. Spectral characteristics of the oxidation product

The fluorescence spectra recorded for laudanosine ($3x10^{-4}$M) in pH 8.5 sodium pyrophosphate solution (0.1M) at 0.7V vs SCE are presented in fig 6.12. The excitation spectrum consists of peaks at 315nm and 361nm while the emission is broad and structureless with a maximum at 470nm. The wavelength combination, λ_{ex} 361nm and λ_{em} 470nm, was chosen for subsequent experiments.

6.3.2. Effect of pH

The fluorescence response curves for laudanosine ($3x10^{-4}$M) in (1) sulphuric acid solution (0.1M), (2) potassium sulphate solution (0.03M), (3) pH 8.5 sodium pyrophosphate solution (0.1M) and (4) sodium hydroxide solution (0.1M) were recorded for excitation at 0.7V vs SCE. The findings are given in table 6.14. The pH dependence of the signal with the requirement that the solution is alkaline before fluorescence

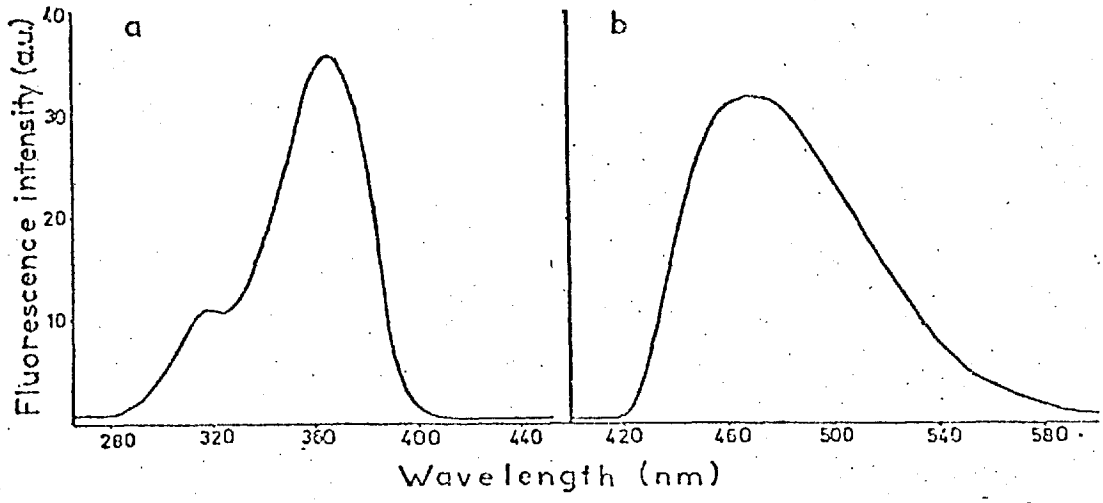

FIG. 6.12. Fluorescence excitation (a) and emission (b) spectra of the oxidation product of laudanosine. Laudanosine ($3x10^{-4}M$) in pH 8.5 sodium pyrophosphate solution (0.1M); electrode potential 0.7V vs SCE; excitation wavelength 361nm, emission wavelength 470nm; bandpass 10nm on both monochromators (respective filters, 7 - 54 and 3 - 73, fitted).

Table 6.14. The effect of pH on the fluorescence of laudanosine during electrolysis.

Background electrolyte Solution	Maximum Fluorescence Intensity (a.u.)
pH 1 Sulphuric acid (0.1M)	0
pH 5.2 Potassium sulphate (0.03M)	0
pH 8.5 Sodium pyrophosphate (0.1M)	40
pH 13 Sodium hydroxide (0.1M)	35

Laudanosine ($3x10^{-4}M$); electrode potential 0.7V vs SCE; excitation wavelength 361nm, emission wavelength 470nm.

is produced suggests that protonation of the tertiary nitrogen of the isoquinoline ring (see fig 6.8) prevents the formation of a fluorescent product on oxidation.

6.3.3. Calibration

Various aliquots of stock laudanosine (0.001M) were diluted to 25ml in pH 10.2 sodium pyrophosphate solution (0.1M) giving solutions covering the range $4x10^{-7}M$ to $2x10^{-5}M$.

The response curves for laudanosine solution (10^{-5}M) were initially recorded for various excitation potentials (0.7V, 0.9V, 1.1V vs SCE) and 0.9V was chosen as the most convenient in terms of development time and maximum signal attained. The fluorescence results and the corresponding logarithmic calibration plot are presented in table 6.15 and fig 6.13 respectively.

Table 6.15. Fluorescence of the oxidation product as a function of laudanosine concentration.

Laudanosine Concentration (M)	(log M)	Maximum Fluorescence Intensity (a.u.)	(log a.u.)
$4x10^{-7}$	-6.40	0.0026	-2.58
10^{-6}	-6.00	0.0073	-2.14
$2x10^{-6}$	-5.70	0.0111	-1.95
$4x10^{-6}$	-5.40	0.0207	-1.68
10^{-5}	-5.00	0.0535	-1.27
$1.2x10^{-5}$	-4.92	0.0715	-1.15
$2x10^{-5}$	-4.70	0.1149	-0.94

Laudanosine in pH 10.2 sodium pyrophosphate solution (0.1M); electrode potential 0.9V vs SCE; excitation wavelength 361nm, emission wavelength 470nm.

It can be seen that approximate linearity over the 100 fold concentration range was attained. Extending the calibration graph to meet the limiting signal ($2\sigma_{bl}$ = $2.4x10^{-4}$ a.u.) provided a limiting detectable laudanosine concentration of $4x10^{-8}$M. This figure corresponds to a limiting detectable weight of 2ng based on a cell volume of 120µl.

6.3.4. Structure of the oxidation product

There is evidence in the literature that oxidation may involve an intramolecular cyclisation reaction. On the basis of

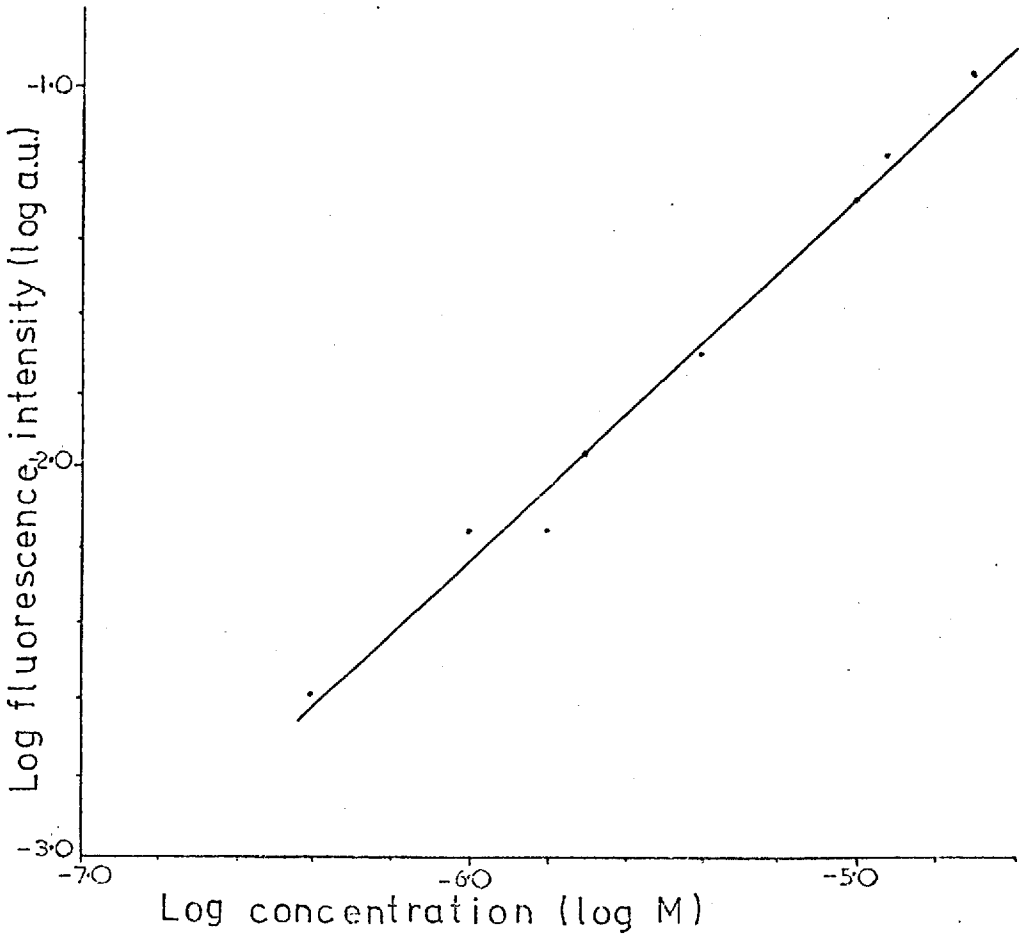

FIG. 6.13. Logarithmic calibration graph for the oxidation product of laudanosine. Laudanosine ($4x10^{-7}$M - $2x10^{-5}$M) in pH 10.2 sodium pyrophosphate solution (0.1M); electrode potential 0.9V vs SCE; excitation wavelength 361nm, emission wavelength 470nm.

cyclic voltammetric studies in acetonitrile, Miller and co-workers[121,122] suggested that the dimethylbenzene moiety of the isoquinoline ring was oxidised (2-electron transfer) and yielded o-methyl flavinantine as the final product. Another possible product is glaucine which has been chemically prepared using vanadium oxytrifluoride as oxidant in trifluoroacetic acid[123]. The structures for both compounds are given below in the overall reaction schemes. Clearly, the high degree of conjugation and structural rigidity for both molecules would be favourable for fluorescence. Lack of fluorescence in acidic solution, however, would tend to disfavour the glaucine product.

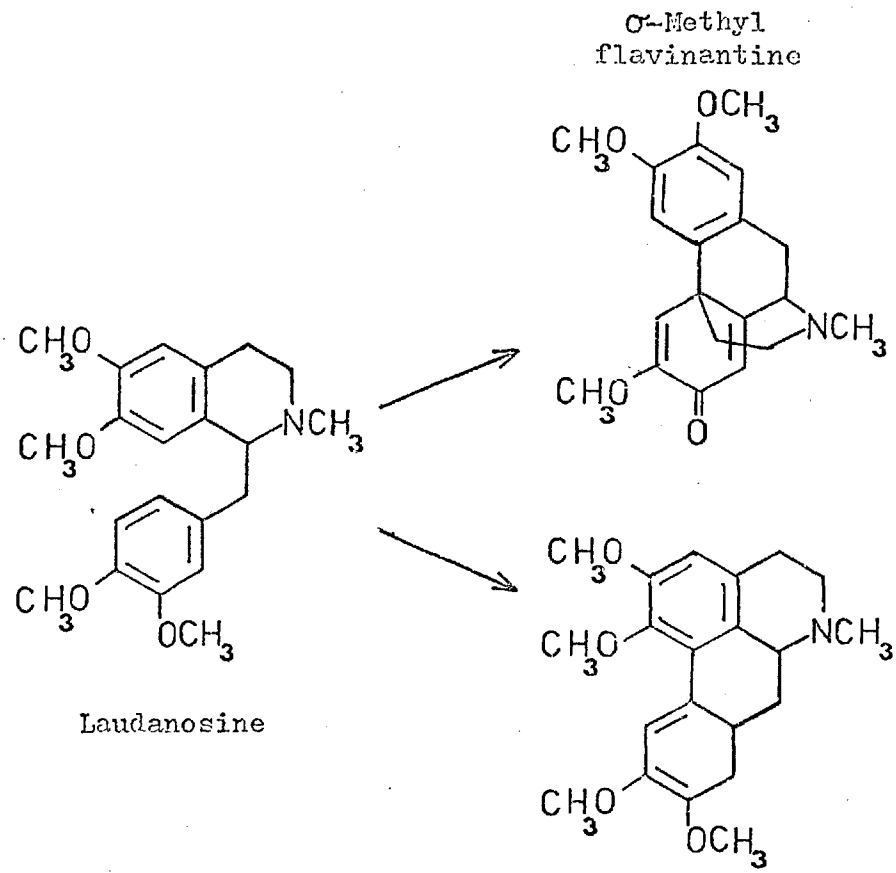

Oxidation products of laudanosine.

6.4. Reserpine

Reserpine, a weakly basic ester alkaloid obtained from the plant Rauwolfia serpentina, has hypnotic and sedative properties and has been used for controlling high blood pressure and in the treatment of mental illness. A sensitive fluorimetric method based on the oxidation of the alkaloid by vanadium pentoxide in ethanolic phosphoric acid solution is available[124]. The oxidation reaction

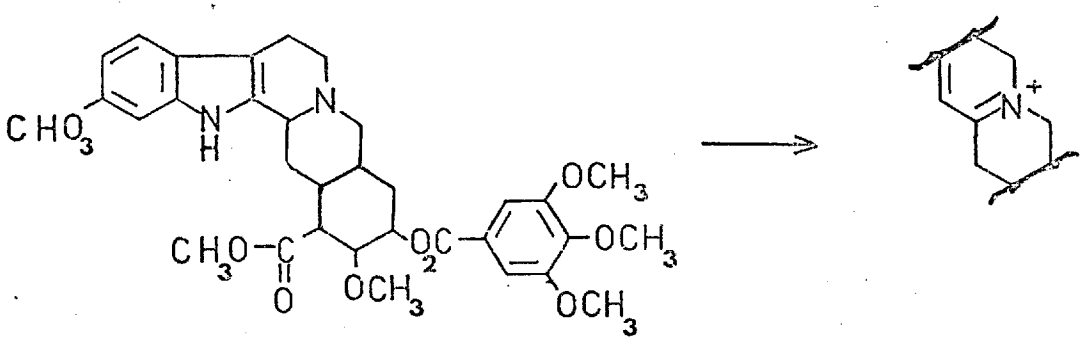

proceeds at the piperdine nitrogen and results in 3,4-dehydroreserpine[124,125]. The fluorescence of the oxidation product (λ_{ex} 365nm, λ_{em} 495nm) was shown to depend markedly on (1) the nature of the oxidant, (2) the nature of mineral acid and (3) the aqueous concentration of the ethanol solvent system.

6.4.1. Voltammetric behaviour

The current - potential curve was recorded for reserpine (500μgml^{-1}) in aqueous ethanol solution (75% vv^{-1} ethanol) containing phosphoric acid (0.6M) as background electrolyte. The voltammogram given in fig 6.14 reveals an oxidation wave commencing at about 0.65V vs SCE with a peak potential of 0.79V vs SCE. Lack of a reduction wave on the reverse scan

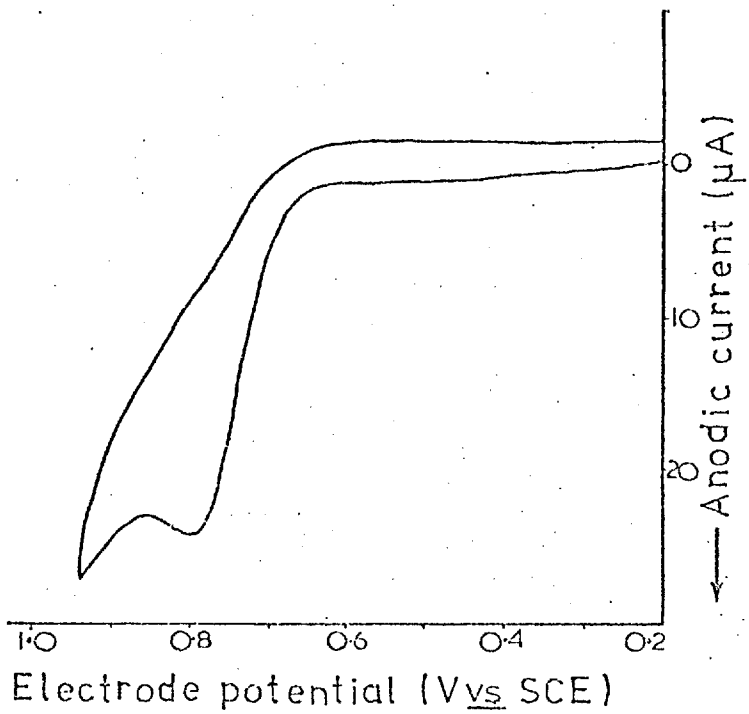

FIG. 6.14. Voltammetric curve for reserpine. Reserpine ($500\mu g ml^{-1}$) in aqueous ethanol (75% vv^{-1} ethanol) containing phosphoric acid (0.6M); working electrode, gold wire; scan rate $20mVs^{-1}$.

indicates an irreversible oxidation.

6.4.2. Fluorescence spectra

The pure drug was not available at the start of the investigations and, instead, a stock reserpine solution was prepared from reserpine tablets (Serpasil 1mg; Ciba). Sample solution was prepared by diluting the stock with aqueous ethanol (75% vv^{-1} ethanol) containing phosphoric acid (0.6M). Appreciable fluorescence was immediately generated on oxidation at 0.8V vs SCE and the recorded spectra are given in fig 6.15. The excitation and emission maxima were 375nm and 500nm respectively.

6.4.3. Effect of electrode potential

The influence of electrode potential on the rate of fluorescence development and the maximum fluorescence attained was similar to the behaviour for morphine. Table 6.16 contains results for excitations at 0.8V, 1.0V and 1.2V vs SCE.

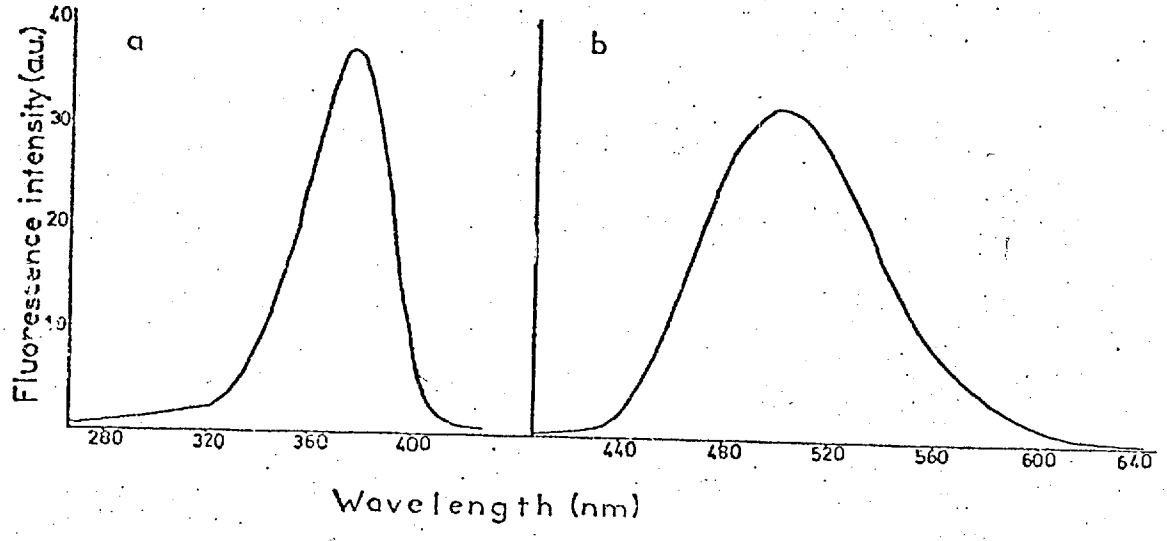

FIG. 6.15. Fluorescence excitation (a) and emission (b) spectra of electrogenerated 3-dehydroreserpine. Reserpine in aqueous ethanol (75%vv^{-1} ethanol) containing phosphoric acid (0.6M); electrode potential 0.8V vs SCE; excitation wavelength 375nm; emission wavelength 500nm; bandpass, 10nm on both monochromators (respective filters, 7 - 54 and 3 - 73, fitted).

Table 6.16. Effect of electrode potential or the fluorescence response of electrogenerated 3-dehydroreserpine product.

Electrode Potential (V vs SCE)	Maximum Fluorescence Intensity (a.u.)	$Time_{MF}$ (min)
0.8	62	26
1.0	42	10.4
1.2	20	2.3

Reserpine in aqueous ethanol (75% vv^{-1} ethanol) containing phosphoric acid (0.6M); excitation wavelength 375nm, emission wavelength 500nm.

6.4.4. Calibration and assay of reserpine tablet

Solution preparation

Standard reserpine solutions (0.1 - 20$\mu g ml^{-1}$) were prepared from stock reserpine solution (1000$\mu g ml^{-1}$) by appropriate dilution with aqueous ethanolic solution (75% ethanol vv^{-1}) containing phosphoric acid (0.6M).

Reserpine tablets (3; 1mg) were crushed in a volumetric flask and left to stand overnight in ethanolic solution containing

phosphoric acid (0.6M). After filtration, the solution was diluted to 10ml. An aliquot (750µl) was then diluted to 25ml with electrolyte solution as above.

Results

The initial experiment for reserpine solution ($2\mu gml^{-1}$) with excitation at 0.9V vs SCE revealed an extremely sensitive fluorescence response, but unfortunately the fluorescence recorded for the repeat run was approximately 50% less intense. It was thought that the signal reduction was caused by electrode poisoning, but it was later noticed that a large air pocket had formed in the cell. It appeared that the alcoholic solution favoured the formation of air bubbles in the tubing which subsequently became lodged in the cell. (This trouble was not experienced with aqueous solution.) Further measurements were, therefore, subject to this difficulty. The response curves for the remaining reserpine solutions with excitation at 0.9V vs SCE were recorded. Unfortunately, maxima were not reached in an acceptable time so that values corresponding to specified times (1.2min, 2.4min, 12.0min) were obtained from the fluorescence - time curves. The results are presented in table 6.17; the values for reserpine, $14\mu gml^{-1}$, were used in a recovery experiment. Approximate linearity was observed for the plots at the three time intervals, but the best experimental fit of data was obtained for t at 1.2 minutes. The calibration graph for t at 1.2 minutes is given in fig 6.16 and the concentration corresponding to the unknown reserpine solution is indicated.

Table 6.17. Assay of reserpine tablet - fluorescence results.

Reserpine Concentration (μgml^{-1})	Fluorescence intensity (a,u.) at 1.2min	2.4min	12.0min
0.1	0.0007	0.0009	0.0020
0.8	0.0065	0.0087	0.0157
2.0	0.0195	0.0267	0.0540
6.0	0.0522	0.0618	0.1356
10.0	0.0891	0.1011	0.1857
14.0	0.1251	0.1749	0.2930
16.0	0.1470	0.2030	0.4010
20.0	0.1530	0.2110	0.4400
Unknown	0.0630	0.0771	0.1695

Reserpine in aqueous ethanol (75% vv^{-1} ethanol) containing phosphoric acid (0.6M); electrode potential 0.9V vs SCE; excitation wavelength 375nm, emission wavelength 500nm.

Calculation

Concentration of unknown reserpine solution = $7.05 \mu gml^{-1}$

Concentration of stock reserpine solution = $235 \mu gml^{-1}$

≡ 2.35mg/10ml

∴ Weight in tablets (3) = 2.35mg

∴ Weight in reserpine tablet = 0.76mg

Labelled content = 1mg

There is considerable deviation between the labelled reserpine content (1mg) and the amount found. Assuming the former to be correct, the discrepancy was probably due to incomplete extraction of the drug from the tablets in the dissolution stage. A repeat experiment to check this was, however, not

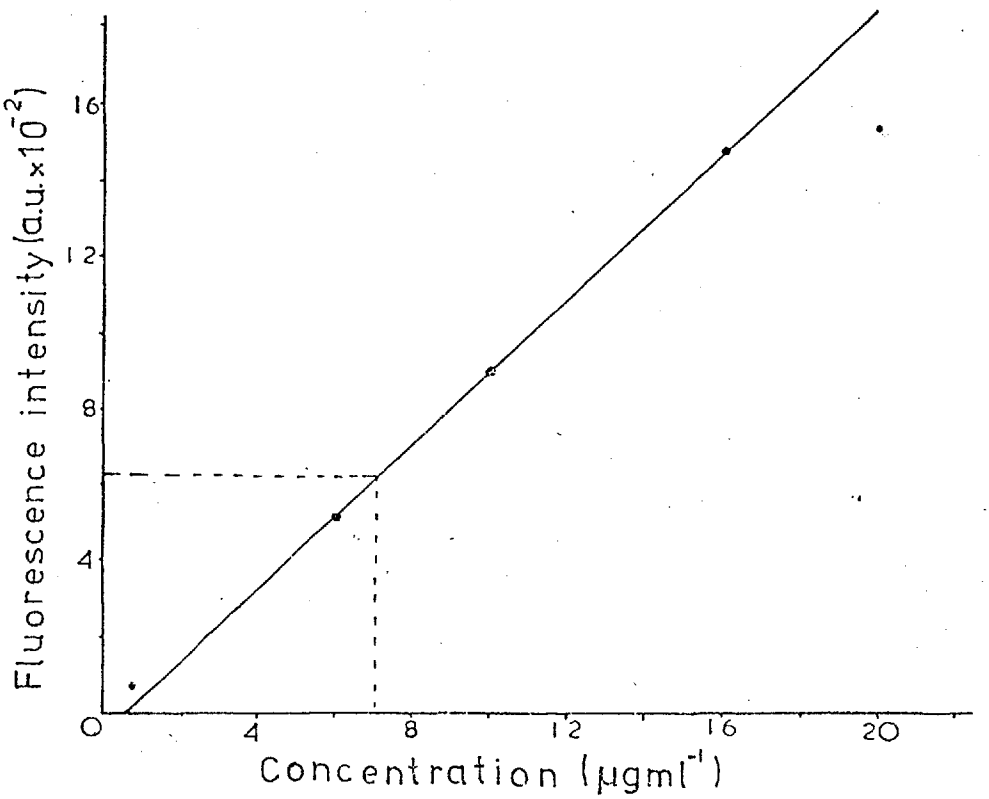

FIG. 6.16. Fluorescence of electrogenerated 3-dehydroreserpine versus reserpine concentration (assay of reserpine tablet). Reserpine in aqueous ethanol (75%vv^{-1} ethanol) containing phosphoric acid (0.6M); electrode potential 0.9V vs SCE; excitation wavelength 375nm; emission wavelength 500nm.

performed. Based on a single recovery experiment, the procedure was shown to be accurate since a recovery of 98.6% (amount recovered, 13.8μgml^{-1}) was obtained for reserpine solution of concentration 14μgml^{-1}.

The limit of detection calculated from the logarithmic calibration graph (t=12min) in the usual manner ($2\sigma_{bl}=3.6\times10^{-4}$) was 40ngml^{-1}. For the cell volume of 120μl, the limiting detectable weight of reserpine was 5ng. Increased sensitivity would have been realised if the air bubble problem had been eliminated.

6.5. Thioguanine

Thioguanine (6-aminopurine-6-thiol) is an important drug for inhibiting neoplastic disease[126]. A sensitive fluorimetric assay, reported by Finkel[126], is based on oxidation of the drug by alkaline permanganate solution to the highly fluorescent sulphonate

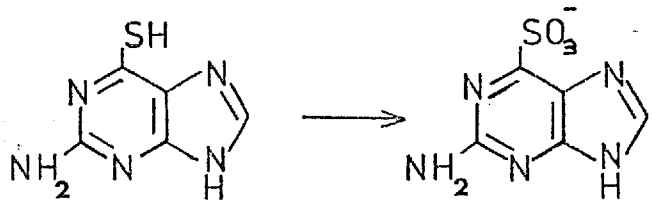

Optimum conditions for the method were pH 10.1 with excitation at 370nm and emission at 410nm. Depending on the reaction conditions, various oxidation products (disulphide, sulphinate, sulphonate) may be formed and these are discussed by Fox and co-workers[127].

6.5.1. Voltammetric behaviour

The current - potential curve for thioguanine (2×10^{-3}M) in pH 10.2 sodium pyrophosphate solution (0.1M) was recorded during a cyclic sweep (0V to 0.75V to 0V vs SCE at $20 mVs^{-1}$) of the gold wire working electrode. Inspection of fig 6.17 reveals an irreversible oxidation wave commencing at about 0.3V vs SCE. The peak observed for the reverse scan is due to reduction of gold oxide.

6.5.2. Fluorescence spectra

Fluorescence monitoring (λ_{ex} 330nm, λ_{em} 410nm) of thioguanine (3×10^{-4}M) in pH 10.2 sodium pyrophosphate solution

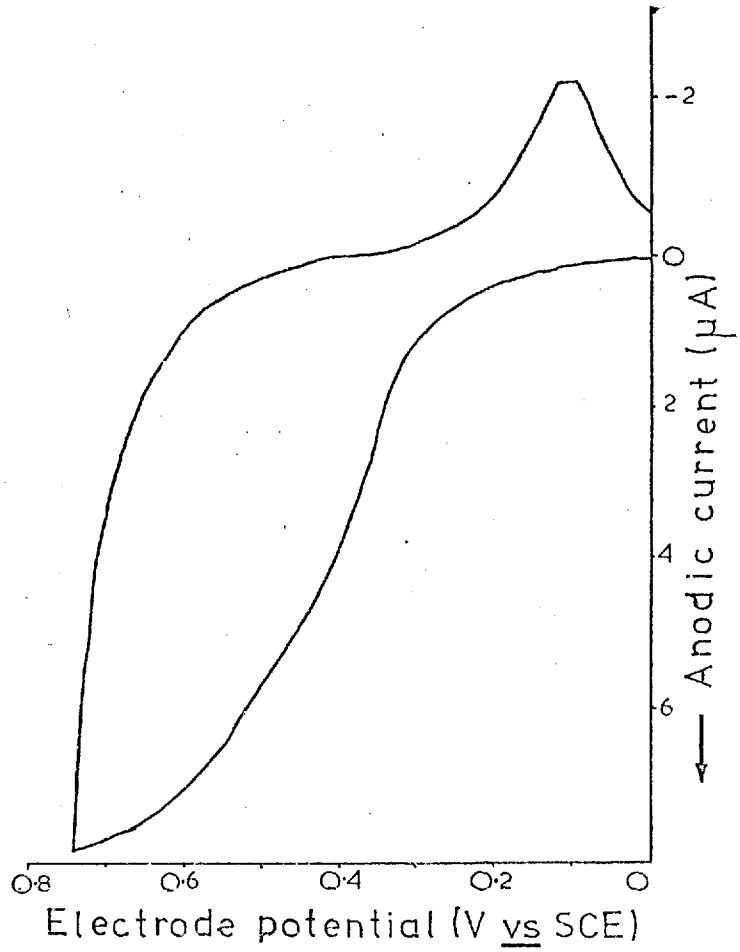

FIG. 6.17.
Voltammetric curve for thioguanine.
Thioguanine ($2x10^{-3}$M) in pH 10.2 sodium pyrophosphate solution (0.1M); working electrode, gold wire; scan rate $20mVs^{-1}$.

(0.1M) with excitation at 0.7V vs SCE was immediately successful. The wavelength of maximum emission (λ_{em} 410nm), however, corresponded to a very low transmission region for the 3-73 filter and it was necessary to remove the filter from the emission monochromator for spectral recording; this introduced a considerable background noise to the fluorescence response. The spectra given in fig 6.18 have characteristic excitation (λ_{ex} 310nm) and emission (λ_{em} 400nm) bands and are in reasonable agreement with that reported by Finkel[126], thus confirming sulphonate production. The background level of the blank solution at 400nm was relatively high and sensitivity was improved by recording at 420nm.

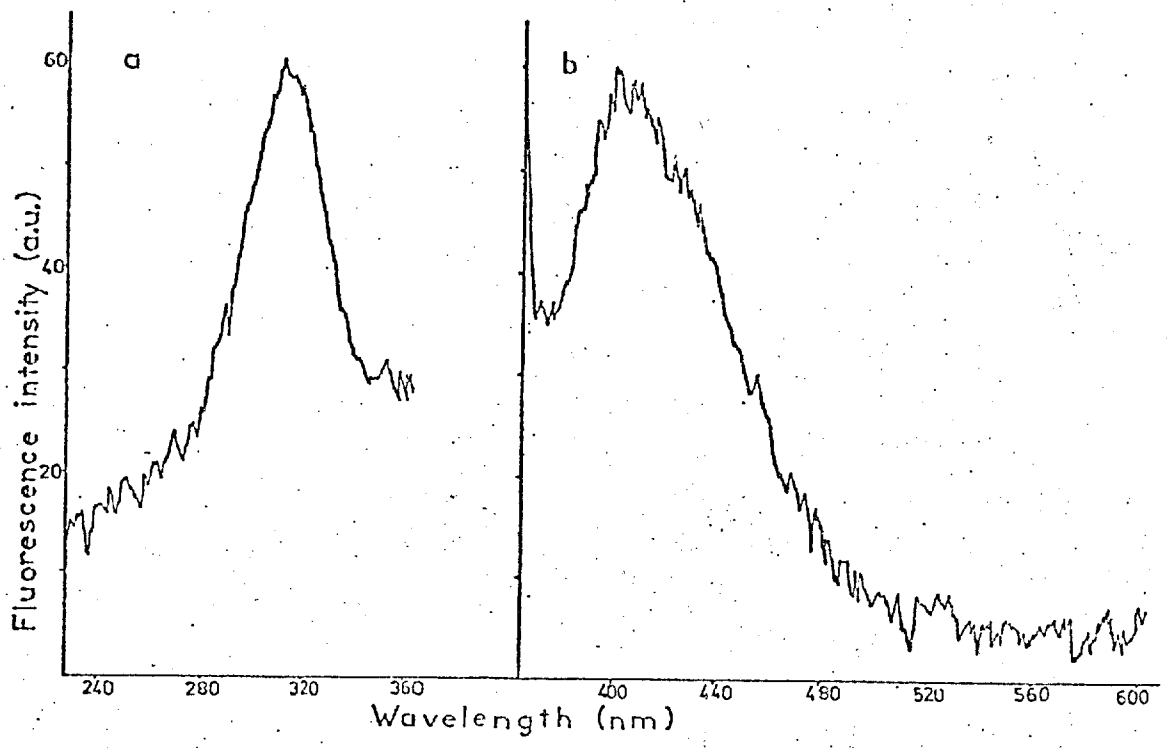

FIG. 6.18. Fluorescence excitation (a) and emission (b) spectra of electrogenerated thioguanine sulphonate. Thioguanine ($3x10^{-4}M$) in pH 10.2 sodium pyrophosphate solution (0.1M); electrode potential 0.7V vs SCE; excitation wavelength 310nm, emission wavelength 400nm; bandpass 10nm on both monochromators (only 7 - 54 filter fitted).

6.5.3. Effect of electrode potential

Excitation potentials of 0.1V to 1.3V vs SCE were imparted on the gold micromesh and the resulting fluorescence response curves for thioguanine ($2x10^{-4}M$) in pH 10.2 sodium pyrophosphate solution (0.1M) were recorded. Surprisingly, significant fluorescence development was noted for excitation at 0.1V vs SCE and this would not have been predicted on the basis of the current - potential curve (fig 6.17). During the recording, maximum fluorescence did not develop within 12 minutes for excitations less than 0.9V vs SCE. Excitation at 1.1V vs SCE yielded a maximum fluorescence of 35units after 5 minutes while at 1.3V vs SCE the corresponding values were 21 units after 2.5 minutes.

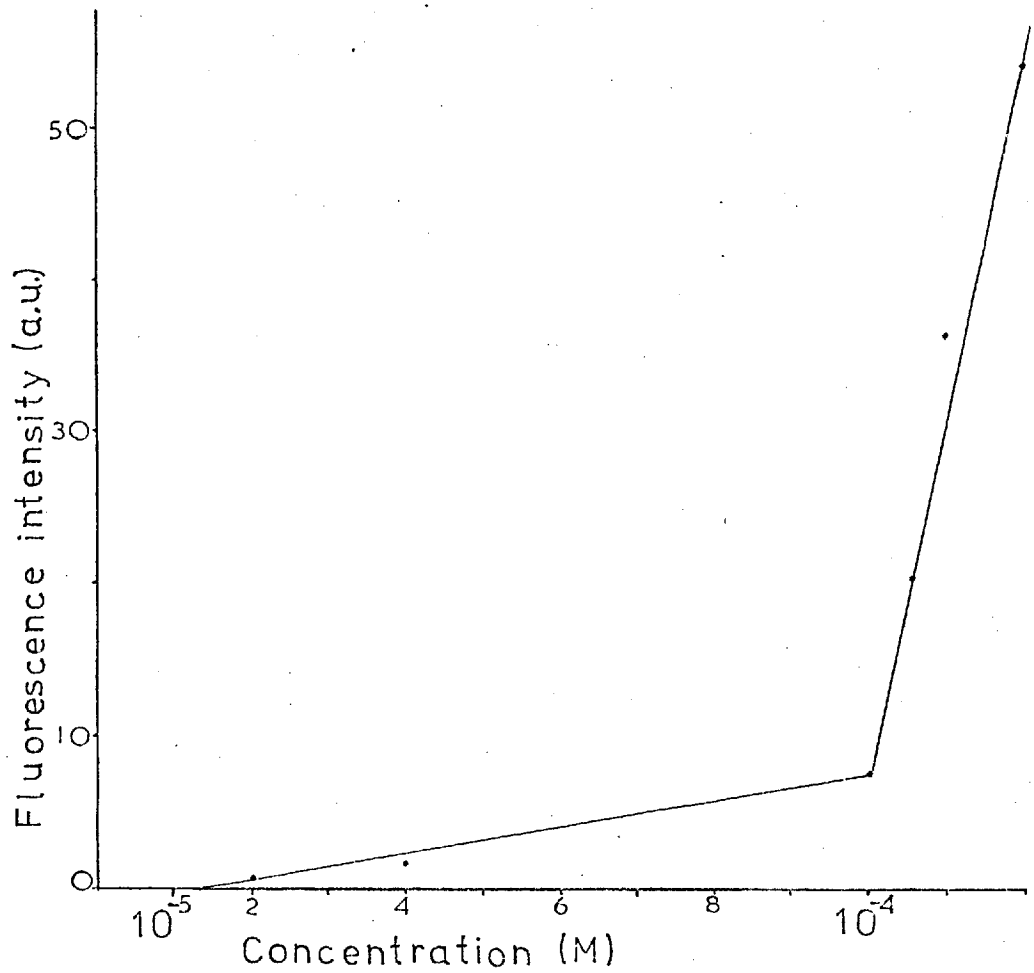

FIG. 6.19. Fluorescence of electrogenerated thioguanine sulphonate versus thioguanine concentration. Thioguanine in pH 9.7 sodium pyrophosphate solution (0.1M); electrode potential 1.1V vs SCE; excitation wavelength 310nm; emission wavelength 420nm.

6.5.4. Calibration

Various concentrations of thioguanine (10^{-5}M - 3×10^{-4}M) in pH 9.7 sodium pyrophosphate solution (0.1M) were oxidised at 1.1V vs SCE and maximum fluorescence was recorded; the results are presented in table 6.18. The calibration plot is given in fig 6.19 and it can be seen that the graph is rather unusual having two distinct regions of linearity.

Table 6.18. Fluorescence of electrogenerated thioguanine sulphonate as a function of thioguanine concentration.

Thioguanine Concentration (M)	Maximum Fluorescence Intensity (a.u.)	$Time_{MF}$ (min)
$2x10^{-5}$	1.65	2.4
$4x10^{-5}$	4.35	2.6
10^{-4}	7.50	3.0
$1.6x10^{-4}$	20.28	4.2
$2x10^{-4}$	36.50	5.2
$3x10^{-4}$	54.30	8.2

Thioguanine in pH 9.7 sodium pyrophosphate solution (0.1M); electrode potential 1.1V vs SCE; excitation wavelength 310nm, emission wavelength 420nm.

6.6. Homovanillic Acid

The assay of urinary homovanillic acid (HVA, 4-hydroxy-3-methoxyphenylacetic acid), the major metabolite of dopamine, is an important indicator of a number of medical disorders[128]. Fluorogenic oxidation reactions based on ferric chloride[129], potassium ferricyanide[130] and potassium permanganate[128] have been reported. The reaction

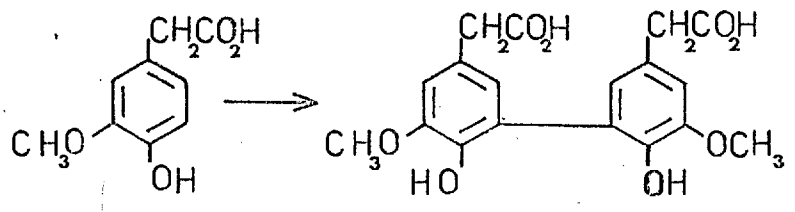

whereby the acid is converted to the highly fluorescent dimer (2,2'-dihydroxy-3,3-dimethyoxybiphenyl-5,5'diacetic acid; λ_{ex} 315nm, λ_{em} 425nm) is an example of phenolic oxidative coupling. Homovanillic acid has been employed as a fluorogenic substrate, the reaction enabling the sensitive determination of the oxidative enzymes, peroxidase, glucose oxidase and xanthine oxidase[131].

6.6.1. Voltammetric behaviour

The current - potential curve for HVA (5×10^{-4}M) in pH 8.5 sodium pyrophosphate solution (0.1M) recorded during a cyclic scan (0V to 0.75V to 0V *vs* SCE at 20mVs^{-1}) of the gold wire working electrode is given in fig 6.20. A well-developed anodic wave ($E_{\frac{1}{2}}$ = 0.28V), corresponding to removal of one electron from the phenoxide moiety, is apparent.

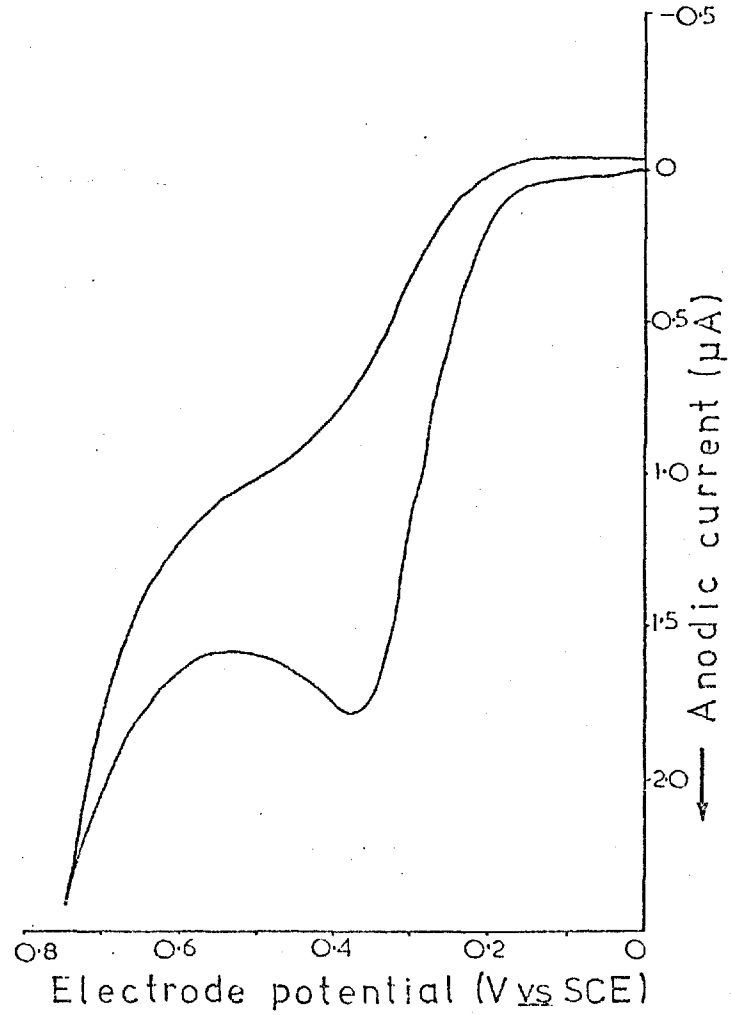

FIG. 6.20.
Voltammetric curve for homovanillic acid ($5x10^{-4}M$) in pH 8.5 sodium pyrophosphate solution (0.1M); working electrode, gold wire; scan rate $20mVs^{-1}$.

6.6.2. Fluorescence spectra

Initial fluorescence monitoring (λ_{ex} 315nm, λ_{em} 425nm) of HVA ($3x10^{-4}M$) in pH 8.5 sodium pyrophosphate solution for excitation at 0.3V vs SCE was successful and the fluorescence spectra of the electrogenerated product were recorded. The spectra are given in fig 6.21 and it can be seen that the excitation maximum, λ_{ex} 315nm, is in agreement with the literature value, but that the emission maximum is shifted to 446nm. This latter feature can be explained since the transmission of the 3-73 filter at 425nm is relatively low. Subsequent measurements were performed at λ_{ex} 315nm and λ_{em} 446nm.

6.6.3. Effect of electrode potential

The fluorescence - time response was recorded for excitations (0.25V to 1.0V vs SCE) of HVA ($2.5x10^{-4}M$) in pH 8.5

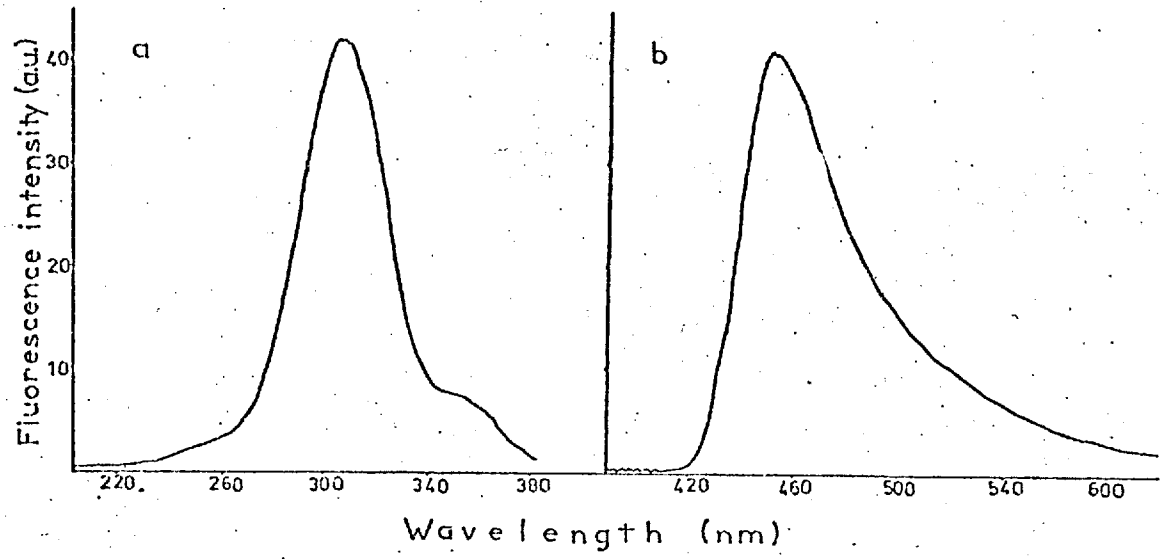

FIG. 6.21. Fluorescence excitation (a) and emission (b) spectra of the oxidation product of homovanillic acid. Homovanillic acid ($3x10^{-4}M$) in pH 8.5 sodium pyrophosphate solution (0.1M); electrode potential 0.3V vs SCE; excitation wavelength 315nm; emission wavelength 446nm; bandpass 10nm on both monochromators (respective filters, 7 - 54 and 3 - 73, fitted).

sodium pyrophosphate solution (0.1M). The maximum fluorescence and development times were dependent on electrode potential in a manner analagous to morphine. The results are given in table 6.19.

Table 6.19. Effect of electrode potential on the fluorescence response of the oxidation product of homovanillic acid.

Electrode Potential V vs SCE	Maximum Fluorescence Intensity (a.u.)	$Time_{MF}$ (min)
0.25	20.85	17.5
0.30	15.48	7.4
0.40	6.66	2.4
0.50	4.24	1.3
0.60	2.98	0.6
0.70	2.30	0.4
0.80	1.98	0.2
0.90	1.76	0.2
1.00	1.69	0.1

Homovanillic acid ($2.5x10^{-4}M$) in pH 8.5 sodium pyrophosphate solution (0.1M); excitation wavelength 315nm, emission wavelength 446nm.

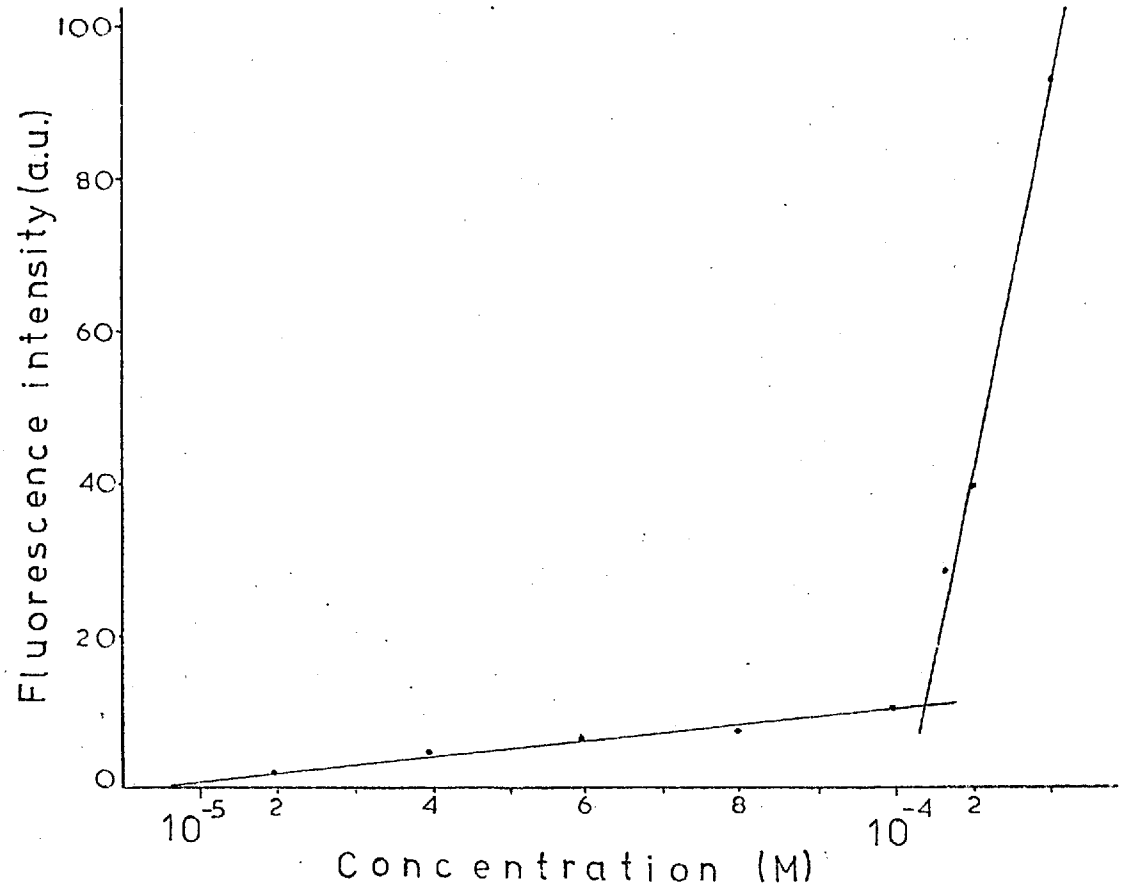

FIG. 6.22. Fluorescence of the oxidation product of homovanillic acid versus homovanillic acid concentration. Homovanillic acid in pH 8.5 sodium pyrophosphate solution (0.1M); electrode potential 0.4V vs SCE; excitation wavelength 315nm; emission wavelength 446nm.

6.6.4. Calibration

Solutions of HVA ($2x10^{-5}$M - $3x10^{-4}$M) in pH 8.5 sodium pyrophosphate solution (0.1M) were oxidised at 0.40V vs SCE and the maximum fluorescence was recorded. The results and calibration plot are presented in table 6.20 and fig 6.22 respectively. The fluorescence concentration graph is similar to the previous plot for thioguanine in that two distinct regions of linearity were obtained.

Table 6.20. Fluorescence of the oxidation product of homovanillic acid as a function of homovanillic acid concentration.

Homovanillic acid Concentration (M)	Maximum Fluorescence Intensity (a.u.)	$Time_{MF}$ (min)
$2x10^{-5}$	1.2	0.7
$4x10^{-5}$	4.2	0.7
$6x10^{-5}$	5.7	0.7
$8x10^{-5}$	6.9	0.7
10^{-4}	10.2	0.7
$1.3x10^{-4}$	28.5	0.7
$2x10^{-4}$	39.0	0.7
$2.5x10^{-4}$	66.6	1.6
$3x10^{-4}$	93.0	2.6

Homovanillic acid in pH 8.5 sodium pyrophosphate solution (0.1M); electrode potential 0.4V vs SCE; excitation wavelength 315nm, emission wavelength 446nm.

6.7. Instrumental Sensitivity

For a concluding experiment, the sensitivity of the Farrand instrument with respect to the gold micromesh cell was determined by estimating the limiting detectable concentration of quinine bisulphate.

Procedure

The instrument was operated at maximum sensitivity and the background noise level of the blank solution was recorded (sulphuric acid, 0.05M). Standard solutions of quinine bisulphate ($10 ngml^{-1}$, $30 ngml^{-1}$, $100 ngml^{-1}$ and $300 ngml^{-1}$) in sulphuric acid (0.05M) were delivered separately to the cell and the fluorescence noted. The results with blank correction are presented in table 6.21 and the logarithmic calibration graph is given in fig 6.23. The limit of detection was taken as that concentration of quinine bisulphate that produced a fluorescence signal equal to twice the standard deviation of the background noise level ($2\sigma_{bl} = 3.04 \times 10^{-4}$ a.u.), the blank

Table 6.21. Fluorescence of quinine bisulphate as a function of concentration.

Concentration of Quinine Bisulphate ($ngml^{-1}$)	(log $ngml^{-1}$)	Fluorescence Intensity (a.u.)	(log a.u.)
10	1.00	0.00044	-3.36
30	1.48	0.00108	-2.97
100	2.00	0.00435	-2.36
300	2.48	0.01230	-1.91

Quinine in sulphuric acid solution (0.05M); excitation wavelength 350nm, emission wavelength 450nm; bandpass 20nm on both monochromators (respective filters, 7-54 and 3-73, fitted); blank subtracted from quinine signal.

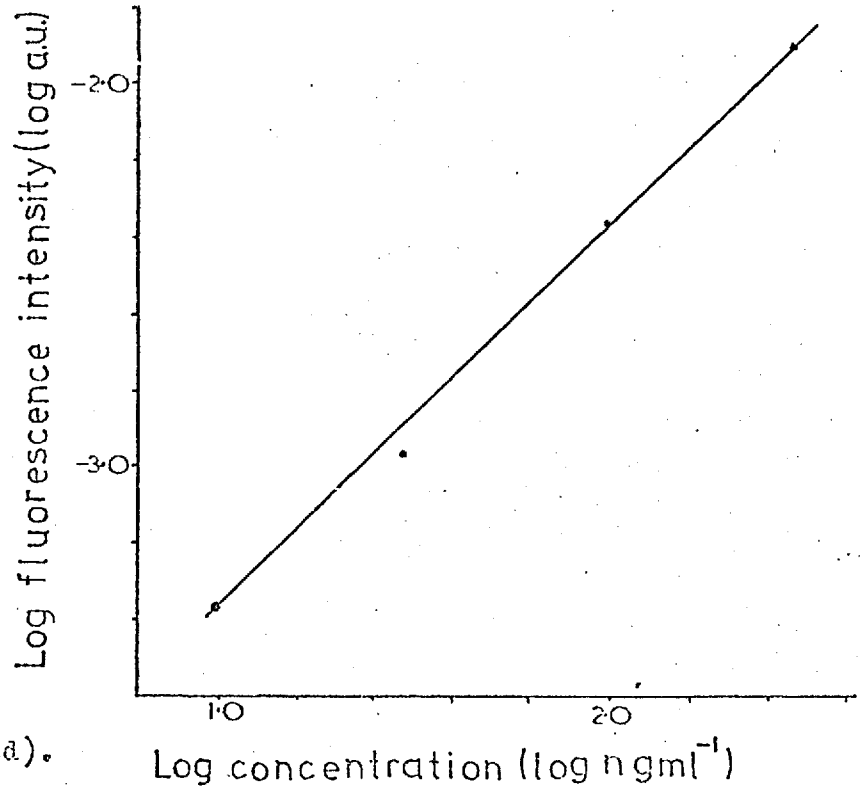

FIG. 6.23. Logarithmic calibration graph for quinine bisulphate. Quinine in sulphuric acid solution (0.05M); excitation wavelength 350nm; emission wavelength 450nm; bandpass, 20nm on both monochromators (respective filters, 7 - 54 and 3 - 73, fitted).

value having been previously subtracted from the quinine signal. Extrapolation of the logarithmic calibration curve to meet the limiting signal enabled the limiting concentration, 7ngml^{-1} (10^{-8}M), to be determined. For the cell volume of 120µl, the limiting detectable weight of quinine bisulphate was calculated to be 0.8ng. Comparison of the detection limits with the values for morphine (19ng), laudanosine (2ng) and reserpine (5ng) indicates the high sensitivity which the spectroelectrochemical technique is capable of attaining. These values, however, may not be used as absolute indicators of fluorescence efficiency since for any particular study the limiting sensitivity depended not only on the quantum efficiency of the oxidation product, but also on product stability with respect to electrode potential and instrumental factors (The transmission characteristics of the filters and the standard deviation of the blank solution were particularly important).

6.8. Conclusions

Fluorescence studies with the gold micromesh cell were very encouraging, the electroinitiation of fluorogenic reactions provided a new semi-automatic method for the determination and characterisation of organic compounds at the trace level. A summary of the electrochemical and fluorescence characteristics of the compounds investigated given in table 6.22 indicates important analytical features of the technique. In addition to the selectivity offered by choice of electrode potential and the two fluorescence wavelengths, selectivity may result from the overall electrode reaction mechanism. For example, phenolic oxidation conferred

Table 6.22. Summary of electrochemical - fluorescence characteristics of compounds.

Compound	Excitation Potential (V vs SCE)	Wavelength Combination (nm) λ_{ex}	λ_{em}	Oxidation Product	Detection Limit (ng)
Morphine	0.25	320	442	Pseudomorphine	19
Homovanillic acid	0.25	315	446	Dimer of HVA	-
Heroin(after hydrolysis)	0.25	320	442	Dimer of Monoacetylmorphine	-
Laudanosine	0.90	361	470	Unknown	2
Reserpine	0.90	375	500	3-dehydroreserpine	5
Thioguanine	1.1	330	400	Thioguanine sulphonate	-
Quinine bisulphate	-	350	450	-	0.8

to morphine a degree of specificity and enabled interference-free determinations in the presence of electroinactive opium alkaloids. The sensitivity of the procedure was comparable to the chemical method of Kupferberg[107] and trace determinations in biological samples should be realised. The semi-automatic capability offered by the gold micromesh cell would be of immediate value in the clinical and forensic fields. These conclusions would apply to heroin (after hydrolysis) determinations. For samples containing the two alkaloids prior separation would be necessary to avoid interference. The spectroelectrochemical approach was applicable to other organic compounds and the studies indicated the value of the gold micromesh cell as a general purpose unit for trace determinations via the redox fluorogenic reaction.

CHAPTER 7 Studies with Polycyclic Aromatic Hydrocarbons

7.1. Introduction

The final research topic was concerned with *in situ* monitoring of polycyclic aromatic hydrocarbons (PAH) in acetonitrile. It was hoped that the fluorescence spectra of the electrogenerated radical ions would provide a new route for characterising these analytically important compounds. Polycyclic aromatic hydrocarbons are formed as a result of inefficient combustion of coal and oil products and pose a serious environmental hazard since they are generally toxic and in some cases are powerful carcinogens[132]. Fortunately the compounds are highly fluorescent and fluorescence-based methods are widely employed for their trace detection and determination[133-137]. The compounds have also been the subject of extensive electrochemical investigations and detailed review articles are available[97,138-141]. Summarising the electrochemical behaviour, aromatic hydrocarbons in aprotic solvents undergo successive one-electron oxidation/reduction steps and depending on the nature of the compound and the experimental conditions, the initially formed radical cation/anion species may be stable or undergo further follow-up chemical reactions. Generally, for reduction in purified solutions and solvents of low proton availability stable radical anions can be prepared, but in the case of oxidation, except in a few cases, the radical cations are highly reactive species and undergo immediate decay reactions. The scheme outlined below where R represents the aromatic hydrocarbon illustrates the initial redox reaction possibilities and also includes the desired fluorescence

routes. In order for fluorescence to be realised the lifetimes of the radical ion species should be sufficient to allow excitation and subsequent fluorescent deactivation of the excited state. Possible interfering mechanisms to be considered are electrogenerated chemiluminescence[44-46] and also the natural fluorescence of the parent compound.

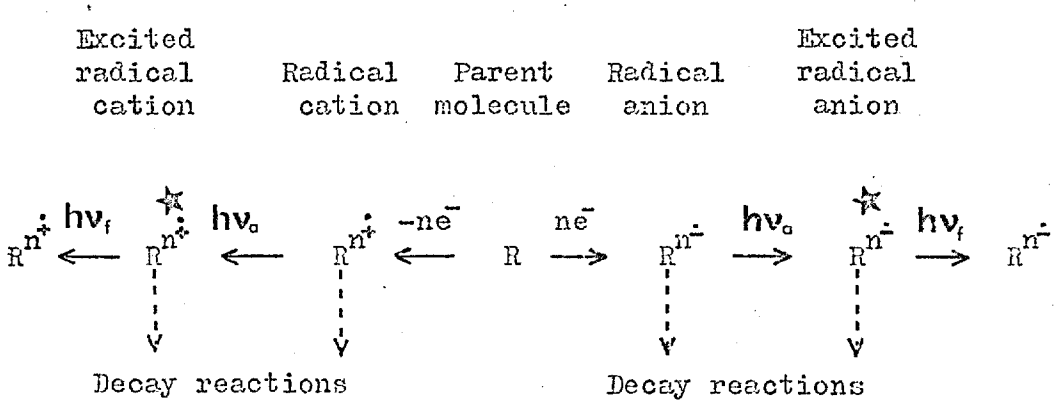

n=1,2

Stable species have been detected by <u>in situ</u> absorption monitoring. The visible spectrum of the radical anion of pyrene[1] and the radical ion (cation and anion) species of 9,10-diphenylanthracene have been reported[30,31,43]. Chemical reduction in tetrahydrofuran using sodium has been employed to enable spectral recording of anionic species[142]. Fluorescence-coupled studies utilising a thin-layer cell have been limited to monitoring the fluorescence decay of rubrene during oxidation[42].

To investigate the proposals, spectral monitoring in a specially designed cell (see section 2.2.3.) was performed during

reduction for acetonitrile solutions of 9,10-diphenylanthracene, perylene and pyrene. Unfortunately, the absorption spectra of the respective radical anions occurred in the visible and near-infrared and thus fluorescence (if realised) recording at longer wavelengths with conventional instrumentation was not possible. The fluorescence experiments described are, therefore, solely concerned with monitoring the fluorescence decay of the parent hydrocarbon during electrolysis. Similar fluorescence decay was also noted for 9,10-diphenylanthracene during oxidation.

7.2. Experimental Details

(1) Apparatus

The Farrand and purpose-built instrument, in conjunction with the quartz cell containing the platinum electrode unit, were employed for fluorescence and absorption monitoring respectively during controlled potential electrolysis. Electrochemical excitation was provided by the PAR 174A.

(2) Solutions and chemicals - purification and preparation

Acetonitrile. Acetonitrile (Spectroscopic grade) was dried by percolation through a column (4ft x 1in) of activated alumina. Acetonitrile (GPR), purified by the method of Walter and Ramaley[143], contained traces of benzene (as evidenced by the ultraviolet spectrum) and was not used.

Tetraethylammonium bromide[144]. Tetraethylammonium bromide (Aldrich) dissolved in chloroform was precipitated with diethylether. The product was recovered and dried at 160°C for 12 hours and stored in a desiccator.

Sodium perchlorate[145]. Sodium perchlorate (Analar grade) was dried at 150°C for 24 hours and stored in a desiccator.

Aromatic hydrocarbons. Aromatic hydrocarbons (Aldrich) were stored in a desiccator and used without further purification.

Electrolyte solutions

Tetraethylammonium bromide (0.1M). The appropriate amount of electrolyte was dissolved in purified acetonitrile contained in a septum-fitted conical flask (250ml). The flask was kept in a desiccator.

Sodium perchlorate (0.1M). Sodium perchlorate solution (0.1M) was prepared and stored as above.

The appropriate electrolyte solution was also used for filling the counter electrode compartment. The reference electrode compartment contained silver nitrate (0.02M) in purified acetonitrile.

Aromatic hydrocarbon solutions

Aromatic hydrocarbon solutions were prepared by transferring, with Hamilton gas-tight syringe, the appropriate background electrolyte solution (tetraethylammonium bromide (0.1M) for reductions; sodium perchlorate (0.1M) for oxidations) to a septum-fitted volumetric flask (10ml) containing a weighed quantity of the appropriate hydrocarbon.

(3) Cell performance and procedure

Sample solution (typically 0.5ml) was transferred from the septum-fitted volumetric flask (10ml) to the cell by Hamilton syringe and the fluorescence decay/absorption was monitored during controlled potential electrolysis. For reduction studies, high-purity (99.999%) and dried argon was used for degassing and to maintain an inert atmosphere during measurement.

Fluorescence was recorded at low instrumental sensitivity using relatively high solution concentrations otherwise an appreciable background signal, due to scattered exciting radiation and fluorescence from the quartz cell, would result. The presence of background electrolyte (tetraethylammonium bromide or sodium perchlorate) at concentrations of 0.1M in acetonitrile did not

affect hydrocarbon fluorescence.

Voltammetric curves were recorded directly in the fluorescence cell, the macro-platinum wire serving as working electrode. Electrode potential measurements were referred to the silver - silver ion reference couple (Ag/Ag^+) which has a value of 0.30V with respect to the aqueous saturated calomel electrode (SCE)[138].

7.3. Reduction Experiments

Aromatic hydrocarbons can undergo successive one-electron reduction steps and follow-up protonation reactions which result in the formation of the dihydrocompound[138],

$$R + e^- \rightleftharpoons R^{\bullet -} \quad (E_{p1})$$

$$R^{\bullet -} + e^- \rightleftharpoons R^{2-} \quad (E_{p2})$$

$$R^{\bullet -} + H^+ \rightarrow RH^{\bullet} \xrightarrow{e^-} RH^- \xrightarrow{H^+} RH_2$$

$$R^{2-} + H^+ \longrightarrow RH^- \xrightarrow{H^+} RH_2.$$

The stability of the radical anions (mono- and di-) depends markedly on the nature of the aromatic hydrocarbon, the proton availability of the solvent and the presence of oxidising agents[146].

Controlled potential reduction experiments with degassed acetonitrile solutions of 9,10-diphenylanthracene, perylene and pyrene were performed with a view to spectrally monitoring the initially formed mono-radical anion species. The internal diameter of the quartz cell at the viewing area was 2mm.

7.3.1. Voltammetric behaviour

The respective current - potential curves were recorded for 9,10-diphenylanthracene ($680\mu gml^{-1}$), perylene ($420\mu gml^{-1}$) and pyrene ($800\mu gml^{-1}$) in the fluorescence cell during cyclic sweep ($50mVs^{-1}$) of the platinum working electrode. The solutions (volume 1ml) containing tetraethylammonium bromide (0.1M) were

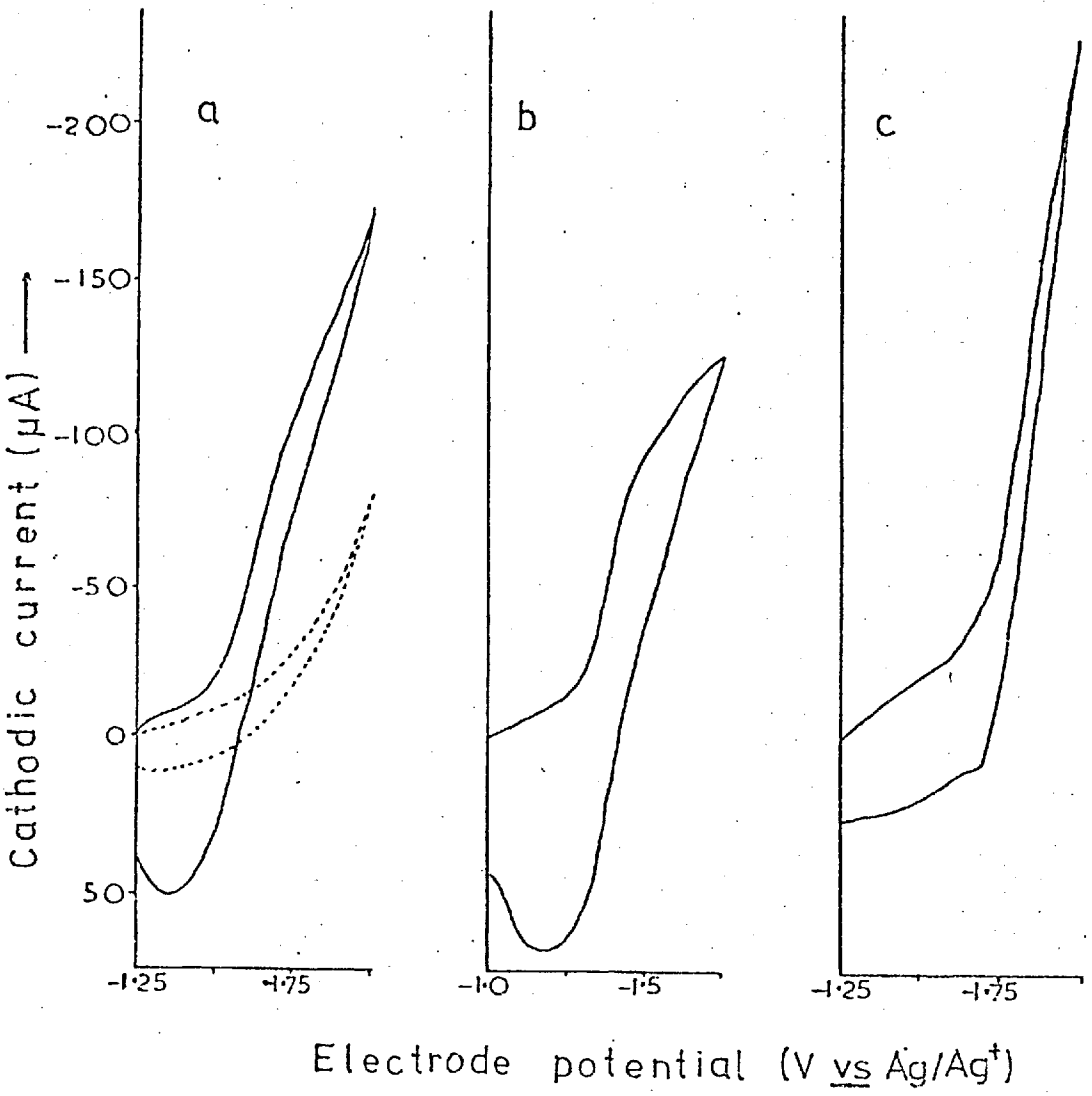

FIG. 7.1. Voltammetric curves for aromatic hydrocarbons. Hydrocarbon in degassed acetonitrile solution containing tetraethylammonium bromide (0.1M); (a) 9,10-diphenylanthracene ($680\mu g ml^{-1}$); broken line, background electrolyte solution only. (b) perylene ($420\mu g ml^{-1}$). (c) pyrene ($800\mu g ml^{-1}$); working electrode, macro-platinum wire; scan rate 50mVs-1.

degassed for five minutes with high-purity argon and an argon blanket was maintained during the scan. The curves are given in fig 7.1 and although the cathodic waves do not exhibit peaks, the commencing reduction potentials (E_c), corresponding to the process

$$R + e^- \longrightarrow R^{\cdot -} ,$$

are evident. The potentials at which reduction approximately

commenced are (1) -1.5V for 9,10-diphenylanthracene (curve a), (2) -1.3V for perylene (curve b) and (3) -1.7V for pyrene (curve c). The cathodic current on the reverse scan particularly for 9,10-diphenylanthracene (curve a) and perylene (curve b) indicated stability of the respective monoradical anion species within the time scale of the sweep.

7.3.2. Absorption spectra of the radical anions

The fluorescence cell was not designed for absorption measurement but this was made possible by employing a rather wide piece of quartz tubing (3mm internal diameter) at the viewing area. The analysing light beam sampled product on either side of the platinum wire working electrode, the wire electrode causing partial obstruction of the light beam. Although the optical pathlength for the cell was short (approximately 2mm), the brilliant colours of the free radical ion solutions (9,10-diphenylanthracene, deep blue; perylene, deep purple; pyrene, yellow) provided significant absorption. The effect of a non-uniform potential distribution along the electrode surface during electrolysis was evidenced with coloured product having formed only around the top portion of the wire.

The respective absorption responses for solutions of (1) 9,10-diphenylanthracene ($680\mu gml^{-1}$), (2) perylene ($100\mu gml^{-1}$) and (3) pyrene ($630\mu gml^{-1}$) in tetraethylammonium bromide (0.1M) were recorded during controlled potential excitation at -2.0V vs Ag/Ag^{+} over the wavelength range 350nm to 1000nm (at 50nm intervals); the absorption signal was fairly rapid and an

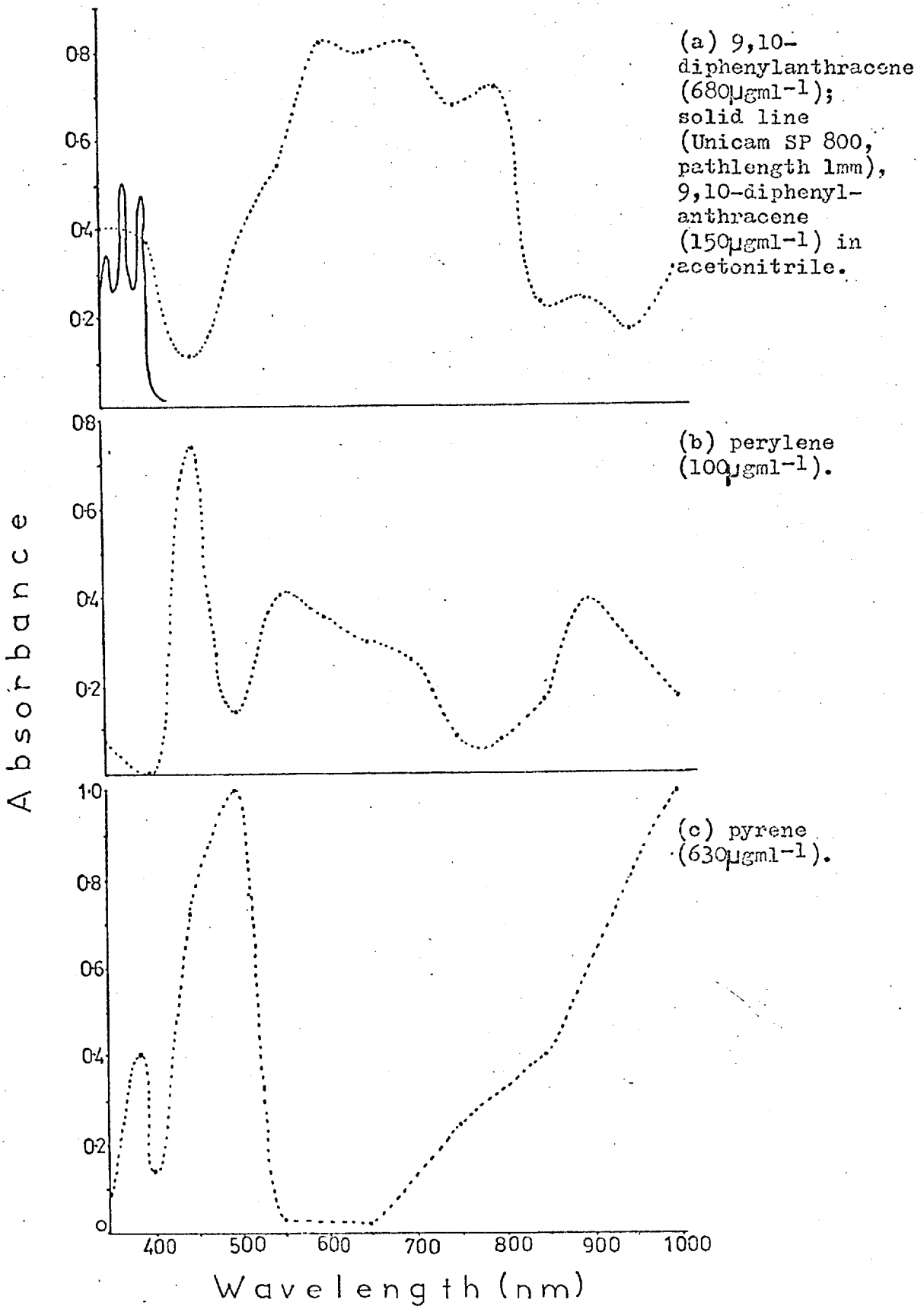

FIG. 7.2. Absorption spectra of electrogenerated radical anions of aromatic hydrocarbons. Hydrocarbon in degassed acetonitrile solution containing tetraethylammonium bromide (0.1M); electrode potential -2.0V vs Ag/Ag^+; quartz cell, internal diameter 3mm; pathlength approximately 2mm.

approximate steady-state maximum was attained in about two minutes. Solutions were degassed prior to measurement at each wavelength and the argon blanket was maintained during electrolysis. A single sample (volume 1ml) of diphenylanthracene served for all measurements, but for pyrene and perylene several samples were required. The "electrogenerated" absorption spectra for the three solutions are given in fig 7.2. The spectrum for 9,10-diphenylanthracene ($150\mu gml^{-1}$) recorded on the Unicam SP 800 instrument is also included (fig 7.2(a), solid line) and the dramatic effect which the one-electron transfer has on the spectral properties of the diphenylanthracene system is evident. Unforturnately, the absorption of the radical anions, although extremely characteristic, occurred in the visible and near-infrared and, therefore, the possibility of fluorescence detection (assuming fluorescence was realised) at longer wavelengths with the Farrand instrument was ruled out. The spectra for the anions of 9,10-diphenylanthracene and pyrene were in good agreement with that reported by Sioda[30] and Kuwana[1] respectively.

7.3.3. Fluorescence monitoring during potential step

The fluorescence reponse (λ_{ex} 370nm, λ_{em} 430nm) of 9,10-diphenylanthracene ($240\mu gml^{-1}$) in tetraethylammonium bromide solution (0.1M) was recorded during repetitive potential step cycling (-1.5V to -2.5V to 1.5V vs Ag/Ag^{+}) of the working electrode. The fluorescence immediately decayed to a low level on application of -2.5V due to removal of 9,10-diphenylanthracene.

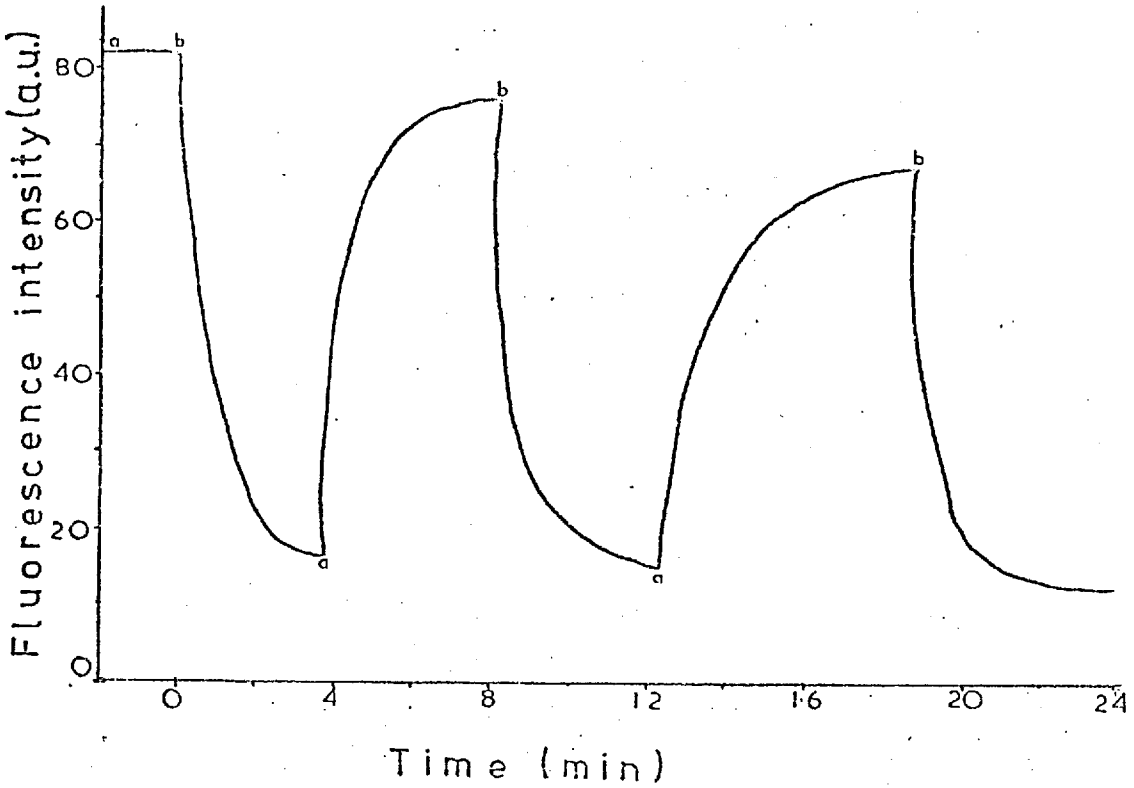

FIG. 7.3. Fluorescence response of 9,10-diphenylanthracene during electrode potential cycling. 9,10-diphenylanthracene ($240\mu g ml^{-1}$) in degassed acetonitrile solution containing tetraethylammonium bromide (0.1M); electrode potential, (a) -1.5V vs Ag/Ag^+, (b) -2.5V vs Ag/Ag^+; excitation wavelength 370nm, emission wavelength 430nm; bandpass, 5mm on both monochromators; quartz cell, 2mm internal diameter.

On returning the potential to -1.5V, the fluorescence increased fairly rapidly indicating oxidation of the radical anion. Repetitive cycling of the electrode potential caused the disappearance/reappearance of fluorescence in a regular manner and indicated reversibility of the 9,10-diphenylanthracene (DPA) system

$$DPA + e^- \underset{-1.5V}{\overset{-2.5V}{\rightleftharpoons}} DPA^{\cdot-}$$

The fluorescence response during electrode cycling is given in fig 7.3 while the emission spectra at -1.5V vs Ag/Ag^+ (curve a, t=0) and at -2.5V vs Ag/Ag^+ (curve b, t=24min) are presented in fig 7.4.

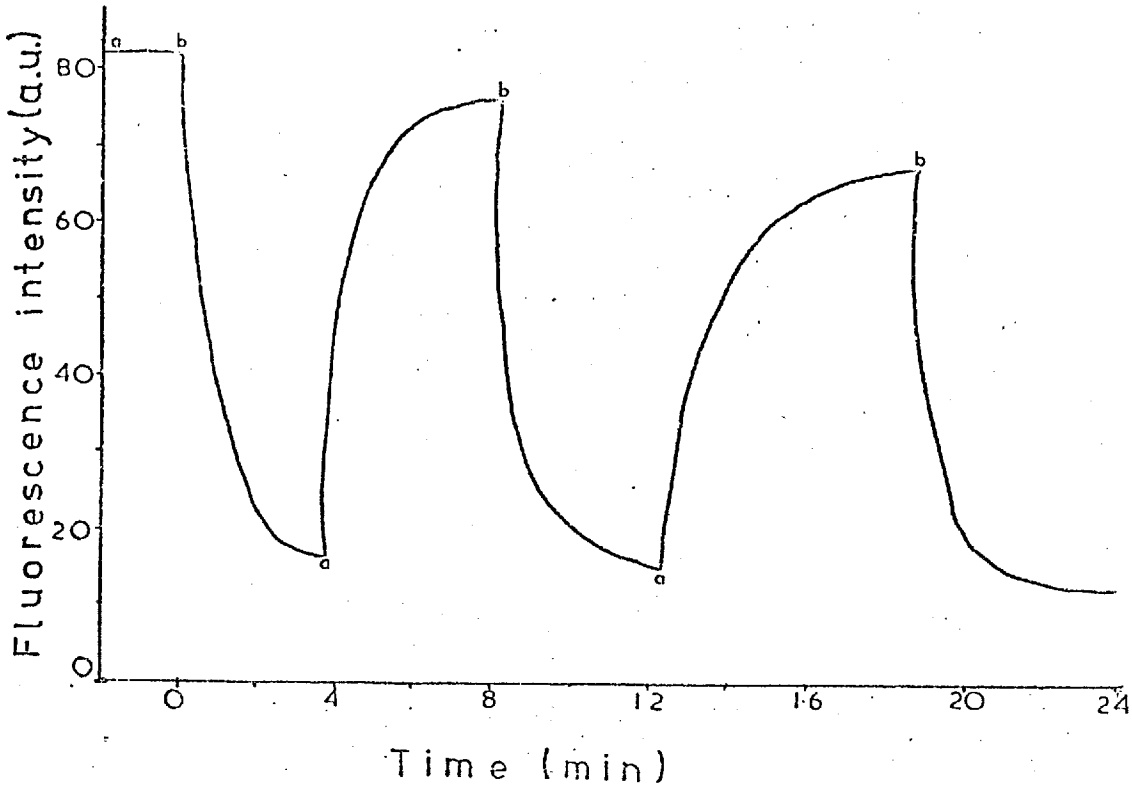

FIG. 7.3. Fluorescence response of 9,10-diphenylanthracene during electrode potential cycling. 9,10-diphenylanthracene ($240 \mu g ml^{-1}$) in degassed acetonitrile solution containing tetraethylammonium bromide (0.1M); electrode potential, (a) -1.5V vs Ag/Ag^+, (b) -2.5V vs Ag/Ag^+; excitation wavelength 370nm, emission wavelength 430nm; bandpass, 5mm on ~~both~~ monochromators; quartz cell, 2mm internal diameter.

On returning the potential to -1.5V, the fluorescence increased fairly rapidly indicating oxidation of the radical anion. Repetitive cycling of the electrode potential caused the disappearance/reappearance of fluorescence in a regular manner and indicated reversibility of the 9,10-diphenylanthracene (DPA) system

$$DPA + e^- \underset{-1.5V}{\overset{-2.5V}{\rightleftharpoons}} DPA^{\cdot -}$$

The fluorescence response during electrode cycling is given in fig 7.3 while the emission spectra at -1.5V vs Ag/Ag^+ (curve a, t=0) and at -2.5V vs Ag/Ag^+ (curve b, t=24min) are presented in fig 7.4.

7.4. Oxidation Experiments

Oxidation of polycyclic aromatic hydrocarbons generally results in unstable cations and complicated follow-up reactions ensue; among the simple aromatic hydrocabons only 9,10-diphenylanthracene exhibits reversible behaviour[139].

Fluorescence monitoring during controlled potential oxidation of acetonitrile solutions of pyrene, perylene, fluorene and naphthalene was attempted, but unfortunately an insulating film formed on the working electrode and prevented further electrolysis. In the case of 9,10-diphenylanthracene the fluorescence decay was recorded. The internal diameter of the quartz cell for this experiment was 1mm and provided a very narrow solution layer, of approximate thickness 0.2mm, in contact with the working electrode.

7.4.1. Voltammetric behaviour

The current - potential curve recorded for 9,10-diphenylanthracene ($150\mu g ml^{-1}$) in sodium perchlorate solution (0.1M) during a cyclic sweep (0V to 1.5V to 0V *vs* Ag/Ag^{+} at $50mVs^{-1}$) of the working electrode is given in fig 7.5. The oxidation wave, corresponding to the loss of one-electron, commenced at about 0.9V and the peak potential was about 1.1V. Further oxidation at potentials beyond about 1.2V, corresponding to the removal of a second electron, occurred. The reduction wave on the reverse scan with a peak potential (E_p) at about 0.8V indicated stability of the free-radical cation.

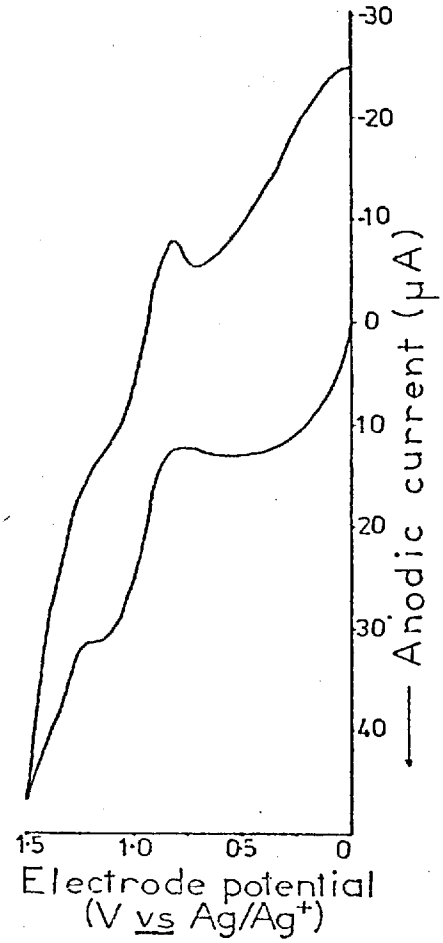

FIG. 7.5. Voltammetric curve for 9,10-diphenylanthracene. 9,10-diphenylanthracene ($150\mu g ml^{-1}$) in acetonitrile solution containing sodium perchlorate (0.1M); working electrode, macro-platinum wire; scan rate $50mVs^{-1}$.

The waves in the region 0V to 0.75V are probably due to platinum surface oxide formation and removal.

7.4.2. Fluorescence monitoring during potential step

The fluorescence (λ_{ex} 370nm, λ_{em} 410nm) of 9,10-diphenylanthracene ($150\mu g ml^{-1}$) in sodium perchlorate solution (0.1M) was monitored during controlled potential oxidation at 1.25V vs Ag/Ag^{+}. The fluorescence decay was very fast and after approximately two minutes the fluorescence level was indistinguishable from the blank solution. The fluorescence decay curve and the emission spectrum before and after oxidation are given in fig 7.6. The high background level, due to fluorescence of the quartz cell and scattered exciting radiation, was severe for the narrow diameter (1mm) cell. After about one hour (at zero applied potential), the fluorescence of the electrolysed solution

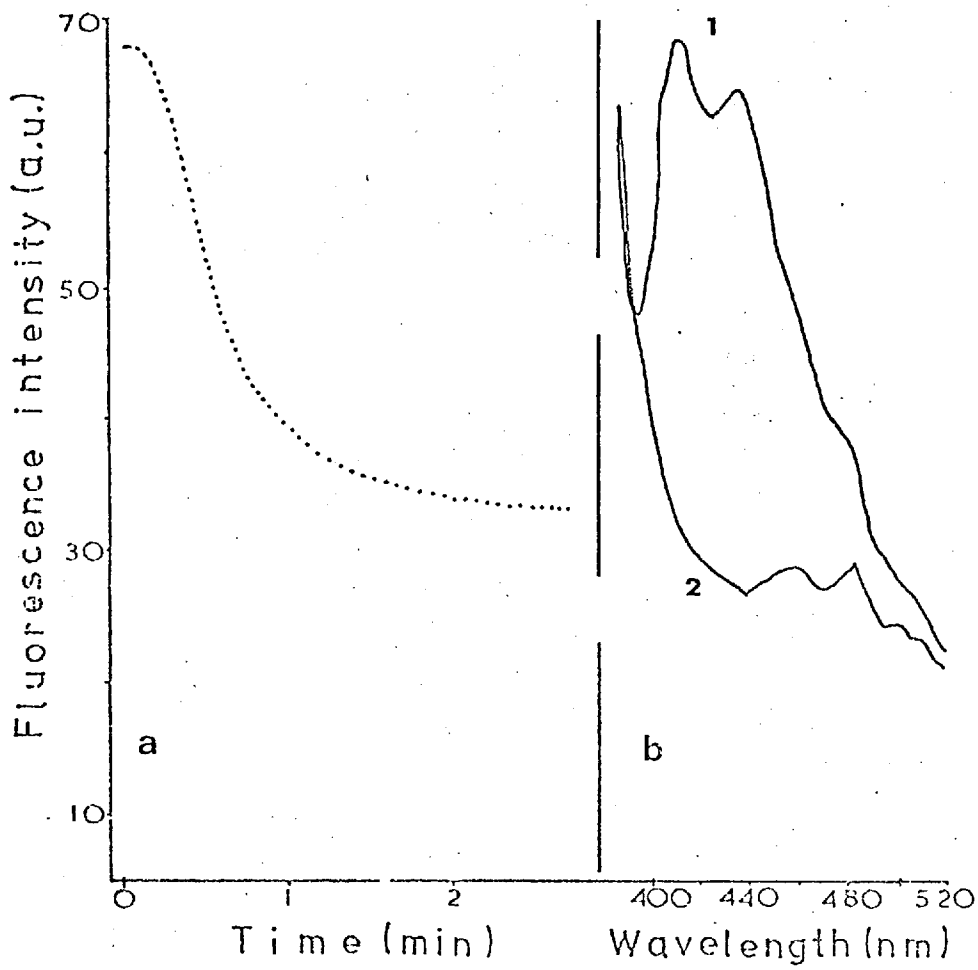

FIG.7.6. Fluorescence response for 9,10-diphenylanthracene during controlled potential oxidation. 9,10-diphenylanthracene ($150\mu gml^{-1}$) in acetonitrile solution containing sodium perchlorate (0.1M). Quartz cell, 1mm internal diameter; bandpass, 5nm on both monochromators. (a) fluorescence - time decay during controlled potential oxidation (1.25 V vs Ag/Ag^+); excitation wavelength 370nm, emission wavelength 410nm. (b) fluorescence emission spectra at (1) zero applied potential (t=0) and (2) 1.25V vs Ag/Ag^+ (t=3min); excitation wavelength 370nm.

returned to approximately 50% of the original value. The explanation for the regeneration of 9,10-diphenylanthracene may have been due to scavenging of the cation radical by residual water

$$2DPA^+ + 2H_2O \longrightarrow DPA + DPA(OH)_2 + 2H^+$$

as proposed by Sioda[30]. Visual examination of the solution during electrolysis revealed the blue colour of the free radical cation species.

7.5. Conclusions

The proposed *in situ* fluorescence studies of electrogenerated ions of polycyclic aromatic hydrocarbons was unsuccessful. The radical anions of (1) 9,10-diphenylanthracene, (2) perylene and (3) pyrene exhibited absorption throughout the visible and near-infrared regions and fluorescence, if realised, would have occurred in the inaccessible infrared. The absorption spectra of the respective anion species were sensitive and characteristic and would be useful for identification purposes. The experiments, although brief, demonstrated the value of the non-aqueous medium for stabilising the primary electrode product and preventing immediate follow-up chemical reactions. The situation is analogous to the aqueous studies of ferrocyanide and o-tolidine but contrasts with the fluorogenic oxidation reactions. The possibility of generating new highly absorbing/fluorescing species in non-aqueous media either as a primary electrode product or as a subsequent follow-up species in a similar manner to the aqueous studies could be realised by suitable choice of solvent and experiments directed along this line would be rewarding. The use of quartz as the cell window material was unsatisfactory and replacement by silica would improve cell performance. For higher sensitivity in absorption, a long optical pathlength cell would be required.

CHAPTER 8 General Conclusion and Recommendations

The spectroelectrochemical procedure whereby electrogenerated species are measured *in situ* by absorption or fluorescence spectroscopy has analytical value. The technique, applicable to inorganic and organic systems, enabled highly absorbing/fluorescent species to be generated, under well-defined conditions, from suitable precursors and concurrent spectral monitoring provided a novel approach for characterisation and determinations at the trace level. Further studies aimed at measuring the primary product or follow-up species of electrode reactions would be rewarding and hopefully would establish the spectroelectrochemical technique as a valuable analytical procedure complimenting its important role in mechanistic studies. The scope for such experiments is almost unlimited, but areas for further research are briefly outlined.

The gold micromesh cell was demonstrated to be an attractive analytical tool for trace determinations via the electro-initiated fluorogenic reaction and further studies should be concerned with assessing its suitability for routine determinations particularly with respect to morphine and heroin. Examination of other potential fluorogenic compounds, for example chlorpromazine[147,148], pyridoxine[149] and thiamine[150], should also be considered.

The chromogenic/fluorogenic approach could be used to improve detector performance in high-pressure liquid chromatography (HPLC) systems. A redox unit (volume ~ 1μl) situated

beyond the column would selectively oxidise/reduce the desired component to enable sensitive detection downstream at the spectroscopic cell (absorption or fluorescence cell; volume ~ 1µl). The technique should be applicable to many electroactive organic compounds that are determined in complex mixtures after HPLC separation.

Finally on the inorganic side, spectral (absorption and fluorescence) monitoring of stable oxidation states of metal ions deserves study. Experiments should be directed at transition metal ions, lanthanides and uranium.

REFERENCES

1. T. Kuwana and N. Winograd in Electroanalytical Chemistry (Ed. A.J. Bard), Vol.7, Marcel Dekker, New York, 1974.

2. T. Kuwana, Ber. der Bunsen-Gesellschaft, 77, 858 (1973).

3. J.F. Tyson and T.S. West, Nature, 250, 139 (1974).

4. J.F. Tyson, Ph.D. Thesis, University of London, London, 1975.

5. T.S. West, Analyst, 99, 886 (1974).

6. H. Bagheri-Sadeghi, Ph.D. Thesis, University of London, London, 1975.

7. A.J.C.L. Hogarth, Ph.D. Thesis, University of London, London, 1977.

8. R.H. Muller (Ed.) in Adv. Electrochem. Electrochem. Engineering (Eds. P. Delahay and C.W. Tobias), Vol.9, John Wiley, New York, 1974.

9. R.N. Adams, J. Electroanal. Chem., 8, 151 (1964).

10. T.M. McKinney in Electroanalytical Chemistry (Ed. A.J. Bard), Vol.10, Marcel Dekker, New York, 1977.

11. T. Kuwana and J.W. Strojek, J. Electroanal. Chem., 16, 471 (1968).

12. T. Kuwana, G. Gruver and J.W. Strojek, Anal. Chem., 41, 481 (1969).

13. T. Kuwana, R.K. Darlington and D.W. Leedy, Anal. Chem., 36, 2023 (1964).

14. T. Kuwana and J.W. Strojek, Disc. Far. Soc., 45, 134 (1968).

15. S.W. Feldberg, T. Kuwana and J.W. Strojek, J. Amer. Chem. Soc., 90, 1353 (1968).

16. T. Osa and T. Kuwana, J. Electroanal. Chem., 22, 389 (1969).

17. G. Gruver, Ph.D. Thesis, Case Western Reserve University, Cleveland, Ohio, 1970.

18. W.J. Blaedel and S.L. Boyer, Anal. Chem., 45, 258 (1973).

19. R.W. Murray, T.E. Neal and M. Petek, Anal. Chem., 43, 1069 (1971).

20. C.N. Reilley, Rev. Pure and Appl. Chem., 18, 137 (1968).

21. F.C. Anson and A.T. Hubbard in Electroanalytical Chemistry (Ed. A.J. Bard), Vol.4, Marcel Dekker, New York, 1970.

22. A.T. Hubbard, Crit. Rev. in Anal. Chem., 3, 201 (1972-4).

23. W.R. Heineman, R.W. Murray and G.W. O'Dom, Anal. Chem., 39, 1666 (1967).

24. R.L. McCreery, Anal. Chem., 49, 206 (1977).

25. W.R. Heineman, M.L. Meckstroth and B.J. Norris, Anal. Chem., 48, 630 (1976).

26. F.M. Hawkridge and T. Kuwana, Anal. Chem., 45, 1021 (1973).

27. W.R. Heineman and T. Kuwana, Anal. Chem., 43, 1075 (1971).

28. Idem, Anal. Chem., 44, 1972 (1972).

29. R.L. McNeely, R.W. Murray, T.E. Neal and M. Petek, Anal. Chem., 45, 32 (1973).

30. R.E. Sioda, J. Phys. Chem., 72, 2322 (1968).

31. Idem, Electrochim. Acta, 13, 375 (1968).

32. W. Kemula and R.E. Sioda, J. Electroanal. Chem., 31, 113 (1971).

33. J.Janata and H.B. Mark, Anal. Chem., 39, 1896 (1967).

34. W.D. Ellis and D.T. Baker, Anal. Chem., 44, 1330 (1972).

35. P.W. Gilles, C.A. Reynolds and E.N. Wise, Anal. Chem., 25, 1344 (1953).

36. Idem, Anal. Chem., 26, 779 (1954).

37. T.C. Franklin and C.C. Roth, Anal. Chem., 27, 1197 (1955).

38. W.N. Hansen, T. Kuwana and R.A. Osteryoung, Anal. Chem., 38, 1810 (1966).

39. T. Kuwana and N. Winograd, J. Amer.Chem. Soc., 93, 4343 (1971).

40. J.N. Burnett, W.R. Heineman and R.W. Murray, Anal. Chem., 40, 1974 (1968).

41. D.H. Evans and D.E. Tallant, Anal. Chem., 41, 835 (1969).

42. A. Yildiz, P.T. Kissinger and C.N. Reilley, Anal. Chem., 40, 1018 (1968).

43. P.T. Kissinger and C.N. Reilley, Anal. Chem., 42, 12 (1970).

44. D.M. Hercules in Physical Methods of Chemistry (Eds. A. Wiesburger and B. Rossiter), Vol.1, Part 2B, Wiley-Interscience, New York, 1971.

45. G.G. Guilbault, Practical Fluorescence - Theory Methods and Techniques, Marcel Dekker, 1973.

46. A.J. Bard and L.R. Faulkner in Electroanalytical Chemistry (Ed. A.J. Bard), Vol.10, Marcel Dekker, New York, 1977.

47. A.J. Bard and S.A. Cruser, Anal. Letters, 1, 11 (1967).

48. Idem, J. Amer. Chem. Soc., 91, 267 (1969).

49. B. Fleet, G.F. Kirkbright and C.J. Pickford, Talanta, 15, 566 (1968).

50. T. Kuwana in Electroanalytical Chemistry (Ed. A.J. Bard), Vol. 1, Marcel Dekker, New York, 1966.

51. D.R. Crow, Proc. Soc. Analyt. Chem., 7, 213 (1970).

52. J.R. Birk and S.P. Perone, Anal. Chem., 38, 1589 (1966).

53. S.P. Perone, Anal. Chem., 44, 443 (1972).

54. S. DasGupta, Ph.D. Thesis, University of London, London, 1975.

55. Z.R. Grabowski and W. Kemula, Coll. Czech. Chem. Comm., 15, 1085 (1950).

56. V.V. Kuznetsov, Zhur. Fiz. Khim., 24, 574 (1950). Chem. Abs., 44, 8801c.

57. P. Gerard, L. Gierst, E. Nicholas and V. Zutic, J. Electroanal. Chem., 44, 107 (1973).

58. N. Ibl in Adv. Electrochem. Electrochem. Engineering (Eds. P. Delahay and C.W. Tobias), Vol.2, Wiley-Interscience, New York, 1962.

59. V.A. Khadeev, Trudy Sredneaziat Gosudarst Univ.im V.I. Lenina Khim, 84, 23 (1958). Chem. Abs., 53, 1881i.

60. P.G. Hansen, J. Inorg. and Nucl. Chem., 12, 30 (1959).

61. Idem, J. Inorg. and Nucl. Chem., 17, 232 (1961).

62. T.M. Ovchinnikova, A.L. Rotinyan and L.A. Taran, Zh. Fiz. Khim., 36, 1909 (1962).

63. R.U. Bondar, V.M. Nagirnyi and V.V. Stender, Zh. Prikl. Khim., 40, 808 (1967).

64. J.P. Hoare, The Electrochemistry of Oxygen, Wiley-Interscience, New York, 1968.

65. A. Damjanovic in Modern Aspects of Electrochemistry (Eds. J.O'M. Bockris and B.E. Conway), No.5, Butterworth, London, 1969.

66. I.M. Kolthoff and C.S. Miller, J. Amer. Chem. Soc., 63, 1013 (1941).

67. I.M. Kolthoff and J.J. Lingane, Polarography (2nd Edit.), Vol.2, Wiley-Interscience, 1952.

68. L. Myuller and L.N. Nekrasov, J. Electroanal. Chem., 9, 282 (1965).

69. J.O'M. Bockris, A. Damjanovic and M.A. Genshaw, J. Electrochem. Soc., 114, 1107 (1967).

70. K.F. Blurton and E. McMullin, J. Electrochem. Soc., 116, 1476 (1969).

71. M.O. Davies, H. Clark, F. Howrka and E. Yeager, J. Electrochem. Soc., 106, 56 (1959).

72. L. Myuller and L.N. Nekrasov, Electrochim. Acta, 9, 1015 (1964).

73. J.P. Hoare, J. Electrochem.Soc., 112, 602 (1965).

74. R.A. Mitchell and D.G. Peters, J. Electroanal. Chem., 10, 306 (1965).

75. W. Bold and M.W. Breiter, J. Electroanal. Chem., 5, 169 (1961).

76. R. Woods in Electroanalytical Chemistry (Ed. A.J. Bard), Vol.9, Marcel Dekker, New York, 1976.

77. J.P. Carr and N.A. Hampson, J. Electroanal. Chem., 17, 2117 (1972).

78. M. Breiter, J. Electroanal. Chem., 7, 38 (1964).

79. J. O'M. Bockris, M. Genshaw and A.K.N. Reddy, J. Electroanal. Chem., 8, 406 (1964).

80. Idem, J. Phys. Chem., 48, 671 (1968).

81. H. Argerstein-Kozlowska, B.E. Conway and W.B.A. Sharp, J. Electroanal. Chem., 43, 9 (1973).

82. B.E. Conway and S. Gottesfield, J. Chem. Soc., I, 69, 1090 (1973).

83. H. Argerstein-Kozlowska, B.E. Conway and B.V. Tilak, J. Electroanal. Chem., 48, 1 (1973).

84. W. Bold and M. Breiter, Electrochim. Acta, 5, 145 (1961).

85. S. Gilman, Electrochim. Acta, 9, 1025 (1964).

86. S. Shibata, Electrochim. Acta, 17, 395 (1972).

87. C.E. Bricker, C.G. Enke and S.W. Feldberg, J. Electrochem. Soc., 110, 826 (1963).

88. A.N. Frumkin in Adv. in Electrochem. and Electrochem. Eng. (Eds. P. Delahay and C.W. Tobias), Vol.1, Wiley-Interscience, New York, 1961.

89. S.S. Mohammad and T. Navaneeth Rao, J. Chem. Soc., 1957, 1077.

90. W. Szafranski and P. Zuman, Anal. Chem., 48, 2163 (1976).

91. R.M. Cassidy, J.R. Dean and D.E. Ryan, Can. J. Chem., 43, 999 (1965).

92. J.A. Dean (Ed.), Langes Handbook of Chemistry (11th Edit), McGraw-Hill, 1973.

93. F.W. Billmeyer in Treatise on Analytical Chemistry (Eds. I.M. Kolthoff and P.J. Elving), Part 1, Vol.5, Wiley-Interscience, New York, 1963.

94. B.Jirgensons and M.E. Strausmanis, A Short Textbook of Colloid Chemistry, Pergamon, London, 1955.

95. W. Heller and E. Vassy, J. Chem. Phys., 14, 565 (1946).

96. W. Heller, H.B. Klevens and H. Oppenheimer, J. Chem. Phys., 14, 566 (1946).

97. R.N. Adams, Electrochemistry at Solid Electrodes, Marcel Dekker, New York, 1969.

98. V.J. Jennings and P.J. Pearson, Anal. Chim. Acta, 82, 223 (1976).

99. E.B. Sandell, Colorimetric Determination of Traces of Metals, Wiley-Interscience, New York, 1944.

100. A. Calderbank and S.H. Yuen, Analyst, 1965, 99.

101. R.J. Argauer and C.E. White, Fluorescence Analysis - A Practical Approach, Marcel Dekker, New York, 1970.

102. S. Udenfriend, Fluorescence Assay in Biology and Medicine, Revised Edition in 2 volumes, Academic Press, New York, 1970.

103. N.D. Cheronis and S. Ehrlich-Rogozinsky, Microchemical Journal 7, 336 (1963).

104. W.C. Evans in Pharmaceutical Chemistry (Ed. L.G. Chatten), Vol.1, Arnold, London, 1966.

105. R.A. Chalmers and G.A. Wadds, Analyst, 95, 234 (1970).

106. K.W. Bentley, The Chemistry of the Morphine Alkaloids, Oxford University Press, London, 1954.

107. A. Burkhalter, H. Kupferberg and E.L. Way, J. Pharmac. Exp. Ther., 145, 247 (1964).

108. A.E. Takemori, Biochem. Pharmac., 17, 1627 (1968).

109. I. Jane and J.F. Taylor, J. Chrom., 109, 37 (1975).

110. G. Nadeau and G. Sobolewski, Can. J. Biochem. Physiol., 36, 625 (1958).

111. G. Fulton, J. Amer. Pharm. Ass., 26, 726 (1937).

112. P.L. Hushin and S.J. Mule, Anal. Chem., 43, 708 (1971).

113. A.F.J. Jackson, Ph.D. Thesis, University of Aberdeen, Aberdeen, 1971.

114. I.A. Pearl and F.J. Vermillon, J. Electrochem. Soc. 111, 1392 (1964).

115. H.P. Deys, Pharm. Weekblad, 99, 737 (1964).

116. A. Kaiser, Z. Analyt. Chem., 209, 1 (1965).

117. A.I. Scott, Quart. Rev., 19, 1 (1965).

118. K. Fukumoto and T. Kametani, Synthesis, 1972, 657.

119. E.G. Clark (Ed), Isolation and Identification of Drugs in Pharmaceuticals, Body Fluids and Post-mortem Material, Pharmaceutical Press, London, 1969, p. 292.

120. K.W. Bentley in The Alkaloids (Eds. R.H.F. Manske and H.L. Holmes), Vol.13, Academic Press, New York, 1971.

121. J.R. Falck, L.L. Miller and F.R. Stermitz, J. Amer. Chem. Soc., 93, 5941 (1971).

122. Idem, J. Amer. Chem. Soc., 95, 2651 (1973).

123. R.F. Bryan, V. Kameswaran, S.M. Kupchan and A.J. Liepa, J. Amer. Chem. Soc., 95, 6861 (1973).

124. H. Stober and T. Urbanyi, J. Pharm. Sci., 59, 1824 (1970).

125. R. Stainier, J. Pharm. Belg., 28, 307 (1973).

126. J.M. Finkel, J. Pharm. Sci., 64, 121 (1975).

127. D.A. Clarke, I.L. Doerr, J.J. Fox and I. Wempen, J. Org. Chem., 26, 3401 (1961).

128. T.J. Mellinger, Amer. J. Clin. Pathol., 49, 200 (1968).

129. D.F. Sharman, Brit. J. Pharmacol., 20, 204 (1963).

130. N.E. Anden, B.E. Roos and B. Werdinius, Life Sc., 7, 448 (1963).

131. P. Brignac, G.G. Guilbault and M. Zimmer, Anal. Chem., 40, 191 (1968).

132. E. Clar, Polycyclic Hydrocarbons, Academic Press, London, 1964.

133. B.L. Van Duuren, Anal. Chem., 32, 1436 (1960).

134. J.F. McKay and D.R. Latham, Anal. Chem., 44, 2132 (1972).

135. T.R. Hauser, E. Sawicki and T.W. Stanley, Int. J. Air Pollut., 2, 253 (1960).

136. F. Funtter and F. Buzzetti, Residue Reviews, 9, 90 (1965).

137. G.F. Kirkbright and C.G. de Lima, Analyst, 99, 338 (1974).

138. K.K. Barnes and C.K. Mann, Electrochemical Reactions in Non-Aqueous Systems, Marcel Dekker, New York, 1970.

139. M. Peover in Electroanalytical Chemistry (Ed. A.J. Bard), Vol.2, Marcel Dekker, New York, 1967.

140. Idem in Reactions of Molecules at Electrodes (Ed. N.S. Hush), Wiley-Interscience, New York, 1971.

141. G.J. Hoijtink in Adv. in Electrochem. Electrochem. Eng. (Eds.P. Delahay and C.W. Tobias), Vol.7, Wiley-Interscience, New York, 1970.

142. G.J. Hoijtink, N.H. Velthorst and P.J. Zandstra, Mol. Physics, 3, 533 (1960).

143. M. Walter and L. Ramaley, Anal. Chem., 45, 165 (1973).

144. A.K.R. Unni, L. Elias and H.I. Schiff, J. Phys. Chem., 67, 1216 (1963).

145. H. Lund, Acta Chem. Scanda, 11, 491 (1957).

146. A.J. Bard and K.S.V. Santhanam, J. Amer. Chem. Soc., 88, 2669 (1966).

147. C.E. Keeler and T.J. Mellinger, Anal. Chem., 35, 554 (1963).

148. Idem, Anal. Chem., 36, 1840 (1964).

149. J. Price, S. Reddy and M. Reynolds, J. Biol. Chem., 233, 691 (1958).

150. F. Eickhorn, E. Kott and A. Rutenberg, Clin. Chem., 17, 296 (1971).